UNIVERSITÀ
DI PARMA

DOTTORATO DI RICERCA IN
INGEGNERIA INDUSTRIALE

CICLO XXX

SOLUTIONS FOR THE DIAGNOSTICS OF HYDRAULIC COMPONENTS AND SYSTEMS – THE CASE OF A HYDRAULIC PUMP AND A HYDRAULIC CRANE

Coordinatore:
Chiar.mo Prof. GIANNI ROYER CARFAGNI

Tutore:
Chiar.mo Prof. PAOLO CASOLI

Correlatore:
Chiar.mo Prof. ANDREA VACCA

Dottorando: FEDERICO CAMPANINI

Anni 2014/2017

Table of Contents

List of Symbols

Symbol	Description	Unit
α	Cyclic frequency	$[Hz]$
α	Swash-plate angle	$[deg]$
β	Volumetric thermal expansion coefficient	$[K^{-1}]$
γ	Skewness	$[-]$
γ_x	Cyclic spectral coherence	$[-]$
Δ	Sampling time	$[s]$
η	Efficiency	$[null]$
η_t	Overall efficiency	$[null]$
η_v	Volumetric efficiency	$[null]$
θ	Angle	$[rad]$
θ	Deviation of the fluid momentum	$[rad]$
μ	Mean value	$[-]$
μ_3	Third central moment	$[-]$
μ_4	Fourth central moment	$[-]$
ρ	Density	$[kg/m^3]$
σ	Standard deviation	$[-]$
τ	Torque	$[N \cdot m]$
τ	Time shift	$[s]$
ω	Angular velocity	$[rad/s]$
A	Set of cyclic frequencies	$[Hz]$
A	Area	$[m^2]$
a	Isothermal factor	$[m^3/kg]$
C_d	Flow coefficient	$[null]$

c	Viscous coefficient	$[N/(m/s)]$
c_p	Specific heat at constant pressure	$[J/(kg \cdot K)]$
E	Internal energy	$[J]$
$E\{\}$	Expected value	$[-]$
F	Force	$[N]$
F_{flow}	Flow force	$[N]$
f	Spectral frequency	$[Hz]$
f_s	Sampling frequency	$[Hz]$
H	Enthalpy	$[J]$
h	Specific enthalpy	$[J/kg]$
I	Moment of inertia	$[kg \cdot m^2]$
J	Optimization cost function	$[Pa \cdot s]$
K	Secant bulk modulus	$[Pa]$
K	Number of frequency shifts	$[null]$
K	Control gain	$[null]$
k	Kurtosis	$[-]$
L	Filter length	$[null]$
M	Mass of the mechanical arms	$[kg]$
m	Mass	$[kg]$
$\dot{m}$	Mass flow rate	$[kg/s]$
N	Signal length	$[null]$
Nu	Nusselt number	$[null]$
n	Angular velocity	$[r/min]$
n	Discrete index	$[null]$
Pr	Prandtl number	$[null]$
P_h	Hydraulic power	$[W]$
P_m	Mechanical power	$[W]$
P_x	Mean instantaneous power	$[-]$

P_x^α	Cyclic modulation spectrum	$[-]$
p	Pressure	$[Pa]$
$\dot{Q}$	Heat exchange	$[W]$
R	Overlap	$[null]$
Ra	Rayleigh number	$[null]$
R_x	Instantaneous auto-correlation function	$[-]$
SC_x	Spectral correlation density	$[-]$
s	Specific entropy	$[J/(kg \cdot K)]$
T	Temperature	$[K]$
T	Period	$[s]$
t	Time	$[s]$
u	Standard uncertainty	$[-]$
u	Control variable	$[-]$
V	Volume	$[m^3]$
$\dot{V}$	Flow rate	$[m^3/s]$
V_d	Pump displacement	$[m^3]$
v	Specific volume	$[m^3/kg]$
W	Weight force	$[N]$
$\dot{W}$	Mechanical power	$[W]$

List of Subscripts

I	First order approximation
II	Second order approximation
1	Suction port
2	Delivery port
21	Difference between the delivery port and the suction port
3	Drainage port
31	Difference between the drainage port and the suction port
a	Ambient
$actual$	Calculated with the actual value of the flow rates ratio
C	Coulomb
c	Combined
cyl	Cylinder
D	Diameter
d	Delivery line
I	Integral
LS	Load sensing
$lookup$	Calculated with the lookup table
$norm$	Normalized
P	Proportional
p	Pump
p	Piston side
r	Radiation
r	Return line
r	Rod side
ref	Reference

s	Supply line
std	Standard method
T	Tank
th	Thermodynamic method
w	Window

List of Abbreviations

BCS	Blind Component Separation
BSE	Blind Signal Extraction
BSS	Blind Source Separation
CCEFP	Center for Compact and Efficient Fluid Power
CF	Cost Function
CMS	Cyclic Modulation Spectrum
CS1	First-Order Cyclostationary
CS2	Second-Order Cyclostationary
CSC	Cyclic Spectral Coherence
DTFT	Discrete-Time Fourier Transform
ECU	Electronic Control Unit
EH	Electro-Hydraulic
ES	Extremum Seeking
FC	Flow Compensator
FDI	Fault Detection and Identification
FGU	Flow Generation Unit
FMEA	Failure Modes and Effects Analysis
FP	Fluid Power
HMM	Hidden Markov Model
LDA	Linear Discriminant Analysis
LPTV	Linear Periodically Time-Varying
LS	Load Sensing
LSPC	Load Sensing Post-Compensated
MB	Main Boom
MCR	Multiple Cyclic Regression

MSE	Mean Squared Error
NN	Neural Network
OB	Outer Boom
PC	Pressure Compensator
PDF	Probability Density Function
PHM	Prognostics and Health Management
PI	Proportional-Integral
PSD	Power Spectral Density
RMS	Root Mean Square
RRCR	Reduced-Rank Cyclic Regression
RUL	Remaining Useful Life
SA	Synchronous Average
SANC	Self-Adaptive Noise Canceller
SCD	Spectral Correlation Density
SOI	Signal of Interest
STFT	Short-Time Fourier Transform
SUBLEX	SUBspace BLind Extraction
SVM	Support Vector Machine
WT	Wavelet Transform

Abstract

This Ph.D. Thesis proposes some Prognostics and Health Management (PHM) solutions in the field of Fluid Power (FP). Two case studies are considered to demonstrate the performance of the proposed PHM approaches: the case study of a variable displacement axial-piston pump and the case study of a truck loading hydraulic crane.

In the last years, the interest of industry towards condition-based maintenance, in opposition to the traditional time-based maintenance, has been growing. Indeed, a condition-based maintenance can increase the system uptime with a consequent economical advantage. As a prerequisite of condition-based maintenance, the PHM has become one of the most studied topic in the engineering field and many PHM solutions have been proposed in many different industrial areas. A similar trend is also present in the FP field, in particular in those applications where the adoption of Electro-Hydraulic (EH) components creates the basis for the introduction of PHM functionalities. The development of any PHM system requires the acquisition of signals from the considered system and therefore it requires the installation of sensors. As a consequence of the growing adoption of EH components and controls, the number of sensors installed in hydraulic systems is constantly growing; these sensors are mainly used for control purposes, but their signals can also be exploited to introduce PHM functionalities. Two main tasks can be identified in a PHM system: diagnostics and prognostics. The objective of diagnostics is to detect and identify a fault within the system, while the objective of prognostics is instead to estimate the Remaining Useful Life (RUL) of the system components. The available approaches for diagnostics and prognostics can be classified in model-based and data-driven. Due to the difficulties in developing models suitable for diagnostics and prognostics, in most cases data-driven methods are proposed in the literature. The main drawback of data-driven approaches is the required availability of experimental data or historical data.

The study conducted on the variable displacement axial-piston pump aimed at the development of a “smart pump” which can return information about its health status. A key parameter for the monitoring of hydraulic machines is the overall efficiency and in this Thesis a method based on the first principle of thermodynamics is proposed for its online estimation. The advantage of this thermodynamic method, in comparison to the “standard” method used for the calculation of the overall efficiency, is that it does not require the installation of bulky and expensive sensors such as flowmeters and torque meters; this makes the thermodynamic approach suitable for online monitoring. The mathematical formulation of this method is derived from the first principle of thermodynamics under the hypotheses of stationary regime and adiabatic system; a demonstration of the suitability of these hypotheses is given. This approach requires the measurement of the pressures and the temperatures at the hydraulic ports of the machine. For the case with external drainage, the ratio between the drainage flow rate and the delivery flow rate appears in the equation of the overall efficiency. Since flowmeters are expensive and difficult to install, the estimation of this flow rates ratio is a crucial point that needs to be addressed in order to make the proposed approach suitable for online condition monitoring. This thermodynamic method requires also the knowledge of the fluid properties and therefore a model of the considered fluid was developed starting from experimental data provided by the manufacturer. The measurement uncertainty is a significant issue for the thermodynamic method and therefore the combined uncertainty was accurately quantified following the relevant standards. An experimental campaign was carried out to validate the proposed method in comparison with the standard approach for the measurement of the overall efficiency. The uncertainty bands of the standard approach and the proposed thermodynamic approach overlap for all the performed tests and this demonstrate that the two approaches are statistically equivalent. The proposed method was then used to calculate the overall efficiency of faulty pumps; the results demonstrate that the proposed methodology can identify the reduction of overall efficiency due to two of the most common faults: worn slippers and port plate eroded by cavitation. These results were obtained by using flowmeters for the evaluation of the flow rates ratio. Some solutions to avoid the use of flowmeters are proposed and their limitations are presented. A solution based on the measurement of the drainage flow rate through an alternative and cheap sensor and the estimation of the delivery flow from the ideal flow is finally proposed. With the adoption of this solution, the proposed thermodynamic method becomes an extremely valuable tool for the online monitoring of the overall efficiency of hydraulic machines.

The proposed thermodynamic method can detect a fault in the machine, but it cannot be used to identify which fault causes the reduction of the overall efficiency. In this Thesis, a methodology

for the analysis of acceleration signals, based on the theory of cyclostationarity, is proposed and exploited to extract features for the fault identification. Acceleration signals convey a lot of information about the machine health status and, along with the delivery pressure signal, are the most used signals for diagnostics and prognostics in hydraulic machines. The proposed methodology requires an angular sampling and allows the decomposition of the signal in the various components related to different sources of vibration. The Synchronous Average (SA) is proposed for the extraction of the periodic part of the signal and the Multiple Cyclic Regression (MCR) algorithm is proposed for the extraction of the second-order cyclostationary part of the signal. Experiments with the pump in healthy and faulty conditions were performed; the two considered faults are worn slippers and port plate eroded by cavitation. The proposed methodology was used to analyze the signals acquired from two accelerometers; the tests were performed in a test bench and a relative encoder was used for the angular sampling. The adoption of a relative encoder is an expensive solution and alternative solutions to achieve an angular sampling are discussed. The decomposition of the acceleration signals performed through the proposed methodology permitted to extract specific features that distinguish each fault from the flawless condition. The extracted features can be used as inputs of an automatic diagnostic algorithm.

The activity on the hydraulic crane is the result of a collaboration between the University of Parma and the MAHA fluid power research center, Purdue University. The research goal of this project is to combine advanced control strategies with diagnostic and prognostic features for Electro-Hydraulic (EH) systems. The idea is to take advantage of the Electronic Control Unit (ECU) and the sensors already available for control purposes to enable diagnostic and prognostic functionalities. The reference machine, i.e. a hydraulic crane for truck applications, is equipped with an independent metering valve and the system is of Load Sensing Post-Compensated (LSPC) type. The control challenge considered is the opening of the meter-out valve, that has to be defined so as to keep the actuator controllability and guarantee an energy efficient actuation. The proposed control algorithm is composed of a feedforward and a feedback part. The feedforward part requires the knowledge of the value of some system parameters that are known, but with some uncertainties; therefore, a feedback part based on a Proportional-Integral (PI) controller is introduced to reduce the steady state error. The parameters of the feedback control are optimized through an Extremum-Seeking (ES) algorithm. A numerical model of the reference machine was developed, and its results were validated by means of a comparison with experimental results. This numerical model was used as a “virtual” test-rig to test the performance of the proposed control and of the optimization algorithm. The outer boom unfolding movement was identified as

a valuable reference cycle for the diagnostics and the verification of the control capabilities. The performance of the proposed control was demonstrated by simulation results and the numerical model was also exploited to simulate the occurrence of common faults within the hydraulic circuit. The results of the simulations demonstrated that the values of the cost functions considered for the control optimization are sensible to the introduced faults and can be exploited for the identification of a faulty condition; however, the use of the cost functions is not enough to distinguish which fault occurred. A diagnostic algorithm based on a NN is proposed; a series of simulation in faulty conditions was performed for the NN training while another series was executed for the NN validation. The results demonstrate the capability of the proposed approach in recognizing which fault occurred in the system; furthermore, the trained NN is also able to quantify the fault intensity and this information is very useful not only for diagnostics, but also for prognostics. In this Thesis, only single fault scenarios were considered, and future steps of this project will be the consideration of multiple faults scenarios and the definition of the minimum set of sensors for the identification of the faults of interest.

In conclusion, this Thesis gives a contribution to the development of PHM systems in the field of Fluid Power, both for systems and components. The results obtained are encouraging and create the basis for future developments.

Chapter 1 - Introduction

This chapter introduces the topic of Prognostics and Health Management (PHM) and provides the background and the motivation behind the research presented in this Ph.D. Thesis. This introductory chapter details also the research objectives pursued in this work and summarizes the primarily contributions left to the research community.

1.1 Background and Motivation

In any industrial application, the maintenance of systems and components is an important task to guarantee a proper functioning of the plants and maximize their uptime. Traditionally the maintenance was performed on a time base, i.e. following a schedule that defines periodic inspections. During these inspections, the system is stopped, or anyway its productivity is reduced, therefore, the inspections performed when the system did not require any maintenance lead to a useless system downtime and consequent loss of productivity. In recent years, the trend is to move from a time-based maintenance to a condition-based maintenance, where the inspections are performed only when they are effectively required. The implementation of a condition-based maintenance relies on an effective PHM system whose function is to identify if and when a maintenance action is required. For this reason, in the last years the research in the field of PHM has been growing in many industrial applications, making PHM one of the hottest research topic in the engineering field. Many solutions for the PHM have been proposed so far and, even if they are presented in very different contexts and industrial applications (from the electronic components to complex industrial plants), these solutions can be adapted and successfully applied to different applications. The implementation of a PHM system requires the acquisition of signals from the system and therefore the installation of a set of sensors. The definition of the sensors to install in the system is of primary importance for the effectiveness of the PHM system and therefore needs to be defined based on a detailed Failure Modes and Effects Analysis (FMEA) of the considered system. The FMEA is always the first step for the implementation of a PHM system and its outputs are the set of the most relevant faults, which need to be considered, and the set of their effects, useful for the definition of the most suitable set of sensors to install. Within the field of PHM, two main tasks can be distinguished: diagnostics and prognostics. The objective of diagnostics is to recognize if a fault occurred in the system (fault detection) and, if a fault is detected, identify which fault occurred (fault identification). The objective of prognostics, instead, is to estimate the Remaining Useful Life (RUL) of the system, i.e. estimate how long the system can work in acceptable conditions. The prognostic task is more complex because it requires not only information on the current state of the system, but also information on the development of the failure modes of the system. For this reason, the literature in the prognostic field is poorer than in the diagnostic field and it has not reached a state of maturity yet.

This Thesis addresses the topic of PHM in the field of Fluid Power (FP) and considers two different case studies: a variable displacement axial-piston pump, typically used in mobile

applications such as excavators, and a truck loading hydraulic crane. This work finds its motivation in the strong tendency demonstrated in the FP field to develop “smart components” and “smart systems” which not only implement advanced control strategies, but also which are able to return information about their health status. The research in this field is driven by the applications where there are strong safety issues, like in the hydraulic systems installed on aircrafts, or where a system downtime would lead to a huge money loss, like in the chemical and petrochemical industries. The diagnostic approaches proposed in the literature can be divided in two main classes: model-based approaches and data-driven approaches. The model-based approaches require the definition of a detailed model of the considered system; the outputs of this model are then compared with the signal acquired from the actual system to compute the diagnosis. The development of a model suitable for diagnostic purposes is complex, in particular for components such us hydraulic pumps, therefore in many applications data-driven methods are preferred. Data-driven methods aims at computing the diagnosis of the system by recognizing trends in the acquired signals that are symptoms of faulty conditions. The main drawback of these methods is that faulty data or history data are required to associate a particular trend (sometimes referred to as “fault signature”) to the corresponding fault. The prognostics approaches can also be divided in model-based and data-driven. The latter are preferred in the large majority of applications due to the complexity of developing a model capable of describing the degradation and failure modes. Of course, both for diagnostics and prognostics, hybrid approaches, which exploit both a model and past data, are present in the literature.

In this Thesis, both a model-based approach and a data-driven approach for the online monitoring of hydraulic pumps and motors are presented and demonstrated for the case study of an axial-piston pump. Furthermore, an approach which combines control and diagnostic/prognostic features for Electro Hydraulic (EH) mobile machines is presented and demonstrated considering a hydraulic crane as reference machine.

1.2 Research Objectives

The primarily objective of this Thesis is to investigate and propose solutions for the diagnostics and prognostics for hydraulic pumps and hydraulic systems. In this Thesis, two case studies are considered: a variable displacement axial-piston pump and a hydraulic crane for truck applications.

The study on the variable displacement pump was conducted with the support of the company Casappa® S.p.A. and aimed at proposing solutions for the online condition monitoring of the

hydraulic unit. The final goal was the development of a “smart pump” which can give real-time information about its health status based on online measurements. A very important performance parameter for the pump monitoring is the overall efficiency and the first objective was to develop a solution for its online measurement. The overall efficiency of hydraulic machines is typically calculated through the measurement of the shaft torque and delivery flow rate. This approach, which is referred to as “standard approach”, is not suitable for the online monitoring since it requires the installation of bulky and expensive sensors such as a torque meter and a flowmeter. An available methodology for the online measurement of the overall efficiency is based on the first principle of thermodynamic and it is referred, within this Thesis, to as “thermodynamic approach”. This method requires the measurement of the pressures and the temperatures at the machine ports and it was presented in the literature for pumps without external drainage. In this Thesis, this thermodynamic approach is considered and adapted for the case of hydraulic machines with external drainage. In the case of external drainage, the additional measurement of the temperature and the pressure at the drainage port is required; furthermore, the efficiency formulation requires also the knowledge of the ratio of the drainage flow rate and the delivery flow rate. Since the installation of flowmeters is not suitable and affordable for the online monitoring, in this work some solutions to cope with this ratio are presented and their limitations are discussed.

The overall efficiency is an important indicator of the machine health status, but it is not enough to compute the machine diagnosis, since several fault can be responsible of the efficiency reduction. Another objective of this Thesis was the development of a methodology that can be used to diagnose the most common faults of a hydraulic machine. In line with the general trend in the specific literature, the research effort was focused on data-driven methods. The most significant signals considered in the literature are the delivery pressure and the accelerations of the pump case. In this Thesis, the attention is focused on the acceleration signals and a methodology, based on the theory of cyclostationarity, is developed for their analysis. The proposed methodology decomposes the acceleration signal at different levels, related to different vibration sources, and proposes tools for a proper analysis at each level. The application of this methodology allows the extraction of many features that can be used as inputs of an automated diagnostic/prognostic algorithm.

The study on the hydraulic crane is the result of a collaboration of the University of Parma with the MAHA fluid power research lab, Purdue University, and it is funded by the American Center for Compact and Efficient Fluid Power (CCEFP). The use of EH systems allows the introduction of advance control strategies that can improve consistently the performances and the

efficiency of mobile hydraulic machines. On the other hand, the EH technology has still some drawbacks in terms of cost, reliability and sometimes operator's perception, which limit its diffusion on the market. The research goal of this project is to combine the advanced control strategies of EH systems with diagnostic and prognostic features so as to make the EH technology more appealing and cost-effective. The architecture of EH controls, including sensors and an Electronic Control Unit (ECU), can be exploited to implement a PHM system. The idea is to exploit the information coming from the installed sensors, some of them already required for control purposes, and features extracted from the control algorithm and its adaptation capability to the occurrence of faults. The control challenge considered in this work refers to the meter-out control of an Load Sensing Post-Compensated (LSPC) independent metering system; the validity of this approach is general and can also be used with other controls, such us oscillation damping controls, position and velocity controls and so on. In this Thesis, a meter-out control that combines a feedforward action and a feedback action is proposed. The feedback component is based on a PI control and the feedback parameters are optimized by means of an Extremum Seeking (ES) algorithm. The ES algorithm is a gradient-based algorithm which can also be implemented online in order to adapt the value of the control parameters to system changes due to the occurrence of faults. Within this work, the optimization of the parameters is carried out offline and the value of the optimization cost functions are used as inputs of a NN based diagnostic algorithm. In future works, an adaptive control based on an online optimization will be considered and the deviation of the control parameters from the healthy value will be considered for diagnostic purposes. The performance of the control and the NN-based diagnostic algorithm were tested by means of a complete simulation model of the reference machine.

1.3 Original Contributions

This section summarizes the primarily contribution of this Thesis in the field of PHM for hydraulic systems and components.

- An existing methodology for the online monitoring of the overall efficiency of hydraulic machines is adapted to the case of machines with external drainage. The methodology is validated by means of a comparison with the results of the "standard approach".
- Some solutions to avoid the usage of flowmeters in the application of the thermodynamic approach are proposed and their limitation are discussed. In particular, a solution based on the use of an alternative and cheap sensor for the measurement of

the drainage flow rate is proposed and will be developed in the future steps of this activity.

- An analysis procedure for acceleration signals, based on the theory of cyclostationarity, is proposed for the extraction of features for the fault identification. The procedure is demonstrated for the case study of a variable displacement axial-piston pump, but its validity is general, and it can be applied to a wide range of roto-dynamic machines.
- A control strategy for the control of the meter-out section in a LSPC independent metering system is proposed and its performances are demonstrated by means of simulation results.
- For the case study of a hydraulic crane, the use of the cost functions adopted for the control optimization is proposed to detect a faulty condition.
- A general approach, based on a NN, for the diagnostics and prognostics of hydraulic systems is proposed and it is demonstrated for the case study of the hydraulic crane.

1.4 Dissertation Organization

After the introduction given in this chapter, a review of the state of the art about PHM, in particular in the field of hydraulic systems and components, is reported in chapter 2. The rest of the dissertation is organized in three chapters that refer to the three PHM methodologies presented in this Thesis. The proposed "thermodynamic approach" for the online measurement of the pump overall efficiency is presented in chapter 3. The mathematical formulation that leads to the overall efficiency expression is first derived and the approach is validated through a comparison with the "standard approach". The methodology is tested introducing faulty components in the pump so as to verify if it is capable of quantifying the reduction of the overall efficiency due to the considered faults. Finally, several solutions are proposed to avoid the use of flowmeters and make the approach suitable for online applications. Chapter 4 presents a methodology for the analysis of acceleration signals based on the theory of cyclostationarity. The methodology is applied to analyze experimental acceleration signals acquired from the pump in healthy and faulty conditions. The activity conducted on the hydraulic crane is presented in chapter 5. The proposed control for the meter-out section of the independent metering valve and the ES algorithm used for its optimization are introduced. A complete numerical model of the reference machine is first validated against experimental results and then exploited to demonstrate the performance of the proposed control. Simulations in faulty conditions were performed and the results demonstrate

that the values of the optimization cost functions are sensible to the introduced faults, and therefore can be used to detect a faulty condition. Then a limited set of sensors is considered to extract features for the training of a NN with the scope of computing the system diagnosis. A summary and a final discussion on the PHM methodologies presented in this Thesis is given in chapter 6.

Chapter 2 - State of the Art

In this chapter a review of the methodologies for Prognostics and Health Management (PHM) is reported. This review is obviously limited and addresses mainly the case of hydraulic pumps and hydraulic circuits since they are the subjects of this Thesis. A wider review of the literature on PHM for mechanical systems can be found in [2.1-2.3].

Both diagnostics and prognostics are essential tasks for the implementation of a condition-based maintenance (or predictive maintenance) and they have different objectives. The diagnostics aims at identifying the health state of the system and can be considered the first step for the prognostic process which, in turn, aims at identifying the Remaining Useful Life (RUL) of the system. Many methodologies and approaches for the diagnostic process have been proposed in many engineering fields and they can be separated in two main classes: data-driven approaches and model-based approaches. In most applications, the development of a numerical model which can be exploited for diagnostics is a difficult task, thereby, the data-driven approaches are preferred. The field of prognostics has not reached the same level of maturity of diagnostics and the literature is poorer, at least for the subject covered in this Thesis, i.e. mechanical systems. The calculation of the RUL of a mechanical system or component is a very difficult task because it requires the capacity of foreseeing the evolution of a fault in the future. Even in this field, a first classification in model-based approaches and data-driven approaches can be made, with the former approaches preferred in most applications. Indeed, the development of a fault growth model is extremely difficult for most of the deterioration mechanisms in mechanical systems.

The study of state of the art on PHM reported in this chapter represented the starting point for the development of the diagnostic and prognostic approaches proposed in this Thesis for the case studies of a variable displacement hydraulic pump and a hydraulic crane.

2.1 Diagnostics

The objective of diagnostics can be summarized in the expression Fault Detection and Identification (FDI) which is often used in the literature. Indeed, the diagnostics aims at detecting if a fault is present in the system first (fault detection) and then at identifying which fault occurred (fault identification). Any diagnostic approach requires the acquisition of signals from the system and therefore requires the installation of a suitable set of sensors for the system monitoring. The signals acquired are then used to compute the diagnosis. The diagnostic approaches can be divided in two main classes: data-driven approaches and model-based approaches. The following sections describe the principles of these two approaches and review the relevant literature.

2.1.1 Data-Driven Approach

As stated by the name itself, data-driven approaches are based on data acquired from the system. These data can be laboratory data explicitly acquired for the development of the diagnostic algorithm, or historical and operational data acquired from the system during its normal functioning. The block diagram of a generic data-driven approach for diagnostics is reported in Figure 2-1. This block diagram is general and can be used to describe the phases of many diagnostic approaches, not only in the field of FP.

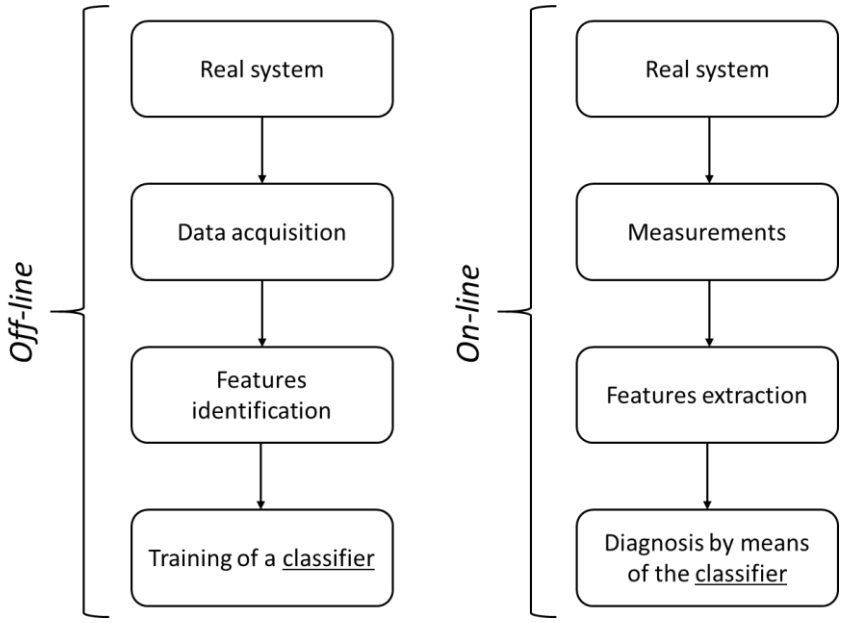

Figure 2-1: Block diagram of a generic data-driven approach for diagnostics.

The data-driven approaches consist of an offline phase and an online phase. The offline phase aims at training a classification algorithm that is then used in the online phase, i.e. when the system is operating, to compute the diagnosis.

2.1.1.1 Data Acquisition

A data-driven approach requires the acquisition of data from the system: laboratory, operational or historical data. These data are used to learn the behavior of the system in healthy and faulty conditions. It is important to select the signals which convey important information about the health state of the system. For this reason, the starting point is a detailed Failures Modes and Effects Analysis (FMEA). The outputs of the FMEA are the identification of the most frequent and significant faults, which need to be considered in the diagnostics algorithm, and the identification of their main effects. The set of sensors to install in the system must be defined so as to acquire the signals where the effects of the faults are more evident.

The vibration of hydraulic pumps, which can be measured using accelerometers installed on the pump case, is affected by the majority of the faults and therefore it is considered in many works which propose diagnostics solutions for hydraulic pumps [2.4-2.9]. Furthermore, the use of accelerometers is the standard for the monitoring and the diagnostics of bearings [2.10, 2.11] that are present in any roto-dynamic machine and also in centrifugal and positive displacement pumps. Acceleration signals have also been exploited for the detection of cavitation in centrifugal pumps [2.6]; for this purpose, also noise measurements have often been considered [2.6, 2.12, 2.13]. In chapter 4 of this Thesis, the acceleration signals acquired by means of two accelerometers are considered for the development of a diagnostic algorithm for a variable displacement axial-piston pump. Besides the acceleration of the pump case, another important signal which is affected by the faults and can be used for the development of an effective diagnostic algorithm is the delivery pressure signal. Many works in the literature propose diagnostics solutions based on the delivery pressure signal [2.14-2.17].

2.1.1.2 Features Identification

Acceleration signals and the delivery pressure signal convey a lot of information about the state of hydraulic pumps; however, the simple comparison of the time series is not effective to compute the diagnosis. The acquired signals need to be elaborated in order to extract parameters or indicators, referred to as “features” in the literature, which are affected by the faults and can be

used as inputs in an automatic diagnostic algorithm. The computation of these features can be performed in the time domain, in the frequency domain, in the time-frequency domain or in the frequency-frequency domain. Some examples of features extracted in the time domain are mean values, Root Mean Square (RMS) values, peak to peak values, maximum and minimum values and so on. The extraction of time features, mean values, is considered in chapter 5 of this Thesis for the development of a diagnostic algorithm for the hydraulic circuit of the crane. In this case study no dynamic effects are present, and the use of mean values is enough to obtain an effective diagnosis.

In most applications, the effects of faults are not evident in the time domain, but in the frequency or time-frequency domain. This is the case of roto-dynamic machines, where the effects of faults are evident at particular frequencies that characterize the faulty components. The occurrence of a fault could influence the RMS value of the acquired signal, acceleration signals for example, but more robust and significant features can be extracted in the frequency domain. For instance, a fault in a race of a bearing will alter the acceleration signal at the corresponding ball pass frequency. The extraction of features in the frequency domain is performed by computing the Fast Fourier Transform (FFT) of the considered signal [2.5, 2.16, 2.18, 2.19]. The computation of the FFT returns many frequency features that can be used in the diagnostic algorithm; the results of the FMEA can be exploited to identify the coefficients of the FFT which are of interest for the identification of a particular fault. The FFT coefficients refer to a precise frequency, but lose sensitivity in the time domain. Some faults affect the system response in a way that neither the time domain, nor the frequency domain are suitable for the extraction of effective features, but their "signature" is clearer in a combination of the time and the frequency domains. Some available tools for the extraction of features in the time-frequency domain are the Short-Time Fourier Transform (STFT) and the Wavelet Transform (WT). The WT is considered in many works related to the diagnostics of roto-dynamics machines [2.1, 2.14, 2.15, 2.18, 2.20, 2.21]. The WT extracts time-frequency coefficients by comparing the considered signal with a wave signal, called "wavelet", which is scaled and translated in time. By using different scaled versions of the wavelet, the time resolution and the frequency resolution, which undergo the indetermination principle, can be adapted at the considered application. The capabilities of the WT are demonstrated by the review reported in [2.22].

Other important tools that can be exploited for the features extraction derive from the theory of cyclostationarity. An introduction to this theory can be found in [2.23] and a wider review of the literature on this topic can be found in chapter 4. Basically, the cyclostationarity studies how the power of a signal at different frequencies is modulated in the frequency domain. The features

extracted through cyclostationary tools belong to the frequency-frequency domain; the spectral frequency, the carrier frequency, is distinguished by the cyclic frequency, which is the modulation frequency. In this Thesis, cyclostationary tools are used for the extraction of features from acceleration signals in the development of a diagnostic algorithm for a variable displacement pump.

2.1.1.3 Classifications Algorithms

Once a set of features sensible to the faults is extracted, it can be used to train an automatic algorithm whose purpose is to correlate the features, which are the inputs of the algorithm, to the faults, which are the output. This automatic algorithm is used to perform a classification and therefore is referred to as "classifier". This classifier is trained offline and then is used online to compute the diagnosis. Many algorithms are presented in the literature for this classification task.

In many applications a Neural Network (NN) is used as classifier. The NN is a powerful tool that is used not only for diagnostics and prognostics, but also for many other tasks as demonstrated in the review reported in [2.24]. A NN is composed of many computational unit, called neurons, organized in several layers; the structure of a NN is reported in Figure 2-2.

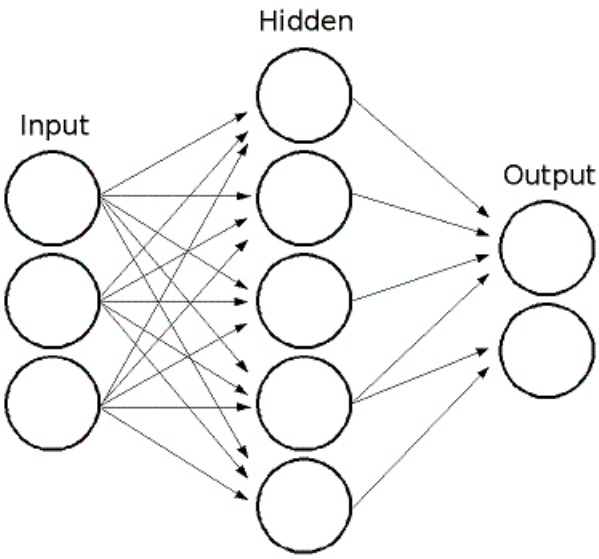

Figure 2-2: Structure of a generic neural network.

The NN is always composed of an input layer, an output layer, and one (as in the figure) or many intermediate or hidden layers. Each neuron is an independent computational unit; the generic structure of a neuron is reported in Figure 2-3.

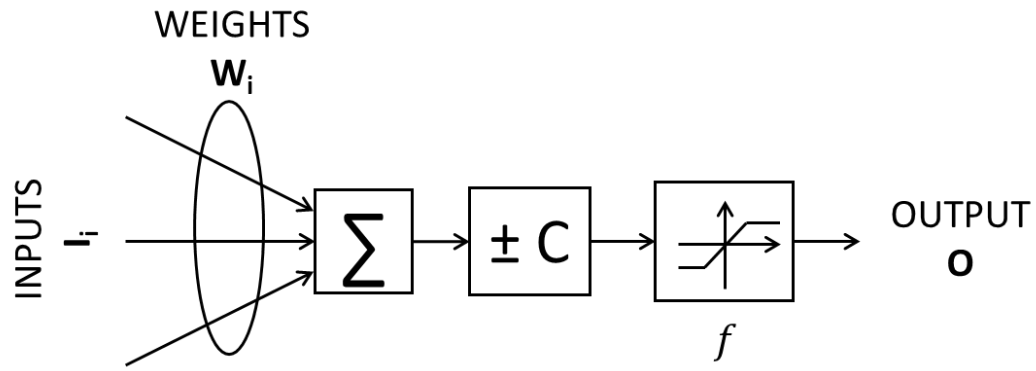

Figure 2-3: Internal structure of a neuron.

A weight is applied to each input of the neuron, then the summation of the weighted inputs is performed, and a bias is applied. The output of the neuron is obtained through a function f that can assume different formulations. The inputs of the neurons in the input layer are the fault features, while the inputs of the neurons of the hidden or the output layers are the outputs of the neurons in the previous layer. The outputs of the neurons in the output layer are the desired diagnosis. The training of the network consists in the definition of the weights and the bias of each neuron in order to associate the features to the faults. The training is performed in a supervised manner, i.e. during the training phase both the inputs and the outputs of the NN are known. Several algorithms are available for the supervised learning; among the most used are the Backpropoagation algorithm and the Levenberg-Marquardt algorithm. Many are the examples of application of NNs for the diagnostics of different mechanical systems: hydraulic circuit [2.25], positive displacement pumps [2.21, 2.26], roto dynamic machines [2.20], ball bearings [2.27-2.29] and for the identification of structural damages [2.30, 2.31].

Apart from the NN, there are many other algorithms which are available for the classification task. Torrika [2.32] presented an interesting comparison of several algorithms for the case study of an axial-piston pump; the performances of a NN are compared to the ones of the following algorithms: Naïve Bayes classifier, Support Vector Machine (SVM), k-nearest neighbor algorithm and decision tree. In that work, the higher classification rate is reached by the SVM, but the performances of the algorithms are very close. Another example of application of the SVM is presented in [2.33] for the case study of a centrifugal pump. Always for the case of a centrifugal

pump, in [2.9] a decision tree algorithm is developed for the fault identification. An approach based on the use of a dynamic Bayesian network is presented in [2.34] for the diagnostics, and also the prognostics, of a hydraulic circuit. A theory which needs to be cited in this brief review is the fuzzy logic. In many works [2.5, 2.16, 2.35] the fuzzy logic is exploited to create inference systems for the fault classification. In many application [2.21 ,2.36] the fuzzy logic is combined to the use of a NN for the classification task. In several works [2.37-2.39], Helwig proposed the use of the Mahalanobis distance classifier for the diagnostics of hydraulic circuits. Helwig proposed also the use of the Linear Discriminant Analysis (LDA) for the reduction of the number of features and the identification of the most relevant features to use as inputs of the classification algorithm.

2.1.2 Model-Based Approach

The main drawback of data-driven methods is the requirement of many data in healthy and faulty conditions. An alternative approach is to use a numerical model of the reference system to compute the diagnosis. The block diagram reported in Figure 2-4 describes the phases of a generic model-based diagnostic algorithm.

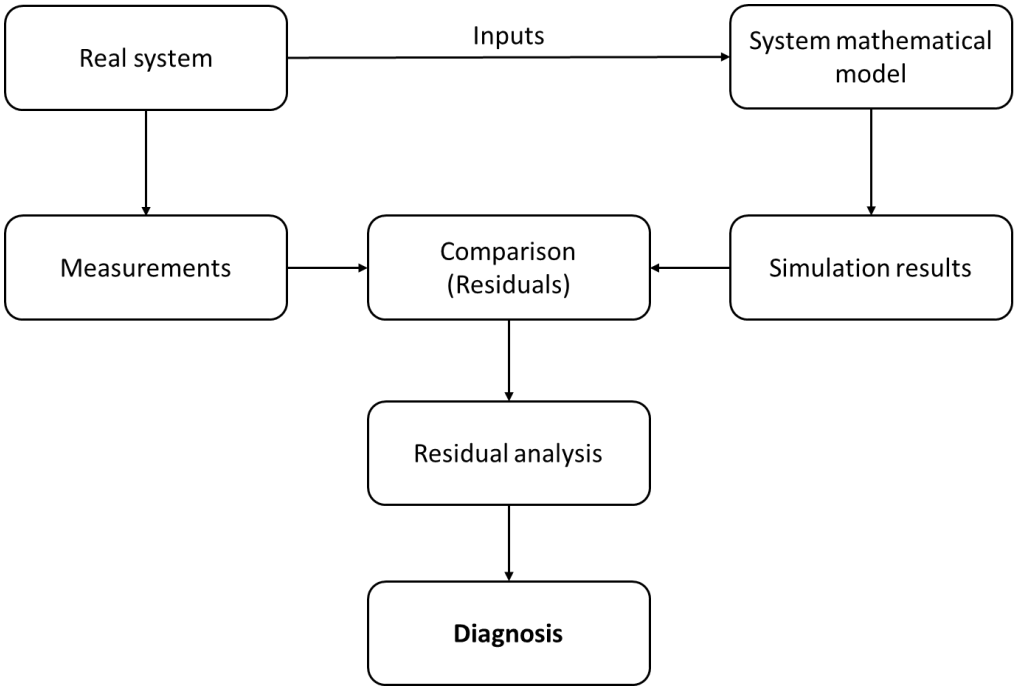

Figure 2-4: Block diagram of a model-based approach for diagnostics.

Firs of all, the development of a numerical model of the system in the flawless condition is required. Once the model is available, it is used to simulate the behavior of the system in the same operating condition of the actual system. The outputs of the model are compared with the outputs of the actual system; the difference between the model output and the actual output is called residual. The model simulates the system in the healthy condition, therefore high values of the residuals are symptoms of a deviation from the correct functioning of the system. The analysis of the residuals is performed not only to detect the presence of a fault, but also to identify which fault occurred in the system; indeed, each fault affects the values of the residuals in a different combination.

The development of a model of the system suitable for diagnostic purposes is not an easy task and in many applications data-driven methods are preferred. Medjaher [2.40] proposed the use of a model, based on bond graphs, for the diagnostics of a hydraulic circuit; the diagnosis is computed by analyzing the values of the residuals. Palazzolo [2.41] proposed the use of a physics-based model for the detection of several types of leakages in a variable displacement axial-piston pump installed on an aircraft. An interesting approach is proposed by Marcu in [2.42]; in this work, the use of a dynamic NN is used to simulate the behavior of several systems in a hydraulic looper. The dynamic NN is trained on past data and then is used online to create residuals which then are analyzed to compute the diagnosis. This last approach is an example of combination of data-driven approach and a model-based approach. It is worth noting that the scheme reported in Figure 2-4 depicts the basic concept of a model-based approach for diagnostics and that not all the model-based approaches presented in the literature adhere strictly to this scheme. The thermodynamic method proposed by Dalla Lana [2.43] for the estimation of the pump overall efficiency can be considered within the class of model-based approaches for the pump diagnostics. This thermodynamic method is derived from the first principle of thermodynamics under the hypothesis of stationary regime and adiabatic system. Dalla Lana presented the method for the case study of an external gear pump with external drainage and, for this application, only the measurements of the pressure and the temperature at the suction and the delivery ports were required for the calculation of the overall efficiency. The main advantage of this method is that it does not require the installation of expensive and bulky sensors and therefore can be applied for the online measurement of the pump efficiency. In chapter 3 of this Thesis an extension of this method to the case of hydraulic pumps with external drainage is presented along with a detailed review of the literature on the topic.

2.2 Prognostics

The objective of prognostics is the estimation of the RUL of a system or a component. The diagnostics of incipient faults can be considered as the first step of the prognostic task; the actual state of the system must be known to infer its future behavior. The basic concept of prognostics and the concept RUL are illustrated in Figure 2-5.

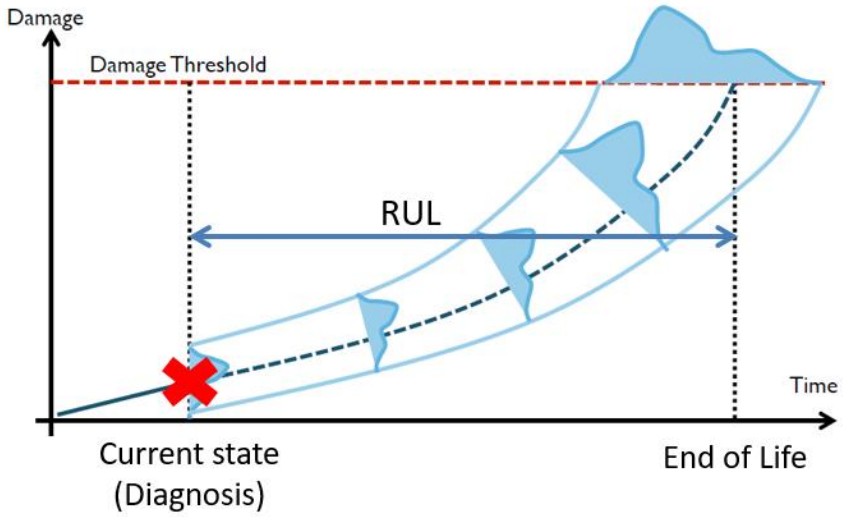

Figure 2-5: Presentation of the concept of prognostics and Remaining Useful Life (RUL).

The current state of the system, i.e. the diagnosis, can be computed through the measurement of the current output of the system. To compute the prognosis the evolution in the future of the fault or degradation must be foreseen. When the fault evolution reaches a threshold beyond which the system functioning is not acceptable, the system is at end of life and the RUL is defined as the difference between the end of life and the current instant. The prognostics of mechanical systems is a difficult task because most of the degradation processes are difficult to foresee. The estimation of the RUL is always computed with some uncertainty as indicated by the probability distributions drawn in the schematic of Figure 2-5.

Also in the field of prognostics, the approaches can be divided in two main classes: model-based and data-driven. The model-based approaches require a model of the degradation mechanism which is used to make an estimate of the RUL. The development of models able to predict the evolution of the degradation processes, such as wear, is a complex task. An example of crack growth model for the prognostics of structural damages is proposed in [2.44]. In most cases, data-driven approaches are preferred and the RUL is computed based on past data relative

to the evolution of the fault. Data driven approaches require data until the end of life of the system; these data can be obtained by monitoring the operations of systems on field or with dedicated "run to failure" experiments. A detailed review of the methodologies presented for the prognostics is reported in [2.1]. The statistical approach of the Hidden Markov Model (HMM) is used to compute the prognosis of many mechanical systems, such as pumps [2.45, 2.46], bearings [2.10] and machining processes [2.47]. An example of use of a dynamic NN architecture is presented in [2.29] for the prognostics of ball bearings. In chapter 5 of this Thesis, an approached based on a NN, trained with the Levenberg-Marquardt algorithm, is proposed for the case study of the truck loading crane.

List of references

2.1. J. Lee, F. Wu, W. Zhao, M. Ghaffari, L. liao, D. Siegel, Prognostics and health management design for rotary machinery systems – Reviews, methodology and applications, Mechanical Systems and Signal Processing, 42 (2014) 314–334.

2.2. P. A. Higgs, R. Parkin, M. Jackson, A. Al-Habaibeh, F. Zorriassatine, J. Coy, A survey on condition monitoring systems in industry, Proceedings of 7th Biennial ASME Conference Engineering Systems Design and Analysis, July 19-22, 2004 Manchester, UK.

2.3. P. Tchakoua, R. Wamkeue, M. Ouhrouche, F. Slaoui-Hasnaoui, T. A. Tameghe, G. Ekemb, Wind Turbine Condition Monitoring: State-of-the-Art Review, New Trends, and Future Challenges Energies 2014, 7, 2595-2630.

2.4. W. Du, C. Yang, A. Li, L. Wang, Wavelet leaders based vibration signals multifractal features of plunger pump in truck crane, Advances in Mechanical Engineering Vol. 2013, Article ID 676404, 11 pages.

2.5. J. Wang, H. Hu, Vibration-based fault diagnosis of pump using fuzzy technique, Measurement, 39 (2006), 176–185.

2.6. J. Cernetic, The use of noise and vibration signals for detecting cavitation in kinetic pumps, Proc. IMechE Vol. 223 Part C: J. Mechanical Engineering Science, pp. 1645-1655.

2.7. M. R. Hodkiewicz, M. P. Norton, The effect of change in _ow rate on the vibration of double-suction centrifugal pumps, Proc Instn Mech Engrs Vol 216 Part E: J Process Mechanical Engineering, pp. 47-58.

2.8. J. K. Sinha, A. R. Rao, Vibration Based Diagnosis of a Centrifugal Pump, Structural Health Monitoring, Vol. 5(4): 0325–8.

2.9. N.R. Sakthivel, V. Sugumaran, S. Babudevasenapati, Vibration based fault diagnosis of monoblock centrifugal pump using decision tree, Expert Systems with Applications 37 (2010) 4040–4049.

2.10. J. Yu, Machine health prognostics using the Bayesian-inference-based probabilistic indication and high-order particle filtering framework, Journal of Sound and Vibration, 358 (2015), 97–110.

2.11. Z. Fan, H. Li, A hybrid approach for fault diagnosis of planetary bearings using an internal vibration sensor, Measurement 64 (2015) 71–80.

2.12. G. D. Neill, R. L. Reuben, P. M. Sandford, E. R. Brown, J. A. Steel, Detection of incipient cavitation in pumps using acoustic emission, Proceedings of the Institution of Mechanical Engineers, Vol. 211 Part E, pp. 267-277.

2.13. L. Alfayez, D. Mba, Detection of incipient cavitation and determination of the best efficiency point for centrifugal pumps using acoustic emission, Proc. IMechE Vol. 219 Part E: J. Process Mechanical Engineering, pp. 327-344.

2.14. Y. Gao, Q. Zhang, A Wavelet Packet and Residual Analysis Based Method for Hydraulic Pump Health Diagnosis, Proceedings of the Institution of Mechanical Engineers, Part D: Journal of Automobile Engineering, Vol. 220 (2006), issue 6, pp: 735-745.

2.15. Y. Gao, Q. Zhang, X. Kong, Wavelet-based pressure analysis for hydraulic pump health diagnosis, Transaction of the ASAE, Vol. 46(4) (2003), pp. 969-976.

2.16. C. Lu, S. Wang, C. Zhang, Fault diagnosis of hydraulic piston pumps based on a two-step MD method and fuzzy C-means clustering, Proc IMechE Part C: J Mechanical Engineering Science 2016, Vol. 230(16) 2913–2928.

2.17. J. Du, S. Wang, H. Zhang, Layered clustering multi-fault diagnosis for hydraulic piston pump, Mechanical Systems and Signal Processing 36 (2013) 487–504.

2.18. Y. Gao, X. Kong, Q. Zhang, Wavelet approach for performance monitoring and diagnosis of a hydraulic pump, Proceedings of the 6th JFPS International Symposium on Fluid Power, TSUKUBA 2005, November 7-10, 2005.

2.19. J. Wang, A Rough Set Approach of Mechanical Fault Diagnosis for Five-Plunger Pump, Advances in Mechanical Engineering Volume 2013, Article ID 174987, 11 pages.

2.20. T. Kaewkongka, Y. H. Joe Au, R. Rakowski, B. E. Jones, Continuous wavelet transform and neural network for condition monitoring of rotodynamic machinery, IEEE Instrumentation and Measurement Technology Conference, Budapest, Hungary, May 21-23, 2001.

2.21. F. Kong, R. Chen, A combined method for triplex pump fault diagnosis based on wavelet transform, fuzzy logic and neuro-networks, Mechanical Systems and Signal Processing 18 (2004) 161–168.

2.22. Z. K. Peng, F.L. Chu, Application of the wavelet transform in machine condition monitoring and fault diagnostics: a review with bibliography, Mechanical Systems and Signal Processing 18 (2004) 199–221.

2.23. J. Antoni, Cyclostationary by examples, Mechanical Systems and Signal Processing 2009; 23: 987–1036.

2.24. M. Paliwal, U.A. Kumar, Neural networks and statistical techniques: A review of applications, Expert Systems with Applications 36 (2009) 2–17.

2.25. A. El-Betar, M. Abdelhamed, A. El-Assal, R. Abdelsatar, Fault Diagnosis of a Hydraulic Power System Using an Artificial Neural Network, JKAU: Eng. Sci., Vol. 17 (2006), No. 1, pp: 117 – 137.

2.26. J. Backas, K. Huhtala, Modelling the efficiencies of hydraulic pumps with neural networks, The Twelfth Scandinavian International Conference on Fluid Power, May 18-20, 2011, Tampere, Finland.

2.27. M. A. Herzog, T. Marwala, P. S. Heyns, Machine and component residual life estimation through the application of neural networks, Reliability Engineering and System Safety 94 (2009) 479– 489.

2.28. R. Huang, L. Xi, X. Li, C. R. Liu, H. Qiu, J. Lee, Residual life predictions for ball bearings based on self-organizing map and back propagation neural network methods, Mechanical Systems and Signal Processing 21 (2007) 193–207.

2.29. P. Wang, G. Vachtsevanos, Fault Prognosis Using Dynamic Wavelet Neural Networks, AAAI Technical Report SS-99-04.

2.30. X. Wu, J. Ghaboussi, J. H. Garrett, Use of neural networks in detection of structural damage, Computer & Structures, Vol. 42, No. 4, pp. 649-659, 1992.

2.31. W. Yousheng, S. Qiao, P. Xufeng, L. Xiaolei, The Application of Wavelet Transform and Artificial Xeural Networks in Machinery Fault Diagnosis, Proceedings of Third International Conference on Signal Processing (ICSP 96), Beijing, China, 18-18 Oct. 1996.

2.32. T. Torikka, Evaluation of Analysis Methods for Fault Diagnosis on axial-piston pumps, The Twelfth Scandinavian International Conference on Fluid Power, May 18-20, 2011, Tampere, Finland.

2.33. V. Muralidharan, V. Sugumaran, V. Indira, Fault diagnosis of monoblock centrifugal pump using SVM, Engineering Science and Technology, an International Journal 17 (2014), pp. 152-.157.

2.34. G. Bartram, S. Mahadevan, Integration of heterogeneous information in SHM models, Structural Control and Health Monitoring 2014; 21: 403-422.

2.35. A. Azadeh, V. Ebrahimipour, P. Bavar, A fuzzy inference system for pump failure diagnosis to improve maintenance process: The case of a petrochemical industry, Expert Systems with Applications, 37 (2010), 627–639.

2.36. M. M. Gupta and D. H. Rao, On the principle of fuzzy neural networks, Fuzzy Sets and Systems 61 (1994), pp. 1-18.

2.37. N. Helwig, E. Pignanelli, A. Schütze, Condition Monitoring of a Complex Hydraulic System using Multivariate Statistics, Instrumentation and Measurement Technology Conference (I2MTC), May 11-14, 2015, Pisa, Italy.

2.38. N. Helwig, E. Pignanelli, A. Schütze, Detecting and compensating sensor faults in a hydraulic condition monitoring system, AMA Conferences 2015 – SENSOR 2015 and IRS 2015, Nuremberg, Germany.

2.39. N. Helwig, A. Schütze, Data-based condition monitoring of a fluid power system with varying oil parameters, 10th International Fluid Power Conference, Dresden, Germany, 2016.

2.40. K. Medjaher, N. Zerhouni, Residual-based failure prognostic in dynamic systems, Proceedings of the 7th IFAC Symposium on Fault Detection, Supervision and Safety of Technical Processes Barcelona, Spain, June 30 - July 3, 2009.

2.41. J. J. Palazzolo, L. D. Scheuemann, J. R. Hartin, Leakage Fault Detection Method for Axial-Piston Variable Displacement Pumps, Aerospace Conference, 2008 IEEE, 1-8 March 2008, Big Sky, MT, USA.

2.42. T. Marcu, B. Köppen-Seliger, R. Stücher, Design of fault detection for a hydraulic looper using dynamic neural networks, Control Engineering Practice 16 (2008) 192–213.

2.43. E. Dalla Lana, V. J. De Negri, A New Evaluation Method for Hydraulic Gear Pump Efficiency through Temperature Measurements, SAE 2006 Commercial Vehicle Engineering Congress & Exhibition, Rosemont, Chicago, United States, 2006. DOI 10.4271/2006-01-3503.

2.44. K. S. Yen, M. M. Ratnam, 2-D crack growth measurement using circular grating moiré fringes and pattern matching, Structural Control and Health Monitoring, 2011; 18: 404-415.

2.45. M. Dong, D. He, A segmental hidden semi-Markov model (HSMM)-based diagnostics and prognostics framework and methodology, Mechanical Systems and Signal Processing 21 (2007) 2248–2266.

2.46. Y. Peng, M. Dong, A prognosis method using age-dependent hidden semi-Markov model for equipment health prediction, Mechanical Systems and Signal Processing 25 (2011) 237–252.

2.47. P. Baruah, R. B. Chinnam, HMMs for diagnostics and prognostics in machining processes, International Journal of Production Research, Vol. 43, No. 6, 15 March 2005, 1275–1293.

Chapter 3 - Thermodynamic Method

This chapter presents a method for the calculation of the overall efficiency of hydraulic machines with external drainage based on the first principle of thermodynamics. This method extends an existing method for machines without external drainage and is a valuable tool for the online monitoring of the machine overall efficiency.

The mathematical formulation of the method is derived from the first principle of thermodynamics. Some hypotheses are considered to simplify the energy balance equation and obtain an exploitable expression for the overall efficiency. This method requires the measurement of the temperatures at the machine hydraulic ports and is strongly affected by the uncertainty on these measurements. The combined uncertainty of the overall efficiency is studied in detail considering the approach suggested by the standards and an extension to the second-order approximation.

The case study of a variable displacement axial-piston pump with external drainage is considered. An experimental campaign was carried out to validate the proposed approach with reference to the standard approach, based on the direct measurement of the mechanical power. The thermodynamic method resulted statistically equivalent to the standard approach, but showed some limits in transient operations. A series of experiments in faulty conditions was carried out and the proposed methodology demonstrated the capability to detect some of the most common incipient faults. The measurement of the drainage and the delivery flow rates is a limit of the proposed methodology which could prevent its usage in online applications; therefore, some solutions to estimate these flow rates without the usage of expensive and bulky sensors are presented and their limitations are discussed.

3.1 Past Efforts

The application of a thermodynamic approach for the evaluation of the performance of hydraulic machines started at the beginning of the 20th century. The thermodynamic method was proposed for the first time by Poirson [3.1] for the calculation of the efficiency and the internal losses in hydraulic turbines. Several developments of the methodology followed in the 20th century and nowadays the thermodynamic approach is cited in several standards dealing with the calculation of the performance of hydraulic machines [3.2, 3.3]. The literature in this field is not rich and most of the applications of the method are related to the online measurements of the performance of hydraulic machines in power plants [3.4, 3.5]. Indeed, the machines used in power plants for the conversion between hydraulic and mechanical energy have a considerable size (order of magnitude of MW) and the measurement of their efficiency through the standard approach, which requires the measurement of the shaft torque and the flow rate, is not feasible. However, in those applications, a small variation in the machine efficiency corresponds to a significant energy loss, therefore, the thermodynamic approach emerged for the online calculation of the overall efficiency. The thermodynamic method can also be applied to estimate the delivery flow rate if the mechanical input power is known (for example from the measurement of the electric power of the electric motor/generator), some applications can be found in [3.4, 3.6].

In the literature exists also few applications of the method in the field of oil hydraulic machines. A precursory work was presented by Dalla Lana [3.7] who presented the mathematical formulation and applied the method on an external gear pump without external drainage; a good match with the standard approach was obtained, in particular at high values of the delivery pressure. Another application of the thermodynamic method was presented by Kjølle [3.8] for the calculation of the overall efficiency of a hydrostatic transmission with un uncertainty comparable to the standard approach. Andersson [3.9] applied a similar approach for the calculation of the oil temperature in the hydraulic circuit installed on an aircraft.

A crux point in the application of the thermodynamic method is the measurement uncertainty and several works dealt with this problem [3.6, 3.10, 3.11]. The combined uncertainty is mainly affected by the uncertainty on the measurement of the temperature difference between the outlet and the inlet ports. Indeed, this temperature difference is about few K (for the hydraulic pump under study the temperature difference is in the range 0-6 K) and the overall efficiency is very sensitive to any variation of this difference. The uncertainty increases when the operating pressure decreases since the temperature difference decreases and the uncertainty on the temperature

difference approaches the measurement value itself. In the case of hydraulic turbines and storage pumps, the current standards [3.2, 3.3] suggest the use of the thermodynamic method only for machine head above 100 m. Nevertheless, some works applied the thermodynamic method for low head machines and obtained acceptable results [3.12, 3.13]

In this Thesis, the author proposes an extension of the thermodynamic method for hydraulic pumps and motors with external drainage; the case study of a variable displacement axial-piston pump is considered [3.14].

3.2 The Proposed Thermodynamic Approach

3.2.1 Standard Approach

The overall efficiency η_t of a positive displacement machine is defined as the ratio of the hydraulic power P_h and the total mechanical power P_m:

$$\eta_t = \frac{P_h}{P_m} \tag{3.1}$$

The total mechanical power P_m is the power provided to the system through the shaft and can be calculated with Eq. 3.2:

$$P_m = \tau \cdot \omega \tag{3.2}$$

Where τ is the shaft torque and ω is the shaft angular velocity. The hydraulic power P_h is the mechanical power transferred to the fluid. Since for positive displacement pumps, the increment of the fluid potential energy and kinetic energy is negligible, the hydraulic power P_h can be calculated with Eq. 3.3 [3.15]:

$$P_h = \dot{V}_2 \cdot p_2 - \dot{V}_1^* \cdot p_1 \tag{3.3}$$

Where p_1 and p_2 are the relative pressures at the suction and delivery ports, while $\dot{V}_1^*$ and $\dot{V}_2$ are the suction and delivery volumetric flow rates. The suction volumetric flow rate $\dot{V}_1^*$ is not measured directly, but it is calculated starting from the delivery flow rate $\dot{V}_2$ with Eq. 3.4 [3.15]:

$$\dot{V}_1^* = \dot{V}_2 \left[1 + \left(\frac{p_2 - p_1}{K}\right) - \beta(T_2 - T_1)\right] \quad 3.4$$

Where K is the secant bulk modulus and β is the volumetric thermal expansion coefficient. Equation 3.4 requires the measurement of the suction and the delivery fluid temperatures T_1 and T_2. In most cases, the suction pressure p_1 is close to 0 (relative value), therefore, Eq. 3.3 can be simplified to Eq. 3.5 introducing a negligible error:

$$P_h = \dot{V}_2 \cdot \Delta p_{21} \quad 3.5$$

Where Δp_{21} is the pressure difference between the delivery and the suction ports. The *standard approach* for the evaluation of the overall efficiency η_t is based on Eq. 3.1, 3.2 and 3.5 and it requires the measurement of the following variables: shaft torque τ, shaft angular velocity ω, suction pressure p_1, delivery pressure p_2 and delivery flow rate $\dot{V}_2$. This approach is used in laboratories for the evaluation of the overall efficiency with very high accuracy. However, the measurement of the shaft torque and the delivery flow rate requires the use of very expensive and bulky instruments, therefore, the standard approach is not suitable for the online measurement of the overall efficiency.

3.2.2 From the First Principle of Thermodynamics

The thermodynamic approach presented in this Thesis offers an alternative way for the estimation of the total mechanical power P_m. The approach is derived from the first principle of thermodynamics, thereby the name *thermodynamic approach*. For the application of the first principle to the hydraulic pump, the boundaries of the system need to be defined first. The boundaries of the system coincide with the pump external surfaces and the hydraulic ports (suction, delivery and drainage). Through the external surfaces the pump exchanges heat ($\dot{Q}$) with the environment by conduction, convection and radiation. A particular boundary is the shaft interface through which the mechanical power $\dot{W}$, required for pressurizing the fluid, enters the system. The hydraulic ports are permeable interfaces where both energy and mass exchanges occur. Figure 3-1 represents the energy and the mass fluxes for the case of the considered hydraulic pump with external drainage.

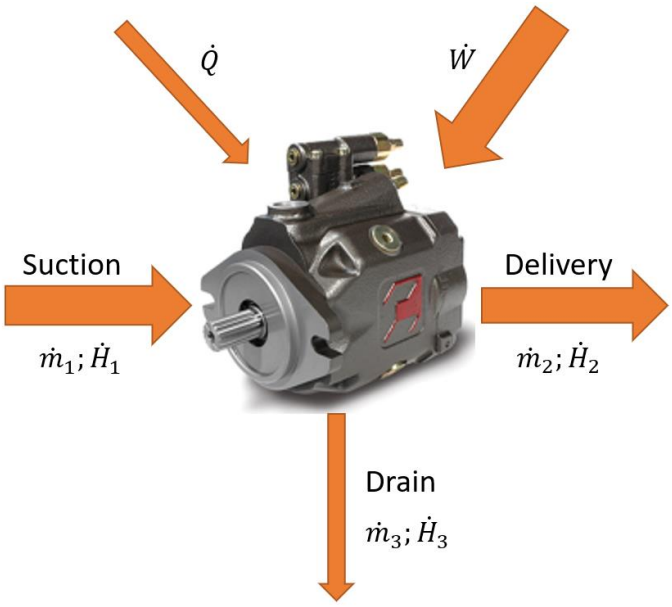

Figure 3-1: Energy and mass fluxes for the hydraulic pump.

The energy balance resulting from the application of the first principle is reported in Eq. 3.6:

$$\dot{Q} + \dot{W} = \dot{H}_2 + \dot{H}_3 - \dot{H}_1 + \dot{E} \qquad 3.6$$

The convection adopted in this Thesis is that the heat flux $\dot{Q}$ and the mechanical work $\dot{W}$ are positive when they enter the system and negative when the exit the system. $\dot{H}$ indicates the enthalpy flux and the subscripts 1, 2 and 3 stand for suction port, delivery port and drainage port respectively. The term $\dot{E}$ represents the time derivative of the system internal energy. The mechanical work $\dot{W}$ has the same physical meaning of the total mechanical power P_m defined by Eq. 3.2:

$$\dot{W} = P_m \qquad 3.7$$

3.2.3 Hypotheses of the Thermodynamic Approach

Some hypotheses are considered to simplify Eq. 3.6 and find an alternative formulation for the mechanical power P_m. The hypothesis of stationary regime is considered; therefore, the pump angular velocity, the pump displacement, the delivery pressure and the inlet fluid temperature are kept constant over time. Under the hypothesis of stationary regime, the time derivative of the

pump internal energy $\dot{E}$ is zero. Another hypothesis is relative to the heat flux $\dot{Q}$ which the pump exchanges with the environment. The pump exchanges heat by convection and radiation through the external surfaces; furthermore, heat exchange by conduction takes place at the hydraulic end (through the pipes and hoses) and at the mechanical end (through the shaft and at the mounting interface). The magnitude of these contributions is difficult to estimate and depends on the pump operating conditions and on many external factors which are related to the installation condition. The sign itself of these contributions depends on the installation condition, even if, in most cases, the heat flows from the pump to the environment. In this Thesis, the term $\dot{Q}$ relative to the heat exchange is considered equal to 0 in order to obtain a fairly simple formula for the estimation of the pump overall efficiency. With the introduction of these two hypotheses, i.e. stationary regime and adiabatic system, Eq. 3.6 reduces to Eq. 3.8:

$$\dot{W} = \dot{H}_2 + \dot{H}_3 - \dot{H}_1 \qquad 3.8$$

This equation states that the mechanical power $\dot{W}$ entering the system through the shaft is entirely transferred to the fluid.

In this paragraph, an estimation of the heat exchange by convection and radiation is given so as to demonstrate that the hypothesis of adiabatic system is acceptable. In this calculation, the geometry of the pump is simplified, and it is considered as a cylinder of approximately the same length and diameter. The temperature of the pump case T_p was assumed 100 °C and the temperature of the environment T_a was assumed 20 °C; the former temperature was assumed relatively high to compute an upper-bound estimate of the heat exchange. It must be noted that T_a can vary in a wide range depending on the installation conditions. The heat exchange by convection was calculated considering free convection; the Nusselt number Nu_D was calculated with Eq. 3.9 [3.16]:

$$Nu_D = \left\{0.60 + \frac{0.387{Ra_D}^{1/6}}{[1 + (0.559/Pr)^{9/16}]^{8/27}}\right\}^2 \qquad 3.9$$

Where Pr is the Prandtl number and Ra_D the Rayleigh number referred to the cylinder diameter; these two dimensionless numbers were calculated considering the air properties at the mean temperature. The resulting heat exchange by free convection is around 100 W; as stated above, this must be considered as the upper-bound estimate of the heat exchange, since favorable conditions were considered. An estimate of the heat exchange by radiation was performed

considering the same temperatures and the same geometrical approximation. The pump was considered as a black body and the heat exchange by radiation $\dot{Q}_r$ was calculated with Eq. 3.10:

$$\dot{Q}_r = A\sigma\left({T_p}^4 - {T_a}^4\right) \qquad 3.10$$

Where A is the area of the pump external surface and σ is the Stefan-Boltzmann constant. The result of this calculation was around 150 W. Summing up the two calculated contributions, the upper-bound estimate of the heat exchange is around 250 W. This value is negligible if compared to the mechanical power required by the considered pump at the design operating point (angular velocity 2200 r/min, full displacement 84 cm^3 and delivery pressure 250 bar), which is around 80000 W; therefore, at this operating condition the hypothesis of adiabatic system is absolutely acceptable. When the pump is operated at different operating conditions with a lower power requirement, the heat exchange, which depends only on the temperatures T_p and T_a, becomes relatively more important. In conclusion, the hypothesis of adiabatic system is acceptable in most of the operating conditions and leads to significant errors only for those operating conditions corresponding to a low power requirement.

3.2.4 An Alternative Formula for the Overall Efficiency

In this paragraph, Eq. 3.8 is manipulated to obtain a new formulation for the pump overall efficiency. The enthalpy flux $\dot{H}$ can be expressed in terms of specific enthalpy h and mass flow rate $\dot{m}$:

$$\dot{W} = \dot{m}_2 \cdot h_2 + \dot{m}_3 \cdot h_3 - \dot{m}_1 \cdot h_1 \qquad 3.11$$

Under the hypothesis of stationary regime, the conservation of mass requires that inlet mass flow rate equals the outlet mass flow rate as reported in Eq. 3.12. Considering the differential enthalpy between delivery and suction and drainage and suction, Eq. 3.13 is obtained:

$$\dot{m}_1 = \dot{m}_2 + \dot{m}_3 \qquad 3.12$$

$$\dot{W} = \dot{m}_2 \cdot (h_2 - h_1) + \dot{m}_3 \cdot (h_3 - h_1) \qquad 3.13$$

The specific enthalpy of the fluid is a function of the temperature and the pressure, Eq. 3.14, and therefore its differential can be expressed as reported in Eq. 3.15:

$$h = h(T, p) \tag{3.14}$$

$$dh = \frac{\partial h}{\partial T}\Big|_p dT + \frac{\partial h}{\partial p}\Big|_T dp \tag{3.15}$$

The temperature derivative of the specific enthalpy at constant pressure is the specific heat coefficient at constant pressure c_p:

$$\frac{\partial h}{\partial T}\Big|_p = c_p \tag{3.16}$$

The pressure derivative of the specific enthalpy at constant temperature is called *isothermal factor* and it is indicated with the letter a in the literature and in the standards. The expression of the isothermal factor reported in Eq. 3.17 is derived from the Maxwell's thermodynamic relation for the pressure derivative of the specific entropy at constant temperature and the definition of the volumetric thermal expansion coefficient β [3.17]:

$$\frac{\partial h}{\partial p}\Big|_T = a = (1 - \beta T)v \tag{3.17}$$

Where v is the fluid specific volume. By substituting Eq. 3.16 and Eq. 3.17 in Eq. 3.15, the differential of the specific enthalpy can be expressed by Eq. 3.18:

$$dh = c_p dT + a dp \tag{3.18}$$

This equation can be integrated to calculate the specific enthalpy differences between the delivery and the suction states and between the drainage and the suction states. If the mean value of c_p and a are considered for the integration, Eq. 3.13 becomes Eq. 3.19:

$$\dot{W} = \dot{m}_2 \left[\bar{c_p}_{21} \Delta T_{21} + \bar{a}_{21} \Delta p_{21}\right] + \dot{m}_3 \left[\bar{c_p}_{31} \Delta T_{31} + \bar{a}_{31} \Delta p_{31}\right] \tag{3.19}$$

Considering the results reported in Eq. 3.1, 3.5 and 3.7, the overall efficiency η_t is given by Eq. 3.20:

$$\eta_t = \frac{\dot{V}_2 \cdot \Delta p_{21}}{\dot{W}} \tag{3.20}$$

By substituting the mechanical power $\dot{W}$ expressed by Eq. 3.19 in Eq. 3.20, the expression for the reciprocal of the overall efficiency given by Eq. 3.21 is obtained:

$$\frac{1}{\eta_t} = \frac{\dot{W}}{\dot{V}_2 \Delta p_{21}} = \frac{\rho_2 \bar{c}_{p_{21}} \Delta T_{21}}{\Delta p_{21}} + \rho_2 \bar{a}_{21} + \frac{\dot{V}_3}{\dot{V}_2} \frac{\rho_3}{\Delta p_{21}} \left(\bar{c}_{p_{31}} \Delta T_{31} + \bar{a}_{31} \Delta p_{31} \right) \tag{3.21}$$

Equation 3.21 offers an alternative way for the calculation of the overall efficiency η_t which is valid under the considered hypotheses of stationary regime and adiabatic system. If only the first two terms of the formula are considered, this formula reduces to the one which can be found in the literature for pump without external drainage [3.7]; therefore, the last term accounts for the external drainage.

The proposed thermodynamic approach for the calculation of the pump overall efficiency, based on Eq. 3.21, requires the measurements of the pressures and the temperatures at the suction, the delivery and the drainage ports. Pressures and temperatures can be measured in an online application since the required sensors are easy to install and relatively cheap. In contrast to the standard approach, this method does not require the measurement of the shaft torque and the pump speed, but in the third term of Eq. 3.21, the ratio between the drainage flow rate $\dot{V}_3$ and the delivery flow rate $\dot{V}_2$ appears. This is a crux point because the installation of flowmeters is not feasible in an online application due to their cost and their size; this problem does not exist for pumps without external drainage because $\dot{V}_3 = 0$ and the third term disappears. In order to use this approach for online applications even for pumps with external drainage, a solution to deal with this flow rates ratio needs to be found. In this activity, the proposed thermodynamic method was first validated with test bench experiments using flowmeters for the evaluation of $\dot{V}_2$ and $\dot{V}_3$; then some solutions were proposed to estimate the ratio between $\dot{V}_3$ and $\dot{V}_2$ without the use of flowmeters.

3.2.5 Fluid Model

The application of the proposed thermodynamic approach requires the availability of a detailed model of the fluid for the estimation of the fluid properties which appear in Eq. 3.21. The fluid properties that need to be known are: the specific heat at constant pressure c_p, the density ρ and the volumetric thermal expansion coefficient β. The fluid considered in this activity is the oil VG 46, a mineral oil typically used in hydraulic applications. Experimental data of the fluid properties

were provided by the manufacturer; these data were interpolated to derive formulae of the fluid properties as a function of the temperature T [°C] and the relative pressure p [bar].

The specific heat at constant pressure c_p depends linearly on the temperature and is calculated through Eq. 3.22:

$$c_p = 1790.05 + 4.47324 \cdot T \left[\frac{J}{kg \cdot °C}\right] \quad 3.22$$

The fluid density ρ can be expressed in function of the fluid density ρ_0, i.e. the fluid density at the same temperature, but at the reference relative pressure p_0 (0 bar):

$$\rho = \rho_0[1 + (p - p_0)/K] \left[\frac{kg}{m^3}\right] \quad 3.23$$

In this equation, K stands for the secant bulk modulus which accounts for the variation of the fluid volume due to a variation of the pressure p. The density at reference pressure ρ_0 depends only on the temperature as reported in Eq. 3.24:

$$\rho_0 = 879.9 - 0.66 \cdot T \left[\frac{kg}{m^3}\right] \quad 3.24$$

The secant bulk modulus K is a function of the temperature and the pressure; the polynomial expression of Eq. 3.25 was derived from the experimental data:

$$K = 0.0000003 \cdot T^4 - 0.0004 \cdot T^3 + 0.2479 \cdot T^2 + \\ -94.51 \cdot T + 17857 + 5.6 \cdot p\ [bar] \quad 3.25$$

The specific volume v is simply the reciprocal of the density and can be calculated with Eq. 3.26:

$$v = \frac{1}{\rho} \left[\frac{m^3}{kg}\right] \quad 3.26$$

Once the other fluid properties are known, the volumetric thermal expansion coefficient β can be calculated through its definition reported in Eq. 3.27:

$$\beta = \rho_{(p,T)} \left(\frac{\partial v}{\partial T}\right)_p \left[\frac{1}{K}\right] \quad 3.27$$

With the knowledge of the fluid properties given by Eq. 3.22 - 3.27, the enthalpy-entropy diagram of the fluid can be calculated. The differential of the enthalpy is reported in Eq. 3.18, while the differential of the entropy can be calculated with Eq. 3.28:

$$ds = \frac{c_p}{T} \cdot dT - \beta v \cdot dp \qquad 3.28$$

A portion of the enthalpy-entropy diagram is reported in Figure 3-2; some isobaric curves and some isothermal curves are also drawn on the plot.

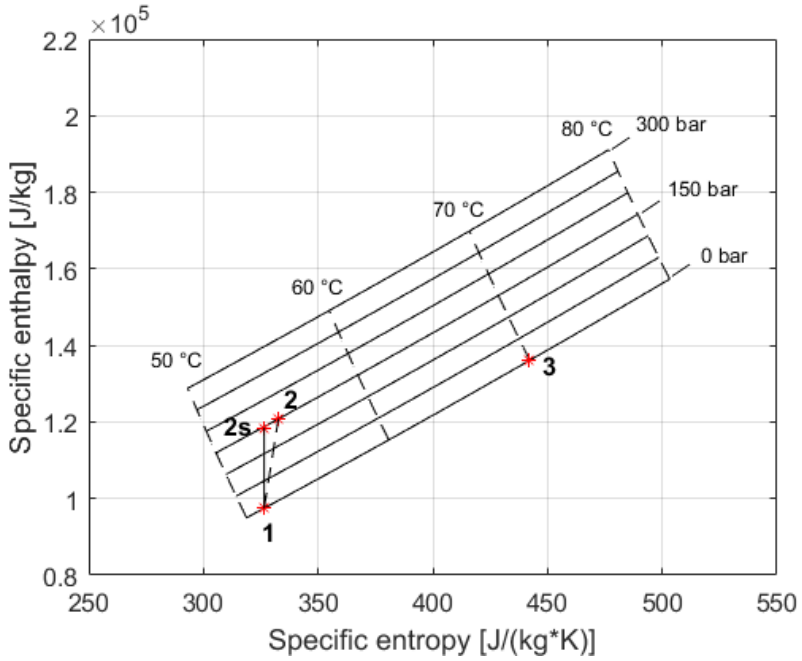

Figure 3-2: A portion of the enthalpy-entropy diagram for the mineral oil VG 46; the figure reports the fluid states (1 suction, 2 delivery and 3 drainage) for an example case (angular velocity 2000 r/min, displacement 51 cm^3 and delivery pressure 150 bar).

The markers of Figure 3-2 indicate the fluid states at the different ports for an example case where the pump was operated at 2000 r/min, with displacement 51 cm^3 and delivery pressure 150 bar. The state 2s corresponds to the final state of the ideal isentropic compression from the suction state 1 to the pressure of the delivery state 2; as expected, the entropy of state 2 is greater than state 2s. It is interesting noting that the enthalpy of state 3 (drainage) is greater than the enthalpy of state 2. The drainage flow is due to leakages which theoretically undergo a lamination from the delivery state and therefore h_3 should be equal to h_2. In the considered case $h_3 > h_2$ and this

means that a heat flow due to the pump internal friction is transferred to the drainage flow in the pump case.

3.3 Uncertainty Evaluation

A well-known problem related to the application of the thermodynamic approach for the evaluation of the machine efficiency is the measurement uncertainty [3.6, 3.10, 3.11]. The uncertainty on the temperature measurements is the most critical due to the small temperature difference among the different ports of the hydraulic pump. Therefore, the measurement uncertainty must be properly calculated and the sensors must be selected in order to maintain the uncertainty at acceptable levels.

3.3.1 First-Order Standard Uncertainty

The measurement of the overall pump efficiency η_t is an indirect measurement. Indeed, the overall efficiency is calculated through Eq. 3.21 and depends on the value of other variables which need to be measured. In the general case, the output value y of a variable Y that is measured indirectly, is calculated through an equation of the type of Eq. 3.29, i.e. its value is function of the value of input variables X_1, X_2, X_3 ... X_n that are measured directly:

$$Y = f(X_1, X_2, X_3 \dots X_n) \qquad 3.29$$

Where $x_1, x_2, x_3 \dots x_n$ are the measured values of the input variables. The uncertainty of the output variable has to be calculated by propagating the uncertainties on the measurements of the input variables; the standard uncertainty of the output variable is a combination of the standard uncertainties of the input variables and is referred to as *combined uncertainty* u_c. The GUM standard [3.18] proposes an expression for the combined uncertainty which is based on a first-order series expansion of the function *f*. Therefore, the output variable is considered linearly dependent on each of the input variable and the combined standard uncertainty $u_{cI}(y)$ (where the subscript I stands for the first-order approximation) can be calculated from the standard uncertainties of the input variables $u(x_i)$ with Eq. 3.30:

$$u_{cI}^2(y) = \sum_{i=1}^{n} \left(\frac{\partial f}{\partial X_i}\right)^2 u^2(x_i) \qquad 3.30$$

This formulation is valid under the hypothesis that all the input variables are independent each other. The overall efficiency is calculated through Eq. 3.21 and therefore this is the equation which links the overall efficiency to the input variables. Considering that the fluid properties are all function of the temperature and the pressure, the input variables are the temperatures and the pressures at the three hydraulic ports and the volumetric flow rates at the delivery and the drainage ports. The equivalent of Eq. 3.29 for the overall efficiency η_t is Eq. 3.31:

$$\eta_t = f(T_1, T_2, T_3, p_1, p_2, p_3, \dot{V}_2, \dot{V}_3) \qquad 3.31$$

The combined standard uncertainty $u_{\eta_t I}$ of the overall efficiency can therefore be calculated with Eq. 3.32:

$$u_{\eta_t I} = \pm \left[\left(\frac{\partial \eta_t}{\partial T_1} u_T\right)^2 + \left(\frac{\partial \eta_t}{\partial T_2} u_T\right)^2 + \left(\frac{\partial \eta_t}{\partial T_3} u_T\right)^2 + \left(\frac{\partial \eta_t}{\partial p_1} u_{p_1}\right)^2 + \left(\frac{\partial \eta_t}{\partial p_2} u_{p_2}\right)^2 + \left(\frac{\partial \eta_t}{\partial p_3} u_{p_3}\right)^2 + \left(\frac{\partial \eta_t}{\partial \dot{V}_2} u_{\dot{V}_2}\right)^2 + \left(\frac{\partial \eta_t}{\partial \dot{V}_3} u_{\dot{V}_3}\right)^2 \right]^{\frac{1}{2}} \qquad 3.32$$

3.3.2 Selection of the Sensors

The combined uncertainty expressed by Eq. 3.32 depends on eight contributions, each of them given by the derivative of the overall efficiency with respect to an input variable multiplied by the uncertainty on the measurement of the same input variable. In the first phase of the activity, the relative impact of these contributions was evaluated in order to focus on the most delicate measurements and select a proper and equilibrate set of sensors.

The estimation of the contributions requires the knowledge of all the input variables listed in Eq. 3.31. Since no experimental tests were available where all the input variables were measured (obviously because we were at the stage of selecting the sensors), the data relative to the evaluation of the overall efficiency with the standard approach were considered and the missing input variables were estimated. In the considered tests, the following input variables were directly

measured: suction temperature T_1, delivery pressure p_2 and delivery flow rate $\dot{V}_2$. The remaining five input variables were estimated based on the following hypotheses:

- The suction pressure p_1 is equal to the zero gauge pressure. The actual suction pressure could be slightly higher or lower, but this hypothesis introduces a negligible error.
- $p_3 = 1\ bar$. For the hydraulic pump under study, the actual drainage pressure assumes values around 1 bar in most of the operating conditions.
- The drainage flow rate $\dot{V}_3$ is calculated with Eq. 3.33 which requires the conservation of mass in stationary regime:

$$\dot{V}_3 = \frac{\rho_1 \cdot \dot{V}_1 - \rho_2 \cdot \dot{V}_2}{\rho_3} \tag{3.33}$$

  Where $\dot{V}_1$ is calculated with Eq. 3.34:

$$\dot{V}_1 = V_d \cdot \frac{n}{60} \tag{3.34}$$

  V_d is the pump displacement and n is the pump angular velocity [r/min].
- The drainage temperature T_3 is calculated considering an isenthalpic transformation from the delivery state (even if Figure 3-2 demonstrated that this is not exactly true):

$$h_3 = h_2 \tag{3.35}$$

- The delivery temperature T_2 is calculated with Eq. 3.36, obtained by inverting Eq. 3.21, where the overall efficiency η_t is known from the standard approach:

$$T_2 = T_1 + \frac{\Delta p_{21}}{\rho_2 \bar{c}_{p_{21}}}\left[\frac{1}{\eta_t} - \rho_2 \bar{a}_{21} - \frac{\dot{V}_3}{\dot{V}_2}\frac{\rho_3}{\Delta p_{21}}\left(\bar{c}_{p_{31}} \Delta T_{31} + \bar{a}_{31} \Delta p_{31}\right)\right] \tag{3.36}$$

This last hypothesis forces the estimate of the overall efficiency with the thermodynamic approach to be coherent with the standard approach as reported in Figure 3-3.

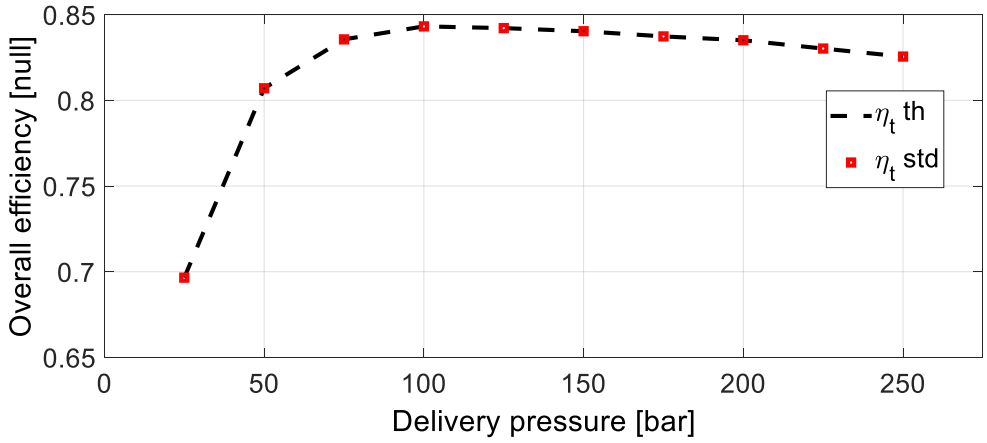

Figure 3-3: Comparison between the overall efficiency measured with the standard approach and the one estimated with the thermodynamic approach (angular velocity 1500 r/min and displacement 84 cm^3).

The percentage influence of the input variables on the combined standard uncertainty given by Eq. 3.32 was calculated for one relevant operating condition (angular velocity 1500 r/min, displacement 84 cm^3 and delivery pressure 150 bar) and the results are reported in Table 3-1. These results were obtained considering a standard uncertainty of ± 0.5 K for the temperature sensors, ± 2 bar for the pressure sensors and 1 % of the actual value for the flowmeters; these values of the uncertainties are in line with the typical values of commercial sensors. The value of the overall efficiency based on Eq. 3.21 and 3.32 is $\eta_t = 0.8404 \pm 0.0578$.

Table 3-1: Percentage influence of the input variables on the combined standard uncertainty of the overall efficiency.

T_1	T_2	T_3	p_1	p_2	p_3	$\dot{V}_2$	$\dot{V}_3$
50.08	48.96	4.031e-3	0.4931	0.4621	1.244e-4	1.702e-4	1.702e-4

The values reported in the table demonstrates that the combined uncertainty is almost completely due to the uncertainty in the measurements of the suction and the delivery temperatures. This result was expected because the temperature difference between the delivery and the suction ports ΔT_{21} is small ($\Delta T_{21} = 3.6\,K$ in the considered case) and the overall efficiency η_t is very sensitive to ΔT_{21}; therefore, the temperature sensors at the suction and at the

delivery ports must be extremely accurate. The other variables do not constitute a problem and the use of standard commercial sensors is acceptable.

The use of temperature sensors with high accuracy is particularly important at low values of the delivery pressure. Indeed, when the delivery pressure reduces, also the temperature difference ΔT_{21} reduces accordingly (see Figure 3-2 where some isothermal curves are reported on the enthalpy-entropy diagram) and reaches values lower than 1 K ($\Delta T_{21} = 1\ K$ with $p_2 = 25\ bar$). Since the uncertainty on the measure of the temperature difference ΔT_{21} depends only on the adopted sensors and is constant, the relative uncertainty on the measurement of ΔT_{21} increases and, consequently, the uncertainty on the overall efficiency increases. This trend is well represented in Figure 3-4 which reports a comparison between the uncertainty bands for two values of the temperature sensor uncertainty.

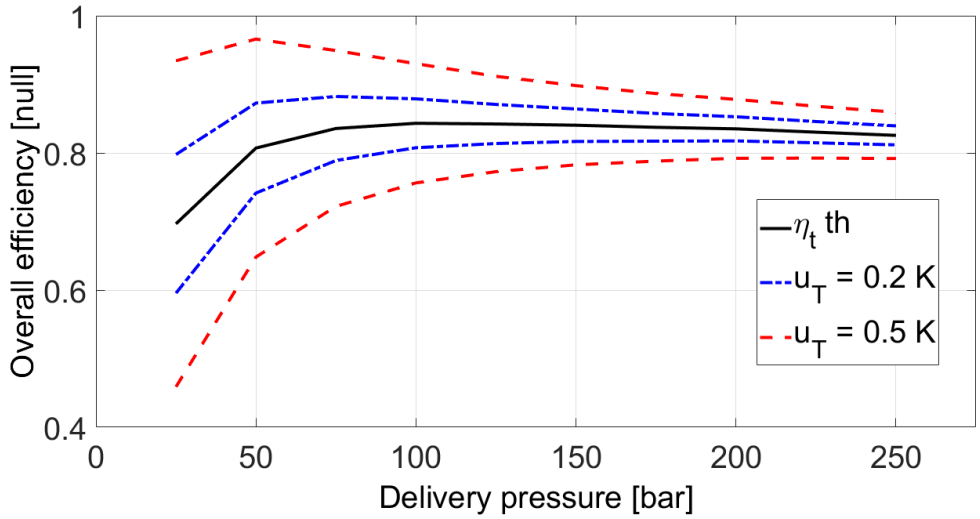

Figure 3-4: Comparison of the uncertainty bands of the overall efficiency between temperature sensors with uncertainty $u_T = \pm 0.2\ K$ and temperature sensors with uncertainty $u_T = \pm 0.5\ K$ (angular velocity 1500 r/min and displacement 84 cm^3).

The considerations reported in this paragraph guided the authors towards the choice of very high accuracy temperature sensors ($u_T = \pm 0.2\ K$) for the suction and the delivery ports. With this choice, the uncertainty on the overall efficiency is acceptable even at relatively low values of the delivery pressure.

3.3.3 Second-Order Standard Uncertainty

The approach followed by the GUM standard [3.18] for the calculation of the combined uncertainty is based on the first-order approximation as shown in § 3.3.1. This approximation considers a linear dependency between the output variable and each of the input variables. However, Eq. 3.21 is non-linear and therefore the first-order approximation could be not suitable for the application. The combined standard uncertainty was also calculated considering a second-order series expansion for the function f of Eq. 3.31. With the second-order approximation, the combined standard uncertainty $u_{cII}(y)$ (where the subscript II stands for the second-order approximation) is given by Eq. 3.37 [3.19]:

$$\begin{aligned} u_{cII}^2(y) = \sum_{i=1}^{n}\left[\left(\frac{\partial f}{\partial X_i}\right)^2 u^2(x_i) + \gamma_i\left(\frac{\partial f}{\partial X_i}\right)\left(\frac{\partial^2 f}{\partial X_i^2}\right)u^3(x_i)\right] \\ + \sum_{i=1}^{n}\left(\frac{k_i-1}{4}\right)\left(\frac{\partial^2 f}{\partial X_i^2}\right)u^4(x_i) \\ + \frac{1}{2}\sum_{i=1}^{n}\sum_{\substack{j=1 \\ j\neq i}}^{n}\left(\frac{\partial^2 f}{\partial X_i \partial X_j}\right)^2 u^2(x_i)u^2(x_j) \end{aligned} \qquad 3.37$$

In this equation γ_i is the skewness and k_i is the kurtosis of the input variable X_i. The summations consider the all set of n input variables. The skewness γ is a measure of the asymmetry of the Probability Density Function (PDF) g and it is defined from the third central moment μ_3 defined in Eq. 3.38:

$$\mu_3 = E(x-\mu)^3 = \int_{-\infty}^{+\infty}(x-\mu)^3 \cdot g(x)\,dx \qquad 3.38$$

In this equation μ represents the expected value $E(x)$ of the random variable X. The skewness γ is defined as the normalized third central moment as reported in Eq. 3.39:

$$\gamma = \frac{E(x-\mu)^3}{[E(x-\mu)^2]^{\frac{3}{2}}} = \frac{\mu_3}{\sigma^3} \qquad 3.39$$

Where σ represents standard deviation of the random variable X. The kurtosis k is a measure of the concentration of the PDF g about the expected value and is a normalized version of the fourth central moment μ_4 (Eq. 3.40) as reported in Eq. 3.41:

$$\mu_4 = E(x-\mu)^4 = \int_{-\infty}^{+\infty} (x-\mu)^4 \cdot g(x)\, dx \tag{3.40}$$

$$k = \frac{E(x-\mu)^4}{[E(x-\mu)^2]^2} = \frac{\mu_4}{\sigma^4} \tag{3.41}$$

For a normal probability distribution, the skewness is identically zero, $\gamma = 0$, because the distribution is symmetric and $k = 3$. Considering a normal distribution for all the input variables, the second-order combined uncertainty can be calculated with Eq. 3.42:

$$u_{cII}^2(y) = \sum_{i=1}^{n} \left(\frac{\partial f}{\partial X_i}\right)^2 u^2(x_i) + \frac{1}{2}\sum_{i=1}^{n} \left(\frac{\partial^2 f}{\partial X_i^2}\right) u^4(x_i) + \frac{1}{2}\sum_{i=1}^{n}\sum_{\substack{j=1 \\ j\neq i}}^{n} \left(\frac{\partial^2 f}{\partial X_i \partial X_j}\right)^2 u^2(x_i) u^2(x_j) \tag{3.42}$$

A comparison between the combined uncertainty obtained with the second-order approximation u_{cII} (Eq. 3.42) and with the first-order approximation u_{cI} (Eq. 3.32) was done so as to test if the first-order approximation is acceptable in this application. The percentage deviation between the two approximations was calculated with Eq. 3.43:

$$Deviation\ \% = \frac{u_{cI} - u_{cII}}{u_{cI}} \cdot 100\% \tag{3.43}$$

The comparison was carried out considering a set of different operating conditions and the results are reported in Table 3-2.

Table 3-2: Percentage deviation between the first-order approximation and the second-order approximation for the calculation of the combined uncertainty of the overall efficiency.

		Delivery pressure			
Displacement	**Speed**	**100 bar**	**150 bar**	**200 bar**	**250 bar**
20 cm^3	**1500 r/min**	-0.13%	-0.07%	-0.04%	-0.02%
40 cm^3	**1500 r/min**	-0.16%	-0.07%	-0.04%	-0.03%
20 cm^3	**2000 r/min**	-0.13%	-0.06%	-0.04%	-0.03%
40 cm^3	**2000 r/min**	-0.13%	-0.07%	-0.05%	-0.03%

The deviation is extremely small in all the operating conditions and therefore the first order approximation is acceptable in the considered application. In the remaining of this work, the reported combined uncertainties were always calculated with the first-order approximation.

3.4 Experimental Activity

3.4.1 Experimental Layout

The proposed thermodynamic approach for the evaluation of the overall efficiency was applied to the case study of the hydraulic pump Casappa® MVP 60-84. This pump is a variable displacement axial-piston pump, the maximum displacement is 84 cm^3 obtained with a swash plate angle of 21°. The pump was tested on the test bench for hydraulic components available at the Industrial Engineering Department of the University of Parma.

The pump was instrumented with all the sensors required for the measurement of the overall efficiency with the standard approach and the thermodynamic approach. The hydraulic schematic of the experimental layout is reported in Figure 3-5 and a photo of the instrumented pump installed on the test bench is reported in Figure 3-6.

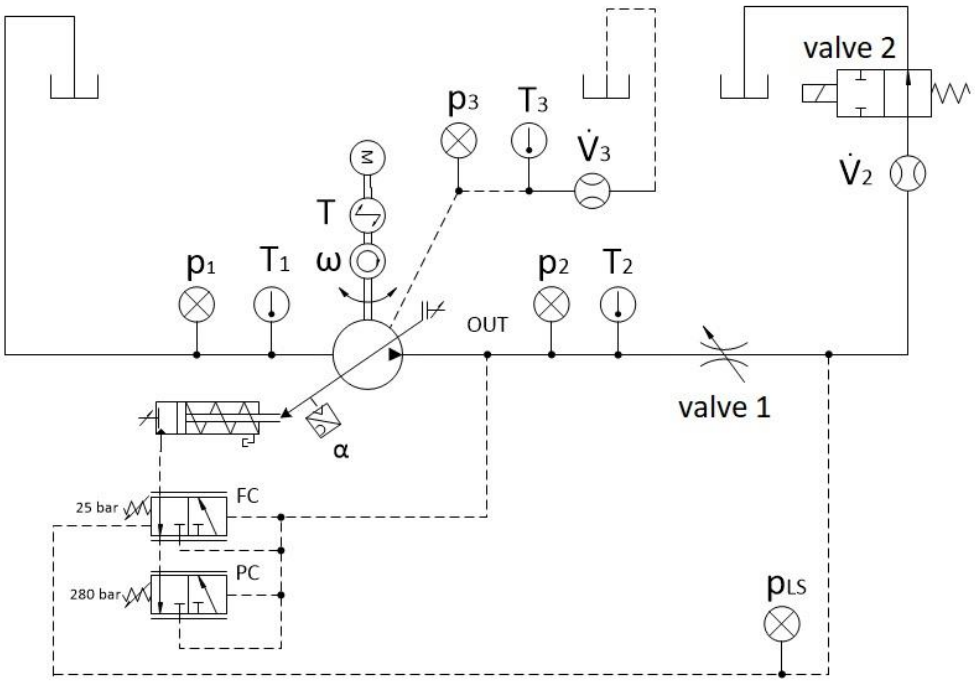

Figure 3-5: Hydraulic schematic of the experimental layout.

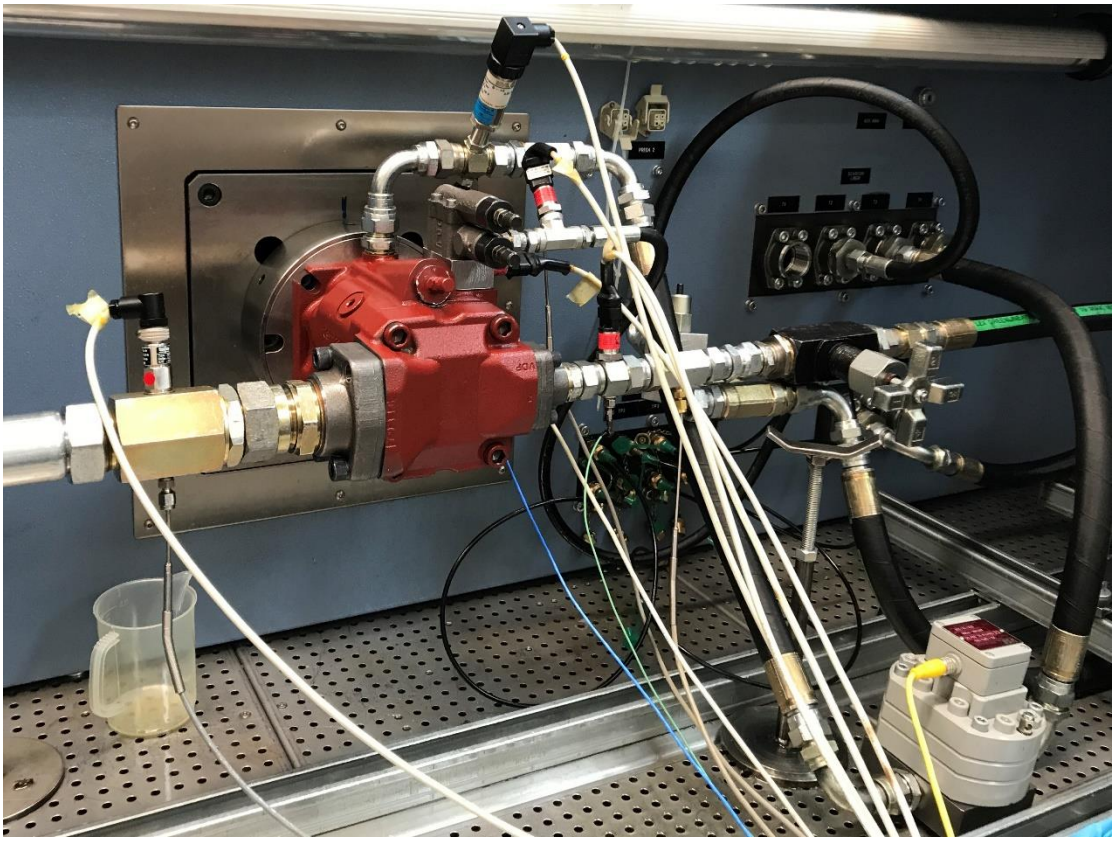

Figure 3-6: Photo of the instrumented pump on the test bench.

The pump is equipped with a Flow Compensator (FC) and with a Pressure Compensator (PC) and is installed in a Load Sensing (LS) logic. The FC regulates the displacement of the pump to keep a constant pressure drop (25 bar in this application), referred to as *pump margin*, between the LS pressure p_{LS} and the pump delivery pressure p_2. The PC acts in order to limit the pump displacement when the delivery pressure reaches the maximum tolerable value (280 bar in this application). The pump is driven by an electric motor whose angular velocity ω can be regulated; the shaft torque τ is measured by means of a torque sensor. The pump displacement can be regulated by acting on a variable orifice (valve 1 in the schematic) installed in the delivery line; the pump displacement can be indirectly measured through the indication of the swash plate angle α given by an angular sensor installed on the pump. The pump delivery pressure is set through another 2/2 valve (valve 2 in the schematic). With this experimental layout, the pump can be tested at different operating conditions by varying the angular velocity ω, the delivery pressure p_2 and the pump displacement V_d (proportional to the swash plate angle α). The schematic of Figure 3-5 reports also the position of the sensors installed for the experimental activity; the specifications of the sensors are reported in Table 3-3.

Table 3-3: Specifications of the adopted sensors.

Variable	Sensor	Range	Accuracy
T_1, T_2, T_3	Tersid® Thermistor Pt100	0 to 100 °C	± 0.2 °C
p_1	Wika® S-10	-1 to 9 bar	± 0.5% FS
p_2, p_{LS}	Danfoss® MBS 1250	0 to 400 bar	± 0.5% FS
p_3	Trafag® NAT 8251	0 to 10 bar	± 0.5% FS
$\dot{V}_2$	VSE® VS 2	0.1 to 120 l/min	± 0.3% measured value
$\dot{V}_3$	VSE® VS 1	0.05 to 80 l/min	± 0.3% measured value
α	Custom angular sensor (Walvoil®)	0° to 360°	± 0.02°
τ	HMB® T10FS	0 to 500 Nm	Class 0.05
ω	HMB® T10FS	0 to 20000 r/min	Class 0.05

In section § 3.3.2 it was shown that the measurement of the suction and the delivery temperatures is critical since it strongly affects the uncertainty on the overall efficiency. Therefore, three high accuracy thermistor Pt100 with standard uncertainty ± 0.2 °C were selected for the measurement of the temperatures at the hydraulic ports. The three thermistors were also calibrated together in order to eliminate any existing offset among the sensors. This last point is very important since the overall efficiency in Eq. 3.21 is function of the temperature differences ΔT_{21} and ΔT_{31}, therefore any existing offset among the sensors would affect in a critical manner the measurement. Two positive displacement flowmeters were also installed to measure the delivery and the drainage flow rates. These flowmeters are very expensive and difficult to install in an online application; they were used to validate the mathematical formulation of the proposed method. The expected flow rate in the drainage line is of few liters per minute, however, a flowmeter with a much larger range had to be selected to maintain the pressure in the pump case under the limit declared by the manufacturer (2 bar).

3.4.2 Experimental Tests

3.4.2.1 Validation Tests

A first series of experiments was carried out to validate the proposed thermodynamic approach. With this series of experiments, the objective was to verify that the value of the overall efficiency calculated with the thermodynamic approach was coherent with the value obtained

with the standard approach, used as reference method. The two approaches are coherent, and statistically equivalent, if their error bands overlap over the all set of operating conditions. Therefore, the pump was tested at different operating conditions varying the delivery pressure, the swash plate angle, the angular velocity and the oil temperature. The operating conditions investigated are reported in Table 3-4. The acquisitions were performed in stationary conditions, i.e. waiting for all the variables to reach the steady-state value; this is particularly important for the thermodynamic method since the temperature measurements are affected by the thermal capacitance of the pump. The sampling frequency was set to 1000 Hz (a relative low value since the focus was not on dynamic effects) and the values of the overall efficiency with the two approaches were calculated by averaging over an acquisition of 5 s.

Table 3-4: Static tests performed to validate the thermodynamic approach, the tests were performed with the oil temperature at 50 °C and 70 °C.

Angular velocity	**Swash plate angle**	**Delivery pressure**			
		100 bar	**150 bar**	**200 bar**	**250 bar**
1500 r/min	**5°**	✓	✓	✓	✓
	10°	✓	✓	✓	✓
2000 r/min	**5°**	✓	✓	✓	✓
	10°	✓	✓	✓	✓

3.4.2.2 Dynamic Tests

A test was also carried out to assess the performance of the method in transient conditions. Indeed, in most of the applications where variable displacement pump are used, the pump operating condition is not constant in time, but changes rapidly and continuously (this is particularly true on mobile applications). This method is interesting for online applications and therefore its performance in transient conditions need to be verified. The considered dynamic test consisted in a step variation, from 50 to 150 bar, of the delivery pressure (both the pressure rise and the pressure decrease were considered). Also for this test, the performance of the thermodynamic approach was compared to the performance of the standard approach. The overall efficiency is calculated with Eq. 3.21 which was obtained under the hypothesis of stationary

regime ($\dot{E} = 0$), therefore, the proposed approach cannot be theoretically used in non-stationary conditions. However, in transient conditions, the time derivative of the internal energy $\dot{E}$ is negligible if compared with the other terms of the energy balance equation (Eq. 3.6), therefore, this approach can be used with good approximation even in non-stationary conditions.

3.4.2.3 Tests in Faulty Conditions

A series of tests in faulty conditions was carried out. The faulty conditions were obtained by introducing faulty components in the pump; both naturally worn components and artificially damaged components were considered. The faults were selected among the most relevant ones based on the Failure Modes and Effects Analysis (FMEA) executed with the partner company, manufacturer of the considered pump. For each faulty condition, the overall efficiency was calculated with the proposed thermodynamic approach and compared to the one of the flawless pump; in the case of a significant difference, the proposed method can be used to detect the fault.

The following faults were considered:

- fault 1: worn port plate (Figure 3-7);
- fault 2: port plate with cavitation erosion (Figure 3-8);
- fault 3: worn swash plate (Figure 3-9);
- fault 4: worn slippers (Figure 3-10);
- fault 5: bearing with worn outer race (Figure 3-11);
- fault 6: artificially damaged piston (Figure 3-12);
- fault 7: artificially damaged cylinders block (Figure 3-13);
- fault 8: control actuator with worn cylinder.

Only faults 6 and 7 consider artificially damaged components, all the other faults consist of naturally worn components provided by the pump manufacturer. All the considered conditions recreate faults which can occur in actual applications. All the considered faults are light faults since the objective is to exploit the proposed method to detect incipient faults which could grow and lead to a complete pump failure.

Figure 3-7: Worn port plate.

Figure 3-8: Port plate with cavitation erosion.

Figure 3-9: Worn swash plate.

Figure 3-10: Worn slippers.

Figure 3-11: Bearing with worn outer race.

Figure 3-12: Artificially damaged piston.

Figure 3-13: Artificially damaged piston block.

Each faulty condition was tested keeping constant the pump displacement, but at different values of the delivery pressure and the angular velocity as reported in Table 3-5.

Table 3-5: Tests performed with the faulty components (swash plate angle 12.8° equivalent to a displacement of 51 cm^3).

Angular velocity	**Delivery pressure**	
	150 bar	**250 bar**
500 r/min	✓	✓
1500 r/min	✓	✓
2000 r/min	✓	✓

Only one pump was considered for the experimental campaign; the faulty components were installed into the pump one at a time to reproduce the faulty conditions. It as to be noted that when the pump is disassembled and the assembled again, without changing any components and respecting the tightening torque for each bolt, slight differences in the pump efficiency can be measured; these differences are due to the different interaction among the pump components.

3.4.3 Experimental Results

3.4.3.1 Validation Tests

Steady-state tests were carried out to validate the thermodynamic approach with reference to the standard approach. The results of the tests of Table 3-4 with oil temperature 50 °C are reported in Figure 3-14:

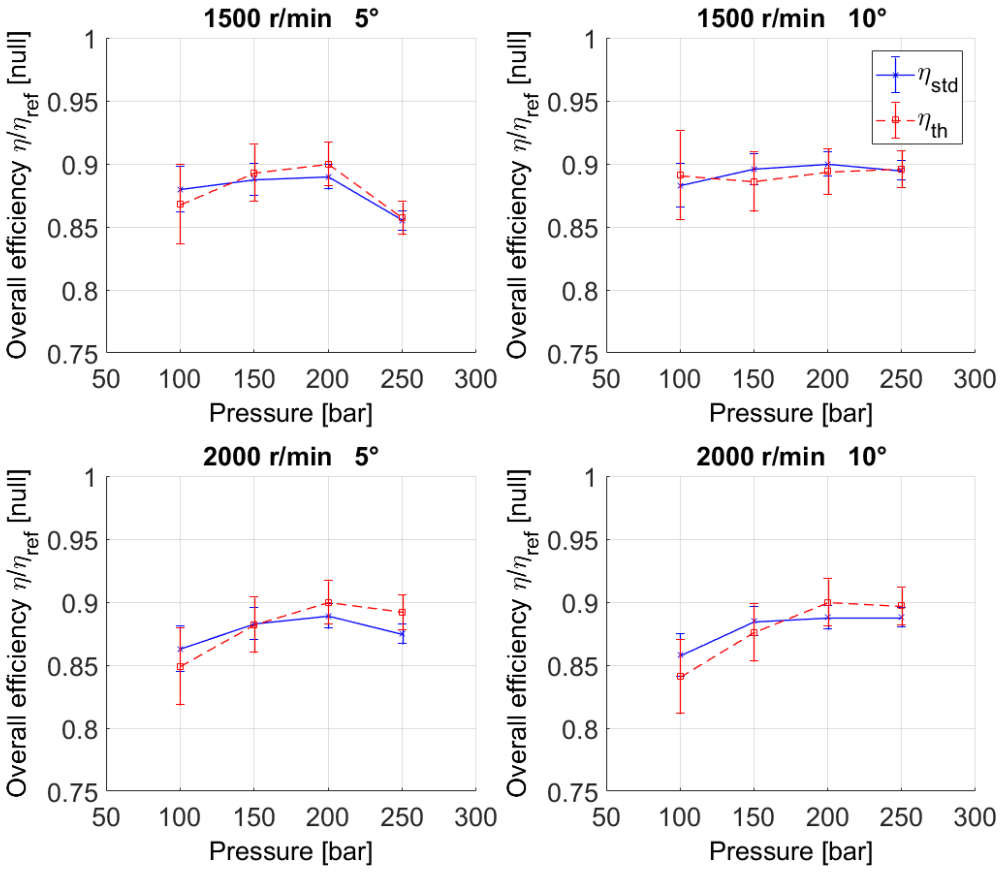

Figure 3-14: Comparison between the thermodynamic approach and the standard approach in steady-state conditions (oil temperature 50 °C).

The values of the overall efficiency were normalized for confidential reasons. For each plot, the reference value η_{ref} was defined so as to make the maximum value of the efficiency equal to 0.9; the comparison between the thermodynamic approach and the standard approach, which is the objective of these plots, is still valid. The comparison of the efficiency values among different

plots is meaningless since η_{ref} changes from plot to plot. The figure represents the uncertainty bands calculated with the first-order approximation as described in section § 3.3.1. The uncertainty bands of the two approaches overlap for all the considered operating conditions and therefore the two approaches are statistically equivalent. Figure 3-15 reports the results of the tests executed with oil temperature 70 °C.

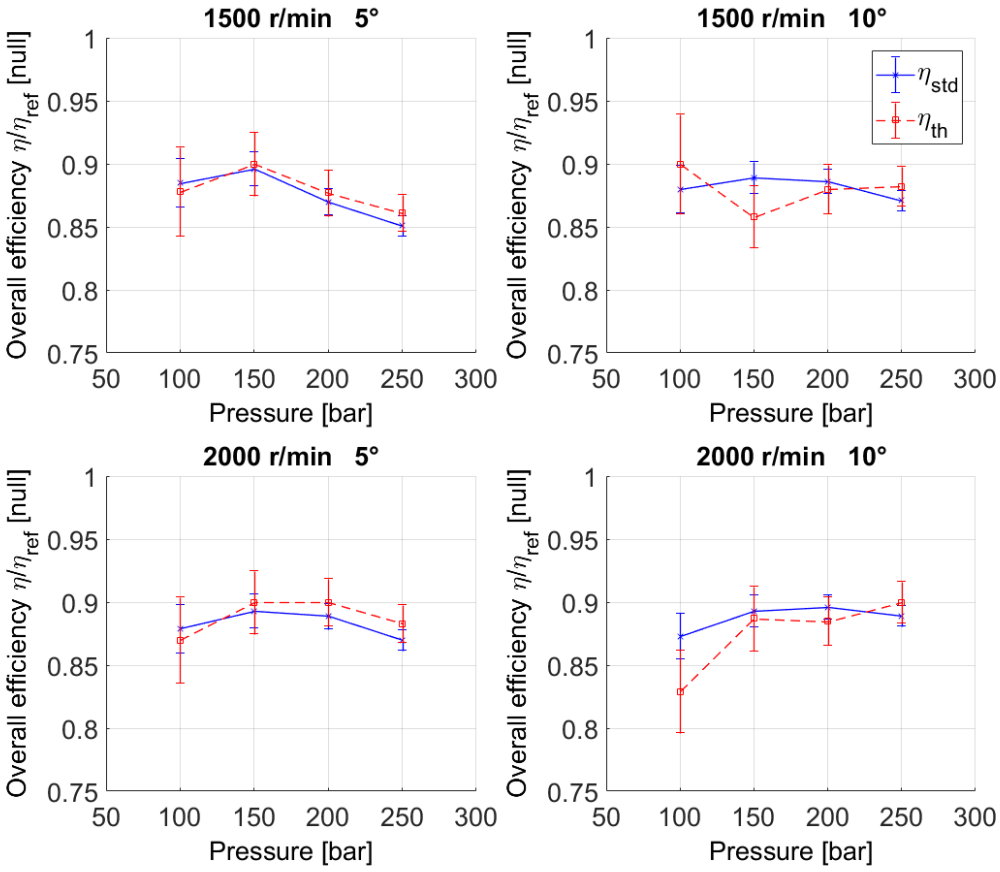

Figure 3-15: Comparison between the thermodynamic approach and the standard approach in steady-state conditions (oil temperature 70 °C).

Also for these tests, the uncertainty bands overlap for all the considered operating conditions and the two approaches are statistically equivalent. The uncertainty of the thermodynamic method is higher at low values of the delivery pressure because the temperature difference ΔT_{21} becomes small and the relative uncertainty on its measurement increases (see section § 3.3.2). Considering the results reported in Figure 3-14 and Figure 3-15, it can be concluded that the proposed thermodynamic approach is a valid alternative to the standard approach for the measurement of

the overall efficiency of a pump with external drainage. It is worth noting that this approach can be easily adapted to the case of a hydraulic motor with external drainage.

3.4.3.2 Dynamic Tests

The performance of the proposed thermodynamic approach in transient conditions was assessed through a step variation of the delivery pressure. The test was performed with angular velocity 1500 r/min and swash plate angle 10°; a step variation between 50 bar and 150 bar was imposed to the delivery pressure, both the rise and the descent phases were considered. The comparison between the overall efficiencies calculated with the thermodynamic and the standard approaches is reported in Figure 3-16.

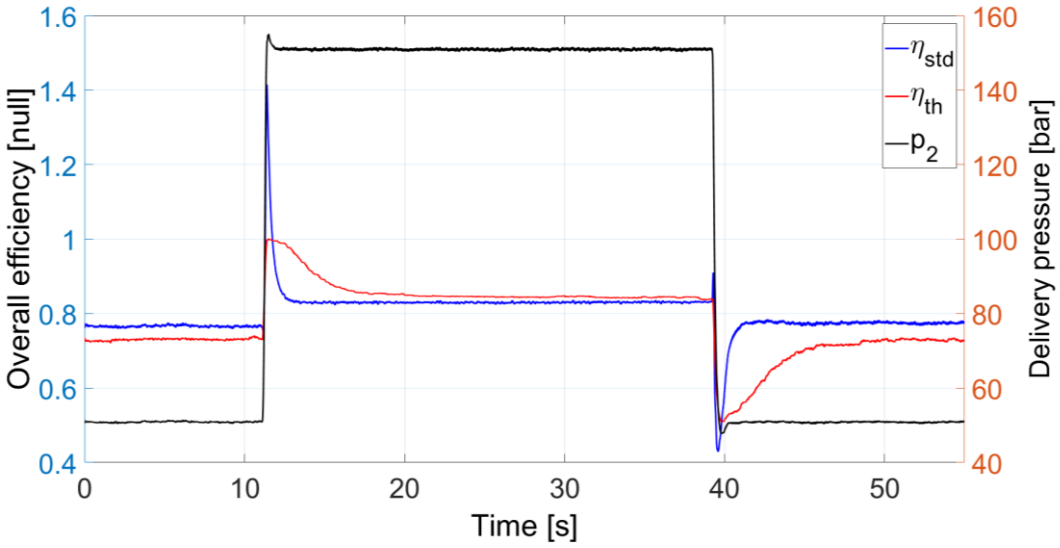

Figure 3-16: Comparison between the thermodynamic approach and the standard approach in the dynamic test, delivery pressure step from 50 bar to 150 bar (angular velocity 1500 r/min, swash plate angle 10°).

The pressure variation is very fast and both approaches experience some delay; however, the thermodynamic approach is slower than the standard approach. Both methods measure the overall efficiency indirectly and the delays are caused by the delays of the sensors used for the direct measurements of the input variables. Apart from the delivery pressure p_2 and the delivery flow rate $\dot{V}_2$, which affect both methods, the input variables mainly involved in this dynamic test are: the torque τ for the standard approach; the delivery temperature T_2, the drainage temperature T_3 and the drainage flow rate $\dot{V}_3$ for the thermodynamic approach. In the transient phase, the two

approaches return incorrect values, sometimes unfeasible values above unity, as illustrated by the zoom on the rise step reported in Figure 3-17.

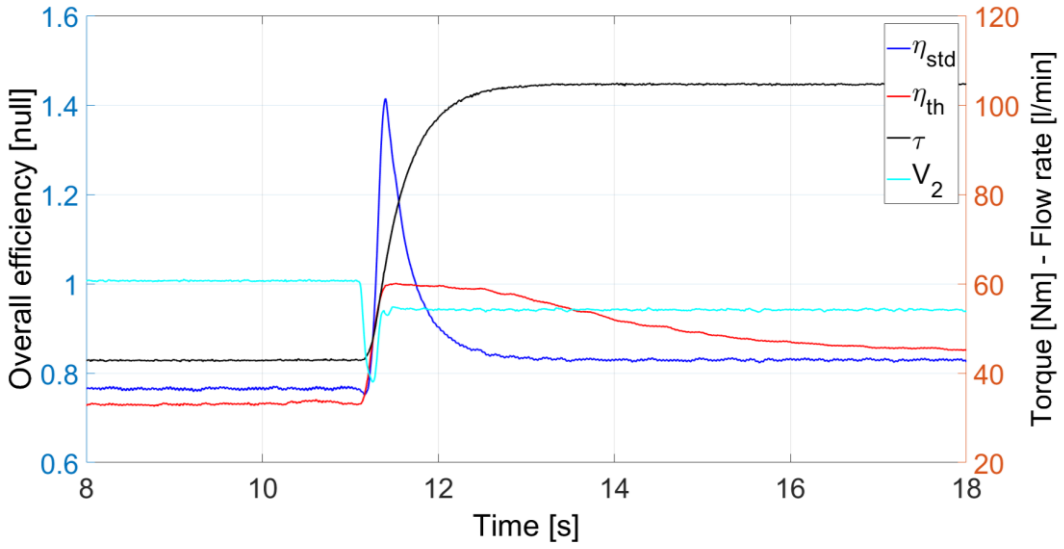

Figure 3-17: Zoom on the pressure rise step of the dynamic test.

Both approaches are affected by the measurements of the delivery flow rate $\dot{V}_2$ whose trend is reported in Figure 3-17; the time response of the flowmeter is fast, and the collapse of the flow is due to the closed-loop control (load sensing logic) of the pump. Immediately after the pressure step, the standard approach returns values above unity and this is caused by the delay of the torque sensor which underestimate the torque in the first phase. The thermodynamic method is slower because it is affected by the time response of the temperature sensors. A comparison between the trends of the overall efficiency calculated with the thermodynamic method η_{th} and the temperature difference ΔT_{21} is reported in Figure 3-18. The delivery temperature changes immediately when the pressure changes, therefore, the delay of ΔT_{21} to reach the steady state value is due to the time constant of the temperature sensor, which can be estimated around 4 s. The delay of the overall efficiency is comparable to the one of the temperature difference ΔT_{21}. The overall efficiency strongly depends on ΔT_{21} and therefore, any delay on the measurement of ΔT_{21} affects the measurement of the overall efficiency. Figure 3-19 reports the comparison between the trends of the overall efficiency calculated with the thermodynamic method η_{th} and the temperature difference ΔT_{31}.

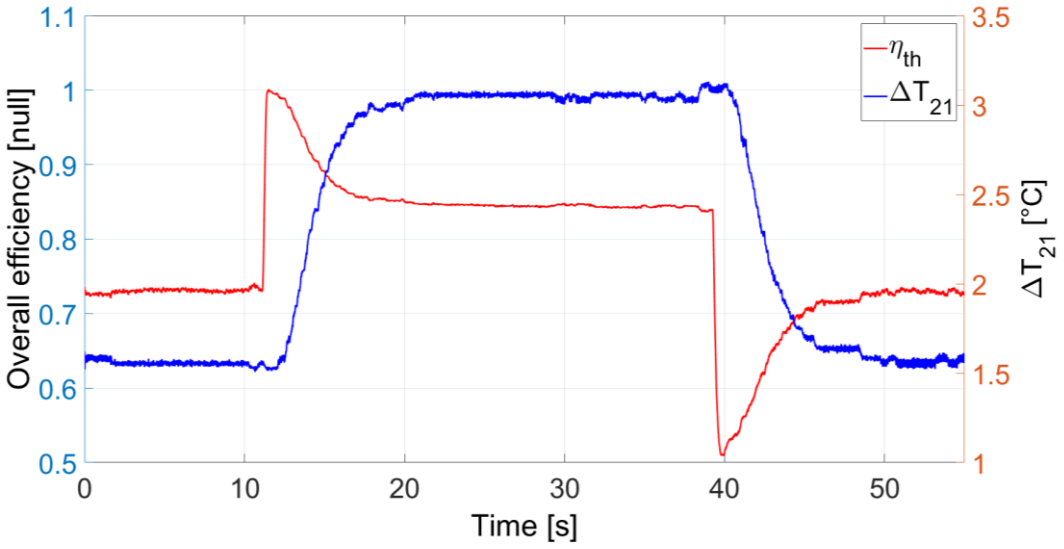

Figure 3-18: Comparison between the trend of the overall efficiency and the temperature difference ΔT_{21} in the dynamic tests.

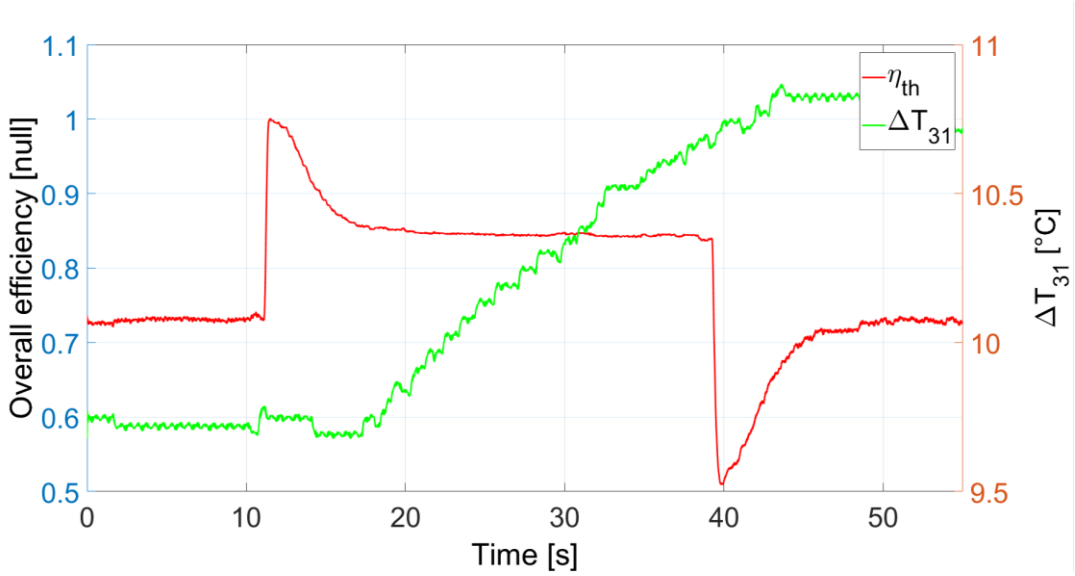

Figure 3-19: Comparison between the trend of the overall efficiency and the temperature difference ΔT_{31} in the dynamic tests.

The delay of the overall efficiency seems to be independent on the delay of ΔT_{31} which is much bigger. The two variables seem to be independent because the small variation of ΔT_{31} (around 2 °C) do not cause a significant variation of the overall efficiency. The delay of ΔT_{31} is not only due to the time constant of the temperature sensors (the same of ΔT_{21}), but it is due to an

actual delay of this temperature difference in reaching the steady-state value. Before reaching the drainage port, the leakages have to pass through the pump case (volumetric capacitance around 1 l) where a heat exchange with the metal parts of the pump takes place. The drainage temperature T_3 is affected by this physical phenomenon which causes a significant delay as illustrated in Figure 3-19.

The performance of the proposed thermodynamic approach in transient conditions, strongly depends on the time constant of the temperature sensors. The time constant of the thermistors Pt 100 used in this activity is around 4 s; faster sensors could be used, but in general, any temperature sensor will induce a delay. Therefore, the proposed approach is unsuitable for the measurement of the overall efficiency in applications where the operating conditions change rapidly and continuously. For the application of the proposed method in online applications, the operating condition must change slowly or, at least, some windows where the operating conditions are constant must exist. It has to be noted that also the standard approach showed some delay in the dynamic tests and therefore it will fail in rapid transient conditions.

3.4.3.3 Tests in Faulty Conditions

This section reports the results of the tests performed in faulty conditions. The thermodynamic method was used to calculate the overall efficiency of the faulty pumps and its value was compared to the value of the flawless pump to quantify the reduction of the overall efficiency and detect the fault. At this test of the project, only few tests were performed for each fault and only one component for each fault type was considered, therefore statistical tools or tests could not be applied. However, the comparison proposed in this section is still significant to show the capability of the proposed thermodynamic method to detect the efficiency reduction due to a faulty component.

Table 3-6 reports the difference between the overall efficiency of the flawless pump and the overall efficiency of the faulty pump. This difference was calculated with Eq. 3.44:

$$\Delta\eta\,\% = [\eta_t(flawless) - \eta_t(faulty)] \cdot 100 \qquad 3.44$$

The efficiency differences are rather small since the considered faults are light, incipient faults. A significant reduction of the pump efficiency over a wide set of operating conditions was measured for fault 2 (port plate with cavitation erosion) and fault 4 (worn slippers); these faults are extremely common, and their intensity grows with the pump usage. For the other faults, the

measured efficiency is very close to the one of the flawless pump and the difference is comparable to the measurement uncertainty. In general, the efficiency difference is higher at low angular velocities; the efficiency differences are always small at maximum speed (2000 r/min) and maximum pressure (250 bar).

Table 3-6: Difference between the overall efficiency of the flawless pump and the faulty pump expressed as a percentage (the efficiencies are calculated with the thermodynamic approach).

	500 r/min		**1500 r/min**		**2000 r/min**	
	150 bar	**250 bar**	**150 bar**	**250 bar**	**150 bar**	**250 bar**
Fault 1	0.14	3.80	1.84	1.07	1.55	-1.67
Fault 2	6.28	7.51	2.36	2.62	3.72	-0.83
Fault 3	-1.42	1.27	1.11	0.21	2.11	-1.29
Fault 4	9.19	10.13	1.44	4.00	2.86	1.10
Fault 5	4.05	2.37	0.35	0.46	2.97	-1.49
Fault 6	-0.12	0.43	1.86	0.40	2.53	-3.81
Fault 7	0.73	1.18	1.73	1.66	4.15	-0.16
Fault 8	4.47	3.66	3.67	1.03	-0.17	-2.82

In conclusion, the measurement of the overall efficiency with the proposed method was able to detect two common incipient faults, i.e. the port plate with cavitation erosion and the worn slippers.

3.5 Considerations on the Flow Rates Ratio

The proposed thermodynamic method is a valuable tool to calculate the overall efficiency of hydraulic machines with external drainage and it demonstrated also the potential to detect incipient faults. However, the method requires the measurements of the delivery and drainage flow rates $\dot{V}_2$ and $\dot{V}_3$ (Eq. 3.21). In all the results presented so far, the two flow rates were measured by means of two positive displacement flowmeters. These sensors are expensive and difficult to install in an actual application. Therefore, in order to make this approach suitable for online condition monitoring, an alternative solution for the estimation on the delivery and drainage flow rates needs to be defined.

3.5.1 Hypothesis of Zero Drainage Flow

The flow rates appear in the equation of the overall efficiency as the ratio of the drainage flow rate $\dot{V}_3$ and the delivery flow rate $\dot{V}_2$. Equation 3.45 (identical to Eq. 3.21) defines the efficiency $\eta_t(drain)$ and highlights in parentheses the flow rates ratio:

$$\frac{1}{\eta_t(drain)} = \frac{\rho_2 \bar{c}_{p_{21}} \Delta T_{21}}{\Delta p_{21}} + \rho_2 \bar{a}_{21} + \left(\frac{\dot{V}_3}{\dot{V}_2}\right) \frac{\rho_3}{\Delta p_{21}} \left(\bar{c}_{p_{31}} \Delta T_{31} + \bar{a}_{31} \Delta p_{31}\right) \qquad 3.45$$

The first solution to get rid of the flow rates ratio is to simply neglect it. In this case Eq. 3.45 boils down to Eq. 3.46, which defines the efficiency $\eta_t(no\ drain)$, i.e. the overall efficiency in the case of pump without external drainage:

$$\frac{1}{\eta_t(no\ drain)} = \frac{\rho_2 \bar{c}_{p_{21}} \Delta T_{21}}{\Delta p_{21}} + \rho_2 \bar{a}_{21} \qquad 3.46$$

This first solution is very simple and returns a wrong value of the overall efficiency in case of non-zero drainage flow rate. To quantify the magnitude of this approximation, $\eta_t(drain)$ and $\eta_t(no\ drain)$ were calculated for the tests of Table 3-4 with oil temperature 50 °C. The Flow rates ratio $\dot{V}_3/\dot{V}_2$ for the considered tests is reported in Table 3-7.

Table 3-7: Flow rates ratio $\dot{V}_3/\dot{V}_2$.

Angular velocity	**Swash plate angle**	**Delivery pressure**			
		100 bar	**150 bar**	**200 bar**	**250 bar**
1500 r/min	**5°**	0.0930	0.1302	0.1494	0.1993
	10°	0.0468	0.0630	0.0787	0.0904
2000 r/min	**5°**	0.0719	0.0949	0.1171	0.1515
	10°	0.0379	0.0467	0.0621	0.0706

The trend of the ratio is as expected: it is inversely proportional to the angular velocity and to the displacement, while it is directly proportional to the delivery pressure. The drainage flow rate depends mainly on the delivery pressure, it increases when the delivery pressure increases while the delivery flow rate slightly decreases. The ratio assumes non-negligible values; the maximum

value is around 0.20 at 1500 r/min and 250 bar. To consider the effect of neglecting this ratio on the calculation of overall efficiency, the difference between $\eta_t(no\ drain)$ and $\eta_t(drain)$ was calculated with Eq. 3.47 and the values are reported in Table 3-8:

$$\Delta\eta_t\ \% = [\eta_t(no\ drain) - \eta_t(drain)] \cdot 100 \qquad 3.47$$

Table 3-8: Difference between $\eta_t(no\ drain)$ and $\eta_t(drain)$ expressed as percentage.

Angular velocity	Swash plate angle	Delivery pressure			
		100 bar	**150 bar**	**200 bar**	**250 bar**
1500 r/min	**5°**	11.269	13.834	12.079	13.008
	10°	6.562	7.002	6.445	8.453
2000 r/min	**5°**	8.334	11.005	10.521	11.703
	10°	6.788	4.971	6.686	7.326

The magnitude of the error resulting from neglecting the flow rates ratio is significant (maximum value around 14 %) and dependent on the magnitude of the ratio. This first solution is simple, but leads to considerable and unacceptable errors.

3.5.2 Lookup Table for the Flow Rates Ratio

A second approach to avoid the online measurement of the flow rates consists in substituting the actual flow rates ratio with the value estimated offline on the flawless pump before the installation. The flow rates ratio depends on the pump operating conditions (angular velocity, displacement, delivery pressure and suction temperature), therefore several tests need to be performed offline in order to create a lookup table function of the pump operating conditions. Once the lookup table is available, the ratio is obtained through interpolation and the flow rates are not measured online. This approach does not lead to any error for the flawless pump since the lookup table refers to the same condition. To assess the behavior of this approach when a fault occurs in the system, numerical simulations were performed considering the hypotheses reported in section § 3.3.2.

The numerical simulations considered the effects of faults which lead to a reduction of the volumetric efficiency η_v, with consequent variation of the flow rates ratio with reference to the flawless case. Two cases of volumetric efficiency reduction were considered:

- with leakages towards the suction;
- and with leakages towards the drainage.

In both cases the delivery flow rate reduces, but in the former, the missing outflow flows back to the suction area and the drainage flow rate does not change, while in the latter, the missing outflow flows entirely through the drainage. A reduction of the volumetric efficiency $\Delta\eta_v$ of 5 %, 10 %, 15 % and 20 % was considered for both cases. The data acquired on a flawless pump for calculating the efficiency with the standard approach were used as starting point.

For the case with leakages towards the suction, the delivery flow rate of the simulated faulty pump was calculated according to the reduction of volumetric efficiency with Eq. 3.48:

$$\dot{V}_2(faulty) = V_d \frac{n}{60}(\eta_v - \Delta\eta_v) \qquad 3.48$$

The drainage flow rate was kept unchanged; this case is similar to the case of pumps without external drainage where a reduction of the volumetric efficiency causes an increase of the reflux towards the suction. All the other variables were calculated following the hypotheses reported in section § 3.3.2; in particular, the delivery temperature $T_2(faulty)$ in faulty condition was calculated with Eq. 3.36. The difference between the delivery temperature in faulty condition $T_2(faulty)$ and the delivery temperature in flawless condition $T_2(flawless)$ was calculated with Eq. 3.49:

$$\Delta T_2 = T_2(faulty) - T_2(flawless) \qquad 3.49$$

The values of ΔT_2 for different operating conditions and for the four levels of volumetric efficiency reduction are reported in Figure 3-20.

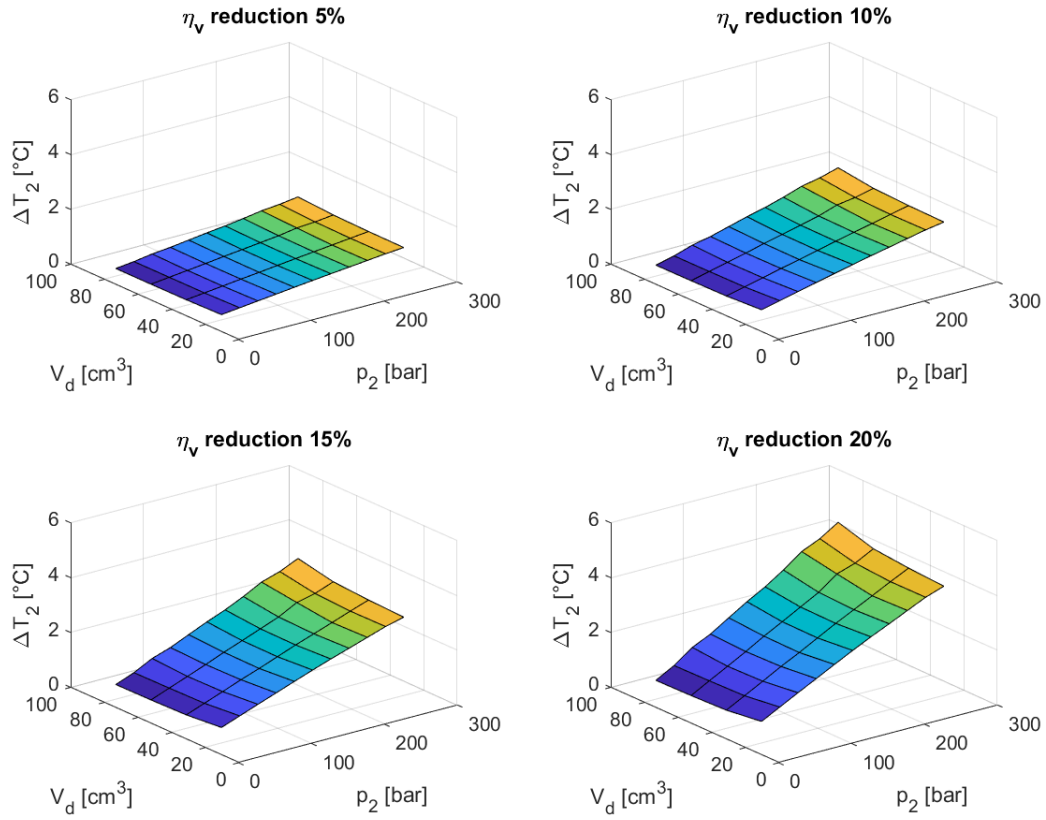

Figure 3-20: Difference between $T_2(faulty)$ and $T_2(flawless)$ for the case with leakages towards the suction.

The temperature difference ΔT_2 is directly proportional to the delivery pressure and increases when the volumetric efficiency reduces. The mechanical power transferred to the fluid reduces (same delivery pressure but lower delivery flow rate) because of the volumetric efficiency reduction, consequently, the specific enthalpy of the delivery flow increases to preserve the energy balance. The overall efficiency $\eta_t(lookup)$ of the simulated faulty condition can be calculated with Eq. 3.50 where the flow rates ratio is obtained through the lookup table, i.e. it is the one in flawless condition:

$$\frac{1}{\eta_t(lookup)} = \frac{\rho_2 \bar{c}_{p_{21}} \Delta T_{21}}{\Delta p_{21}} + \rho_2 \bar{a}_{21} + \left(\frac{\dot{V}_3}{\dot{V}_2}\right)_{lookup} \frac{\rho_3}{\Delta p_{21}} \left[\bar{c}_{p_{31}} \Delta T_{31} + \bar{a}_{31} \Delta p_{31}\right] \quad 3.50$$

The value of $\eta_t(lookup)$ must be compared to the actual overall efficiency $\eta_t(actual)$, Eq. 3.51, where the ratio is the actual one in faulty condition:

$$\frac{1}{\eta_t(actual)} = \frac{\rho_2 \bar{c}_{p_{21}} \Delta T_{21}}{\Delta p_{21}} + \rho_2 \bar{a}_{21} + \left(\frac{\dot{V}_3}{\dot{V}_2}\right)_{actual} \frac{\rho_3}{\Delta p_{21}} \left[\bar{c}_{p_{31}} \Delta T_{31} + \bar{a}_{31} \Delta p_{31}\right] \quad 3.51$$

The difference between $\eta_t(lookup)$ and $\eta_t(actual)$ was calculated with Eq. 3.52 and the results are reported in Figure 3-21:

$$\Delta\eta_t = \eta_t(lookup) - \eta_t(actual) \quad 3.52$$

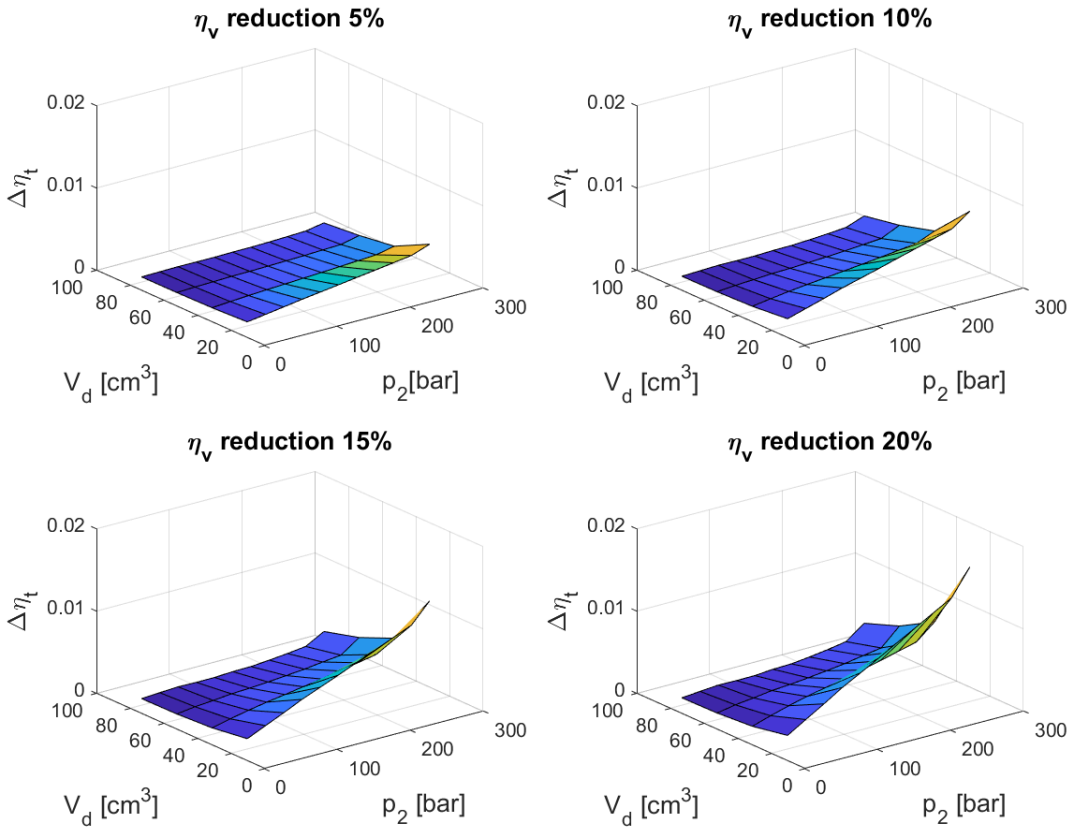

Figure 3-21: Difference between $\eta_t(lookup)$ and $\eta_t(actual)$ for the case with leakages towards the suction.

The value of $\Delta\eta_t$, i.e. the error on the estimation of the overall efficiency, is rather small if compared with the reduction of the volumetric efficiency. Indeed, the thermodynamic method is sensitive to the increase of the delivery temperature and can detect this kind of fault with leakages towards the suction.

For the case with leakages towards the drainage, the delivery flow rate is still calculated with Eq. 3.48 and the drainage flow rate is calculated with Eq. 3.33 preserving the mass balance. The same approach was used to calculate the variables of the faulty condition and, in particular, the value of the delivery temperature. The values of ΔT_2 were calculated with Eq. 3.49 and the results are plotted in Figure 3-22.

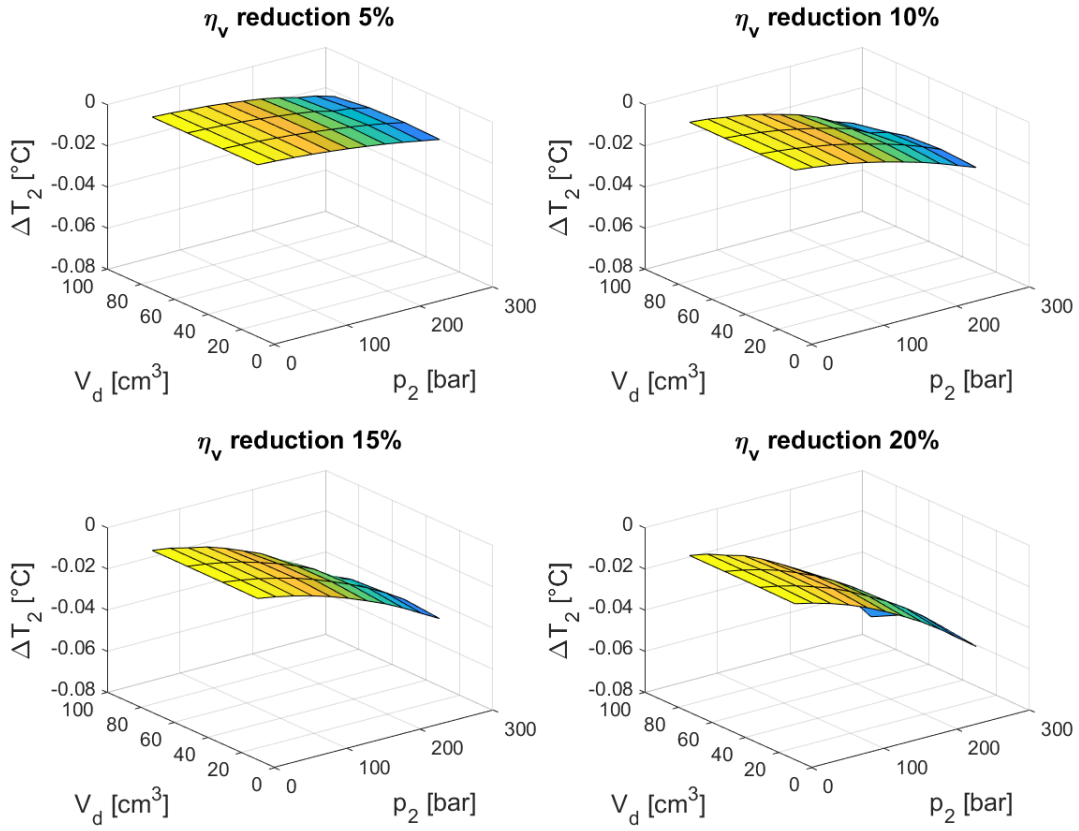

Figure 3-22: Difference between $T_2(faulty)$ and $T_2(flawless)$ for the case with leakages towards the drainage.

The delivery temperature in faulty condition $T_2(faulty)$ is almost equal to the temperature in the flawless condition $T_2(flawless)$. In this case, the reduction of the mechanical power transferred to the fluid is compensated by the increased enthalpy flux at the delivery port and the

delivery temperature remains the same. The difference between $\eta_t(lookup)$ and $\eta_t(actual)$ was calculated with Eq. 3.52 and the values are reported in Figure 3-23.

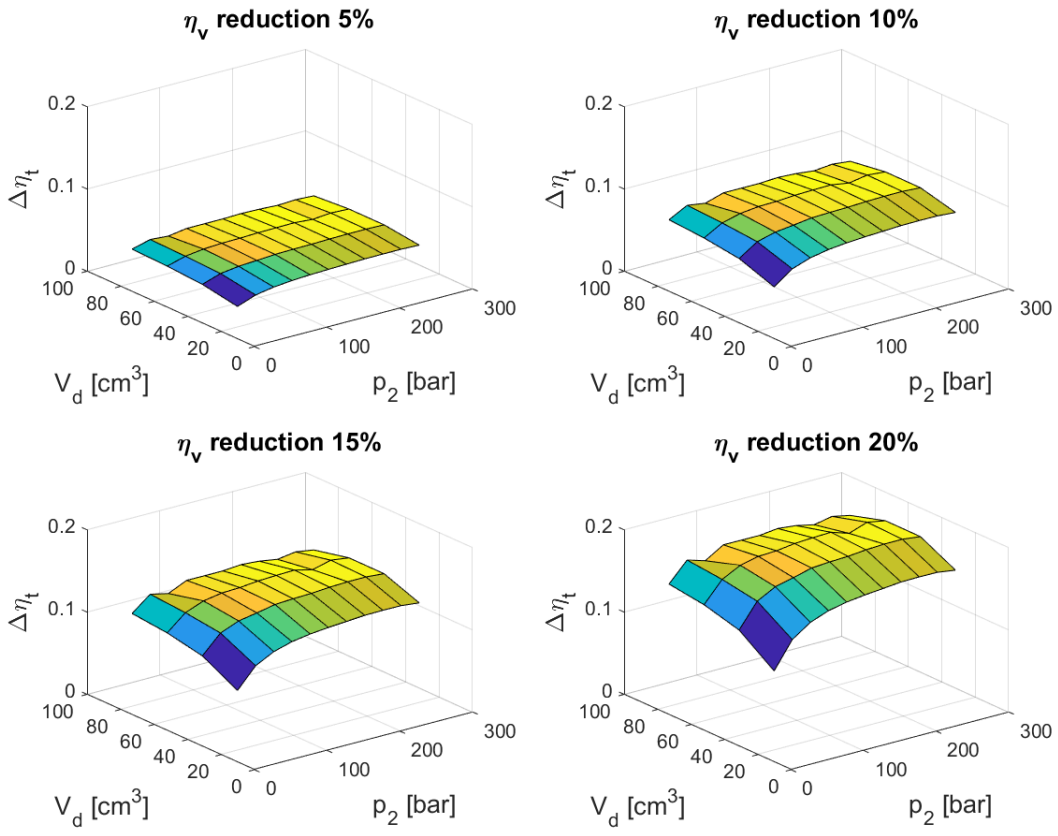

Figure 3-23: Difference between $\eta_t(lookup)$ and $\eta_t(actual)$ for the case with leakages towards the drainage.

In this case, the error in the estimation of the overall efficiency is of the same order of magnitude of the reduction of the volumetric efficiency. Indeed, if the temperatures are the same of the flawless pump and the same ratio is used for the calculation of the overall efficiency, $\eta_t(lookup)$ returns the value of the efficiency of the flawless pump and the error in the evaluation of the efficiency of the faulty pump is significant. This solution to avoid the measurements of the flow rates is basically blind to this kind of fault.

From the analysis of the two faulty conditions, it can be concluded that this approach based on a lookup table is prone to fail when the fault induces a considerable increase of the drainage flow rate. However, to improve the performance of the method, an online estimate of the flow rates must be available and a solution in this direction is proposed in the next section.

3.5.3 Measurement of the Drainage Flow Rate

The measurement of the drainage flow rate is already a valuable parameter to monitor the health state of the pump. The use of standard sensors, like positive displacement flowmeters, is not suitable for an online application because these sensors are expensive and bulky. A cheaper solution for the measurement of the drainage flow rate can be performed by measuring the pressure difference on a calibrated orifice. Another solution could exploit the pressure difference caused by the fluid momentum between the intrados and the extrados of a curve installed in the drainage line [3.20]. Both solutions are cheap, but require a proper design of the measuring system and the measurement of a small pressure difference. Furthermore, these solutions must be designed so as to keep the drainage pressure below the limit defined by the manufacturer (usually 2 bar).

The measurement of the delivery flow rate is more complicated because the flow is one order of magnitude higher. Once a measure of the drainage flow rate is available, the delivery flow rate can be calculated as the difference between the ideal flow rate and the drainage flow rate, as reported in Eq. 3.53:

$$\dot{V}_2 = V_d \frac{n}{60} - \dot{V}_3 \qquad 3.53$$

This solution does not consider the leakages towards the suction, but we demonstrated in the previous section that this approximation does not cause a considerable error in the calculation of the overall efficiency. Furthermore, once the drainage flow rate $\dot{V}_3$ is measured, a small approximation on the estimate of the delivery flow rate $\dot{V}_2$ do not cause a significant error on the estimate of the ratio $\dot{V}_3/\dot{V}_2$.

With this solution for the evaluation of the flow rates ratio, the proposed thermodynamic method becomes an extremely powerful tool for the online monitoring of the overall efficiency of pumps with external drainage. A similar approach can be adopted for hydraulic motors with external drainage.

3.6 Discussion and Future Works

In this chapter a thermodynamic method for the calculation of the overall efficiency of hydraulic machines with external drainage was presented. The reference case of a variable-

displacement axial-piston pump was considered, but the presented approach can be easily adapted to hydraulic motors. The proposed method constitutes an extension of the thermodynamic method already known in the literature for the measurement of the overall efficiency of hydraulic machines without external drainage.

The proposed method was derived from the first principle of thermodynamics under the hypothesis of adiabatic pump and stationary regime. The effects of these two hypotheses were quantified and it was demonstrated that they introduce an acceptable approximation. The final formulation of the overall efficiency requires the measurement of the pressure and the temperature at the three hydraulic ports (suction, delivery and drainage). Besides, the presence of the external drainage requires also the measurement of the ratio between the drainage flow rate and the delivery flow rate. In the case without external drainage, the method requires only the measurement of temperatures and pressures, and therefore it is suitable for the online monitoring of the pump overall efficiency. The measurement of flow rates requires the installation of flowmeters which are expensive and cumbersome sensors; therefore, a solution to deal with the flow rates ratio must be found in order to use the proposed method for the online monitoring of hydraulic machine with external drainage. In the first phase of the project, the focus was on validating the thermodynamic approach by means of a comparison with the standard approach, and therefore the flow rates were measured by means of positive displacement flowmeters. The method requires also the knowledge of the fluid properties and for this reason a model of the fluid was derived from the experimental data provided by the oil manufacturer. To compare properly the results of the thermodynamic method to the results of the standard method, the measurement uncertainties were calculated according to the relevant standards. It was demonstrated that a first-order approximation is enough for the calculation of the combined uncertainty. The greatest impact on the efficiency uncertainty is due to the differential measurement of temperature difference between the delivery and the suction ports. Some simulations were performed to select suitable temperature sensors and three Pt 100 with an accuracy of ± 0.2 K were selected. The thermodynamic method requires the installation of high accuracy temperature sensors to obtain a measurement uncertainty comparable to the standard method.

A series of tests at different operating conditions were performed to validate the proposed thermodynamic method. Over the entire set of tests, the uncertainty bands of the efficiency calculated with the thermodynamic method and the efficiency calculated with the standard method overlap; thereby, the two approaches are statistically equivalent. It can be concluded that the proposed thermodynamic method is a valid alternative to the standard method for the evaluation of the overall efficiency. However, the results of a dynamic test demonstrated that the

proposed method is unsuitable for the measurement of the efficiency when the pump operating conditions change rapidly. The poor performance in dynamic conditions is mainly due to the time constant of the temperature sensors which introduce a delay in the calculation of the efficiency. This drawback hinders the usage of the thermodynamic method in many applications of mobile hydraulics were the operating conditions of the hydraulic machines change rapidly and continuously. The application of this method requires stationary conditions or slowly changing conditions.

Since this method is proposed as a tool for the online monitoring, a series of experiments in faulty conditions was executed at different operating conditions. Eight faults were considered; these faults were selected among the most common based on a FMEA. Most of the tested faults were at an incipient stage and therefore the reduction of the overall efficiency was within the uncertainty band of the method. Two faults, worn slippers and port plate with cavitation erosion, shown a remarkable reduction of the efficiency over a wide range of operating conditions.

The proposed method showed the potential for identifying some common faulty conditions, but the problem relative to the measurement of the flow rates ratio must be addressed. Some solutions were proposed to deal with this ratio. It was demonstrated that the hypothesis of zero drainage flow rate leads to an unacceptable approximation. The use of a lookup table with the values of the ratio in healthy condition is a better option, but it fails in case of faults which cause a significant increase of the drainage flow rate. To overcome this drawback, a solution based on the measurement of the drainage flow rate is proposed; the sensor must be cheap and must introduce a small pressure drop. The design of a flow rate sensors for this application, based on a curve, will be considered as a future development of this project. Once an estimate of the drainage flow rate is available, the delivery flow rate can be calculated as the difference between the ideal flow rate and the drainage flow rate. With this solution for the estimation of the flow rate ratio, the proposed thermodynamic model is an extremely useful method for the online monitoring of the overall efficiency in hydraulic machines with external drainage.

List of references

3.1. L. Barbillon, A. Poirson, Sur une méthode thermométrique de mesure du rendement des turbines hydrauliques, La Houille Blanche (1920) 217–221.

3.2. IEC (Ed.), IEC 60041 – Field acceptance tests to determine the hydraulic performance of hydraulic turbines, storage pumps and pump-turbines, 3rd Edition, IEC, 1991.

3.3. EN ISO 5198:1998, Centrifugal, mixed-flow and axial pumps - Code for hydraulic performance tests - Precision Class, International Organisation for Standardisation, 1998.

3.4. J. Lanzersdorfer, L. Götsch, Analytical solutions using the thermodynamic efficiency method for absolute flow measurement, Flow Measurement and Instrumentation, Volume 44 (2015), 89–96. http://dx.doi.org/10.1016/j.flowmeasinst.2014.11.013.

3.5. S. S. Patil, H.K. Verma, A. Kumar, Efficiency Measurement of Hydro Machine by Thermodynamic Method, Proceedings of the 8th International Group for Hydraulic Efficiency Measurement (IGHEM) Conference, 2010, Roorkee, India, October 21-23, 2010.

3.6. A. J. Milne, Implications of Measurement Uncertainty When Using the Thermodynamic Method of Pump Efficiency Monitoring in Water, Proceedings of the Institution of Mechanical Engineers, Part A: Journal of Power and Energy, Volume 204 (1990) 109-119. doi:10.1243/PIME_PROC_1990_204_016_02.

3.7. E. Dalla Lana, V. J. De Negri, A New Evaluation Method for Hydraulic Gear Pump Efficiency through Temperature Measurements, SAE 2006 Commercial Vehicle Engineering Congress & Exhibition, Rosemont, Chicago, United States, 2006. DOI 10.4271/2006-01-3503.

3.8. A. Kjølle, The thermodynamic method applied to hydraulic transmission, Proceedings of the JFPS International Symposium on Fluid Power, Volume 1993 (1993), Number 2, 639-644. http://doi.org/10.5739/isfp.1993.639.

3.9. J. Andersson, P. Krus, K. Nilsson, K. Storck, Modelling and Simulation of Heat Generation in Electro-Hydrostatic Actuation System, Proceedings of the Fourth JHPS International Symposium on Fluid Power, Tokyo, Japan, November 15-17, 1999. ISBN4-931070-04-3.

3.10. H.D. Feng, L. Xu, R. P. Xu, L. J. Wu, X. H. Shi, J. D. Yan, T. Y. Wang, Uncertainty analysis using the thermodynamic method of pump efficiency testing, Proceedings of the Institution of Mechanical Engineers, Part C: Journal of Mechanical Engineering Science, Volume 218 (2004), 543-555. doi: 10.1243/095440604323052328.

3.11. A. Abgottspon, M. Briggeler, T. Staubli, Corrective terms of thermodynamic efficiency measurements, Proceedings of the 8th International Group for Hydraulic Efficiency Measurement (IGHEM) Conference, Roorkee, India, October 21-23, 2010.

3.12. J. Ramdal, Efficiency measurements in low head hydro power plants, Doctoral thesis at Norwegian University of Science and Technology, 2011. ISBN 978-82-471-2883-4.

3.13. S. L. Merry, M. T. Thew, Evaluation of a thermodynamic method for efficiency measurements on a low-pressure pump in water and mercury, Journal of Physics E: Scientific Instruments, Volume 17 (1984), Number 11.

3.14. P. Casoli, F. Campanini, A. Bedotti, M. Pastori, A. Lettini (2017), Overall efficiency evaluation of a hydraulic pump with external drainage through temperature measurements, ASME - Journal of Dynamic Systems, Measurement and Control, doi:10.1115/1.4039084.

3.15. ISO 4409:2007, Hydraulic fluid power - Positive displacement pumps, motors and integral transmissions - Determination of steady-state performance, International Organization for Standardization, 2007.

3.16. Theodore L. Bergman, Adrienne S. Lavine, Frank P. Incropera, David P. DeWitt, Fundamentals of Heat and Mass Transfer, 7th Edition, Jonh Wiley & Sons, Jefferson City, 2011.

3.17. Neil E. Todreas, Mujid S. Kazimi, Nuclear System I – Thermal Hydraulic Fundamentals, CRC Press Taylor & Francis Group, Boca Raton, 2011.

3.18. JCGM 100:2008, Evaluation of measurement data - Guide to the expression of uncertainty in measurement, Bureau International des Poids et Mesures, 2008.

3.19. M.A.F. Martins, R. Requião, R.A. Kalid, Generalized expressions of second and third order for the evaluation of standard measurement uncertainty, Measurement, Volume 44 (2011), Issue 9, 1526–1530.

3.20. Charles W. Groepper, T. Cui, Perry Y. Li, Kim A. Stelson, Design of integrated pressure, flow, and temperature sensor for hydraulic systems, Proceedings of the Power Transmission and Motion Control Symposium, Bath, UK, September 13-15, 2006. ISBN 08 6197 135 3.

Chapter 4 - Pump Diagnostics Based on Acceleration Signals

This chapter presents a methodology for the analysis of acceleration signals and demonstrates its application for the diagnostics of a variable displacement axial-piston pump. This methodology relies on the theory of cyclostationarity, therefore, an introduction to this theory and to its signal processing tools is given in the first part of the chapter.

The acceleration signals are currently used for the monitoring and the diagnostics of a variety of mechanical systems, indeed, the acceleration signals convey a lot of information about the system health status. In most cases the raw signal is useless for diagnostic purposes and processing is needed to extract features which are related to the machine faults. Following the theory of cyclostationarity, the proposed methodology decomposes the acceleration signal in its periodic (first-order cyclostationary) and second-order cyclostationary components. These two parts contain information about different phenomena and need to be separated and processed with different tools. The Synchronous Average (SA) is used for the extraction of the periodic part and the Multiple Cyclic Regression (MCR) algorithm is exploited for the separation of the second-order cyclostationary part from the remaining noise. The extraction capabilities of the MCR algorithm are tested and calibrated on synthetic signals.

The proposed methodology is then applied on experimental signals acquired from two accelerometers installed on the pump case. The experiments were carried out in healthy and faulty conditions; the faulty conditions were created by introducing worn components within the pump. The results show that the proposed methodology for the analysis of the acceleration signals can extract features which highlight the presence of the considered faults. These fault features can be used in an automatic diagnostic system.

4.1 Theory of Cyclostationarity

In dealing with acceleration signals issued by mechanical systems, the cyclostationary analysis allows to take advantage of the transient events which are lost with the classical stationary approach. Indeed, most of the signals collected from mechanical systems (not only acceleration signals, but also noise signals and pressure signals) are cyclostationary signals.

The theory of cyclostationarity was mainly developed in the field of communication signals [4.1] and in the last years this theory started to be applied to mechanical signals. The theory of cyclostationarity has reached its maturity and the literature in this field is rich, as it is demonstrated by these two reviews on the subject [4.2, 4.3]. For the beginners, a good introduction to this theory can be find in this reference [4.4].

4.1.1 Definition of Cyclostationarity

A stationary signal is, by definition, a signal which can be described by statistical parameters which are constant over time. Starting from this definition of stationary signal, a first definition of cyclostationary signal can be given [4.5].

Definition 1. A cyclostationary signal is a signal whose statistical descriptors change periodically over time; the period is referred to as the *cycle*.

At first glance, this definition seems to be suitable to describe the signals issued by mechanical systems, because in most of the mechanical systems the phenomena repeat themselves on a cyclic basis even when the system is operated in "stationary condition", i.e. when its control parameters are kept constant over time. A variety of examples of cyclic phenomena can be reported: the gear meshing in a gearbox, the gas combustion in an internal combustion engine, the inversion of forces in reciprocating mechanisms, the turbulence generated by the blades in dynamic pumps and fans, etc. These cyclic phenomena induce a cyclic behavior on the signal. Furthermore, when a fault occurs in the system, it is likely that it induces a periodic variation in the signal at the frequency followed by the faulty component, which is the reciprocal of the cycle. Therefore, by detecting the frequency of the variation, the fault can be identified in a precise component.

The stationary approach considers parameters which are averages over time, such as the mean value, the mean power (or the Root Mean Square (RMS)) and the Power Spectral Density (PSD). These time-averaged parameters can be relevant for the system diagnostics; in many cases for example, an increase of the RMS value of an acceleration signal is the symptom of a faulty system.

Furthermore, the PSD reveals which are the frequency components in the signal and this spectrum can be a powerful tool for the system diagnostics. However, the cyclic phenomena of mechanical systems induce typically a cyclic modulation of the signal power; in this case, the stationary approach shows its limits and fails in detecting the cyclic behavior. A simple example will make it clearer.

Example 1. Let us consider the signal $x(t)$ described by Eq. 4.1:

$$x(t) = \sin(\pi \cdot \alpha_0 \cdot t) \cdot n(t) \qquad 4.1$$

Where $\alpha_0 = 25\ Hz$ and $n(t)$ is a band limited $[2000 - 4000\ Hz]$ random noise. Basically, the amplitude of the random noise is periodically modulated with frequency $\alpha_0/2$. The example signal is showed in Figure 4-1 (a) over a period of 0.4 s; the mean value and the RMS value are also reported in the same figure. Figure 4-1 (b) instead reports the PSD of the example signal. In the graphs u stands for the generic unit of the signal.

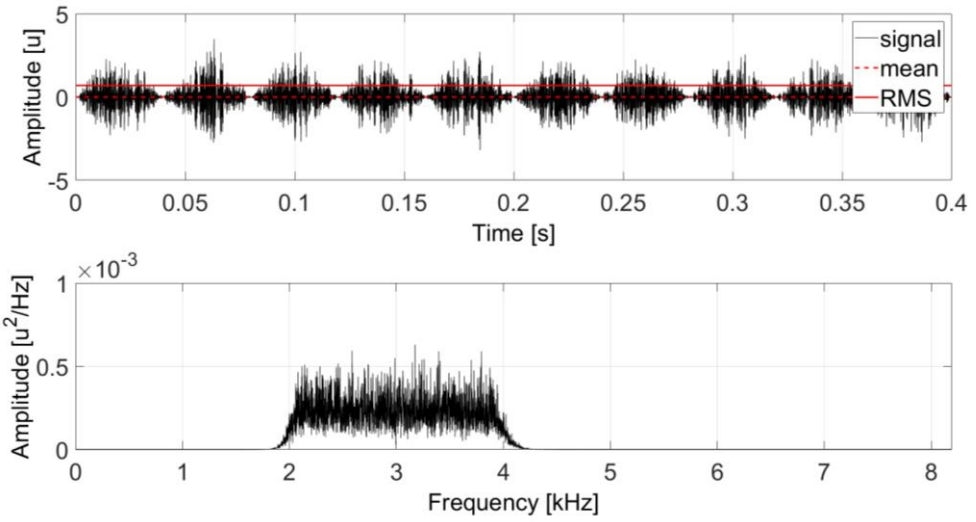

Figure 4-1: (a) Example 1 signal together with its mean value and its RMS value, (b) PSD of the example 1 signal computed with the Welch's estimator.

The signal shows an evident beating phenomenon with frequency α_0, i.e. the signal power changes periodically with frequency α_0, which is referred to as the *cyclic frequency*. Even if this example signal is very simple, it well represents a typical acceleration signal issued by a mechanical system (in an actual signal the presence of the background noise can make difficult to detect the beating phenomenon from the analysis of the time series). From Figure 4-1, it is

evident that neither the mean value (which is zero) nor the RMS value can represent the characteristic beating phenomenon of the signal. The PSD shows that the signal is completely random over the spectral support 2000 – 4000 Hz and it does not contain any information about the beating phenomenon. Both the RMS and the PSD are related to the signal power, but, since they are computed as time averages, they are unable to extract its periodic changes. We can conclude that the standard stationary approach is unable to detect the beating phenomenon of this example signal.

The cyclostationary approach considers a cyclic decomposition of the signal power. This cyclic decomposition leads to the definition of the *mean instantaneous power* $P_x(t)$ [4.4]:

$$P_x(t) = \sum_{\alpha \in A} \left(\lim_{T \to \infty} \frac{1}{T} \int_T |x(t)|^2 \cdot e^{-j2\pi\alpha t} dt \right) \cdot e^{j2\pi\alpha t} \qquad 4.2$$

Basically, the mean instantaneous power is obtained by computing the Fourier coefficient of the power signal corresponding to the cyclic frequency α and then multiplying this coefficient by the complex exponential so as to return a sinusoidal signal at frequency α. The set A contains all the cyclic frequencies whose Fourier coefficients are above a level of significance. The mean instantaneous power is obtained as a summation over the set A. The instantaneous power of the example 1 signal is reported in Figure 4-2 (a) while the amplitude of its FFT is reported in Figure 4-2 (b).

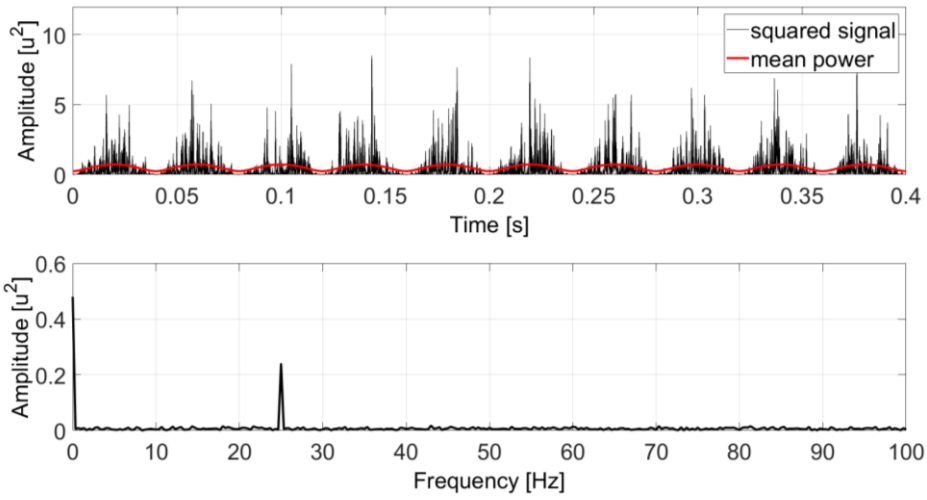

(a)

(b)

Figure 4-2: (a) Instantaneous power of the example 1 signal and its mean instantaneous power computed considering only its main frequency components [0 Hz and 25 Hz], (b) amplitude of the FFT of the squared signal.

The spectrum shows significant components only at the nil frequency and at the cyclic frequency $\alpha_0 = 25\ Hz$. Therefore, the FFT of the instantaneous power signal highlights clearly the cyclic frequency α_0. Figure 4-2 (a) reports also the mean instantaneous power calculated with Eq. 4.2 where the set A contains the two frequencies 0 Hz and 25 Hz, i.e. the only two frequencies which have shown a significant amplitude in the FFT. Therefore, in the cyclostationary analysis the mean power is not a constant value averaged over time, as in the stationary analysis, but a time-dependent signal which extracts the periodic trends related to the cyclic frequencies.

At this point a general definition of cyclostationarity can be given. In the following definition, a slight difference exists between a signal that exhibit cyclostationarity at the cyclic frequency α and a signal which is cyclostationary at cyclic frequency α.

Definition 2. A signal is said to exhibit cyclostationarity at the cyclic frequency α if after the application of linear and non-linear transformation it shows periodic components at that cyclic frequency. In particular, a signal is said to be cyclostationary at the cyclic frequency α if the set A of cyclic frequencies contains only α and its integer multiples.

The cyclostationary analysis looks for *hidden periodicities* in the signal by applying a transformation and then trying to extract the periodic components at specific cyclic frequencies. In the case of example 1, the transformation was the squaring operator (a second-order transformation) to compute the signal power and the cyclic frequency was $\alpha_0 = 25\ Hz$.

Different orders of cyclostationarity can be defined. The order of cyclostationarity depends on the order of the transformation applied to generate periodic components. The signal of example 1 showed periodic components after applying the squaring operator and therefore it is *second-order cyclostationary (CS2)*. A *first-order cyclostationary (CS1)* signal can also be defined, in this case the signal contains periodic components when a linear transformation is applied. This linear transformation can be the *do-nothing* operator, therefore, a CS1 signal is simply a signal which contains periodic components. Considering the signal of example 1, it is CS2, but, since it is completely random, it is not CS1. Finally, higher-orders cyclostationary signal can be defined in the same way.

4.1.2 The Cyclic Modulation Spectrum

This paragraph introduces the *Cyclic Modulation Spectrum (CMS)*, which is one of the most important tools to detect and represent CS2 signals. In the previous paragraph, it was shown that second-order cyclostationarity refers to the presence of periodic components in the signal power.

In most cases, the acceleration signals issued by mechanical systems show second-order cyclostationarity because the cyclic phenomena which happen within the systems induce a periodic energy release. Therefore, in dealing with signals collected from mechanical systems, the analysis of second-order cyclostationarity is the most important along with the analysis of first-order cyclostationarity.

Let us consider a generic signal $x(t)$ and its filtered versions $x_{\Delta f}(t;f)$, which are obtained through filters with bandwidth Δf and centered at frequency f. Starting from these filtered signals, the cyclic modulation spectrum $P_x^{\alpha}(f;\Delta f)$ is defined by Eq. 4.3:

$$P_x^{\alpha}(f;\Delta f) = \lim_{T\to\infty}\frac{1}{T}\int_T \left|x_{\Delta f}(t;f)\right|^2 \cdot e^{-j2\pi\alpha t}dt \qquad 4.3$$

Basically, the CMS is the Fourier coefficient evaluated at frequency α of the power of the filtered version of the signal around the central frequency f. This spectrum is function of two frequencies: the frequency f is referred to as the *spectral frequency*, while the frequency α is referred to as the *cyclic frequency*. The spectral frequency is related to the frequency components of the signal, while the cyclic frequency is related to the periodic variation in the signal power. The CMS indicates, for each spectral frequency, which are the modulating frequencies of the signal power and with which intensity. Therefore, the spectral frequency f can also be interpreted as the carrier frequency, while the cyclic frequency α is the modulating frequency. The analysis of the CMS of a signal can reveal immediately if the considered signal is CS2; if non-zero coefficients at cyclic frequency $\alpha \neq 0$ are present, it means that the signal exhibits cyclostationarity at that cyclic frequency. Furthermore, the analysis of CMS reveals the set A of cyclic frequencies which modulate the signal power. It has to be noted that the coefficients of CMS depend on the bandwidth Δf of the filter.

In the case of a finite-length discrete signal $x[n]$, an estimate $\widehat{P_x^{\alpha}}(f;\Delta f)$ of the CMS can be computed with Eq. 4.4 [4.6]:

$$\widehat{P_x^{\alpha}}(f;\Delta f) = \frac{1}{I}\sum_{i=1}^{I}\left|X_{N_w}(t_i;f;\Delta f)\right|^2 \cdot e^{-j2\pi\alpha t_i} \qquad 4.4$$

Where $X_{N_w}(t_i;f;\Delta f)$ is defined by Eq. 4.5:

$$X_{N_w}(t_i; f; \Delta f) = \sum_{n=iR}^{iR+N_w-1} w_i[n] \cdot x[n] \cdot e^{-j2\pi fn} \qquad 4.5$$

Basically, $X_{N_w}(t_i; f; \Delta f)$ is the Short-Time Fourier Transform (STFT) of the signal $x[n]$ and $w_i[n]$ is a data-tapering window (for example the Hamming window) of length N_w with the following property:

$$w_i[n] = w[n - iR] \qquad 4.6$$

In these equations, the parameter R is defined so as to create a desired overlap between two consecutive blocks and I is the number of overlapping blocks. Therefore, the estimate of the CMS given by Eq. 4.4 is the Discrete-Time Fourier Transform (DTFT) of the quantity $\left|X_{N_w}(t_i; f; \Delta f)\right|^2$ which is known as the *spectrogram* of the signal $x[n]$.

The spectrogram of the signal of example 1 is reported in Figure 4-3 (a). The spectrogram was computed with a Hanning window and an overlap equal to 2/3 of the window length; the time resolution of the STFT is $\Delta t = 5.2\, ms$ and the frequency resolution $\Delta f = 32\, Hz$. The spectrogram gives a valid time-frequency representation of the signal from which the cyclic behavior at the cyclic frequency $\alpha_0 = 25\, Hz$ is clear. The CMS of the same signal is instead reported in Figure 4-3 (b); the CMS was computed through Eq. 4.4 with a spectral frequency resolution $\Delta f = 32\, Hz$, a cyclic frequency resolution $\Delta\alpha = 0.18\, Hz$ and a maximum detectable cyclic frequency $\alpha_{max} = 95.16\, Hz$. In Figure 4-3 a gray scale is used; a darker point corresponds to a higher value. The CMS presents a clear line at the cyclic frequency $\alpha_0 = 25\, Hz$ and therefore detects clearly the power modulation at that cyclic frequency over the spectral frequency interval $[2000 - 4000\, Hz]$ (the example 1 signal contains only these spectral frequencies by construction).

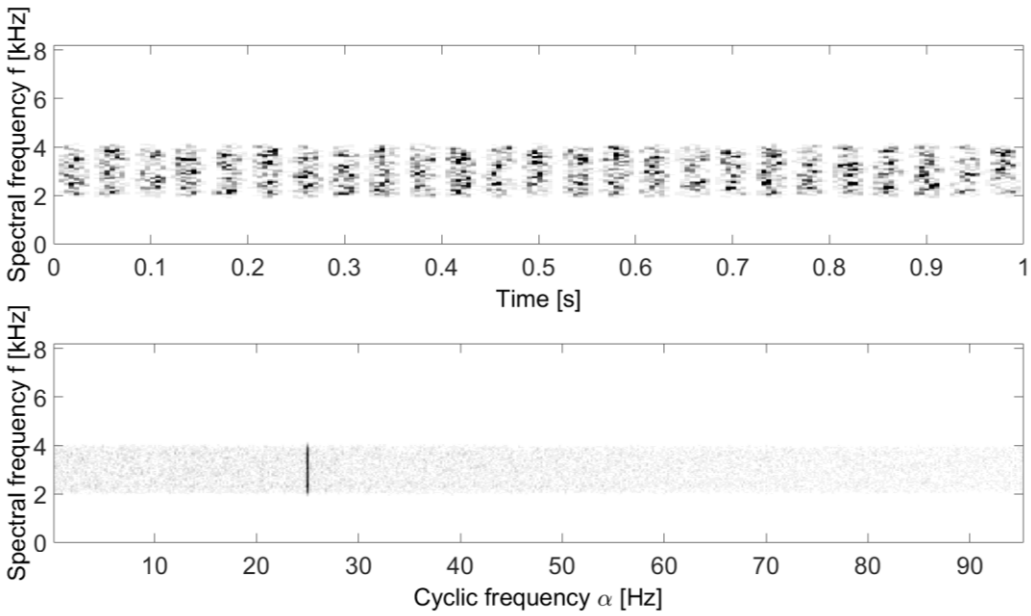

Figure 4-3: (a) Spectrogram $[u^2]$ of the example 1 signal ($\Delta f = 32\ Hz$, $\Delta t = 5.2\ ms$), (b) cyclic modulation spectrum $[u^2]$ of the same signal ($\Delta f = 32\ Hz$, $\Delta \alpha = 0.18\ Hz$, $\alpha_{max} = 95.16\ Hz$).

The CMS is an extremely powerful tool to analyze CS2 signals. However, the frequency resolution Δf and the time resolution Δt cannot be arbitrarily reduced, but they are constrained by the uncertainty principle [4.4] stated by Eq. 4.7:

$$\Delta f \cdot \Delta t \geq \frac{1}{4\pi} \tag{4.7}$$

This uncertainty principle defines a limit, Eq. 4.8, on the maximum cyclic frequency α_{max} which can be analyzed in the CMS:

$$\alpha_{max} \leq 4\pi \cdot \Delta f \tag{4.8}$$

It is now interesting to point out that the cyclostationary analysis expressed by the CMS generalizes the *envelope analysis* [4.7] which has been extensively used for the analysis of acceleration signals. The classical envelope analysis consists in band-pass filtering the signal around a specific spectral frequency and then computing the FFT of the absolute value of the signal. It is simple to note that the CMS returns, at the same time, the envelope spectra for all the spectral frequencies and, therefore, generalizes the envelope analysis.

4.1.3 The Spectral Correlation Density

This paragraph introduces a valuable tool for the analysis of CS2 signals, i.e. the *Spectral Correlation Density (SCD)*. This tool exploits the key property that the amplitude modulation in the time domain corresponds to a correlation in the frequency domain as will be showed after in this section.

Let us consider a generic discrete signal $x[n]$ where L is the signal length and Δ is the time between two consecutive samples. The second-order analysis of a cyclostationary signal can be summarized by the analysis of the s*ymmetric instantaneous auto-correlation function* presented in Eq. 4.9:

$$R_x[n;\tau] = E\left\{x\left[n+\frac{1}{2}\tau\right]x\left[n-\frac{1}{2}\tau\right]^*\right\} \quad 4.9$$

In this equation, E indicates the expected value operator which in the context of cyclostationarity has to be interpreted as an *ensemble average* and not as a time average [4.8]. Ensemble average means that the expected value is computed by considering a series of different repetitions of the stochastic process (in particular, a series of acquired signals or, at least, an acquisition which covers a series of *cycles*) and then averaging them together. The symbol $*$ indicates the complex conjugate. The instantaneous auto-correlation function considers the interaction between two values of the signal spaced apart by the time-lag τ. The instantaneous autocorrelation function applies a second-order transformation and therefore its study refers to a CS2 analysis. The instantaneous autocorrelation function can also be exploited for a definition of second-order cyclostationarity [4.5].

Definition 3. Random signals with periodic auto-correlation function are CS2 signals. For these signals, the property described in Eq. 4.10 holds:

$$R_x[n;\tau] = R_{2x}[n+N;\tau] \quad 4.10$$

Where N is the cycle length.

Given the property of definition 3, the instantaneous auto correlation function of CS2 signals accepts a Fourier series whose coefficients can be calculated through Eq. 4.11:

$$R_x[\tau;\alpha_i] = \lim_{L\to\infty}\frac{1}{L}\sum_{n=-L/2}^{L/2} R_x[n;\tau]\cdot e^{-j2\pi\alpha_i n\Delta} \qquad 4.11$$

These Fourier coefficients are called *cyclic auto-correlation function* because they are different from zero only for the cyclic frequencies $\alpha_i \in A$. In the particular case $\alpha_i = 0$, the cyclic auto-correlation function is equivalent to the conventional auto-correlation function considered in the stationary approach. Therefore, the cyclic auto-correlation function is an extension of the conventional auto-correlation function and extracts the periodic components of the instantaneous auto-correlation function at each time lag τ.

The CMS demonstrated that CS2 signals can be effectively represented in the f, α plane. To obtain a frequency descriptor from the cyclic auto-correlation function, the time lag τ needs to be converted into the spectral frequency f. This is done be computing the DTFT of $R_x[\tau;\alpha_i]$, thus obtaining the *spectral correlation density* $SC_x(f;\alpha_i)$:

$$SC_x(f;\alpha_i) = \Delta\sum_{\tau\to-\infty}^{+\infty} R_x[\tau;\alpha_i]\cdot e^{-j2\pi f\tau\Delta} \qquad 4.12$$

This formulation of the SCD makes difficult the explanation of the terminology spectral correlation, therefore, an equivalent formulation, based on the Cramér's spectral decomposition [4.5], is given in Eq 4.13:

$$SC_x(f;\alpha_i) = \lim_{L\to\infty}\frac{1}{L\Delta}E\left\{X_L\left(f+\frac{1}{2}\alpha_i\right)X_L\left(f-\frac{1}{2}\alpha_i\right)^*\right\} \qquad 4.13$$

Where $X_L(f)$ is the DTFT of the signal x[n]:

$$X_L(f) = \Delta\sum_{n=0}^{L-1} x[n]\cdot e^{-j2\pi fn\Delta} \qquad 4.14$$

This alternative formulation shows that the SCD quantifies the correlation between the spectral components centered at the spectral frequency f and spaced apart by the cyclic frequency α_i. Indeed, a periodic carrier at frequency f_0 whose amplitude is modulated with frequency α_0 is equivalent to two periodic carriers at frequency $f_0 + (1/2)\alpha_0$ and $f_0 - (1/2)\alpha_0$ (and the corresponding components in the negative frequencies) as shown in Eq. 4.15:

$$x(t) = \cos(\pi\alpha_0 t) \cdot \cos(2\pi f_0 t) = \frac{1}{4}e^{j2\pi(f_0+\alpha_0/2)t} + \frac{1}{4}e^{-j2\pi(f_0+\alpha_0/2)t} + \frac{1}{4}e^{j2\pi(f_0-\alpha_0/2)t} + \frac{1}{4}e^{-j2\pi(f_0-\alpha_0/2)t} \quad 4.15$$

This equation shows the fundamental link between the most important CS2 tools, i.e. the CMS and the SCD.

When an actual signal is considered, the signal length *L* is finite and Eq. 4.13 cannot be directly used for computing the SCD. In this work, the Welch's method [4.5], based on the *averaged cyclic periodogram* [4.9], is used for computing an estimate $\widehat{SC}_x(f;\alpha;L)$ of the SCD:

$$\widehat{SC}_x(f;\alpha_i;L) = \frac{1}{K\Delta}\sum_{k=0}^{K-1} X_{N_w}^{(k)}\left(f+\frac{1}{2}\alpha_i\right) X_{N_w}^{(k)}\left(f-\frac{1}{2}\alpha_i\right)^* \quad 4.16$$

Where $X_{N_w}^{(k)}(f)$ is the short-time DTFT of the windowed signal $x[n]$:

$$X_{N_w}^{(k)}(f) = \Delta \sum_{n=kR}^{kR+N_w-1} w_k[n]x[n] \cdot e^{-j2\pi f n\Delta} \quad 4.17$$

$w_k[n]$ is a window (for example the Hanning window) with the following property:

$$w_k[n] = w[n-kR] \quad 4.18$$

Where N_w is the window length, *R* is defined so as to create the desired overlap between two consecutive segments and *K* is the number of segments. The computational time required for the estimation of the SCD could be a limit for its implementation for onboard diagnostics; this aspect is addressed in [4.10].

It is worth mentioning another tool directly derived from the SCD, i.e. the *Cyclic Spectral Coherence (CSC)* which is defined in Eq. 4.19:

$$\gamma_x(f;\alpha_i) = \frac{SC_x(f;\alpha_i)}{\left(SC_x\left(f+\frac{1}{2}\alpha_i;0\right)SC_x\left(f-\frac{1}{2}\alpha_i;0\right)\right)^{1/2}} \quad 4.19$$

The CSC is a complex value with the same phase of the SCD, but with a normalized magnitude limited between 0 and 1. The amplitude of the CSC is normalized through the value of the frequency components which are considered in the SCD so as to keep it independent by scale effects. Therefore, $|\gamma_x(f;\alpha_i)|$ can be considered a measure of the *degree of second-order cyclostationarity*; the closer its value to one the higher the statistical link between the two frequencies centered at frequency f and spaced apart by the cyclic frequency α_i.

The magnitudes of the SCD and the CSC of the signal of example 1 are reported in Figure 4-4.

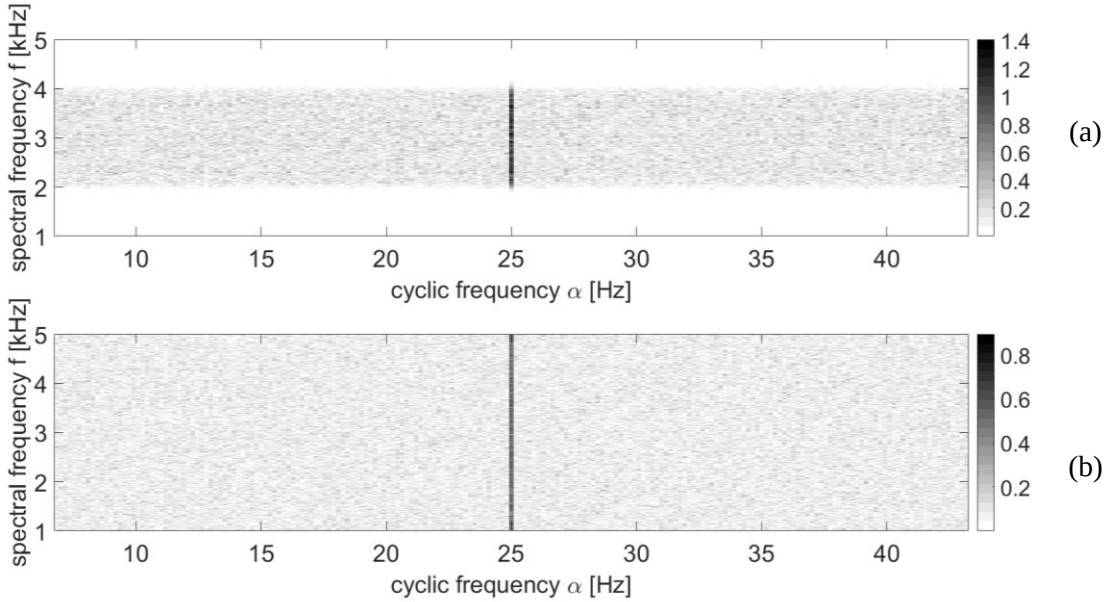

Figure 4-4: (a) Magnitude of the spectral correlation density $[u^2/Hz]$ of the example 1 signal ($\Delta f = 5.46\ Hz$, $\Delta\alpha = 0.18\ Hz$), (b) magnitude of the cyclic spectral coherence $[null]$ of the same signal ($\Delta f = 5.46\ Hz$, $\Delta\alpha = 0.18\ Hz$).

Both the SCD and the CSC highlight in an extremely clear manner the cyclic frequency $\alpha_0 = 25\ Hz$. It has to be noted that the CSC highlights the cyclic frequency α_0 even outside of the spectral support $[2000 - 4000\ Hz]$ and this is due to the normalization effect described above.

4.2 Blind Signal Extraction

The acceleration signals are considered in many applications for the condition monitoring and the diagnostics of mechanical systems. These acceleration signals (it is also the case of noise signals) are the result of excitations due to many sources. Let us consider the complex case of an

internal combustion engine [4.11, 4.12]; the acceleration signal acquired by means of an accelerometer installed on a precise position on the engine is caused by the gas combustion, the reciprocating motion of the pistons, the contacts forces in the cam mechanism and so on. Therefore, the acquired acceleration signals contain contributions due to all these phenomena. From one end, the signal is very rich of information which can be used for condition monitoring or diagnostic purposes, but, on the other end, all these contributions are mixed together and therefore the information carried by the signal is of difficult interpretation.

The objective of the *Blind Source Separation (BSS)* [4.13] is to extract all the independent sources from the analysis of the output measurements. The independent sources are the physically different excitation forces, while the output measurements are the accelerations signals acquired in different positions and different directions. The objective of BSS is extremely ambitious in the case of mechanical systems because there are many sources and their number is hardly even known; a list of the challenges for the application of BSS techniques in the field of mechanical systems is reported in reference [4.13]. However, in many applications, the complete knowledge of the sources is not required, and the ambition of the BSS can be reduced. Instead of extracting the set of independent sources, we can focus on extracting the independent contribution of any source on each observation signal, this introduce the concept known in the literature as *Blind Component Separation (BCS)* or *Blind Signal Extraction (BSE).*

The methodology proposed in this work for the separation of the different components of an acceleration signal follows the general guideline proposed by Antoni in [4.8]. A generic acceleration signal $x[n]$ is decomposed in three main components as illustrated in Eq. 4.20:

$$x[n] = p[n] + c[n] + n[n] \qquad 4.20$$

- $p[n]$ is the *predictable part* of the signal, this is also the *CS1 part*, i.e. the periodic part, of the signal;
- $c[n]$ is the *CS2 part* of the signal defined over the set A of cyclic frequencies of interest;
- $n[n]$ is the *remaining noise* which contains the contributions which are not of interest, or anyway which are not included in $p[n]$ or in $c[n]$, this part can also contain CS2 contributions which are related to cyclic frequencies not included in the set A.

The proposed decomposition scheme is particularly suitable for the analysis of acceleration signals; Eq. 4.20 is also a valid scheme for modelling acceleration signals. Only the CS1 and the CS2 components are considered because they are the most relevant in acceleration signals; the contribution at higher orders are usually negligible. The three components contain the

contributions of different sources; for example, in rotating machines, the periodic component is usually linked to imbalances, misalignments, eccentricities, etc., while the CS2 part is due to other phenomena like wear, friction forces, fluid turbulence, etc. Typical is the example of the gearbox [4.14, 4.15] where the contributions due to the gear meshing are CS1 and therefore included in $p[n]$, while the contributions due to the ball bearings are CS2 and therefore included in $c[n]$.

The application of the proposed methodology allows the separation of different contributions which then can be analyzed with the most suitable tools. In particular, the periodic part of the signal can be effectively analyzed with the classical Fourier spectrum and do not need the cyclostationary approach presented in the previous paragraph. The CS2 part instead can be analyzed with the CS2 tools previously introduced (cyclic modulation spectrum, spectral correlation density and cyclic spectral coherence). The separation of the different parts is also important so as to eliminate the mutual interferences which can cause misleading results in their analysis. In particular, it is a key point to extract the predictable part before analyzing the CS2 part [4.8].

4.2.1 Extraction of the Periodic Component

The extraction of the predictable part $p[n]$ of the acceleration signal consists in extracting its periodic part (CS1 part). The predictable part of the signal corresponds to its expected value:

$$p[n] = E\{x[n]\} \tag{4.21}$$

Where the expected value operator E refers to *ensemble average* and not to time average. The ensemble average is computed by averaging different repetitions of the same stochastic process. The problem is how to compute the expected value when only one repetition of the process is available. Since the expected value is the periodic part of the signal, it can be computed through the operator P which extracts all the periodic components of the signal; this is true under the hypothesis of *cycloergodicity*. The property of cycloergodicity for cyclostationary signals is equivalent to ergodicity for stationary processes; therefore, for a cyclostationary and cycloergodic signal $x[n]$, the ensemble average is equivalent to the *infinite cycle average* [4.8]:

$$p[n] = E\{x[n]\} = P\{x[n]\} = \lim_{K\to\infty} \frac{1}{2K+1} \sum_{k=-K}^{K} x[n+kN] \tag{4.22}$$

Where N is the cycle length and K is the number of considered cycles. It must be noted that this formulation extracts only the periodic components which are multiples of the cycle, which therefore needs to be known a priori. In the case of the hydraulic pump considered in this work, the basic cycle corresponds to one shaft revolution. In general, for rotating machines, *the basic cycle* can be calculated considering the kinematics of the machine.

4.2.1.1 Synchronous Average

The simplest and most adopted [4.8, 4.16] technique for the calculation of an estimate of the predictable part $\hat{p}[n]$ is the *Synchronous Average (SA)*. Given a signal $x[n]$ of finite-length L corresponding at K cycles of N samples each, the SA is expressed by Eq. 4.23:

$$\hat{p}[n] = E\{x[n]\} = \frac{1}{K}\sum_{k=0}^{K-1} x[m + kN] \qquad 4.23$$

Where the m variable resets at the end of each cycle and it is constrained in the range $[0, N-1]$:

$$m = n - \left\lfloor \frac{n}{N} \right\rfloor N \qquad 4.24$$

Basically, the SA is the cycle average computed on a finite number of cycles (this is always the case for actual signals). An equivalent expression in the frequency domain [4.8] is reported in Eq. 4.25:

$$\hat{p}[n] = E\{x[n]\} = \sum_{k=0}^{[N-1]} e^{j2\pi knK/L} \frac{1}{L}\sum_{m=0}^{L-1} x[m] e^{-j2\pi kmK/L} \qquad 4.25$$

From this expression, it is clear that the SA is only able to extract the predictable part at frequencies which are integer multiples of the cycle. The mathematical implementation of the SA is simple, but it faces some practical problems. Both formulation require an extremely precise estimation of the cycle length N and both require L and K to be integers; furthermore, Eq. 4.23 requires also N to be integer. All these conditions are easily satisfied if the acceleration signal is acquired with an angular sampling; in this case N is integer and is also known exactly since it depends on the acquisition system. If a time sampling is adopted, in general N is not an integer and needs to be estimated since it depends on the sampling frequency and the machine angular

velocity. Some angular resampling techniques [4.17] are available in order to make N an integer and use Eq. 4.23 to compute the SA. These techniques require a tachometer signal, of at least one sample per cycle, to create a precise link between time and angular position. However, not always a tachometric signal is available. Some attempts of computing the angular resampling without a tachometric signal have been done [4.18, 4.19], but the obtained results showed some limitation in comparison to classical angular resampling techniques.

It is important to note that, in rotating machine, the acceleration signals are theoretically cyclostationary in the angular domain and not in the time domain. Indeed, the phenomena which excite the output signal are cyclic with reference to the angular position and not necessarily to the time variable. This point becomes particularly important when the machine angular velocity is not perfectly constant over time, but it experiences some fluctuations. For this reason, an angular sampling, or an angular resampling, is required for a proper analysis of machine signals.

4.2.1.2 Other Methodologies

The task of extracting the predictable part from acceleration signals finds a lot of applications and therefore many methodologies have been proposed in the literature. Some of these methodologies are listed in this paragraph without giving the details of their implementation which can be found in the cited references.

The extraction of the predictable part $\hat{p}[n]$ can be performed by means of a *comb filter* [4.8] in the frequency domain. The transfer function $H(f)$ of the comb filter is described by Eq. 4.26 when the number of considered cycles K tends to ∞:

$$H(f) = \begin{cases} 1 & f = \frac{k}{T}, k \in Z \\ 0 & elsewhere \end{cases} \qquad 4.26$$

Where T is the time cycle. It is worth noting that the time domain SA leads to an identical transfer function when K tends to ∞.

The two methodologies presented so far can extract the periodic components which are integer multiples of the cycle. Some *adaptive algorithms* have been proposed to extract any periodic component present in the signal. These adaptive algorithms, also called *blind algorithms*, are particularly important in machine when it is impossible to define a common cycle for all the periodic phenomena (the common cycle is theoretically infinite or extremely long). All these algorithms are based on the *prediction theory* and the most relevant among them is the *Self-*

Adaptive Noise Canceler (SANC) presented in [4.20]. This algorithm is based on the concept that a periodic component is fully predictable in the future and therefore can be inferred from the knowledge of a past segment of the signal. On the other end, the random part of a signal is uncorrelated with a past segment of the signal and therefore, when a limit delay is reached, the best estimation of the random part is zero and the estimation error equals the signal itself. This algorithm therefore allows to decompose the signal in its deterministic (periodic) part and its non-deterministic (random) part. A frequency version of this algorithm is presented in the reference [4.21].

4.2.2 Extraction of the CS2 Component

The methodologies presented in the previous paragraph extract the predictable part $p[n]$ of a signal; by subtracting this component to the raw signal $x[n]$, the *residual part* $r[n]$ is obtained:

$$r[n] = x[n] - p[n] \tag{4.27}$$

Since the CS1 component of the signal has been removed, $r[n]$ contains only *pure CS2* components or higher-order cyclostationary components along with noise:

$$r[n] = c[n] + n[n] \tag{4.28}$$

Here the distinction between *pure* and *impure* cyclostationarity needs to be clarified.

Definition 4. In simple words, a signal is said to be *purely cyclostationary* at order n, if its cyclostationarity (definition 2) at order n is not due to lower order cyclostationary components. A formal definition based on the cumulant theory was given by Gardner [4.22]

Following this definition, the signal of example 1 is purely cyclostationary at order two, because it is a CS2 signal and it is not a CS1 signal. The residual signal does not contain CS1 components since they are all removed by subtracting the predictable part, therefore, the CS2 components are also pure CS2 components.

In most cases, the acceleration signals issued from rotating machines contain CS2 components due to the power modulations caused by the internal phenomena synchronized with the machine angular velocity. The CS2 components related to a source exhibit the second-order cyclostationarity over the set of cyclic frequencies which characterizes the source; different sources refer to different set of cyclic frequencies. In condition monitoring and diagnostic

problems, only one CS2 component is of interest, i.e. the component over the set of cyclic frequencies related to the analyzed source. For instance, if our focus is to detect a bearing fault in a gearbox, we will consider the CS2 components at the bearing cyclic frequencies and we will not consider the CS2 components related, for example, to the gears meshing. In this paragraph, some methodologies for extracting the desired CS2 component $c[n]$ from the residual signal are presented. The remaining noise $n[n]$ includes also the CS2 components which do not refer to the cyclic frequencies of interest (these components are referred to as *interferences*).

The existing methodologies for the extraction of the CS2 part take advantage of the spectral correlation (also called *spectral redundancy*) of CS2 signals, in the same way as the periodicity is exploited for the extraction of the CS1 component. Three are the most important methodologies in the literature: Multiple Cyclic Regression (MCR) [4.23], SUBspace BLind Extraction (SUBLEX) [4.24] and Reduced-Rank Cyclic Regression (RRCR) [4.25]. All these three methodologies are said to be *blind* because they do not require any information neither about the noise nor the interferences. The only requirement is the knowledge of the cyclic frequency of the *Signal of Interest (SOI)* to be extracted; for a proper and effective extraction, this cyclic frequency must not be shared with any other *undesired* source. The RRCR algorithm was designed as a combination of MCR and SUBLEX, and it is demonstrated in [4.25] that the RRCR algorithm outperforms the other two methodologies. In the single sensor case, i.e. when only one output measurement is available, the RRCR algorithm is equivalent to the MCR algorithm. Since in this work only the single sensor case is investigated, the MCR algorithm is considered for the extraction of the CS2 component. The details of the implementation of the MCR algorithm are given in the next section.

4.2.2.1 MCR Algorithm

The Multiple Cyclic Regression (MCR) algorithm takes advantage of the spectral redundancy of CS2 signals to extract the CS2 component of interest from the residual signal. In this case the SOI is the CS2 component at a precise cyclic frequency α_k which needs to be known a priori. The method separates the SOI form the other CS2 components at different cyclic frequencies (interferences) and the background noise. The cyclic frequency of the SOI needs to be known accurately and, if not already known, can be calculated by computing the SCD of the residual signal. It is important to point out that this algorithm should be applied on the residual signal, if a periodic component linked to the CS2 part of interest is present, the extracted result contains both CS1 and CS2 components.

In this paragraph the mono-sensor case of the MCR algorithm is presented, the general multi-sensors version of this algorithm is presented in [4.23]. This method combines several frequency-shifted versions of the residual signal $r(n)$ which are optimally filtered to yield the desired SOI. This method is similar to the application of a Linear Periodically Time-Varying (LPTV) Wiener filter [4.26]. The method starts by calculating several frequency-shifted versions of the residual signal as reported in Eq. 4.29:

$$a_k = r(n) \cdot e^{2\pi j \alpha_k n} \tag{4.29}$$

These frequency-shifted signals are complex vectors. The cyclic frequencies considered for the shifting are the cyclic frequency of interest; positive frequencies and the corresponding negative frequencies are considered. The null cyclic frequency is not considered and the number of cyclic frequencies K considered affects the extraction of the SOI as will be demonstrated later in this section. These frequency-shifted versions of the signal are then filtered and combined to obtain an estimate $\hat{c}(n)$ of the SOI as shown in Eq. 4.30:

$$\hat{c}(n) = \sum_{k=1}^{K} g_k(n) * a_k(n) \tag{4.30}$$

Where $*$ indicates the convolution operator. The summation is performed over the set of the considered cyclic frequencies $\alpha_k, k = 1 \cdots K$. The idea behind the MCR algorithm is that the averaging effects obtained through the summation of the frequency-shifted signals are destructive for the noise, but not for the SOI. To derive the set of filters $g_k(n)$, the filters are considered of a generic length L form τ_1 to τ_L, $L = \tau_L - \tau_1 + 1$, and written as $[Lx1]$ vectors:

$$\underline{g_k} = [g_k(\tau_1) \cdots g_k(\tau_L)]^T \tag{4.31}$$

The corresponding frequency-shifted signals can be written as a $[1\ x\ L]$ vectors as reported in Eq. 4.32:

$$\underline{a_k}(n) = [a_k(n - \tau_1) \cdots a_k(n - \tau_L)] \tag{4.32}$$

By combining Eq. 4.31 and 4.32, the estimate of the SOI $\hat{c}(n)$ can be calculated with the summation of matrix products reported in Eq. 4.33:

$$\hat{c}(n) = \sum_{k=1}^{K} \underline{a}_k(n) \cdot \underline{g}_k \tag{4.33}$$

The formulation can become even more compact by considering the extended vectors $\underline{g}$ $[LK\ x\ 1]$, for the filter, and $\underline{a}(n)$ $[1\ x\ LK]$, for the modulated signal, as reported in Eq. 4.34 and 4.35:

$$\underline{g} = \left[\underline{g}_1{}^T \cdots \underline{g}_K{}^T\right]^T \tag{4.34}$$

$$\underline{a}(n) = \left[\underline{a}_1(n) \cdots \underline{a}_K(n)\right] \tag{4.35}$$

Now $\hat{c}(n)$ is simply given by the matrix product reported in Eq. 4.36:

$$\hat{c}(n) = \underline{a}(n) \cdot \underline{g} \tag{4.36}$$

If the considered residual signal $r(n)$ is of length N, the MCR algorithm can be applied on $N - L + 1$ samples returning the SOI $\underline{\hat{c}}$ given by Eq. 4.37:

$$\underline{\hat{c}} = \boldsymbol{a} \cdot \underline{g} \tag{4.37}$$

Where $\underline{\hat{c}}$ is a $[N - L + 1\ x\ 1]$ vector as presented in Eq. 4.38, $\boldsymbol{a}$ is a $[N - L + 1\ x\ LK]$ matrix presented in Eq. 4.39 and $\underline{g}$ has already been presented in Eq. 4.34:

$$\underline{\hat{c}} = [\hat{c}(N + \tau_1) \cdots \hat{c}(1 + \tau_L)]^T \tag{4.38}$$

$$\boldsymbol{a} = \left[\underline{a}^T(N + \tau_1) \cdots \underline{a}^T(1 + \tau_L)\right]^T \tag{4.39}$$

The matrix $\boldsymbol{a}$ is completely known from the frequency-shifted signals, the vector $\underline{g}$ containing the KL parameters of the optimal filters needs instead to be calculated. The filters parameters can be calculated through Eq. 4.40:

$$\boldsymbol{C_{a,a}} \cdot \underline{g} = \underline{C}_{a,r} \tag{4.40}$$

Where the $[LK\ x\ LK]$ matrix $\boldsymbol{C_{a,a}}$ and the $[LK\ x\ 1]$ vector $\underline{C}_{a,x}$ are described in Eq. 4.41:

$$\boldsymbol{C_{a,a}} = \boldsymbol{a}^H \cdot \boldsymbol{a}; \quad \underline{C_{a,r}} = \boldsymbol{a}^H \cdot \underline{r} \tag{4.41}$$

The unknown correlation vector $\underline{C_{a,r}}$ can be calculated with the signal $r(n)$ instead of the signal $c(n)$ provided the assumption that the SOI is uncorrelated with the noise. The vector of the filter parameters can be obtained by inverting the matrix $\boldsymbol{C_{a,a}}$; the complexity of the inversion of this matrix increases with the number LK of filters parameters.

The MCR algorithm for the mono-sensor case described by Eq. 4.29-4.41 was implemented in the Matlab® software and its performances were evaluated on the following example.

Example 2. Let us consider the synthetic signal $x(n)$ of length $N = 81920$ (to simulate an acquisition of 5 s with a sampling frequency $f_s = 16384\ Hz$). This signal is composed of a pure CS2 part $c(n)$ with cyclic frequency $\alpha = 225\ Hz$ and a noise part $n(n)$ as presented in Eq. 4.42:

$$x(n) = c(n) + n(n) \tag{4.42}$$

The CS2 part is given by Eq. 4.43:

$$c(n) = n_c(n) \cdot \sin\left(\pi j \alpha \frac{n}{f_s}\right) \tag{4.43}$$

The two signals $n(n)$ and $n_c(n)$ are two white noise signals with mean power 2 and with frequency support $[2000 - 4000\ Hz]$ and $[5000 - 7000\ Hz]$ respectively. The signals $n(n)$, $c(n)$ and $x(n)$ are plotted in Figure 4-5 for a period of 0.12 s while the their FFT are reported in Figure 4-6.

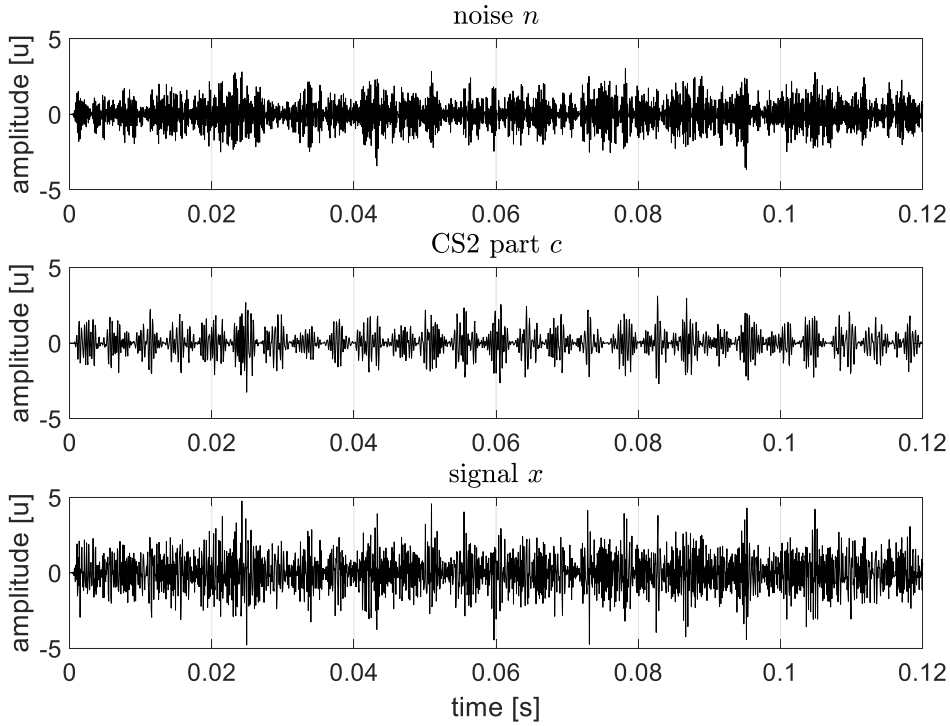

Figure 4-5: The noise component $n(n)$, the CS2 part $c(n)$ and the signal $x(n)$ of example 2.

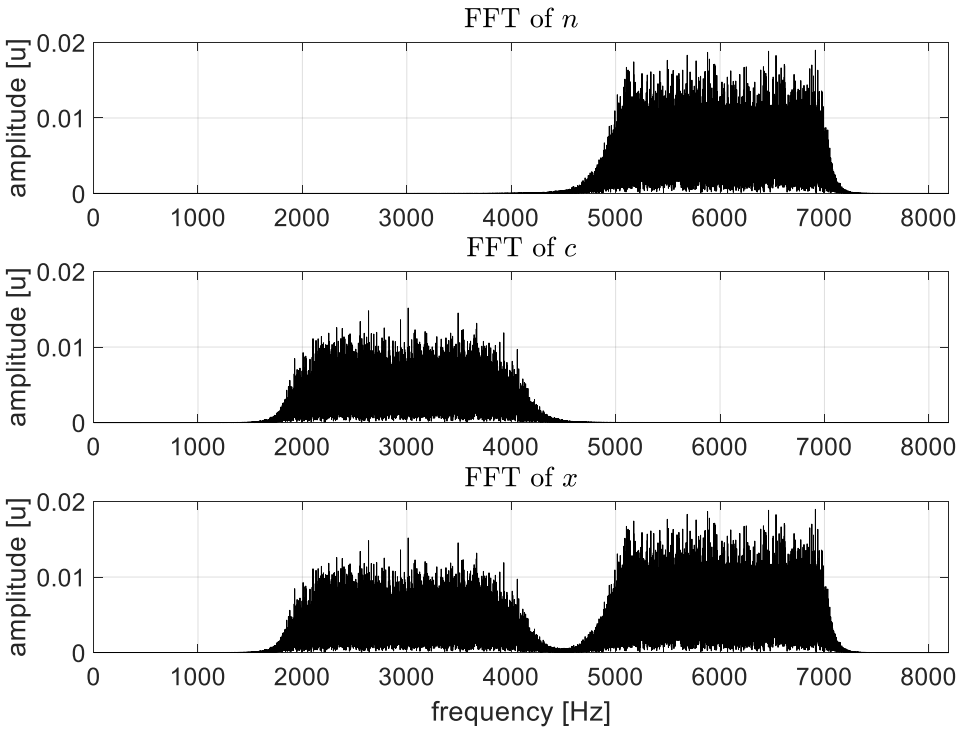

Figure 4-6: FFT of the noise $n(n)$, the CS2 part $c(n)$ and the signal $x(n)$ of example 2.

The beating phenomenon at frequency α of signal $c(n)$ is masked by the noise in the signal $x(n)$. From the FFT, it can be noted that all the signals are completely random in nature.

The described MCR algorithm was used to extract the CS2 component of signal $x(n)$ from the noise. The extraction capability of the algorithm depends on the value of the filter length L and the number of frequency shifts K, therefore the method was applied by varying these two parameters and the results were compared. The quality of the extraction was quantified with the normalized Mean Squared Error (MSE) between the estimate $\hat{c}[n]$ and the actual CS2 part $c[n]$ described in Eq. 4.44 and the results are reported in Figure 4-7:

$$MSE_{norm} = \frac{\sum_{n=1}^{N-L+1}(\hat{c}[n] - c[n])^2}{\sum_{n=1}^{N-L+1} c[n]^2} \qquad 4.44$$

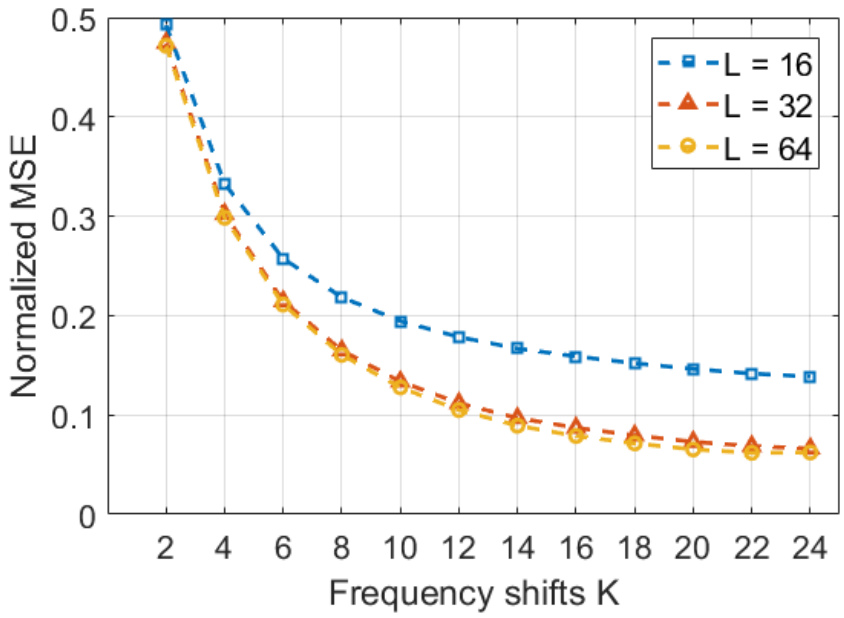

Figure 4-7: Normalized MSE for different values of the filter length L and the number of frequency shifts K.

The extraction performance of the MCR algorithm increases with the number of the frequency shifts K. The normalized MCR reduces with an increased filter length L, but the difference between $L = 32$ and $L = 64$ is small. The minimum value of the MSE was achieved with $L = 64$ and $K = 22$; indeed, when the product LK increases, the precision of the algorithm is affected by the errors in the inversion of matrix $\boldsymbol{C}_{a,a}$ whose dimension becomes important. The comparison

between the extracted signal $\hat{c}[n]$ and the actual CS2 part $c[n]$ obtained with $L = 64$ and $K = 22$ is reported in Figure 4-8.

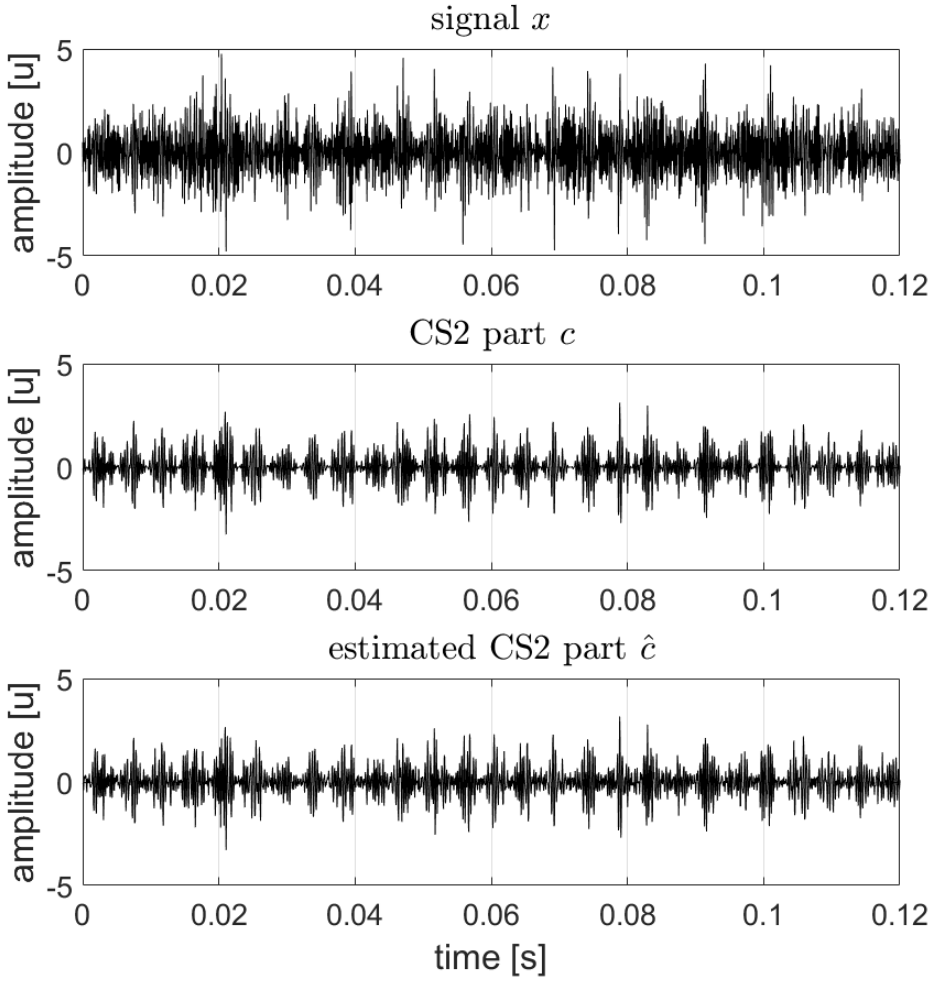

Figure 4-8: Comparison between the CS2 part c and the estimated CS2 part $\hat{c}$ with filter length $L = 64$ and number of frequency shifts $K = 22$.

In this case the extraction of the CS2 component is almost perfect. It has to be noted that the presented MCR algorithm allows the perfect extraction of the CS2 component only if the frequency supports of the CS2 part and the noise do not overlap like in example 2.

4.2.3 Proposed Analysis Procedure

This section synthetizes a procedure for the analysis of acceleration signals which combines the theory and the tools presented in the previous sections. This procedure decomposes the acquired signal in several components; each component has distinct characteristics and needs to

be analyzed with the proper tools. A block diagram of the proposed procedure is reported in Figure 4-9.

The first step of the procedure consists in obtaining an acceleration signal x function of the angular position θ. The signal $x(\theta)$ can be directly obtained through an angular sampling if a relative encoder is available to drive the acquisition. The use of an encoder is expensive and requires installation space; therefore, the angular sampling is not viable in most of the actual applications and its applicability is confined to laboratory tests. In actual applications, the time sampling of the acceleration signal $x(t)$ is simpler to perform. The signal $x(\theta)$ in the angular domain can be obtained through the application of one of the angular resampling procedures presented in [4.17]; these procedures require the availability of a tacho signal $T(t)$. The tacho signal could just be a signal with one impulse per revolution, or it could consist in multiple impulses per revolution; the more impulses the better in order to reduce the errors due to the angular velocity variation within each revolution.

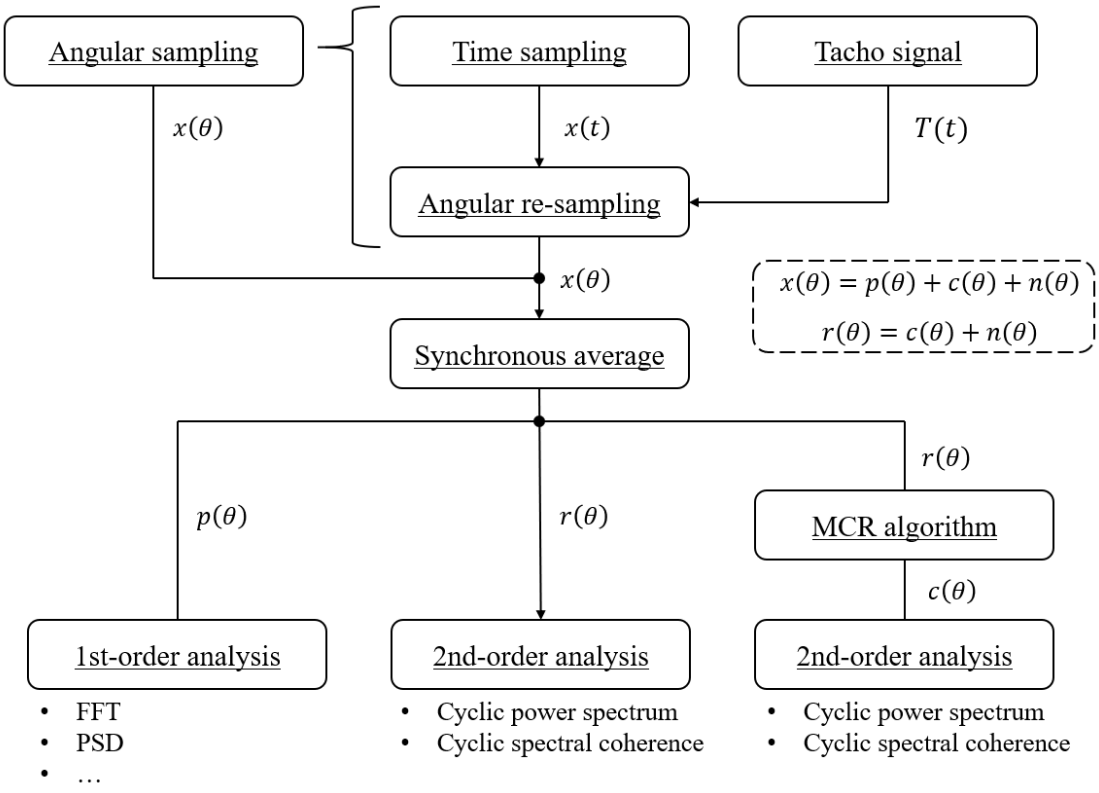

Figure 4-9: Block diagram of the proposed approach for the analysis of acceleration signals.

Once the signal $x(\theta)$ in the angular domain is available, the synchronous average $p(\theta)$ can be extracted with the algorithm presented in section § 4.2.1.1. The SA contains the CS1 components

of the signal and therefore must be analyzed with the standard tools for the frequency analysis, such as the FFT or the PSD. The residual signal $r(\theta)$ can be computed by subtracting the SA from the acceleration signal $x(\theta)$. The residual signal contains the CS2 components and the higher order cyclostationary components of the signal. The CS2 components can be analyzed through the tools presented in section § 4.2.2, such as the SCD and the CSC. It is important to subtract the SA before executing the analysis of the CS2 components because the presence of periodic components could alter the results of the CS2 analysis. The residual signal contains also the background noise which can make the results of the CS2 analysis less clear. The application of the MCR algorithm presented in section § 4.2.2.1 can be used to separate the CS2 component of interest form the background noise and the other CS2 components at different cyclic frequencies (interferences). If CS2 components at different cyclic frequencies are of interest, the MCR algorithm can be applied several times at different cyclic frequencies. The results of the MCR algorithm can be analyzed with the tools for the CS2 analysis.

This analysis procedure allows to separate the effects of different sources and analyze them avoiding interferences. Indeed, different faults induce different effects; for example, some faults could induce a modification of the periodic part of the signal, evident from the CS1 analysis, while other faults could induce a different power modulation of the signal, evident from the CS2 analysis.

4.3 Experimental Activity

The methodology proposed in section § 4.2.3 for the analysis of accelerations signal was applied on the data collected from two accelerometers installed on a variable-displacement axial-piston pump. The pump was tested both in healthy and faulty conditions and the final goal of the analysis was to extract suitable parameters for the pump diagnostics. This section presents the experimental layout and the experimental tests.

4.3.1 Experimental Layout

The hydraulic pump considered in this activity is the same pump considered for the activity on the thermodynamic method for the evaluation of the machine overall efficiency. The pump is the MVP 60-84 produced by the company Casappa®. This pump is of axial-piston swash plate type, with a maximum displacement of 84 cm^3. The pump is equipped with a hydro-mechanical LS regulator and was tested in load sensing configuration. All the tests carried out within this

project, were executed on the test bench available in the laboratory of the Industrial Department of the University of Parma.

Two piezoelectric accelerometers were installed on the pump case as illustrated in Figure 4-10.

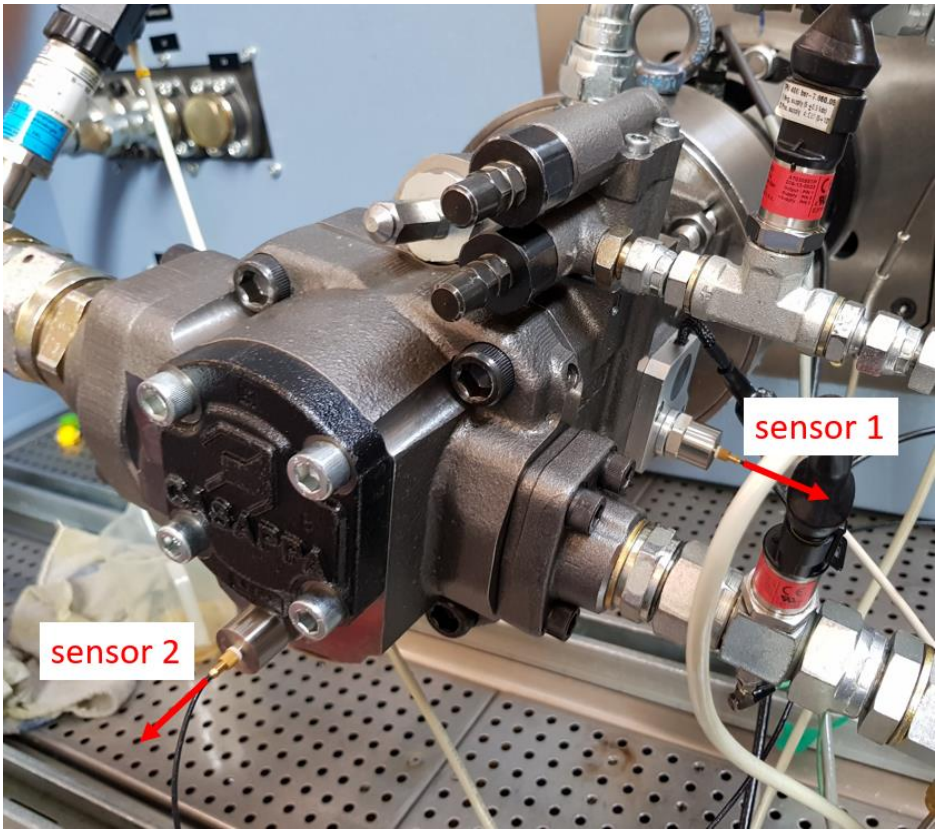

Figure 4-10: Position of the two accelerometers on the pump.

The accelerometer referred to as sensor 1 was installed on the angular sensor of the pump which measures the angular position of the swash plate; this sensor measures the accelerations in the direction of the suction-delivery flow. The second accelerometer (sensor 2 in the figure) is installed on the cover of the pump, at the hydraulic end, and measures the acceleration in the direction of the pistons. Both accelerometers are the Brüel & Kjær type 4370 with a bandwidth up to 10 kHz and a maximum continuous sinusoidal acceleration of 20000 m/s^2.

The acquisitions were performed using a relative encoder for the angular sampling. The installation of the relative encoder is illustrated in Figure 4-11.

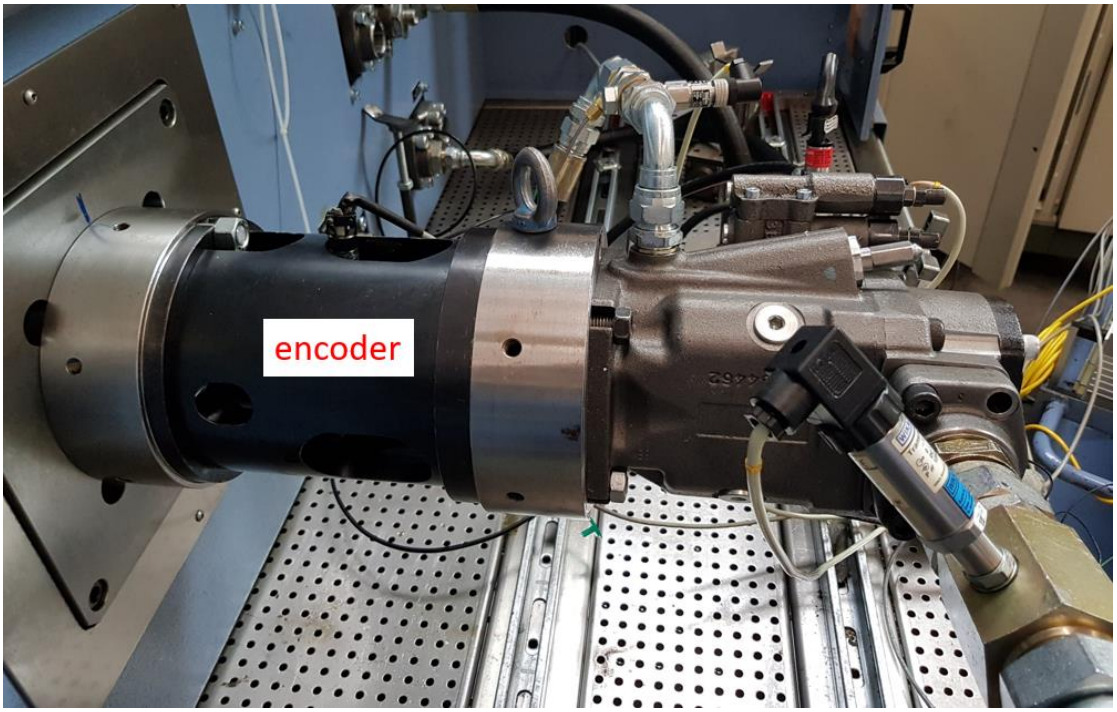

Figure 4-11: Installation of the relative encoder (within the black manifold).

The relative encoder counts 3600 steps per revolution corresponding to an angular resolution of 0.1 deg. The angular resolution of the relative encoder leads to very high sampling frequencies when the pump is operated at the most common operating conditions; for example, at 2000 r/min the sampling frequency is 120000 kHz. This sampling frequency is much higher than the frequency required to exploit the accelerometers bandwidth.

4.3.2 Experimental Tests

The pump was tested in flawless condition and in two faulty conditions. The two faults considered are: worn piston slippers and port plate eroded by cavitation. These two faults were already considered in the activity on the thermodynamic method for the calculation of pump efficiency. The two faulty conditions were obtained by introducing naturally worn components in the flawless pump. A photograph of the worn slippers, fault 1, is reported in Figure 4-12 while a photograph of the port plate eroded by cavitation, fault 2, is reported in Figure 4-13.

Figure 4-12: Photograph of the tested worn slippers (left), fault1, along with the slippers of the flawless pump (right).

Figure 4-13: Photograph of the tested port plate damaged by cavitation, fault 2.

The considered worn slippers, shown in the left photograph of Figure 4-12, have a rounded edge, in contrast to the sharp edge of the flawless slippers; furthermore, the worn slippers have a different height because of a different wear. The geometrical variations of the worn slippers can excite the pump case in a different manner, therefore inducing different vibrations. The damage due to cavitation in the port plate, Figure 4-13, is located between the delivery and the suction

holes and, in particular, in the transition from the delivery to the suction. The damage is quite light and consists of an erosion which can cause a reflux from the delivery to the suction. The flawless condition and the two faulty conditions were tested in the four different operating conditions reported in Table 4-1.

Table 4-1: Operating condition considered for the measurements of the accelerations in healthy and faulty conditions.

Angular velocity	Swash angle	Delivery pressure	
		150 bar	250 bar
1500 r/min	**12.8 deg**	✓	✓
2000 r/min	**12.8 deg**	✓	✓

For each acquisition, 900000 samples, corresponding to 250 revolutions, were acquired. The tests were repeated 10 times for each operating condition in order to assess the repeatability of the acquisitions and extract robust features for the fault identification.

4.4 Experimental Results

The objective of this section is to show how the proposed methodology for the analysis of acceleration signals can be used to identify the considered faults. In order to reduce the amount of data presented, two significant operating conditions are considered: the tests at 1500 r/min and 150 bar for sensor 1 and the tests at 2000 r/min and 150 bar for sensor 2. Results at other operating conditions are also shown to illustrate general trends.

4.4.1 Root Mean Square Values

A simple parameter that can be used for the fault detection is the RMS value of the acceleration signal. In this paragraph the RMS values for all the acquired signals are reported. The RMS values of the signals acquired with sensor 1 are reported in Figure 4-14, while the RMS values of the signals acquired with sensor 2 are reported in Figure 4-15.

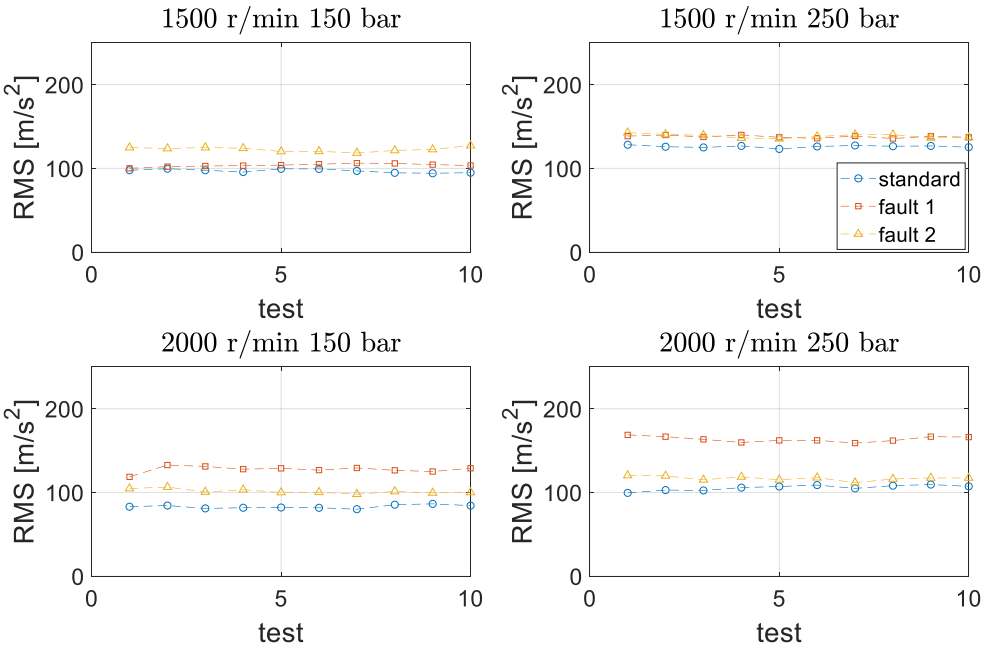

Figure 4-14: RMS values of the acceleration signals acquired with sensor 1.

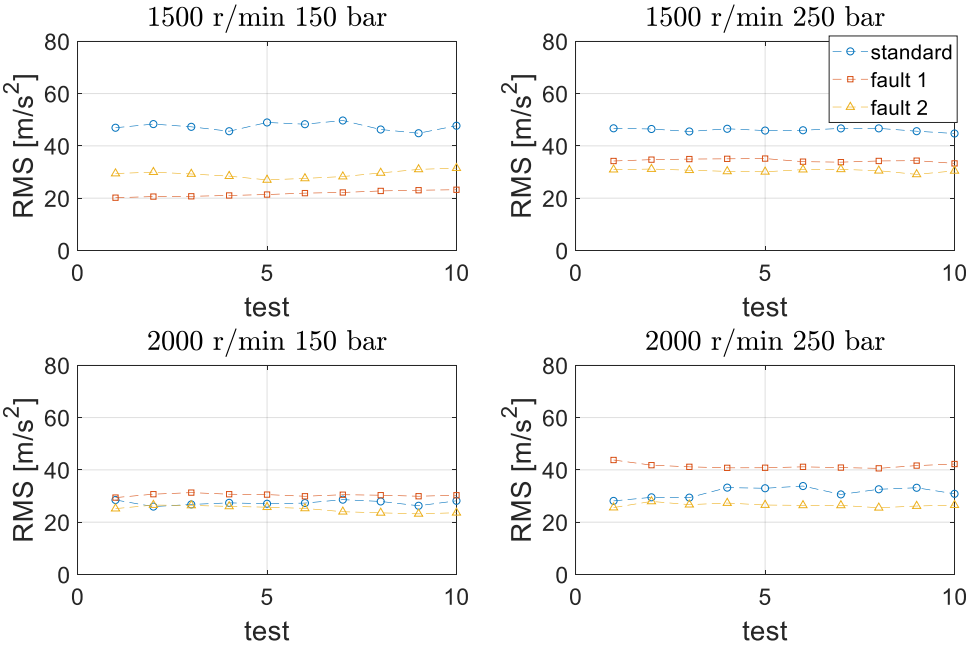

Figure 4-15: RMS values of the acceleration signals acquired with sensor 2.

For both sensors, a general and clear trend which can be used to identify a fault based on the RMS value does not exist; therefore, further analyses are required for the identification of the considered faults. The RMS value is a measure of the mean power of the signal and this information can be used to explain the different intensity of some parameters presented in the next sections.

4.4.2 Synchronous Average

The first step of the proposed methodology consists in the calculation of the SA to extract the CS1 components from the raw signal. The residual signal, obtained by subtracting the SA from the raw signal, contains only pure CS2, or higher-order, components. Figure 4-16 reports the raw signal, the SA and the residual signal for the signal acquired with sensor 1 in the case of flawless pump; the signals are reported over a period of two revolutions (720 deg).

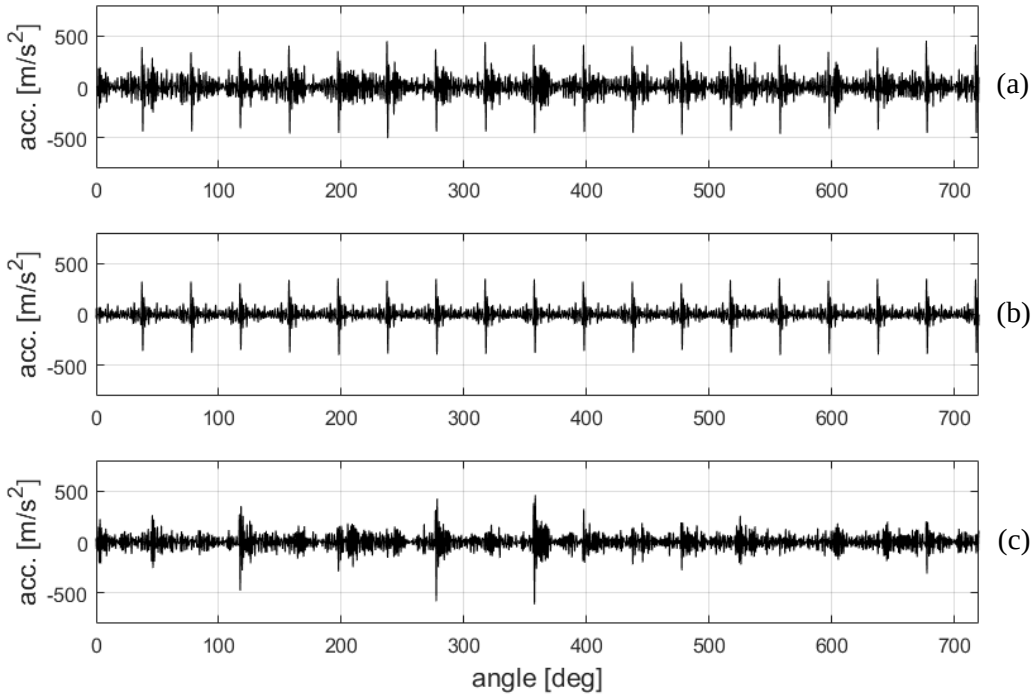

Figure 4-16: (a) Raw signal, (b) synchronous average and (c) residual signal for the signal acquired with sensor 1 in the case of flawless pump (1500 r/min, 150 bar).

The SA is a cycle average and is repeated two times to cover the period of 720 deg. The SA shows a clear periodic behavior at the piston frequency (9 impulses per revolution). The residual signal collects the random part of the signal and does not show any repeatable behavior. A

comparison of the SA of the signals acquired from sensor 1 with the pump in healthy and faulty conditions is reported in Figure 4-17.

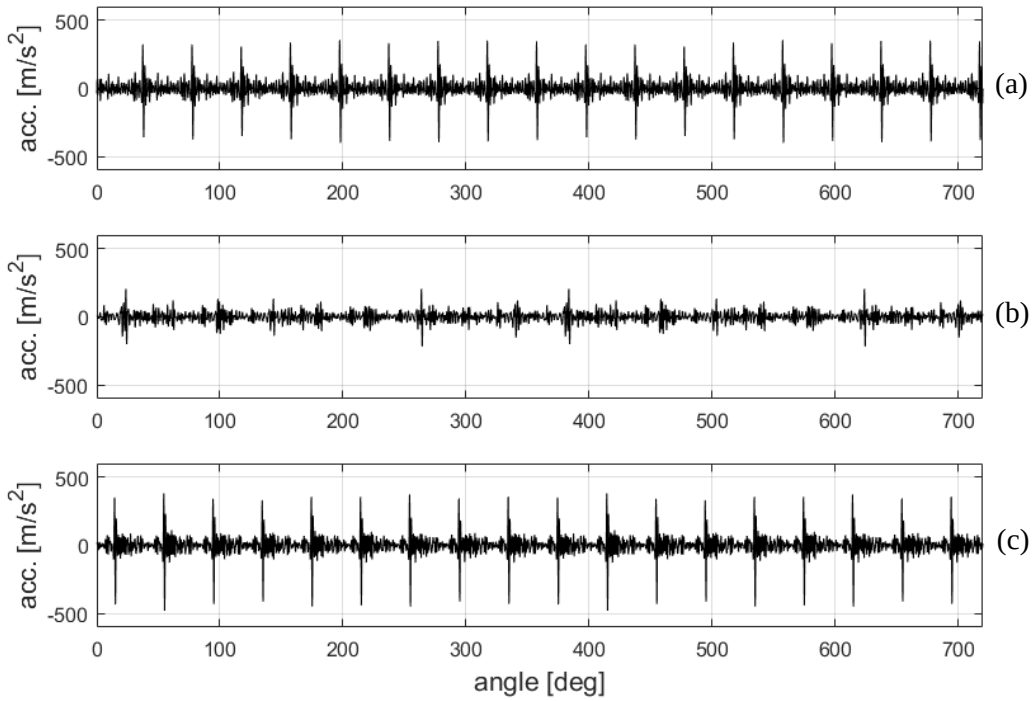

Figure 4-17: Synchronous average for (a) the flawless pump, (b) fault 1 and (c) fault 2 for the signal acquired with sensor 1 (1500 r/min, 150 bar).

The SA signals for the flawless pump and for fault 2, i.e. port plate eroded by cavitation, look very similar and both show a clear periodic behavior at the piston frequency. The SA for fault 1, i.e. worn slippers, does not show any remarkable periodic behavior at the piston frequency and seems to be random. From this first result, the analysis of the SA of sensor 1 seems to be effective for the identification of fault 1.

Figure 4-18 reports the raw signal, the SA and the residual signal for the signal acquired with sensor 2 in the case of flawless pump. In this case, the shape of the SA does not show the impulses at the piston frequency found in Figure 4-16 for sensor 1.

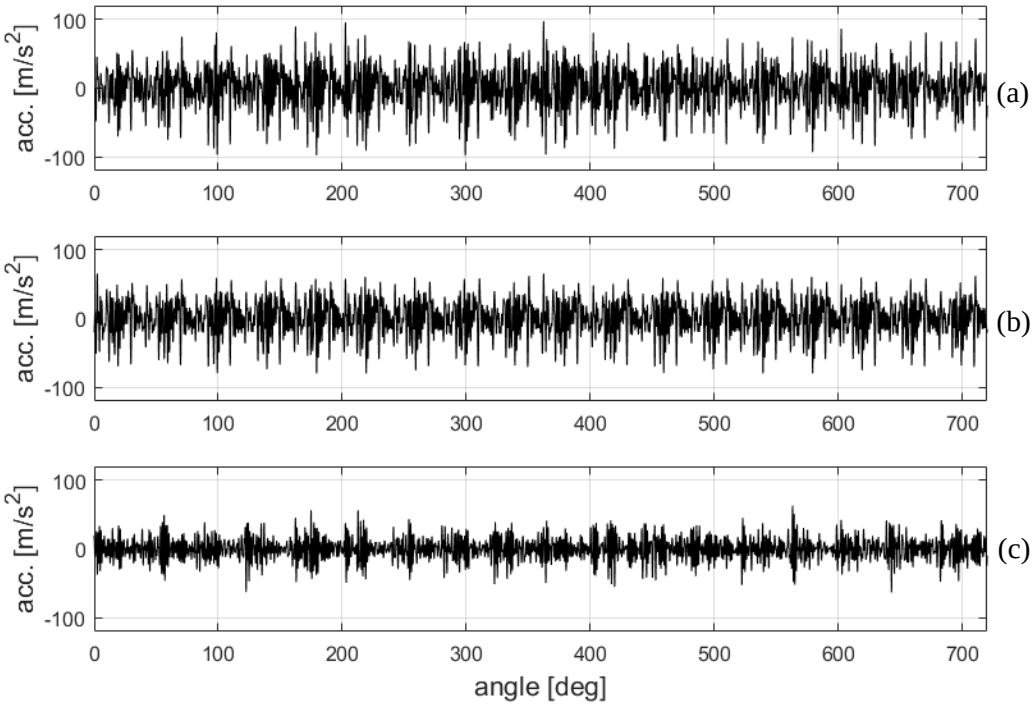

Figure 4-18: (a) Raw signal, (b) synchronous average and (c) residual signal for the signal acquired with sensor 2 in the case of flawless pump (2000 r/min and 150 bar).

The comparison among the SA of the flawless pump and the faulty pumps for the signals acquired with sensor 2 is reported in Figure 4-19. Also in this case, the SA signals of the flawless pump and of fault 2 show a similar periodic behavior at the piston frequency, while the SA of fault 1 seems to be more random. The analysis of the signals in the angle domain showed some differences; however, in the next sections the tools presented in this chapter will be applied to highlight the differences between the flawless case and the faulty cases.

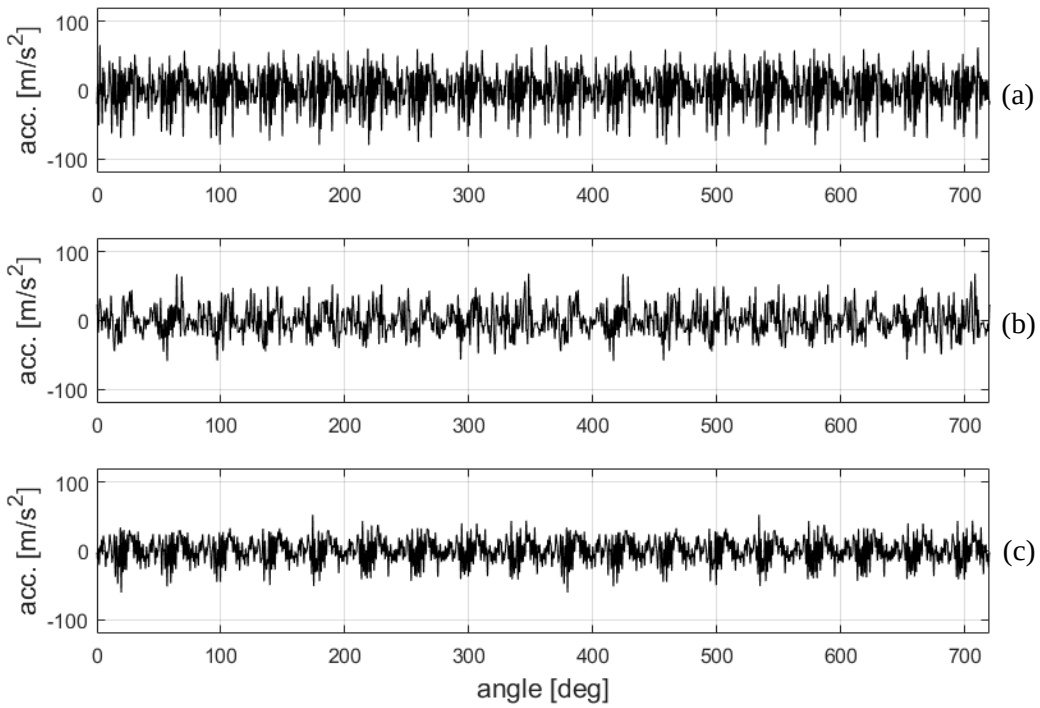

Figure 4-19: Synchronous average for (a) the flawless pump, (b) fault 1 and (c) fault 2 for the signal acquired with sensor 2 (2000 r/min, 150 bar).

4.4.3 First-Order Cyclostationary Analysis

The first-order analysis is performed by computing the FFT of the SA and the residual signals. Figure 4-20 reports the FFT of the signals reported in Figure 4-16. The FFTs are shown up to order 400, which corresponds to the higher limit of the bandwidth of the accelerometers (10 kHz); order 1 corresponds to the shaft frequency and order 9 to the piston frequency. The SA collects all the periodic components and the residual signal remains completely random; the CS2, or higher-order, components are not highlighted by the FFT. The peaks in the FFT of the raw signal are the same of the FFT of the SA; these peaks are at order 9 and at its multiples.

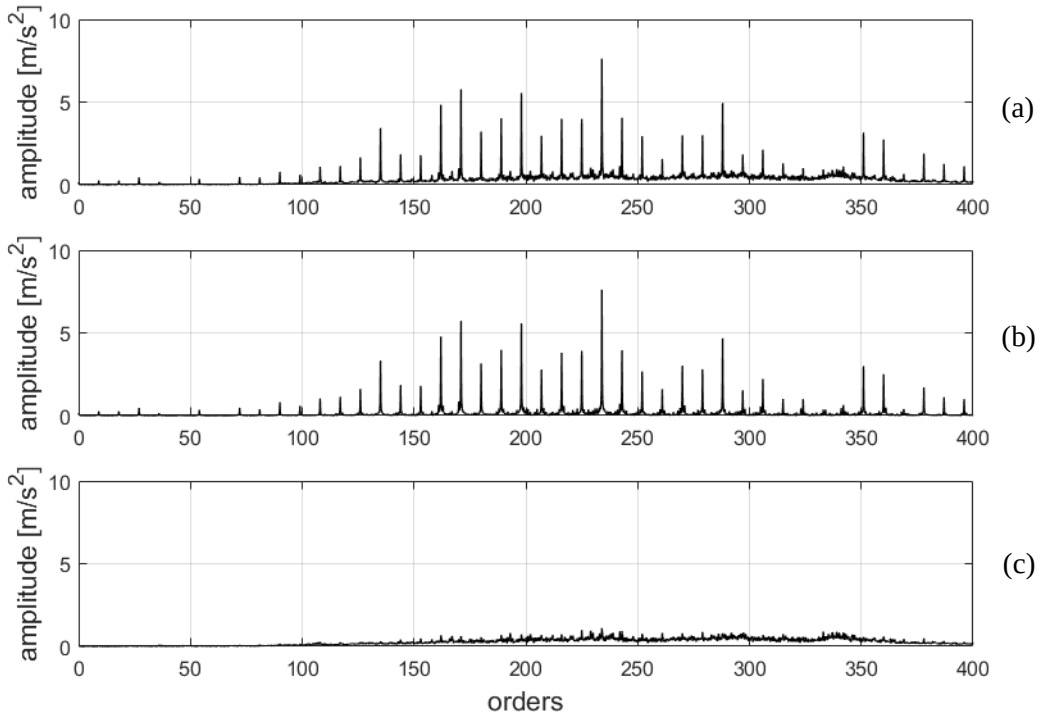

Figure 4-20: FFT of (a) acceleration signal, (b) synchronous average and (c) residual signal for the signal acquired with sensor 1 in the case of flawless pump (1500 r/min,150 bar).

A comparison of the FFTs of the SA with the pump in healthy and faulty conditions for the signals acquired with sensor 1 is reported in Figure 4-21. The SA of fault 1 does not show remarkable periodic components and looks random. On the other hand, the SA of fault 2 shows significant periodic components, similar to the ones of the flawless condition. This result confirms the result found in the analysis of the SA signals in the angle domain, Figure 4-17.

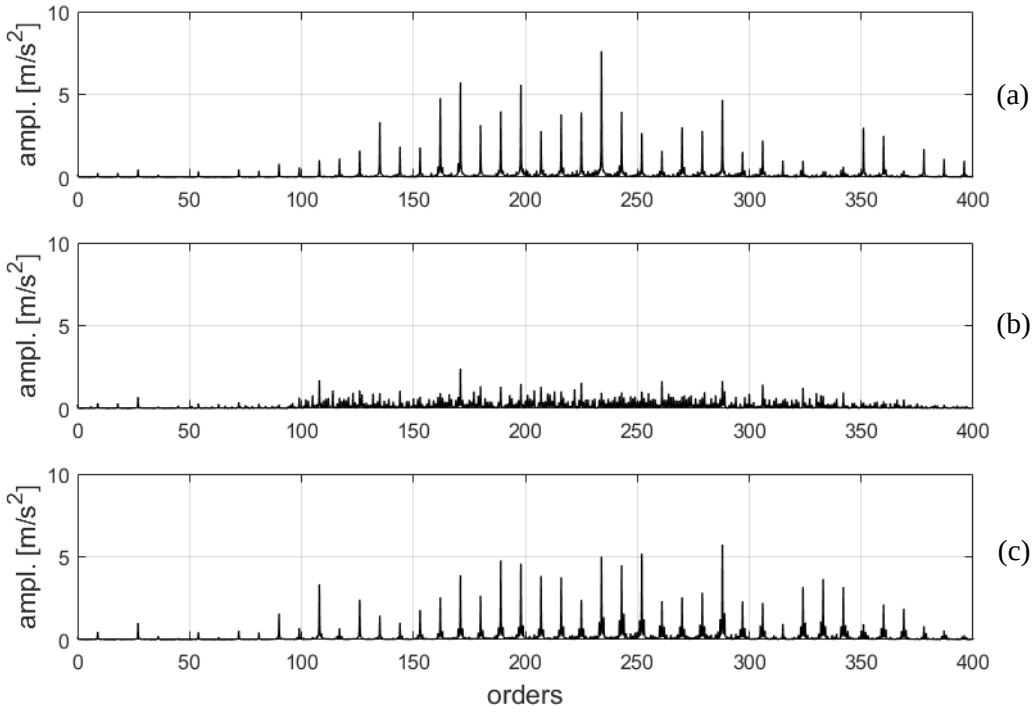

Figure 4-21: FFT of the synchronous average for (a) the flawless pump, (b) fault 1 and (c) fault 2 for the signal acquired with sensor 1 (1500 r/min, 150 bar).

The acceleration signal acquired from sensor 1 loses its periodic components in the case of worn slippers (fault 1). This result is very important because allows the identification of the fault related to worn slippers, which is one of the most common faults occurring in swash-plate type pumps. This result can be explained looking at Figure 4-12, which reports the comparison between the healthy and the worn slippers. The slippers of the healthy case have a very similar height, while the slippers of the faulty case present different levels of wear and, in particular, different heights. In the healthy case, the slippers excite the pump vibration in an analogous way leading to high harmonics at order 9 and its multiples. In the faulty case, the slippers excite the pump vibration in different ways, therefore the harmonic at order 9 and its multiples reduce their intensity and the energy is distributed over the set of harmonics multiple of order 1, i.e. the shaft frequency.

Figure 4-22 reports the FFTs of the residual signals corresponding to the SA signals considered in Figure 4-21. The residual signals in the flawless case and in the faulty cases are random since the periodic part was extracted by the SA. The behavior of the three FFTs is similar, but higher values can be identified for fault 2 around order 330.

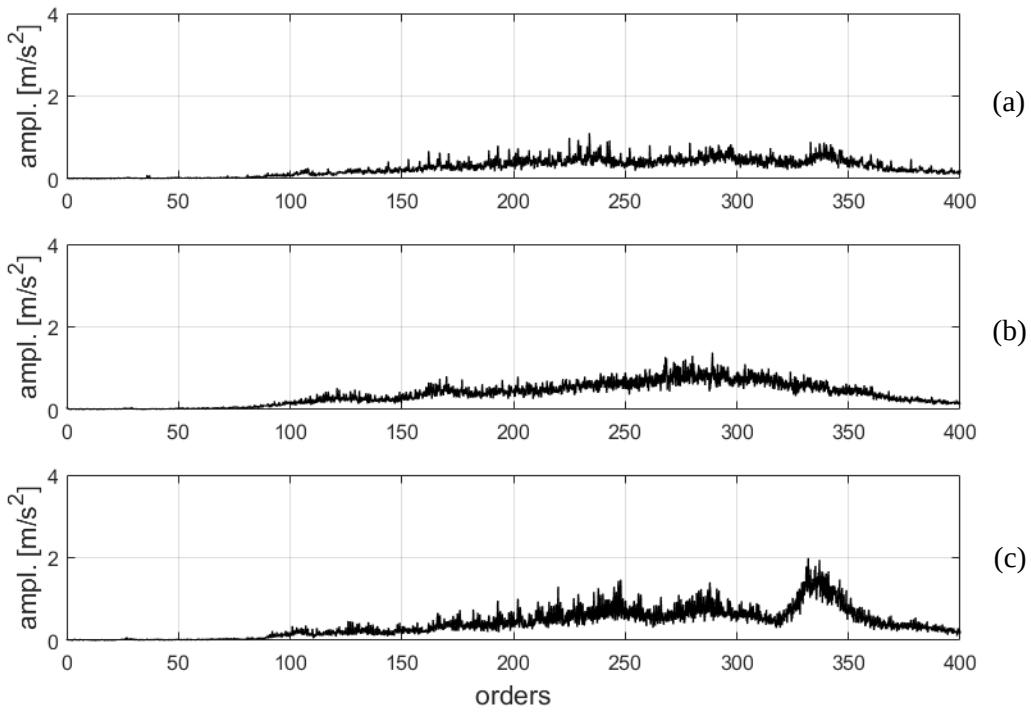

Figure 4-22: FFT of the residual signal for (a) the flawless pump, (b) fault 1 and (c) fault 2 for the signal acquired with sensor 1 (1500 r/min, 150 bar).

A comparison of the FFTs of the SA with the pump in healthy and faulty conditions for the signals acquired with sensor 2 is reported in Figure 4-23. The result highlighted in Figure 4-21 for sensor 1 is confirmed also for the signals acquired with sensor 2. In case of worn slippers, the harmonics at order 9 and at order 18 are remarkable and comparable to the ones found in case of flawless pump and fault 2; at higher frequencies the harmonics at multiples of order 9 are not evident and become comparable to the harmonics at multiples of order 1.

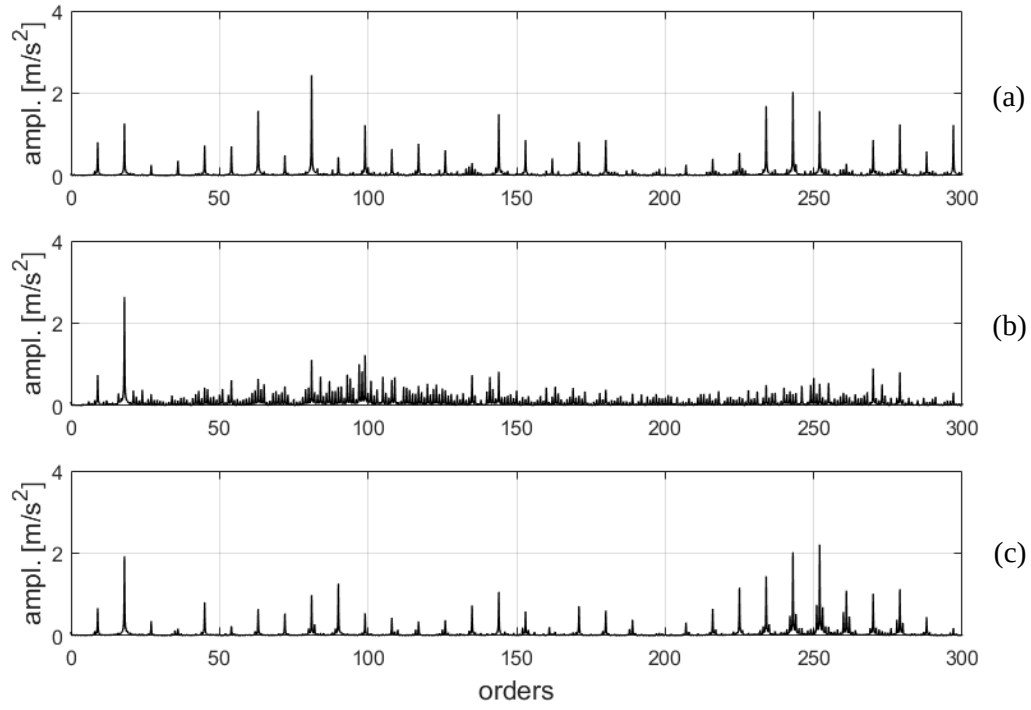

Figure 4-23: FFT of the synchronous average for (a) the flawless pump, (b) fault 1 and (c) fault 2 for the signal acquired with sensor 2 (2000 r/min, 150 bar).

Figure 4-24 reports the FFTs of the residual signals corresponding to the SA signals considered in Figure 4-23. The trend of the FFT for the flawless pump is similar to the one of fault 2, apart from higher values in the latter case around order 250. Since these tests are performed with the pump operated at 2000 r/min, the higher values at order 250 correspond to the higher values at order 330 found in Figure 4-22, where the pump angular velocity was 1500 r/min; the corresponding frequency is around 8250 Hz. The port plate eroded by cavitation seems to introduce a modification of the pump vibration around 8250 Hz. This difference in the residual signals is investigated in the next section using CS2 tools.

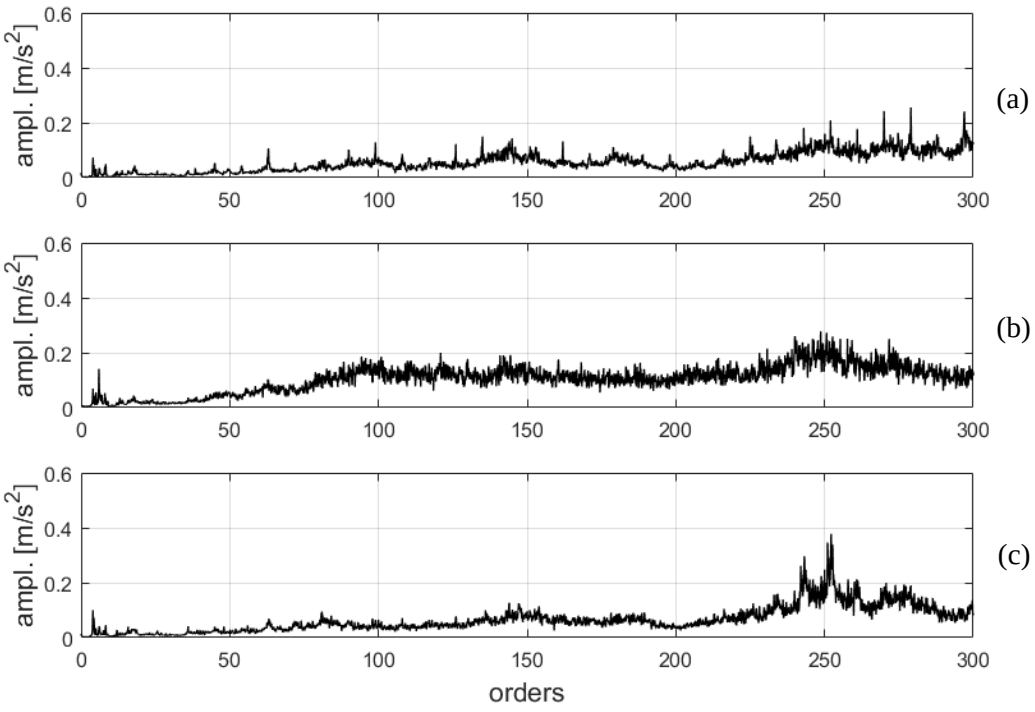

Figure 4-24: FFT of the residual signal for (a) the flawless pump, (b) fault 1 and (c) fault 2 for the signal acquired with sensor 2 (2000 r/min, 150 bar).

4.4.4 Second-Order Cyclostationary Analysis

The CS2 analysis is performed by computing the spectral correlation density and the cyclic spectral coherence of the residual signals. The SCD, Eq. 4.13, highlights at which frequencies (orders in the angle domain) the signal power is modulated. The CSC, Eq. 4.19, is a normalized index that can be considered a measure of the degree of second-order cyclostationarity. Both these tools were calculated considering a signal length of 36000 samples, corresponding to 10 revolutions, and a window length of 720 samples. With these parameters, the resulting resolutions are 0.1 orders for the cyclic frequency and 2.5 orders for the spectral frequency. Since the principal cyclic phenomenon is the one related to the pistons, only the cyclic frequencies around order 9 were considered to reduce the computational time.

Figure 4-25 reports the SCD calculated for the signals acquired with sensor 1 with the pump operated at 1500 r/min and 150 bar. The plots show on the x-axis the cyclic order and on the y-axis the spectral order. For the flawless pump (standard) and for fault 2 a clear modulation at order 9 is present; the power of the random part of the acceleration signal is clearly modulated at

the pistons frequency. For fault 1, modulations at other orders, multiples of order 1, are present. In case of worn slippers, not only the periodic part, but also the power modulation of the random part loses the dominant component at order 9 and shows components at multiples of the shaft frequency. The explanation of these phenomena is the differential wear of the slippers, each of them excites the pump vibration in a different manner and the component at order 9 reduces. For the case of fault 2, higher values of the spectral correlation are found around the spectral order 330; this result is in line with the higher values around the same order found in the FFT of the residual signal, Figure 4-22.

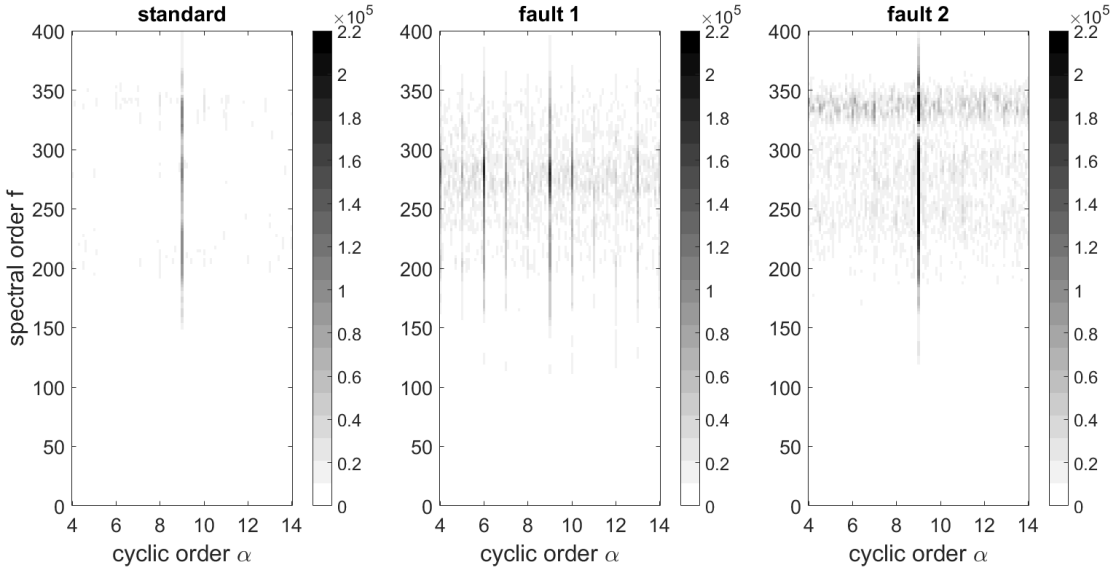

Figure 4-25: Spectral correlation density around the cyclic order 9 for the signals acquired with sensor 1 at 1500 r/min 150 bar ($\Delta\alpha = 0.1$, ($\Delta f = 2.5$).

Figure 4-26 reports the CSC for the same signals considered in Figure 4-25. For the flawless pump and for fault 2 a clear line at order 9 is present, therefore both these signals show a clear CS2 behavior at the piston frequency. In the case of fault 1, the degree of second-order cyclostationarity at order 9 is lower and comparable to the degree found at multiples of order 1.

Figure 4-27 reports the spectral correlation density calculated for the signals acquired with sensor 2 with the pump operated at 2000 r/min and 150 bar. Also in this case, fault 1 presents power modulations at multiples of order 1. Fault 2 shows a strong component at cyclic order 9 and at spectral frequencies around order 250, which corresponds to the same frequency of order 330 at 1500 r/min.

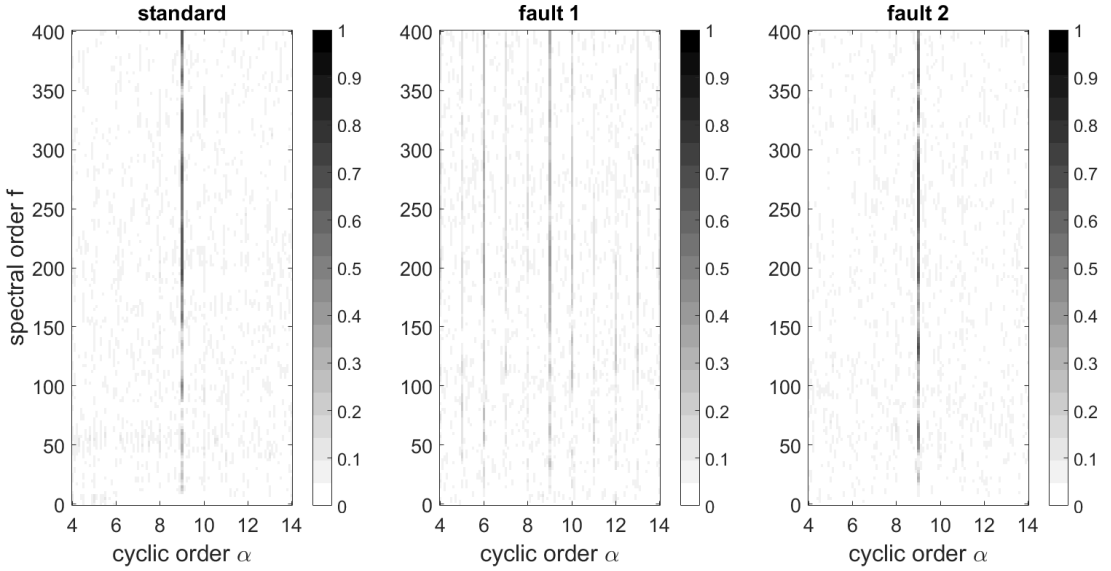

Figure 4-26: Spectral coherence around the cyclic order 9 for the signals acquired with sensor 1 at 1500 r/min 150 bar ($\Delta\alpha = 0.1$, ($\Delta f = 2.5$).

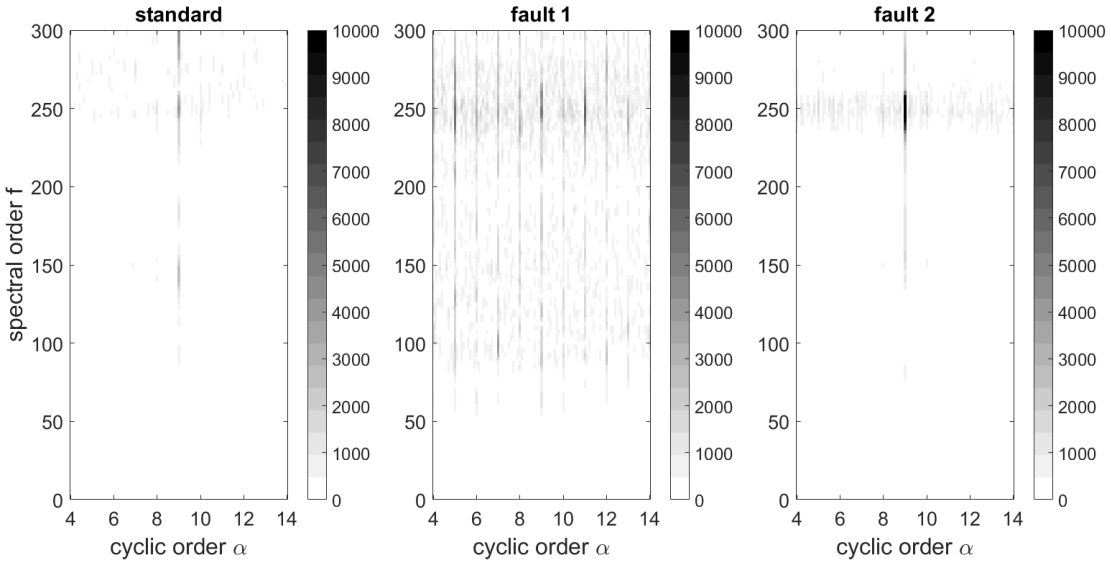

Figure 4-27: Spectral correlation density around the cyclic order 9 for the signals acquired with sensor 2 at 2000 r/min and 150 bar ($\Delta\alpha = 0.1$, ($\Delta f = 2.5$).

Figure 4-28 reports the spectral coherence of the signal considered in Figure 4-27. High values of the coherence are found for fault 2 at spectral frequencies around order 250 and at cyclic order

9. The spectral coherence of fault 1 is comparable at each multiple of order 1. Figure 4-29 and Figure 4-30 reports the SCD and the CSC for the signals acquired with sensor 2 with the pump operated at 2000 r/min and 250 bar.

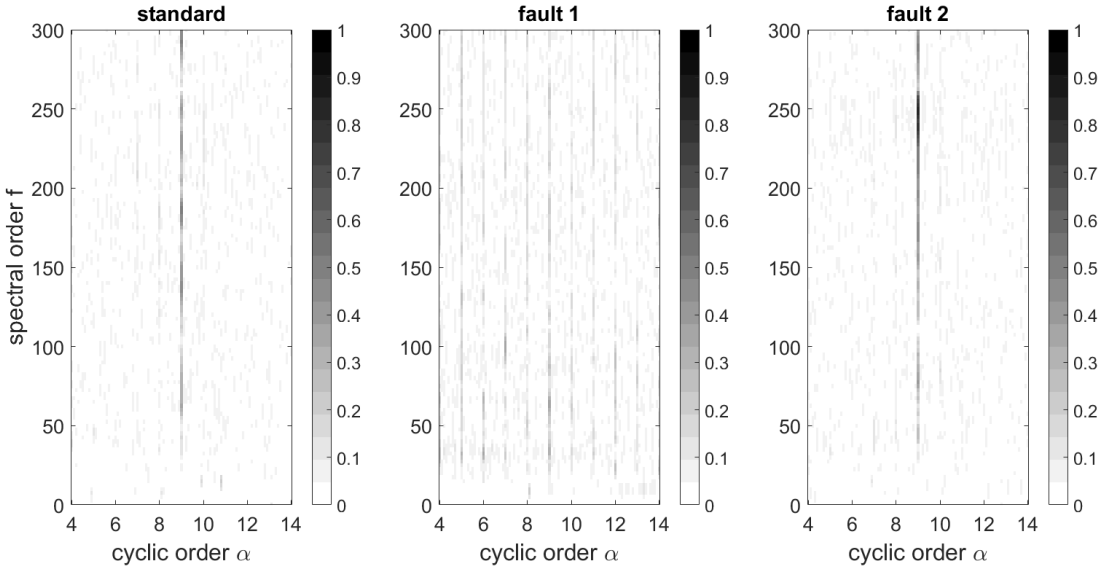

Figure 4-28: Spectral coherence around the cyclic order 9 for the signals acquired with sensor 2 at 2000 r/min and 150 bar ($\Delta\alpha = 0.1$, ($\Delta f = 2.5$).

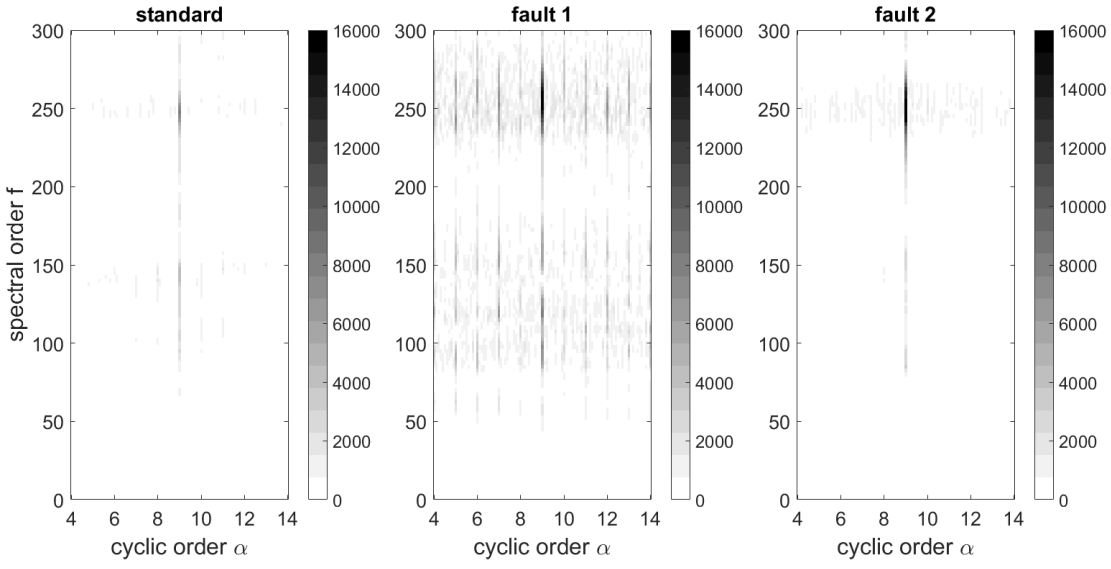

Figure 4-29: Spectral correlation density around the cyclic order 9 for the signals acquired with sensor 2 at 2000 r/min and 250 bar ($\Delta\alpha = 0.1$, ($\Delta f = 2.5$).

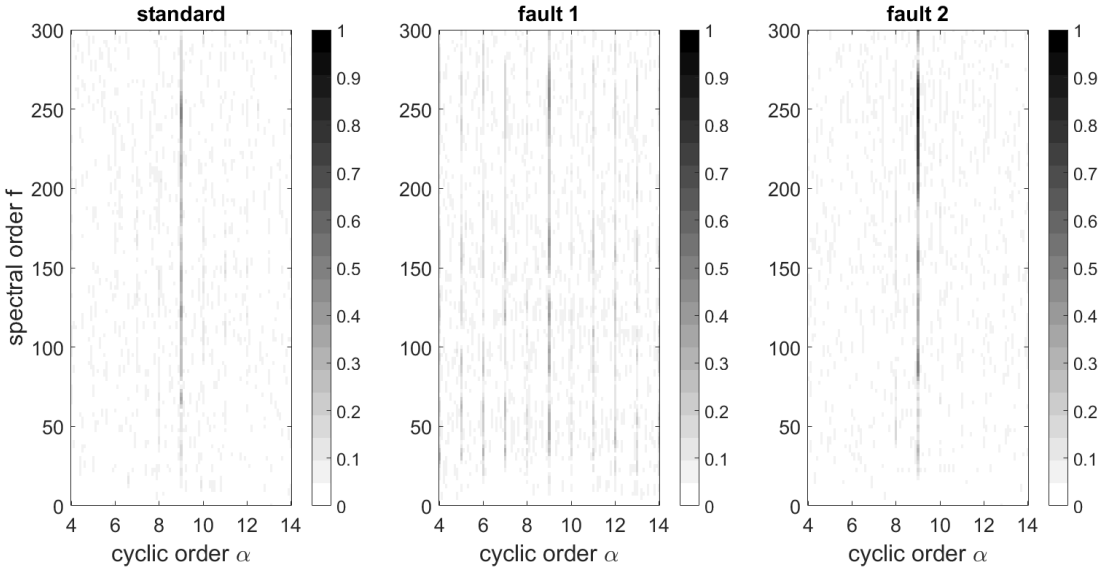

Figure 4-30: Spectral coherence around the cyclic order 9 for the signals acquired with sensor 2 at 2000 r/min and 250 bar ($\Delta\alpha = 0.1$, ($\Delta f = 2.5$).

The trends found in the tests performed at 150 bar and represented in Figure 4-27 and in Figure 4-28 are confirmed. In particular, the fault 2 presents higher values of the SCD and the CSC at cyclic order 9 and around spectral order 250. The introduction of the port plate eroded by cavitation seems to introduce higher CS2 components in the acceleration signals around the spectral frequency 8250 Hz (order 330 at 1500 r/min and order 250 at 2000 r/min). This behavior is particularly evident in the signals acquired with sensor 2, which is installed closer to the port plate and therefore closer to the fluid dynamic and mechanic modifications induced by the introduction of fault 2.

4.4.5 MCR Algorithm

The MCR algorithm, presented in section § 4.2.2.1, can be applied to filter the residual signal and keep only the CS2 part of interest. The results of the previous section showed that the dominant CS2 component is at order 9; this component is due to the power modulation induced by the pistons. The MCR algorithm was used to filter the residual signal at cyclic order 9. The algorithm was applied using a filter length $L = 32$ and $K = 16$ frequency shifts; these parameters are a good trade-off between accuracy and computational time, as shown in Figure 4-7.

A comparison of the SCD before and after the application of the MCR algorithm is reported in Figure 4-31 for the signal acquired from sensor 1 with worn slippers. With the application of

the MCR algorithm, the component at cyclic order 9 is exalted and the other components are reduced; for example, the significant component at order 6 is heavily reduced. Figure 4-32 reports the corresponding CSC. The filtered residual shows a high coherence at order 9, while in the unfiltered residual the coherence at order 6.

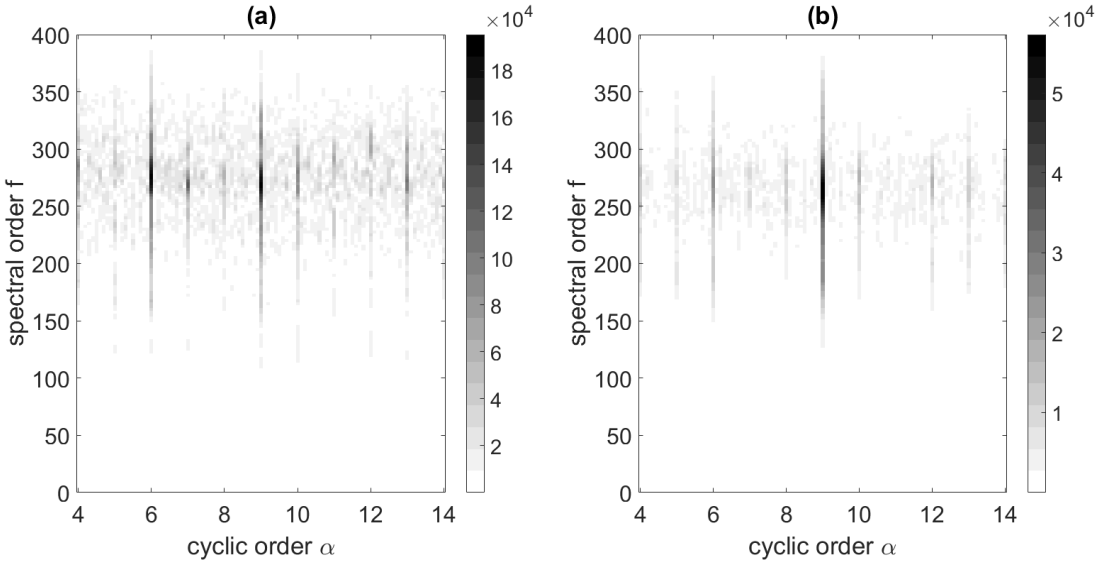

Figure 4-31: Spectral correlation density before (a) and after (b) the application of the MCR algorithm; signal acquired with sensor 1 in case of fault 1 at 1500 r/min and 150 bar.

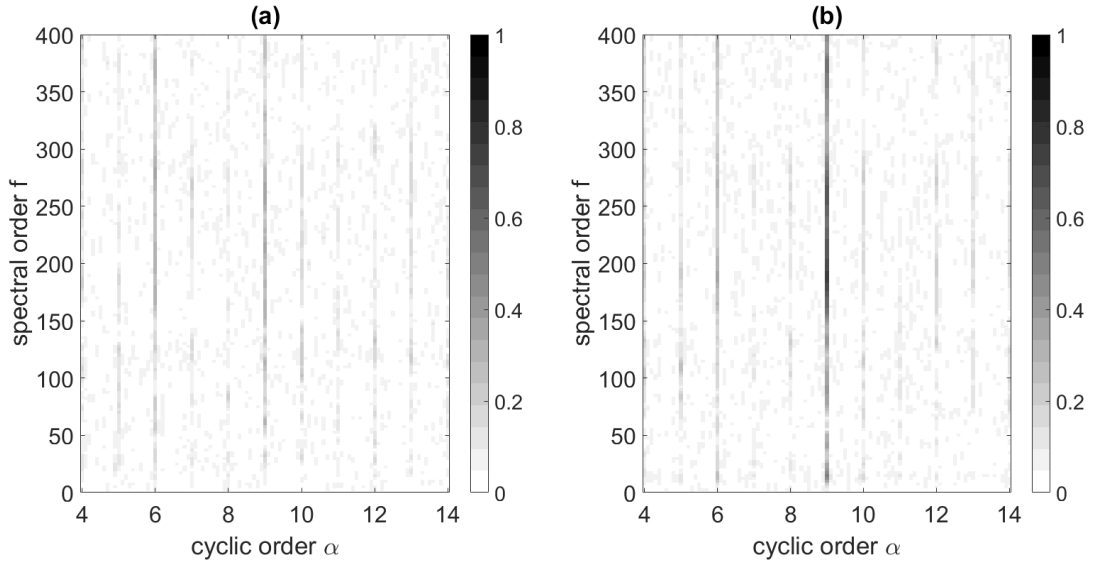

Figure 4-32: Spectral coherence before (a) and after (b) the application of the MCR algorithm; signal acquired with sensor 1 in case of fault 1 at 1500 r/min and 150 bar.

The results presented in the last two figures demonstrate that the MCR algorithm works properly and keeps the component of the signal which shows a high coherence at the considered cyclic frequency. From the SCD reported in Figure 4-31, it can be noted that, by keeping only the CS2 component at order 9, the overall signal power is reduced.

Figure 4-33 reports the comparison of the SCD before and after the application of the MCR algorithm for the signal acquired from sensor 2 with the port plate eroded by cavitation. The significant component around the spectral order 250 and cyclic order 9 is kept and the background noise is reduced. Considering the spectral coherence reported in Figure 4-34, higher values can be found at the spectral frequencies where the power of the signal is low. Also in this second case, the MCR algorithm is able to exalt the CS2 components at cyclic order 9 and reduce the background noise.

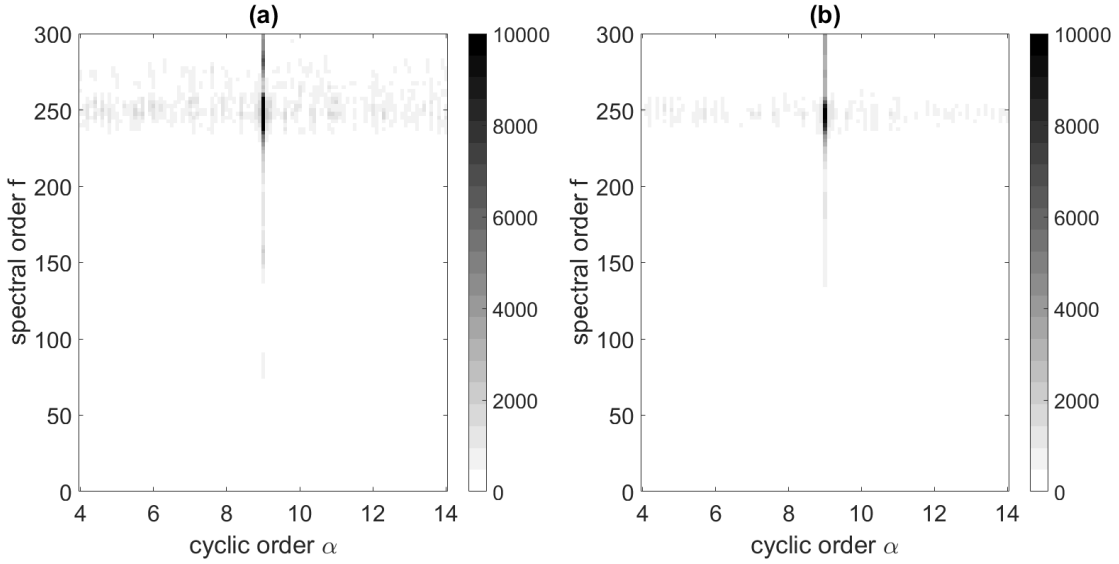

Figure 4-33: Spectral correlation density before (a) and after (b) the application of the MCR algorithm; signal acquired with sensor 2 in case of fault 2 at 2000 r/min and 150 bar.

The CS1 analysis of the SA and the CS2 analysis of the residual signal were already able to extract features for the identification of the two considered faults and the application of the MCR algorithm is not necessary. However, the application of the MCR algorithm at order 9 can highlight the difference between fault 2 and the flawless case, as illustrated in Figure 4-35.

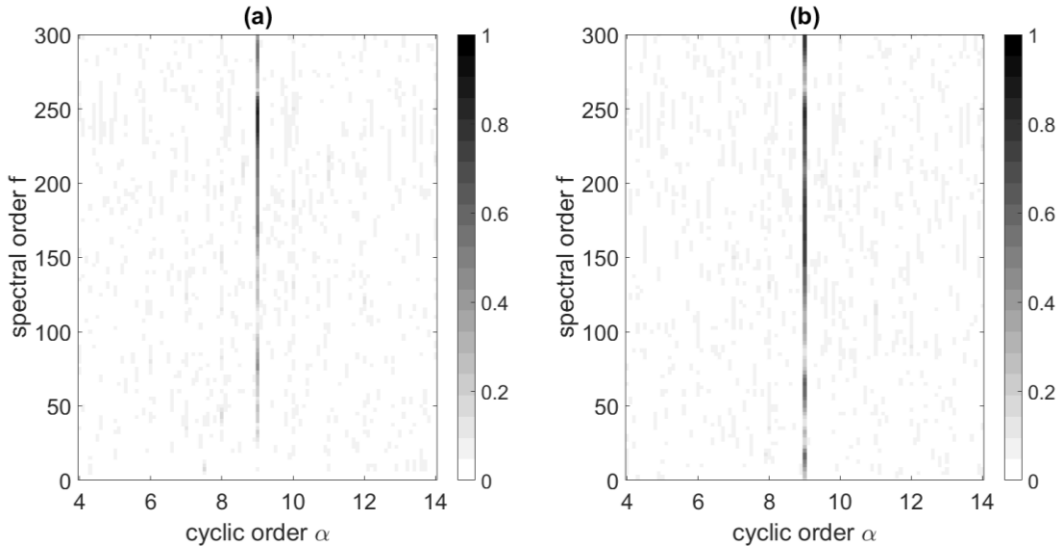

Figure 4-34: Spectral coherence before (a) and after (b) the application of the MCR algorithm; signal acquired with sensor 2 in case of fault 2 at 2000 r/min and 150 bar.

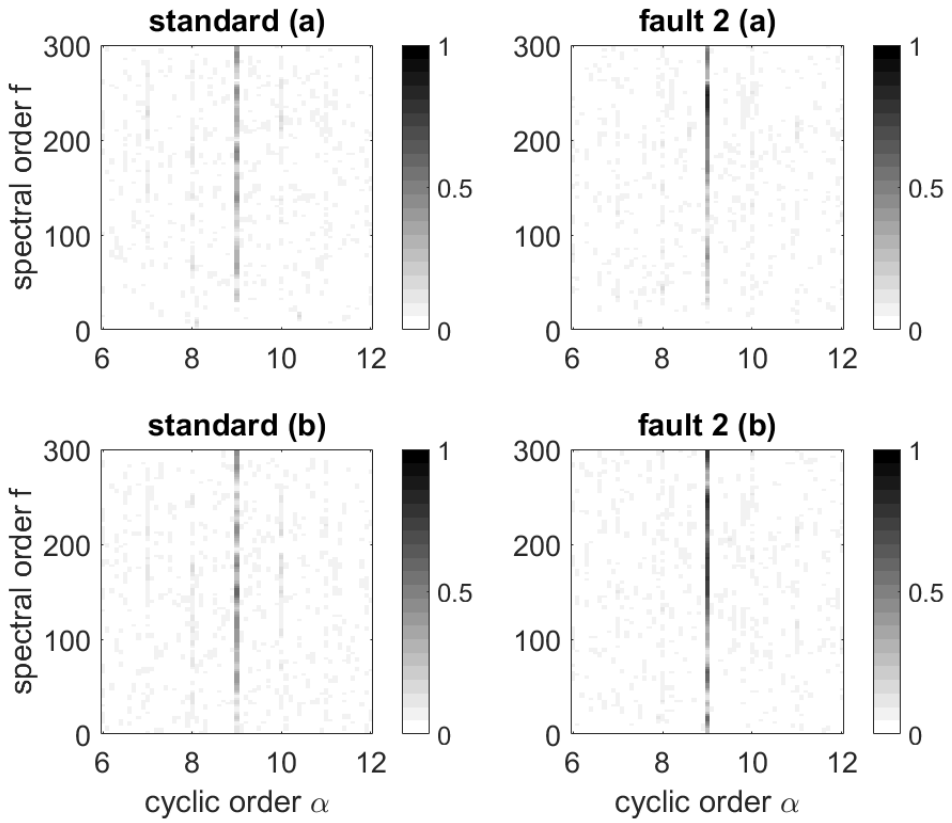

Figure 4-35: Comparison of the CSC before (a) and after (b) the application of the MCR algorithm for the flawless pump and the fault 2 (sensor 2, 2000 r/min and 150 bar).

The application of the MCR algorithm becomes very important when it is used to extract a CS2 component that is masked by other CS2 components of higher intensity. In case of fault 2, the CS2 component of interest is at order 9 and it is not masked by other CS2 components. The MCR algorithm is very useful for the detection of a bearing fault. In this case, the MCR algorithm must be used to extract the CS2 component at the specific frequency of the bearing fault; this CS2 component is most probably masked by the component at the piston frequency.

4.5 Discussion and Future Works

In this chapter a methodology for the analysis of acceleration signals was proposed. This methodology is based on the theory of cyclostationarity and it is suitable for the analysis of acceleration signals issued by roto-dynamic machines. The features extracted by the methodology are useful for the machine monitoring and diagnostics.

The machine vibrations are the result of the contributions of different sources; an effective signal analysis requires the separation of these contributions in order to avoid interferences. The proposed methodology starts with the extraction of the periodic, i.e. CS1, component by computing the SA of the signal. The calculation of the SA requires an angular sampling, and in the experiments performed in this activity a relative encoder was used as trigger for the acquisitions. The CS1 component was analyzed by computing the FFT. The residual signal, obtained by subtracting the SA from the raw signal, contains only CS2 or higher order cyclostationary components. In this Thesis, only the analysis of the CS2 components was addressed because they are the most significant in roto-dynamic machines. The SCD was proposed to analyze the CS2 components in the frequency-frequency domain. The SCD indicates how the power of the signal at spectral frequency f is modulated at the cyclic frequency α. The CSC is a normalized parameter limited between 0 and 1 which was proposed to measure the degree of second-order cyclostationarity at specific f and α. The MCR algorithm was proposed to extract the CS2 component at a specific cyclic frequency and avoid interferences with other CS2 components and the background noise.

The proposed methodology was applied to the case study of a variable displacement axial-piston pump. The goal was to extract features for the machine diagnostics and the acceleration signals were acquired by means of two accelerometers installed on the pump case in two different positions. Experimental tests were performed with the pump in healthy and faulty conditions and at different operating conditions. The two faults considered are worn slippers (fault 1) and port

plate eroded by cavitation (fault 2). The fault 1 was already detectable from the first-order cyclostationary analysis and was also evident in the second-order cyclostationary analysis of the residual signal. The differential wear of the slippers reduces, almost cancels, the excitation at the piston frequency (order 9) and this is evident in the CS1 component and in the power modulation of the CS2 components. The identification of the fault related to the worn slippers is an important result since this fault is one of the most common for pumps of the swash plate type. Fault 2 is an incipient fault due to cavitation erosion. This fault was not detectable from the analysis of the periodic component, but the application of CS2 tools permitted to highlight a difference with the flawless case. The results showed higher values for the CS2 components around the spectral frequency 8250 Hz and at cyclic frequency corresponding to the pistons frequency. This result was evident in all the tested operating conditions for the sensor installed at the hydraulic end, i.e. closer to the port plate. The performance of the MCR algorithm were demonstrated on the experimental signals. For the considered faults, the benefits coming from the application of the MCR algorithm were moderate since the CS2 components of interest were not masked by other CS2 components. However, the application of the MCR algorithm can be very useful if the identification of other faults is addressed. For example, in case of a bearing fault, the CS2 component of interest is probably masked by the greater CS2 components due to the pistons and the proposed MCR algorithm can be used to extract the CS2 component related to the fault.

The results of this chapter demonstrated that the proposed methodology can be effectively applied for the detection of incipient faults in an axial-piston pump. The parameters extracted can be used as inputs of an automatic decision making diagnostic algorithm; for example, based on the use of a neural network for the faults classification. In future works, a larger set of frequent and significant incipient faults and several samples for each fault will be considered. The acceleration signals will be analyzed with proposed methodology to extract a large set of fault features. In this Thesis the objective was to demonstrate the capabilities of the analysis procedure and the results were visualized and analyzed manually. This approach becomes ineffective if the data set is large and a procedure will be studied to automatically analyze the set of features and extract the most significant parameters for the fault identification, i.e. the features which highlight the difference between a specific fault and the other cases. Based on this reduced set of features, an automatic and effective diagnostic system can be developed. In this activity the angular sampling was implemented by using a relative encoder. This solution is expensive and unsuitable for onboard diagnostics; therefore, a solution based on the time sampling of the acceleration signals and a tacho signal for the angular resampling will be studied. Another aspect which limit the application of the proposed approach for onboard diagnostics is the important computational

effort required for the second-order cyclostationary analysis. To address this point, the methodology can be applied offline, where the computational effort is not a problem, to define the reduced set of features as reported above; then, for the onboard and online application, only the features of interest can be calculated, thus reducing the computational effort and avoiding the calculation of useless parameters. In conclusion, even if this methodology was demonstrated for the case of an axial-piston pump, it can be successfully applied to other similar roto-dynamics machines.

List of references

4.1. W. Gardner, Cyclostationarity in Communications and Signal Processing, IEEE Press, New York, 1994.

4.2. W. Gardner, A. Napolitano, L. Paura, Cyclostationarity: half a century of research, Signal Processing 86 (4) (2006) 639–697.

4.3. E. Serpedin, F. Panduru, I. Sari, G.B. Giannakis, Bibliography on cyclostationarity, Signal Processing 85 (12) (2005) 2233–2303.

4.4. J. Antoni, Cyclostationary by examples, Mechanical Systems and Signal Processing 2009; 23: 987–1036.

4.5. J. Antoni, Cyclic spectral analysis in practice, Mechanical Systems and Signal Processing 21 (2) (2007) 597–630.

4.6. G. D. Elia, M. Cocconcelli, E. Mucchi, G. Dalpiaz, Combining blind separation and cyclostationary techniques for monitoring distributed wear in gearbox rolling bearings, Proc IMechE Part C: J Mechanical Engineering Science 0(0) 1–16.

4.7. R.B. Randall, J. Antoni, S. Chobsaard, The relationship between spectral correlation and envelope analysis in the diagnostics of bearing faults and other cyclostationary machine signals, Mechanical Systems and System Processing 15 (5) (2001) 945–962.

4.8. J. Antoni, F. Bonnardot, A. Raad, M. El Badaoui, Cyclostationary modelling of rotating machine vibration signals, Mechanical Systems and Signal Processing 2004; 18: 1285–1314.

4.9. R. Boustany, J. Antoni, Cyclic spectral analysis from the averaged cyclic periodogram, in: Proceedings of the 16th IFAC World Congress, Prague, Czech Republic, July 4–8, 2005.

4.10. J. Antoni, G. Xin, N. Hamzaoui, Fast computation of the spectral correlation, Mechanical Systems and Signal Processing 92 (2017) 248–277.

4.11. J. Antoni, J. Danière, F. Guillet, Effective vibration analysis of IC engines using cyclostationarity. Part I: a methodology for condition monitoring, Journal of Sound and Vibration 257(5) (2002) 815–837.

4.12. J. Antoni, J. Danière, F. Guillet, R. B. Randall, Effective vibration analysis of IC engines using cyclostationarity. PartI I: new results on the reconstruction of the cylinder pressure, Journal of Sound and Vibration 257(5) (2002) 839–856.

4.13. J. Antoni, Blind separation of vibration components: principles and demonstrations, Mechanical Systems and Signal Processing 2005; 19: 1166–1180.

4.14. J. Antoni, R.B. Randall, Differential diagnosis of gear and bearing faults, ASME Journal of Vibration and Acoustics 124 (2) (2002) 165–171.

4.15. C. Capdessus, M. Sidahmed, J.L. Lacoume, Cyclostationary processes: application in gear faults early diagnosis, Mechanical Systems and Signal Processing 14 (3) (2000) 371–385.

4.16. P.D. McFadden, M. M. Toozhy, Application of synchronous averaging to vibration monitoring of rolling element bearings, Mechanical Systems and Signal Processing (2000) 14(6), 891-906.

4.17. K. Fyfe, E. Munk, Analysis of computed order tracking, Mechanical Systems and Signal Processing 11 (2) (1996) 187–205.

4.18. F. Bonnardot, R.B. Randall, J. Antoni, F. Guillet, Enhanced unsupervised noise cancellation (E-SANC) using angular resampling – Application for planetary bearing fault Diagnosis, Surveillance 5 CETIM, Senlis, France, 11-13 October 2004.

4.19. F. Bonnardot, M. El Badaoui, R. B. Randall, J. Danière, F. Guillet, Use of the acceleration signal of a gearbox in order to perform angular resampling (with limited speed fluctuation), Mechanical Systems and Signal Processing 19 (2005) 766–785.

4.20. J. Antoni, R. B. Randall, Unsupervised noise cancellation for vibration signals: part I – evaluation of adaptive algorithms, Mechanical Systems and Signal Processing 2004; 18: 89–101.

4.21. J. Antoni, R. B. Randall, Unsupervised noise cancellation for vibration signals: part II – a novel frequency domain algorithm, Mechanical Systems and Signal Processing 2004; 18: 103–117.

4.22. W.A. Gardner, C.M. Spooner, The cumulant theory of cyclostationary time-series, Part I: foundations, IEEE Transactions on Signal Processing 42 (12) (1994) 3387–3408.

4.23. F. Bonnardot, R.B. Randall, F. Guillet, Extraction of 2nd order cyclostationary sources - application to vibration analysis, Mechanical Systems and Signal Processing 19 (6) (2005) 1230–1244.

4.24. R. Boustany, J. Antoni, A subspace method for the blind extraction of a cyclostationary source: application to rolling element bearing diagnostics, Mechanical Systems and Signal Processing 19 (6) (2005) 1245–1259.

4.25. R. Boustany, J. Antoni, Blind extraction of a cyclostationary signal using reduced-rank cyclic regression – unifying approach, Mechanical Systems and Signal Processing 2008; 22: 520–541.

4.26. W.A. Gardner, Cyclic wiener filtering: theory and method, IEEE Transaction on Communications 41 (1) (1993) 151–163.

Chapter 5 - Control and Diagnostics on a Hydraulic Crane

This chapter presents the results of a project aiming at combining an advanced control strategy with a diagnostic system for Electro-Hydraulic (EH) mobile machines. This activity was carried out at the MAHA Fluid Power Research Center of the Purdue University (Indiana, USA).

The reference machine is a truck loading hydraulic crane with a maximum capacity of 5 t. The crane is equipped with an independent metering system which allows the independent control of the meter-in and the meter-out valves. In this activity, a control algorithm for the meter-out valve, which combines a feedforward action and a feedback action, is presented. The feedback control is based on a Proportional-Integral (PI) regulator whose parameters were optimally defined through the application of an Extremum Seeking (ES) optimization algorithm. A detailed numerical model of the reference machine was developed in order to obtain a "virtual test-rig". This model was exploited to evaluate the performance of the control algorithm, and also to simulate the behavior of the system in faulty conditions without the need of performing time-consuming experimental tests. An algorithm based on a static Neural Network (NN) was developed for the system diagnostics. This algorithm utilizes the cost functions used for the control optimization as parameters for the identification of the system health state.

The results reported in this Thesis demonstrate that the presented control is able to guarantee the controllability of the actuators in an efficient way and that the optimization cost functions are valuable parameters for the machine diagnostics. The proposed diagnostic system demonstrated to be able to identify the machine health state even when a reduced set of sensors, including only pressure sensors, is used.

5.1 Project Rationale

In the last decades, the development and the diffusion of the electro-hydraulic technology led to consistent improvement in the efficiency and the performance of mobile hydraulic machines. However, the potential of the EH technology is still partially exploited because many applications are reluctant to its adoption in place of traditional and robust hydraulic-mechanical solutions. The rationale behind this project is to exploit the potential of the EH technology not only for improving the machine performance, controllability and efficiency, but also to introduce diagnostic features which can make the system safer and more reliable.

The Prognostics and Health Management (PHM) has been acquiring more and more interest in recent years, but it has not reached its state of maturity yet. Several works can be found on the application of diagnostic techniques for the case of hydraulic components, such as a hydraulic pump. In this field, some relevant methodologies were presented by Torrika [5.1], who proposed a vibration-based method and compared the results of different algorithms (such as the neural network and the support vector machine) for the classification task, and Gao [5.2], who presented a methodology based on the delivery pressure signal and the wavelet transform. On the other hand, only few works dealt with the diagnostics of complex hydraulic systems. Helwig et al. [5.3] proposed a method based on the Linear Discriminant Analysis (LDA) to reduce the dimension of the features vector and on the Mahalanobis distance classifier to detect the degradation condition of a hydraulic system. El-Betar et al. [5.4] proposed the use of a static neural network to recognize the actuator leakage and a valve fault in a basic hydraulic system. The original contribution of this work is to demonstrate that the parameters used for the control of an EH mobile machine can be effectively exploited as diagnostics features. The idea is to exploit the time-adaptation characteristic of many control algorithms which adjust their parameters so as to adapt to machine changes. Some important works in this fields were published by Vacca [5.5-5.7], who, for the case study of a hydraulic crane, applied an ES algorithm to optimize the control parameters of an open-center valve system with the objective of minimizing the system oscillations and improving the system efficiency. These studies demonstrated that the proposed control algorithm can potentially adapt to the unavoidable changes experienced by the machine during its life.

The work presented in this Thesis aims at demonstrating that an advanced control for EH machines, capable of adapting to the machine changes, can be also successfully exploited for diagnostic purposes. The addition of diagnostic capabilities to an advanced control algorithm will make the EH technology more appealing also for those applications, such as mobile hydraulics,

which have always been reluctant to this technology. Many branches of the hydraulic are still reluctant to the introduction of control complexities even if the advantages in terms of performance and efficiency are evident. The case of EH independent metering systems is a clear example of this; many solutions have been studied and proposed in recent years [5.8-5.9], but the applications on commercial vehicles are extremely rare. Indeed, the adoption of an independent metering system introduces a control issue related to the separation of the meter-in and meter-out valve with the introduction of an additional degree of freedom. In the last years, several studies dealt with the control complexity of independent metering systems and some examples are the works by Yao [5.10, 5.11] and Pedersen [5.12].

The reasons reported above justify the choice of installing an EH independent metering system on the reference machine. The reference machine is a hydraulic crane for truck applications which was available at the MAHA Fluid Power Research Center and which, in its standard version, is equipped with an open-center valve system. This reference machine exalts the control complexities of an EH independent metering system since the load can be resistive or overrunning and also the transition between the two types of load must be properly managed. The reference machine is presented in section § 5.2 and its numerical model, developed in the first part of this project, is presented in section § 5.3. The hydraulic system is of LSPC type and in this Thesis a control algorithm to define the meter-out valve opening is proposed, the meter-in valve is under the direct control of the operator. The control algorithm, presented in section § 5.4, combines a feedforward contribution and a feedback contribution to achieve a precise control. The feedback control is based on a PI regulator whose parameters must be defined according to the considered actuation; the signal used for the feedback is the pressure measured at the inlet side of the hydraulic actuator. An ES algorithm, presented in section § 5.5, was considered for the optimization of the control parameters. This optimization procedure must be applied offline to define the optimal control parameters and then can be applied online to adapt the control parameters to the machine changes due, for example, to aging and temperature variations.

The numerical model of the reference machine was exploited to simulate the system in faulty conditions and the obtained data were used to develop a data-based diagnostic algorithm based on a static NN. The cost functions used for the optimization of the control parameters are sensible to the considered system faults [5.13] and are used as inputs of the diagnostic algorithm presented in section § 5.6. The cost functions alone do not carry enough information to distinguish among different faults, therefore, a set of features were extracted from sensors installed in the system and used as inputs of the NN. Two set of sensors were considered, a full set which requires the installation of 13 sensors and a reduced set which requires only the installation of 7 pressure

sensors. The results reported in section § 5.7 demonstrate that the proposed diagnostic system based on a NN can identify if a fault occurred in the system and also give an indication of the fault intensity. This last feature constitutes the starting point for the development of a prognostic system.

5.2 Reference Machine

The reference machine is a hydraulic crane whose maximum capacity is about 5 t. This crane is designed to be installed on a truck for loading and unloading goods and materials, but during this activity the crane was fastened to a concrete base as shown in Figure 5-1. The crane is installed at the MAHA Fluid Power Research Center (Purdue University).

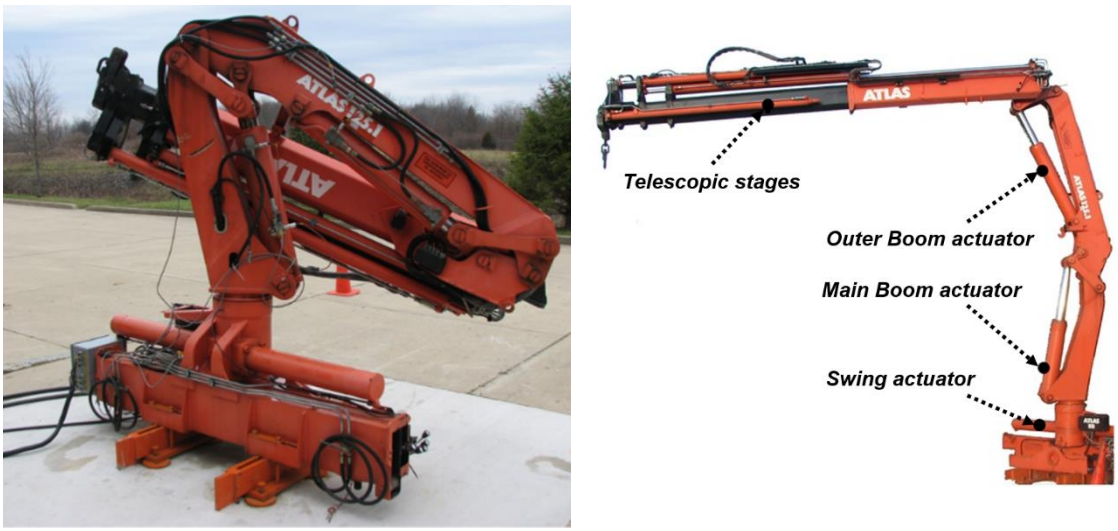

Figure 5-1: Hydraulic crane installed at the MAHA Fluid Power Research Center.

The crane counts four linear actuators as shown in Figure 5-1: the actuator for the swing rotation; the main boom actuator; the outer boom actuator and the multi-stage actuator for the telescopic extension. In this activity, only the main boom actuator and the outer boom actuator were considered. The swing angular position was always kept constant and the telescopic arm was kept to its minimum extension.

The reference machine is equipped with two hydraulic valve blocks which can be interchanged: a standard open center valve block and an independent metering valve block. The two valve blocks are shown in the photograph of Figure 5-2.

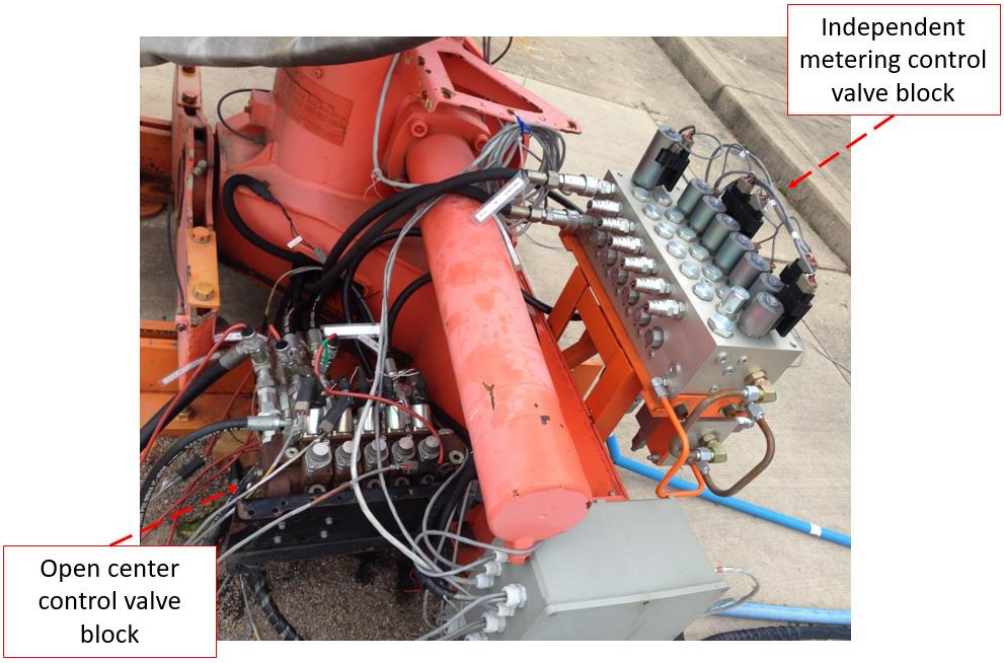

Figure 5-2: Hydraulic valve blocks installed on the reference machine.

In this activity, the independent metering valve was considered. The hydraulic system is of Load Sensing Post-Compensated (LSPC) type, i.e. a post-compensator keeps the pressure drop across the meter-in valve constant and the actuator velocity is directly proportional to the valve opening. Furthermore, the use of post-compensators allows the flow sharing functioning when the flow capacity of the Flow Generation Unit (FGU) is saturated. The hydraulic pump of the FGU is a fixed-displacement pump and an unloading valve is present in the system to enable the LS functioning.

The hydraulic schematic of the considered system is reported in Figure 5-3 (only the system relative to the considered actuators, i.e. main boom and outer boom, is reported). The system is composed of two valve manifolds. The first manifold contains the LS unloading valve (valve 1) and the pressure relief valve. The second manifold contains an independent metering section for each actuator; the telescopic stages are actuated through a standard closed center 4/3 distributor and a valve for the sequential actuation of the actuators. Each independent metering section is composed of four 2/2 cartridge valves, two for the meter-in (valves 2) and two for the control of the discharge flow (valves 4). The system is of LSPC type and a post-compensator (valve 3) is installed downstream each meter-in valve.

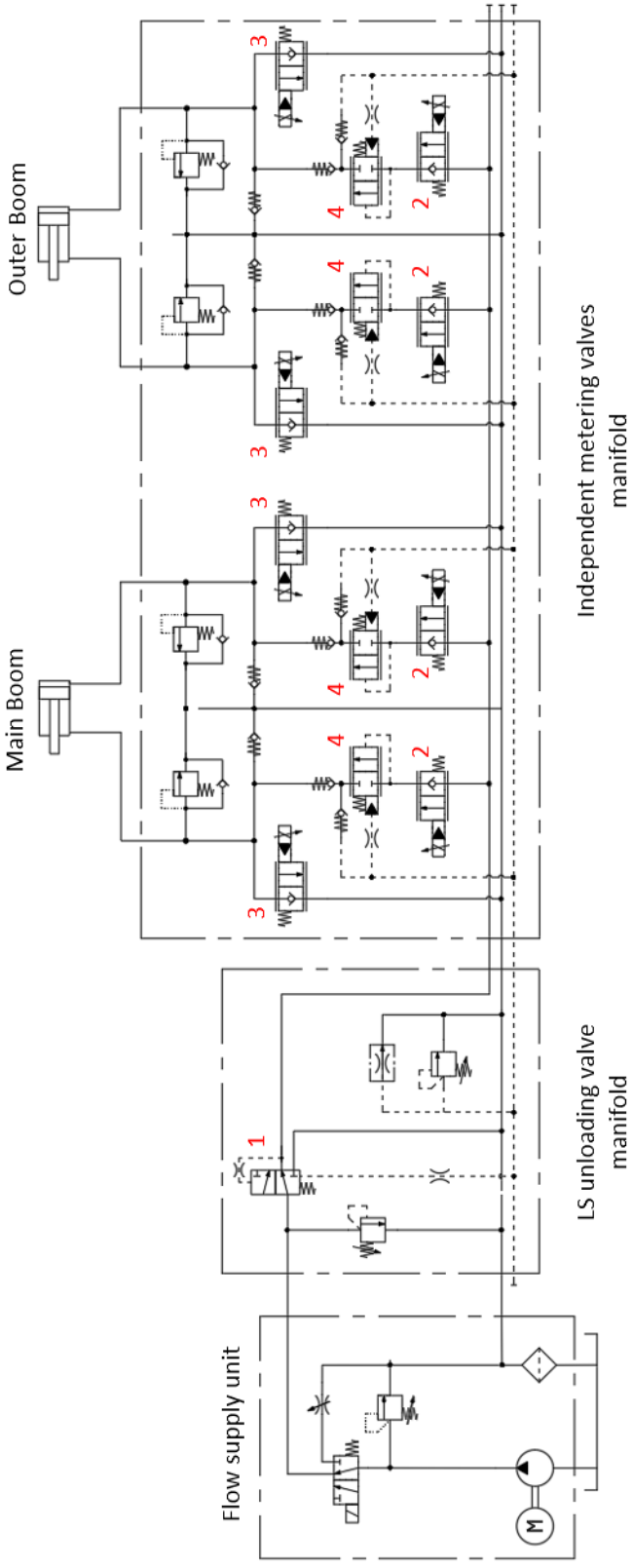

Figure 5-3: ISO schematic of the hydraulic circuit of the crane.

In such a system, the velocity of the actuator is directly proportional to the meter-in valve opening which is directly defined by the operator. The meter-out valve is independently controlled and therefore an additional degree of freedom is available to improve the machine performance.

The reference machine was connected to the central FGU of the MAHA laboratory. Within this activity, a new FGU was designed and built in order to create an independent test-rig for the crane. A photograph and the hydraulic schematic of the designed FGU are reported in Figure 5-4.

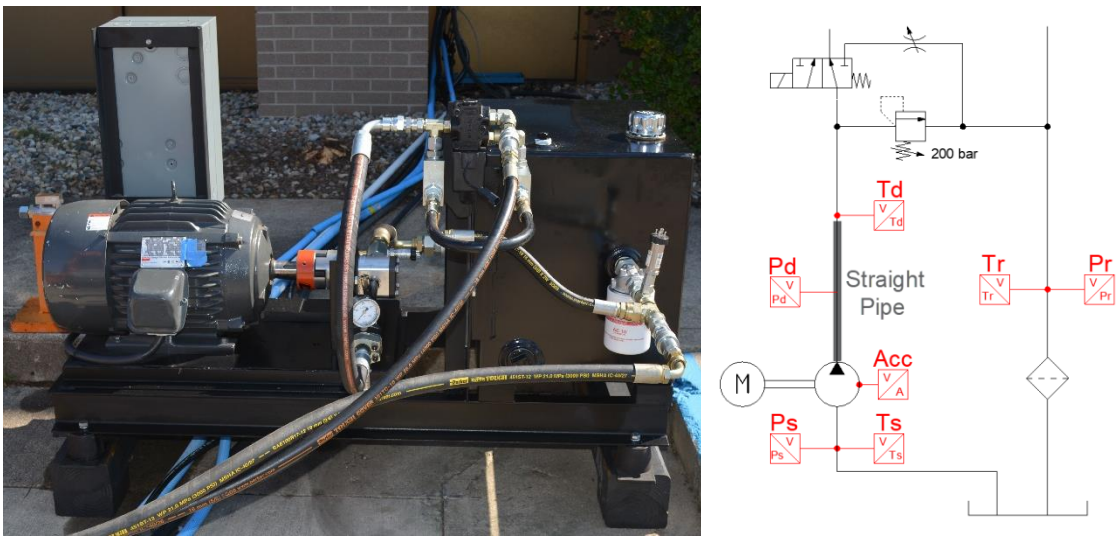

Figure 5-4: The designed flow generation unit.

The hydraulic pump is a fixed-displacement external gear pump, Casappa® PL 20, with a displacement of 21 cm^3. The pump is powered by an electric motor at 1800 r/min. The FGU was equipped with a set of sensors for the online monitoring of its condition; the position of the installed sensors is reported in Figure 5-4, while the sensors specifications are reported in Table 5-1.

Table 5-1: Sensors installed on the designed flow generation unit.

Variable	Sensor	Range	Accuracy
T_s, T_d, T_r	Wika® TR31	-50 to 150 °C	Class A
p_s	Wika® S-10	-1 to 9 bar	± 0.5% FS
p_r	Wika® S-10	0 to 25 bar	± 0.5% FS
p_d	Keller® PA23/8465	0 to 600 bar	± 0.5% FS

Three temperature sensors were installed to monitor the suction temperature T_s, the delivery temperature T_d and the temperature T_r of the return flow. The measurement of the suction and the delivery temperatures allows the calculation of the pump overall efficiency with the thermodynamic method presented in chapter 3. The temperature sensors were selected with a high accuracy class (class A) to keep the combined uncertainty on the estimated efficiency at an acceptable value. The delivery pressure ripple is an important signal for the pump condition monitoring and a high bandwidth pressure sensor was installed; a straight pipe was installed to reduce the wall compliance and exalt the pressure ripple. Another important signal for the pump condition monitoring is the acceleration signal acquired on the pump case; the acceleration sensor was not installed in the first stage of the project covered by this Thesis, but its installation is planned for the future development of the project.

5.3 Numerical Model

A numerical model of the reference machine was developed so as to create a "virtual test-rig" which was used for the development of the control algorithm for the independent metering system. Indeed, the execution of numerical simulations instead of experimental tests allows to save time and resources. The numerical model was also exploited to create data in faulty conditions to be used as inputs for the diagnostics algorithm; the execution of tests in faulty conditions requires the availability of faulty components and time for their installation, besides safety issues.

The crane model was developed in the AMESim® environment with a lumped parameters approach. The level of detail of the numerical model was tailored on the application; the parameters which are affected by the most common faults are introduced in the model so as to simulate the effects of these faults by changing the parameters values. The model follows the actual system causality and describes all the sub-systems which are involved in the energy transformation, from the hydraulic pump to the end effector. The main sub-systems described in the numerical model are:

- the flow generation unit;
- the valve manifolds;
- the linear hydraulic actuators;
- the mechanical arms.

In the following sections, the details of the numerical model are presented.

5.3.1 Flow Generation Unit

The FGU consists of a fixed displacement pump operated at constant angular velocity; the delivery flow $\dot{V}_d$ is calculated with Eq. 5.1:

$$\dot{V}_d = \frac{V_d \cdot n}{\eta_v} \tag{5.1}$$

Where V_d is the pump displacement and n is the pump angular velocity. η_v indicates the pump volumetric efficiency which depends on the delivery pressure and was introduced in the model through a lookup table.

5.3.2 Valve Manifolds

The two valve manifolds are composed of cartridge valves of diverse types (see Figure 5-3) interconnected by volumes and hoses (between the two manifolds). The model was developed following a filling-emptying approach and volumes, where the time derivative of the pressure is calculated, alternate with orifices, where the flow between two volumes is calculated. The model is of lumped parameters type therefore the pressure is considered uniform in each volume and the flow rate is uniform in each line.

The time derivative of the pressure in a generic volume i is calculated with Eq. 5.2 which is obtained combining the mass conservation equation with the state equation of the fluid:

$$\frac{dp_i}{dt} = \frac{K(p_i)}{V_i}\left(\frac{\sum_j \dot{m}_j}{\rho(p_i)} - \frac{dV_i}{dt}\right) \tag{5.2}$$

In this equation K is the bulk modulus, V_i is the volume, ρ is the fluid density and $\sum_j \dot{m}_j$ is the summation of the mass flow rates (positive if entering the volume). For the volumes of the hoses the model of the hydraulic lines embedded in the commercial software [5.14] was considered. This model considers the effect due to the wall compliance through an effective bulk modulus and computes also the friction losses in laminar or turbulent conditions depending on the Reynolds number.

The flow rate through a generic orifice j is calculated with Eq. 5.3 in the hypotheses of incompressible flow and stationary regime:

$$\dot{m}_j = sign(\Delta p) \cdot C_d \cdot A_j \cdot \sqrt{2 \cdot |\Delta p| \cdot \rho} \qquad 5.3$$

Where C_d is the flow coefficient, A_j is the cross-section area of the orifice and Δp is the pressure difference across the orifice. The flow area A of the orifice depends on the spool position which needs to be calculated. Figure 5-5 reports the modeling scheme adopted for the post-compensator valve; a similar approach was used for the other valves of the circuit.

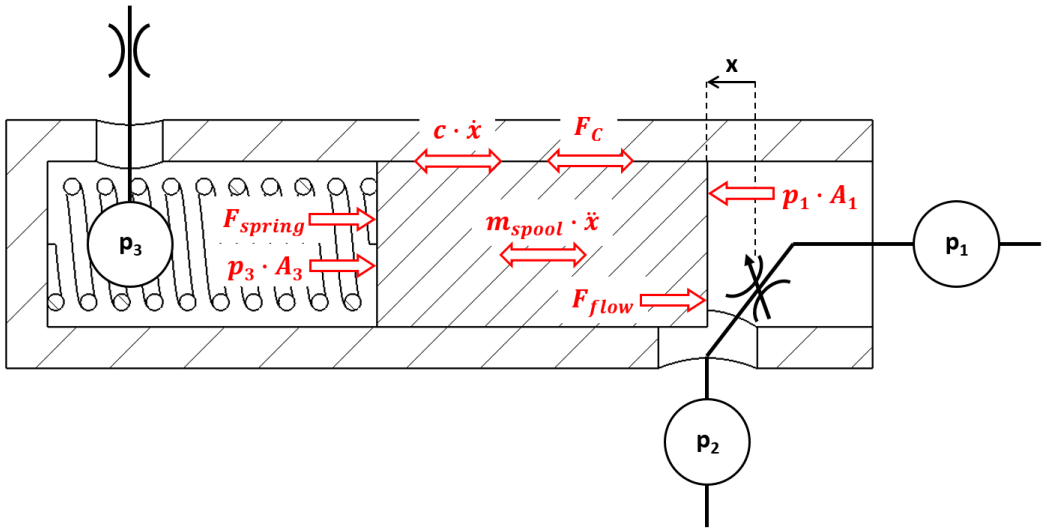

Figure 5-5: Lumped parameters model for the post-compensator valve.

The position x of the valve spool is calculated with Eq. 5.4 which corresponds to the Newton's second law applied to the spool mass m_{spool}:

$$m_{spool} \cdot \ddot{x} = p_1 \cdot A_1 - p_3 \cdot A_3 - F_{flow} - F_{spring} \pm c \cdot \dot{x} \pm F_C \qquad 5.4$$

This equation describes the spool dynamics considering all the most relevant contributions. The static pressure forces are considered by multiplying the static pressures p_1 and p_3 by the corresponding surfaces A_1 and A_3. The force due to the variation of the fluid momentum, i.e. the flow force F_{flow}, is calculated with Eq. 5.5 [5.14]:

$$F_{flow} = 2 \cdot C_d \cdot A \cdot \Delta p \cdot \cos\theta \qquad 5.5$$

Where A is again the flow area of the orifice and θ is the angle which quantifies the deviation of the fluid momentum between the inlet and the outlet of the orifice. The force exerted by the

valve spring is proportional to the valve displacement and the spring stiffness is considered constant. The parameter c indicates the viscous coefficient and therefore a viscous effect proportional to the spool velocity $\dot{x}$ is considered. Finally, the Coulomb friction F_C is considered; the stiction friction (not reported in Eq. 5.4) is considered as well when the spool is in condition of incipient motion. The described valve model requires the knowledge of several parameters, such as the spool mass, the spool geometry, the flow area as a function of the spool displacement, etc., which were defined on the basis of the technical drawings and the technical specifications provided by the valves manufacturer. The definition of other parameters, such as the flow coefficient and the viscous coefficient, were calibrated by comparing the simulation results with the performance curves provided by the valves manufacturer.

5.3.3 Linear Hydraulic Actuators

The force exerted by a linear actuator F_{cyl} is calculated with Eq. 5.6:

$$F_{cyl} = p_p \cdot A_p - p_r \cdot A_r - F_{C,cyl} - c_{cyl} \cdot \dot{x}_{cyl} \qquad 5.6$$

Figure 5-6 illustrates the several contributions of Eq. 5.6.

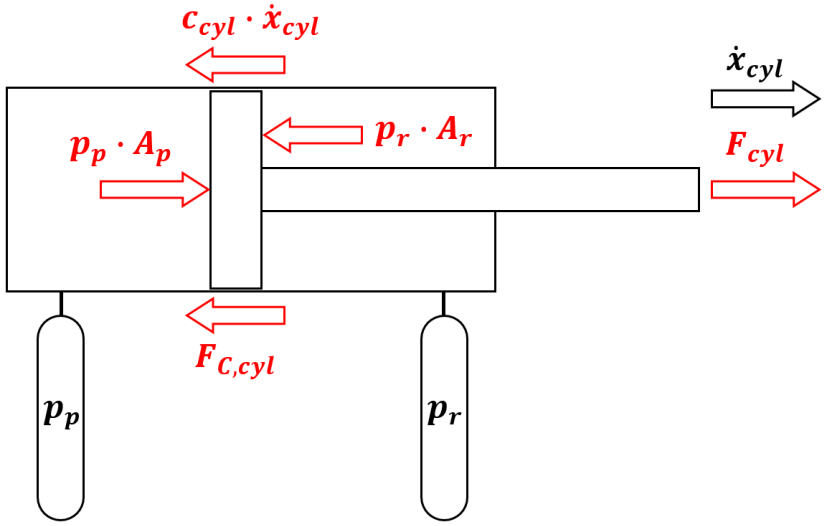

Figure 5-6: Lumped parameters model for the hydraulic linear actuator.

The cylinder force F_{cyl} depends primarily on the piston pressure p_p and the rod pressure p_r acting on the corresponding areas. The effective force applied to the mechanical arms is reduced

by the Coulomb friction force $F_{C,cyl}$ and a viscous friction force proportional to the viscous coefficient c_{cyl}. The inertial effect of the cylinder mass is indirectly considered in the dynamic model of the mechanical arms.

5.3.4 Mechanical Arms

The model of the crane is completed with a multi-body model of its mechanical arms. This dynamic model consists of six rigid bodies: the main boom, the outer boom and the rods which connect the main boom and outer boom cylinders to the mechanical arms. Since the swing rotation is not considered, the model represents a planar mechanism and the mathematical formulation is much simpler than a 3D dynamic model. The model is based on the Lagrange's equations and calculates the planar motion of the bodies under the effect of the external forces; therefore, the forces are the inputs of the model and the bodies positions are its outputs. Constraints to the body motion are introduced in the model to simulate the pivot joints. Figure 5-7 reports the free body diagram of the outer boom (directions x and y define the plane of motion).

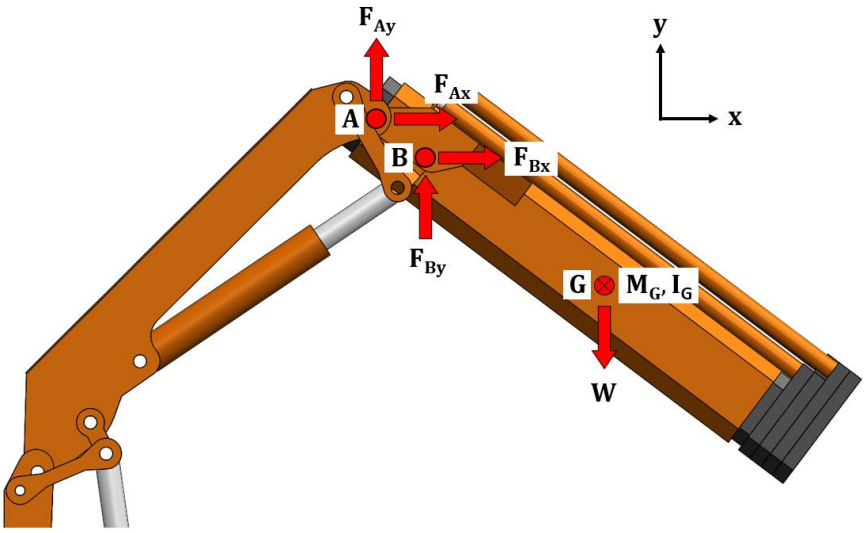

Figure 5-7: Free body diagram of the outer boom.

The pivot joints in A and B are modelled as two orthogonal forces. The other external force acting on the outer boom is the weight acting on the center of gravity. The force due to the load is not considered in this Thesis, but can be easily introduced. Any rigid body is completely described by the knowledge of the mass M_G, the position of the center of gravity G and the moment of inertia along the axis orthogonal to the plane of motion and passing for the center of

gravity. The knowledge of these three parameters for each rigid body was derived from the 3D geometrical model of the mechanical arms.

5.4 Meter-Out Control Strategy

In the independent metering system of the crane (presented in section § 5.2) the velocity of the linear actuators is directly proportional to the meter-in valve opening. Indeed, the system is of LSPC type and the pressure difference across the meter-in valve is kept constant by a post-compensator. The operator command defines directly the opening of the meter-in valve, and therefore the actuation velocity, without the need of any addition control. Unlike a standard single-spool valve system, the meter-out orifice is independent from the meter-in orifice and a proper strategy to control this additional degree of freedom needs to be defined. In this Thesis, a control strategy which combines a feedforward part and a feedback part to control the meter-out valve is proposed. The control strategy is presented for the extension phase of the cylinder, but the same strategy can be applied for the retraction phase. The simplified hydraulic schematic of Figure 5-8 is taken as reference for the presentation of the strategy.

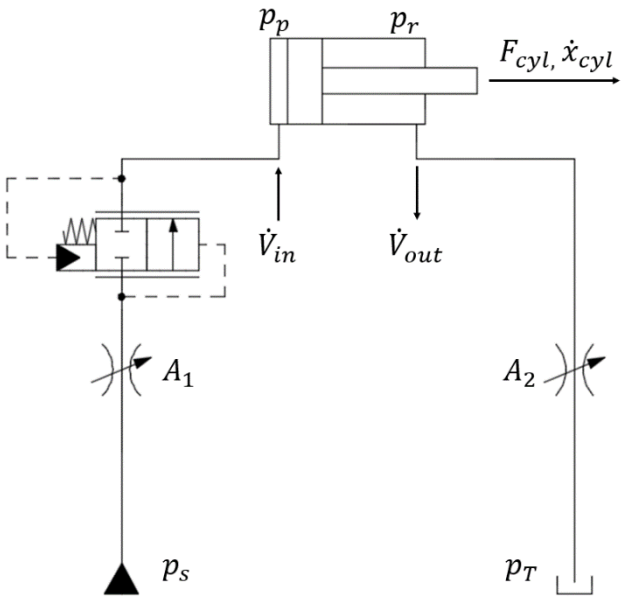

Figure 5-8: Simplified hydraulic schematic.

The control strategy distinguishes between the case of resistive load and overrunning load. In case of resistive load, the meter-out valve is kept completely open so as to optimize the machine energy efficiency. In case of overrunning load, the outlet flow must be throttled otherwise

cavitation occurs in the inlet side of the cylinder and the actuator velocity is no more controlled by the meter-in valve. Indeed, in the considered LSPC system the actuator velocity is directly proportional to the meter-in valve opening until the LS pressure is higher than the tank pressure and the anti-cavitation valves are closed. Figure 5-8 refers to the case of an overrunning load.

The condition of resistive load and overrunning load are distinguished by calculating the force F_{cyl} exerted by the cylinder with Eq. 5.7 where the friction effects are neglected:

$$F_{cyl} = p_p \cdot A_p - p_r \cdot A_r \tag{5.7}$$

p_p and p_r are the piston side and the rod side pressures which are measured through sensors installed on the cylinder. When $F_{cyl} > 0$ the load is resistive and when $F_{cyl} < 0$ the load is overrunning. In case of overrunning load, the cylinder force F_{cyl} can be exploited to calculate the rod pressure required to balance the overrunning force and keep the piston pressure at 0 gauge pressure. In this case the efficiency of the system is maximized, but the system works in condition of incipient cavitation. A reference pressure $p_{p_{ref}}$ higher than the 0 gauge pressure is therefore defined to guarantee a margin against the cavitation condition; in this activity a reference pressure of 10 bar was considered. Once the reference pressure is defined, the corresponding rod pressure $p_{r_{ref}}$ to balance the overrunning force can be calculated with Eq. 5.8:

$$p_{r_{ref}} = p_r + \frac{A_p}{A_r}(p_{p_{ref}} - p_p) \tag{5.8}$$

The feedforward part of the proposed control defines the opening of the meter-out valve from the knowledge of the reference rod pressure $p_{r_{ref}}$ and the meter-in valve opening. For any linear actuator, the relation reported in Eq. 5.9 holds:

$$\frac{\dot{V}_{in}}{A_p} = \frac{\dot{V}_{out}}{A_r} \tag{5.9}$$

The inlet flow rate $\dot{V}_{in}$ and the outlet flow rate $\dot{V}_{out}$ can be calculated with Eq. 5.10 and 5.11:

$$\dot{V}_{in} = C_d A_1(u_1)\sqrt{\frac{2\Delta p}{\rho}} \tag{5.10}$$

$$\dot{V}_{out} = C_d A_2(u_2) \sqrt{\frac{2(p_{r_{ref}} - p_T)}{\rho}} \qquad 5.11$$

In these equations, u_1 and u_2 are the control variables of the meter-in and the meter-out valve respectively, Δp indicates the pressure difference across the meter-in valve (theoretically constant) and p_T is the pressure of the return line which must be measured. In Eq. 5.11 the rod pressure $p_{r_{ref}}$ is considered to keep the piston pressure at the reference value $p_{p_{ref}}$. By introducing Eq. 5.10 and 5.11 in Eq. 5.9, a relation between the meter-out opening and the meter-in opening can be obtained, Eq. 5.12:

$$A_2(u_2) = \frac{A_r}{A_p} \sqrt{\frac{\Delta p}{(p_{r_{ref}} - p_T)}} A_1(u_1) \qquad 5.12$$

The relation between the flow area A_2 and u_2, which depends on the valve and its driver, can be inverted to explicit the control variable of the meter-out valve:

$$u_2 = A_2^{-1}\left(\frac{A_r}{A_p} \sqrt{\frac{\Delta p}{p_{r_{ref}} - p_T}} A_1(u_1) \right) \qquad 5.13$$

Where $A_2^{-1}(x)$ returns the control variable u_2 required to have a flow area $A_2 = x$. Eq. 5.13 constitutes the feedforward part of the control. The control output u_2 depends on the control variable of the meter-in valve and the pressures p_p, p_r and p_T which are measured.

In actual applications, several assumptions considered in the feedforward control are not perfectly respected. The pressure difference Δp across the meter-in valve is not exactly constant and equal to the design value. The function $A(u)$ is known with uncertainty and it is slightly different from valve to valve, even if of the same model, because of the manufacturing tolerances; furthermore, the function changes in time because of the wear and aging. The flow coefficients C_d are not the same between different valves and they vary with the valve opening. For these reasons, the feedforward control would not work alone, and a feedback loop based on a Proportional Integral (PI) control is introduced in the control. The block diagram of the proposed control algorithm is reported in Figure 5-9.

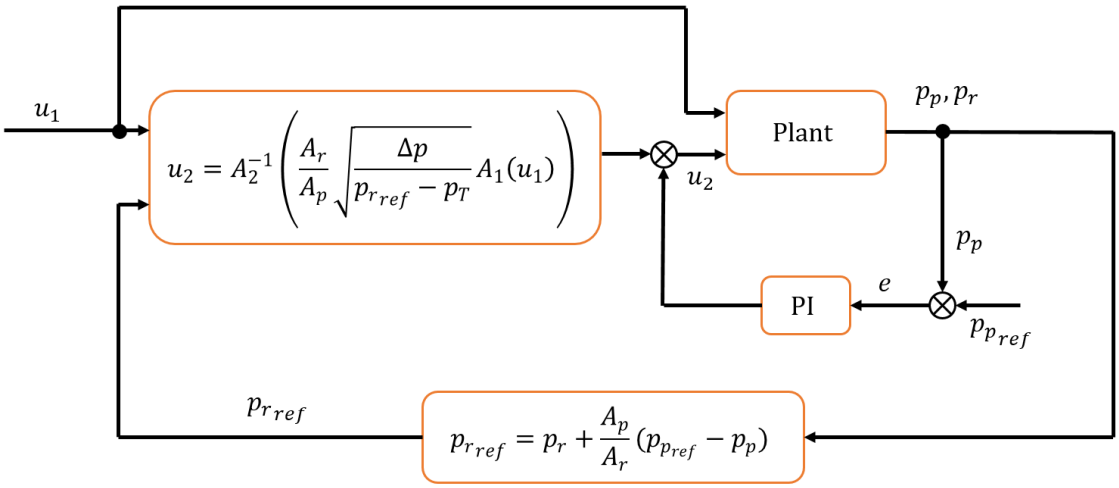

Figure 5-9: Block diagram of the proposed control strategy.

The PI regulator define the correction to apply to the control variable u_2 in order to minimize the error e between the piston pressure p_p and the desired pressure $p_{p_{ref}}$. The procedure adopted for the optimization of the proportional and the integral gains of the feedback loop is presented in the next section.

5.5 Optimization Procedure

The performance of the proposed control algorithm depends on the values of the feedback parameters, i.e. the proportional gain K_P and the integral gain K_I. The definition of these parameters was performed with the Extremum Seeking (ES) optimization algorithm proposed by Aryur [5.15]. The conceptual block diagram of this optimization algorithm is reported in Figure 5-10. This algorithm is of gradient based type. At each iteration, a reference cycle is executed, the value of the cost function J is calculated and a new value of the parameter θ is defined. The optimization continues until the convergence is reached within a defined range.

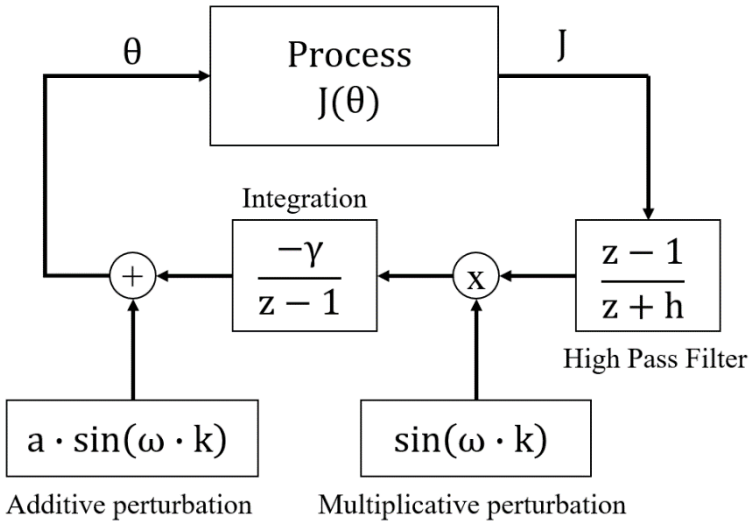

Figure 5-10: Block diagram of the optimization procedure.

The procedure begins with an initial guess for the parameter θ (in this case θ stands for the couple of parameters K_P and K_I). At each iteration the reference cycle is executed with the value of the parameter θ defined in the previous iteration and the value of the cost function J is calculated. A discrete high-pass filter is applied to keep only the variable part of the cost function signal, since this is the interesting part for the optimization procedure. A multiplicative perturbation with pulsation ω is then applied to the output of the filter. The result is integrated with a gain $-\gamma$, where the minus sign forces the algorithm to look for the minimum of the cost function. The integration result is modified by the introduction of an additive perturbation to define the new value of the parameter θ. This algorithm is of gradient based type, therefore could get stuck to a local minimum; the additive perturbation forces the algorithm to look for lower minima around. In this application, the parameters to be optimized are two: the proportional gain K_P and the integral gain K_I. Different values of the pulsation ω must be defined for the two parameters, otherwise the algorithm does not search properly in the two-dimensional space. Furthermore, the values of ω must be higher than the cutoff frequency of the high pass filter.

At each iteration, the algorithm repeats a reference cycle to compute the cost function. In this activity, the considered reference cycle was the outer boom unfolding actuation illustrated in Figure 5-11; in this cycle the meter-in valve of the boom actuator is kept at fully open position for 4 s. This cycle was selected because in the first part of the actuation the load is resistive while in the second part the load is overrunning; this cycle is therefore challenging for the proposed control algorithm. The optimization of the parameters was performed with the simulation model presented above.

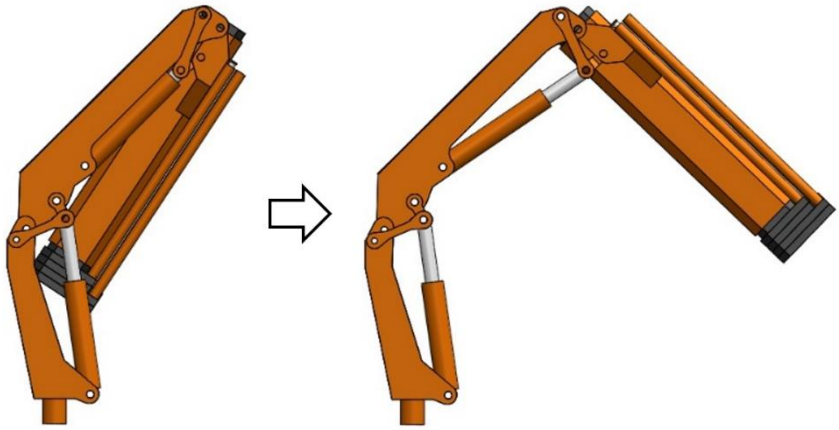

Figure 5-11: Outer boom unfolding movement considered for the optimization of the feedback control parameters.

The objectives of the optimization process must be synthesized in the formulation of the cost function. The objective of the meter-out control is to guarantee the actuator controllability, i.e. throttle the outlet flow so as to avoid cavitation, or anyway the opening of the anti-cavitation valves in the inlet side of the actuator (in this case the piston side). On the other end, the objective of the control is to avoid an unnecessary pressurization of the actuator and the consequent energy losses. These two objectives are achieved by keeping the piston pressure p_p to the reference value $p_{p_{ref}}$ (introduced in section § 5.4). Two cost functions CF_1 and CF_2 were defined to account for these two opposing objectives:

$$CF_1 = \int \max\left(p_p - p_{p_{ref}}, 0\right) \qquad 5.14$$

$$CF_2 = \int \max\left(p_{p_{ref}} - p_p, 0\right) \qquad 5.15$$

Both these cost functions are defined integrating the value of the piston pressure and therefore their calculation does not require the installation of any additional sensor. A graphical representation of the cost functions is reported in Figure 5-12.

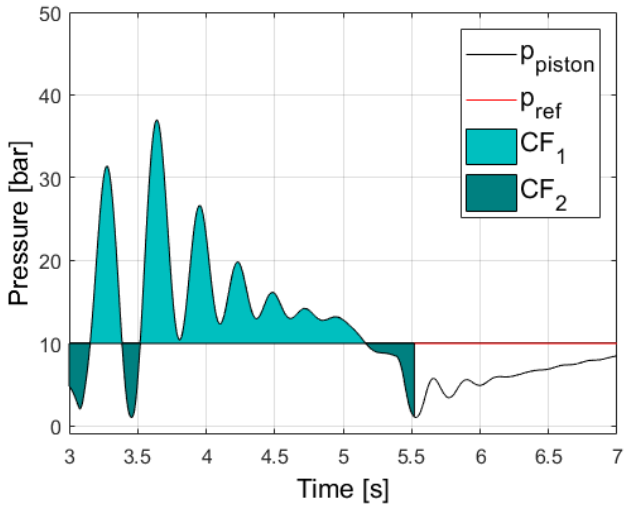

Figure 5-12: Graphical representation of the cost functions.

The cost function CF_1 is proportional to the energy efficiency while the cost function CF_2 is proportional to the risk of cavitation. These cost functions must be combined since the algorithm requires only one cost function. The value of the cost function J was calculated with Eq. 5.16:

$$J = \alpha_1 \cdot CF_1 + \alpha_2 \cdot CF_2 \qquad 5.16$$

The value of the weights α_1 and α_2 was defined considering the different values which the cost functions can assume. The cost function CF_2 assumes smaller values than CF_1 since the minimum value for p_p is -1 bar (gauge pressure). The values considered for α_1 and α_2 are 0.1 and 0.9 respectively. By minimizing the cost function J the optimization process converges towards a solution which avoid the cavitation and an unnecessary pressurization at the same time.

5.6 Diagnostics Approach

The rationale of this project is to combine an advanced control with a diagnostics system for an Electro-Hydraulic (EH) machine. The electronic hardware and a set of sensors are already required for the control of the independent metering system and can also be exploited to infer the machine health condition. This section presents the diagnostics approach developed in this work.

The diagnostics approach is of data-based type and consists of an offline phase and an online phase. The offline phase aims at obtaining a classifier which can identify some faults in the

system. This approach requires to execute tests or obtain historical data of the system in faulty conditions; the faulty conditions considered in the offline phase are those which the classifier can identify. The data are acquired through a set of sensors and then need to be elaborated to define a set of features related to the faults. The definition of the set of sensors to install on the machine and the features extraction are two key points of the methodology. The extracted features are used to train a classifier to distinguish between the healthy condition and the set of the considered faults. In this activity, the cost functions of the optimization process are considered among the features selected for the diagnostics. The defined cost functions (presented in section § 5.5) are indeed performance parameters related to the actuation efficiency and the risk of cavitation whose deviation is symptom of a modification of the system. The classifier is an algorithm whose inputs are the extracted features and whose output is the diagnosis of the system. Different algorithm can be used for the classification task, in this work a static NN is considered. NNs are used in many fields to perform a wide set of different tasks and are the most used also for the classification task in diagnostics systems. The NN trained in the offline phase is used online to identify when a fault occurs in the system. In the online application, the NN receives as inputs the same inputs used in the offline phase and, therefore, the defined set of sensors needs to be installed on the machine and the procedure for the features extraction must be performed online as well.

A data-based diagnostics approach requires the execution of tests in faulty conditions. The reference machine (the hydraulic crane presented in section § 5.2) is equipped with a set of sensors to monitor the value of pressures, flow rates, accelerations and temperatures in different points of the system. The experimental activity is time-consuming, in particular when faulty components need to be inserted in the system to reproduce actual faults; therefore, in the first part of the project presented in this Thesis, the developed model was exploited as a virtual test-rig to simulate the system response in healthy and faulty conditions. This approach allowed to collect easily data in faulty conditions and focus on the development and the test of the diagnostics methodology.

5.6.1 Simulations in Faulty Conditions

The simulation of faults within the system was obtained by changing the value of some relevant parameters of the model. As presented in section § 5.3, the numerical model was designed with a level of detail suitable for the simulation of the most common faults. The following faults were considered in this activity:

- fault 1: volumetric efficiency (η_v) reduction of the hydraulic pump;
- fault 2: increased Coulomb friction in the post-compensator of the outer boom;

- fault 3: increased Coulomb friction in the outer boom hydraulic cylinder;
- fault 4: increased Coulomb friction in the LS unloading valve.

Figure 5-13 shows the position of the considered faults within the system.

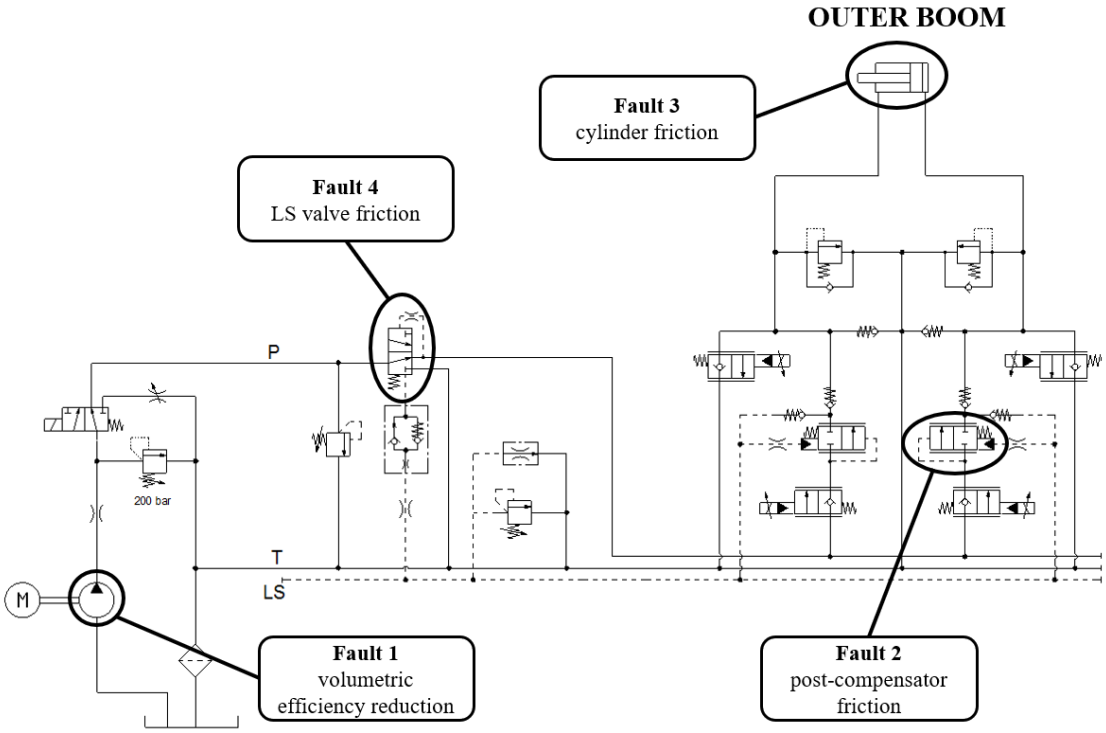

Figure 5-13: Simulated faults.

Each fault was simulated by changing the value of the corresponding parameter, i.e. the volumetric efficiency of the pump for fault 1 and the value of the Coulomb friction for the other three faults. For each fault, four levels of intensity were considered by introducing an increasing deviation of the parameter from the healthy value. The values of the parameters adopted to simulate the considered faults are reported in Table 5-2; these values were defined starting from an estimate of the parameters in the flawless condition.

For the healthy condition and for each faulty condition (4 levels for each of the 4 faults, therefore 16 different faulty conditions) the simulations were repeated 5 times. The 5 simulations were performed by adding a gaussian noise to the faulty parameters; indeed, if a simulation is repeated without changing any input, the results are exactly the same. In actual application, if a cycle is repeated, the results are different because of the effects of many phenomena not included in the model. The gaussian noise is introduced to simulate the typical randomness of the experimental results. The values of the parameters considered to simulate the faults are reported

in Figure 5-14, the values reported in Table 5-2 are represented with continuous lines. In conclusions, 85 simulations were performed to create the set of data to train the static NN.

Table 5-2: Parameters considered to simulate the faults in the hydraulic crane.

	Healthy	**Faulty**				
		Level 1	**Level 2**	**Level 3**	**Level 4**	
Volumetric efficiency	0.95	0.85	0.75	0.65	0.55	[null]
Post-compensator Coulomb friction	1	5	10	15	25	[N]
Cylinder Coulomb friction	1000	2000	4000	7000	10000	[N]
LS valve Coulomb friction	1	5	10	15	25	[N]

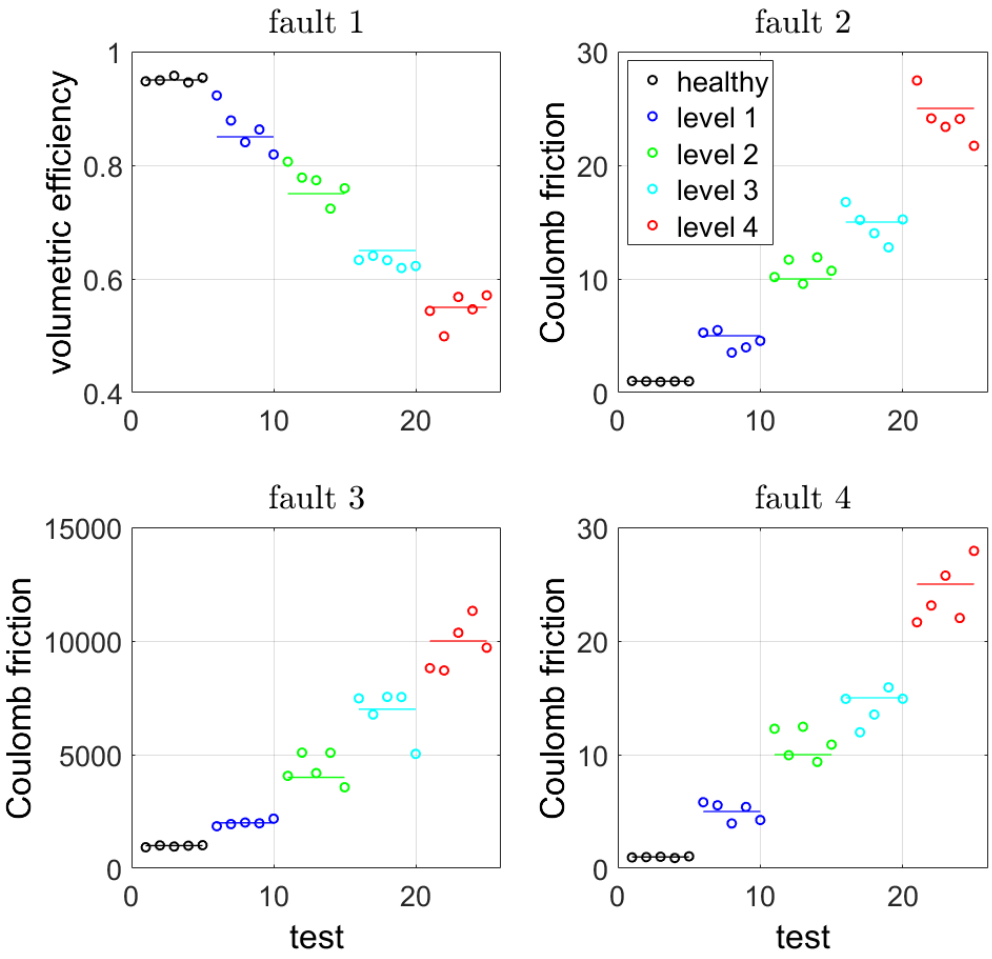

Figure 5-14: Values of the parameters considered to simulate the faults.

The diagnostic approach was tested on the reference cycle described in Figure 5-11, i.e. the same cycle considered for the optimization of the control parameters. In this cycle, only the outer boom actuator is involved, and the considered faults are related to this actuator. The 85 simulations were performed on the reference cycle considering the optimal values of the control parameters obtained in the healthy condition of the system. In this work, only single fault conditions were considered. In actual applications, several faults, even at an incipient level, can be present at the same time and the analysis of multiple faults scenarios is the objective of future steps of this project.

5.6.2 Features Extraction

In actual applications, a set of sensors must be installed on the machine to acquire the signals in healthy and faulty conditions which are required for the training of the classifier. In this activity, virtual sensors are considered to extract the data from the 85 simulations performed. Two set of sensors, referred to as "full set" and "reduced set", were considered in this activity. The full set of sensors corresponds to the set of sensors actually installed on the reference machine. The typology and the position of the sensors are reported in Figure 5-15.

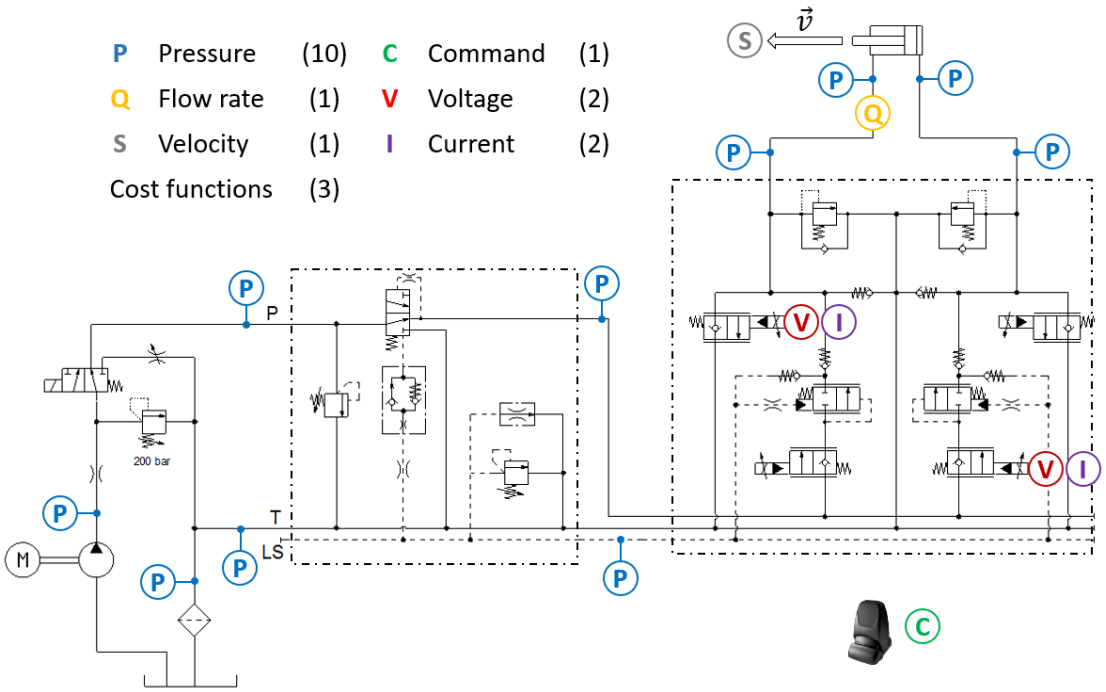

Figure 5-15: Full set of sensors for the diagnostics of the crane.

The full set consists of ten pressure sensors, one flowmeter and one sensor for the measurement of the actuator position/velocity. The voltage and the current of the meter in and the meter out valves are known from the valves drivers and the operator command is a signal defined by the control unit itself. Therefore, the full set of sensors provides seventeen signals for the training of the NN and requires the installation of twelve additional sensors in the system. In addition to these seventeen signals, also the value of the three cost functions, i.e. J, CF_1 and CF_2, calculated on the reference cycle, are considered as inputs for the training of the classifier.

The full set considers the installation of a flowmeter and a velocity sensor on the actuator; these sensors were installed on the reference machine for research purposes, but can difficultly be installed on the actual machine because of their cost and their fragility. Therefore, a reduced set of sensors is considered in this activity. The sensors considered in the reduced set are illustrated in Figure 5-16.

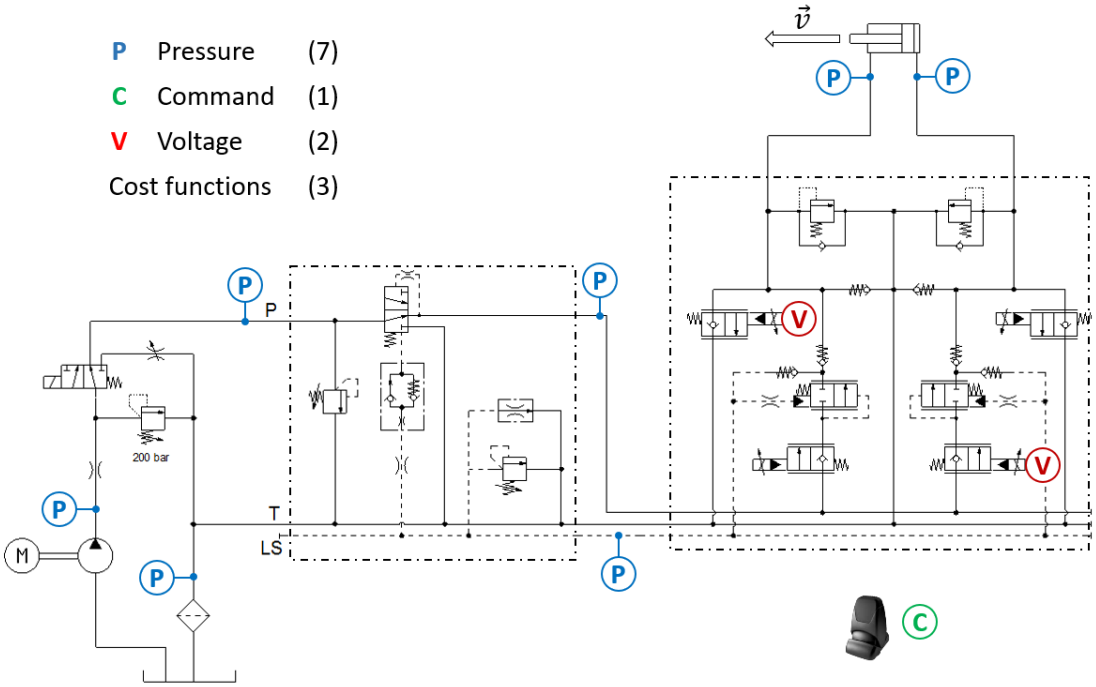

Figure 5-16: Reduced set of sensors for the diagnostics of the crane.

The reduced set requires the installation of seven pressure sensors which are not expensive and are easy to install in the hydraulic circuit. The other three signals, the operator command and the valves voltages, do not require the installation of additional sensors. Also in this case the value of the three cost functions is considered for the training of the classifier.

The full set of sensors provides seventeen signals while the reduced set provides ten signals. From these signals the features for the training of the neural network need to be extracted. The outer boom unfolding cycle considers a valve actuation of 4 s, during which the meter-in valve is kept at the fully open position. In this work, the features were calculated by dividing each signal in four blocks of 1 s each and then computing the mean values of the blocks. The procedure adopted for the features extraction in graphically represented in Figure 5-17 for the case of the pressure measured in the piston side of the outer boom cylinder.

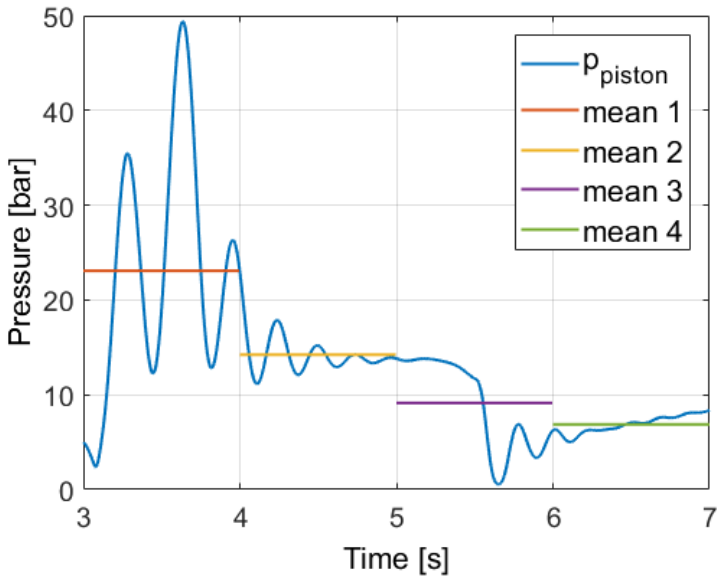

Figure 5-17: Features extraction as mean values (case of the piston pressure signal).

Four features are extracted for each signal and, considering the three features corresponding to the values of the cost functions, this leads to 71 features for the full set of sensors and 43 features for the reduced set of sensors.

5.6.3 Neural Network Training

The extracted features were used to train a static NN through a supervised learning process. The NN considered in this activity is composed of three layers: the input layer, one hidden layer and the output layer. The input layer is made of as many neurons as input features (71 for the full set of sensors and 43 for the reduced set). The hidden layer counts ten neurons characterized by a sigmoid function. The output layer is composed of 4 neurons, one for each faults. The neural network was trained with the features extracted from the 85 simulations; the weights and the

biases of the neurons were calculated with the Levenberg-Marquardt algorithm (the NN was created in the Matlab® environment). The neural network was trained to return an output 0 for the healthy condition, 0.25 for the fault of level 1, 0.5 for the fault of level 2, 0.75 for the fault of level 3 and 1 for the fault of level 4. A schematic of the neural network considered for the classification task is reported in Figure 5-18.

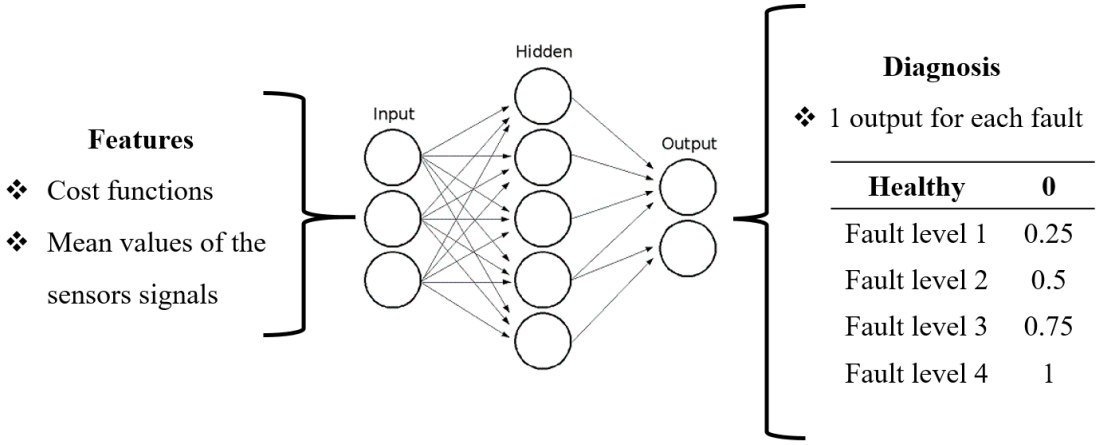

Figure 5-18: Structure of the neural network considered for the diagnostics.

In the online application, i.e. when a set of features extracted from data acquired online is considered, the NN calculates the four outputs which are not discrete, but real numbers which can vary continuously. According to the supervised learning, when the output is close to 0 the diagnosis is that the corresponding fault did not occur, while when the output is greater than 0 the diagnosis is that the fault occurred; the greater the value of the output the greater the fault intensity with a value of 1 when the fault intensity reaches the maximum value used for the network training. This algorithm not only identifies a fault, but returns also an estimate of the fault intensity and this feature can be exploited for prognostic purposes. If the maximum acceptable fault intensity is used to define the value 1 of the output, this NN can be used to monitor the development of the fault and recognize when maintenance is required or when a component of the system must be substituted.

The performance of the NN must be verified on a set of data not used for the training. Indeed, the training algorithm used is extremely powerful and the risk is to train a network with optimal performance on the training data and poor performance on different data, this phenomenon is referred to as overfitting. To verify the performance of the network, two simulations for the healthy condition and two simulations for each of the faulty conditions (34 simulations overall) were executed. The parameters used for the verification of the network were defined in the same

way adopted for the definition of the parameters used for the training and are reported in Figure 5-19.

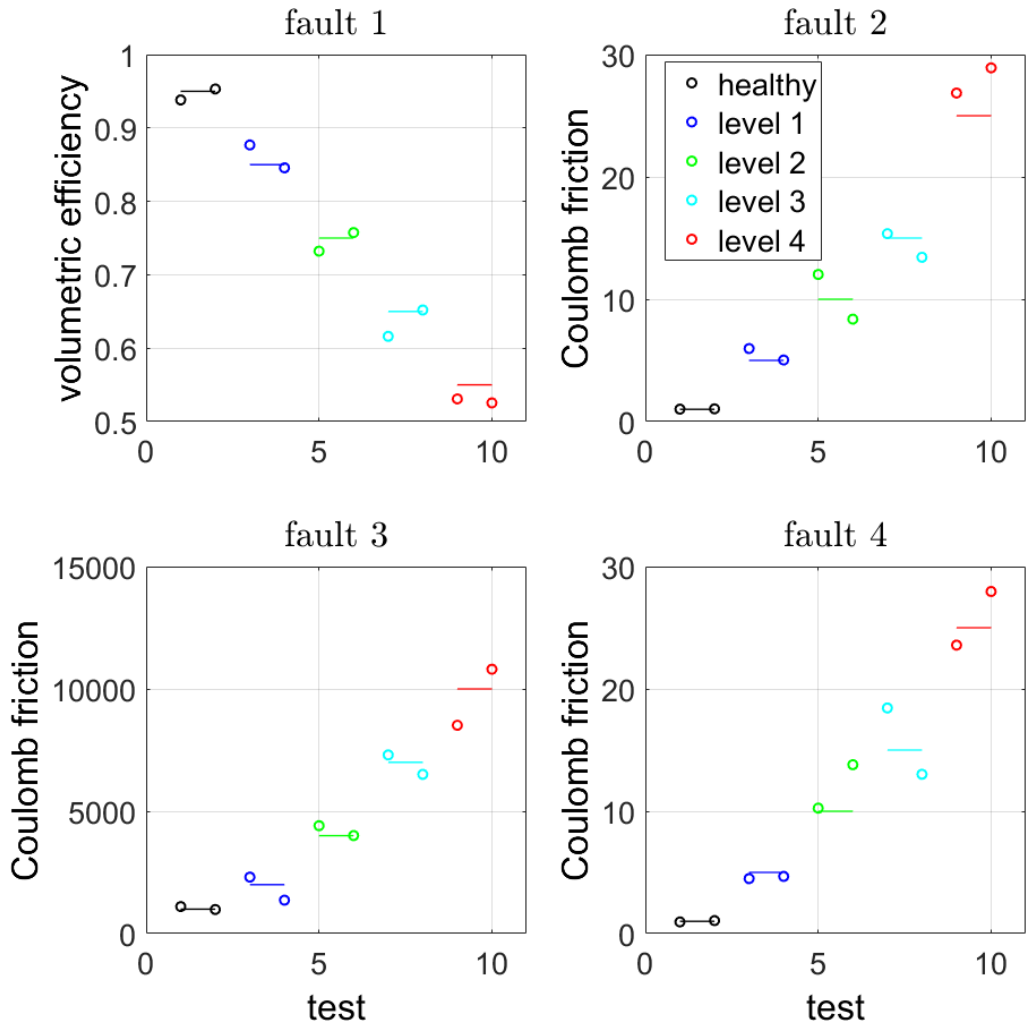

Figure 5-19: Parameters considered for the validation of the neural network.

5.7 Experimental and Simulation Results

This section presents the experimental results used for the validation of the model and the results obtained with the simulation model for the optimization of the control parameters and the crane diagnostics.

5.7.1 Validation of the Numerical Model

The model of the hydraulic crane (presented in section § 5.3) was validated through the comparison with experimental results acquired on the reference machine available at the MAHA Fluid Power Research Center. The cycle considered for the model validation is described in Figure 5-20 and is composed of a main boom unfolding phase followed by an outer boom unfolding phase.

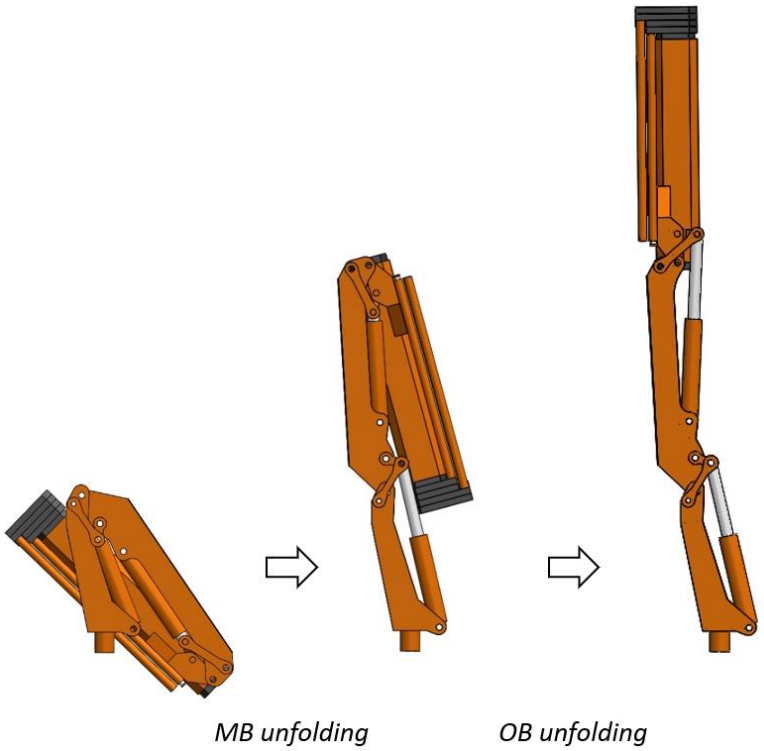

Figure 5-20: Cycle considered for the model validation.

The cycle starts with the main boom and the outer boom actuators at their minimum extension, i.e. with the crane in the closed position. The main boom is actuated with the meter-in valve at the fully opened position until the actuator end stop is reached. In a second time, the outer boom is actuated, always with the meter-in valve at the fully open position, until the actuator end stop is reached. The same cycle with the same input commands was repeated with the developed numerical model and the comparison with the experimental results was performed. Figure 5-21 for the main boom phase and Figure 5-22 for the outer boom phase report the comparison for four pressure signals: the pump delivery pressure p_{pump}, the pressure in the return line p_{tank}, the pressure in the piston side of the considered actuator p_{piston} and the pressure in the rod side p_{rod}.

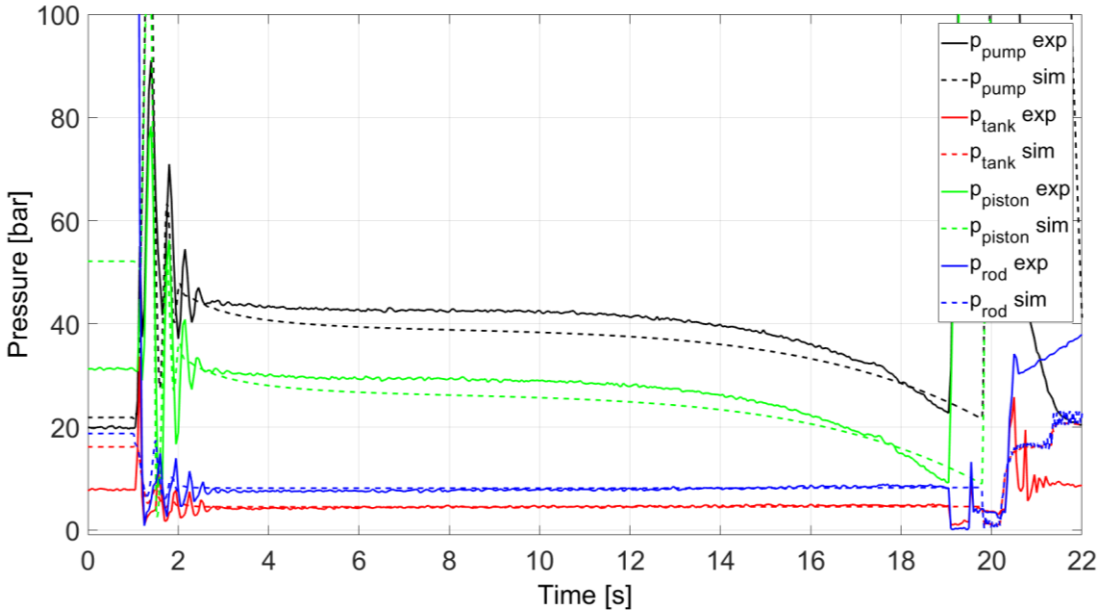

Figure 5-21: Comparison of experimental and simulation results for the MB unfolding movement.

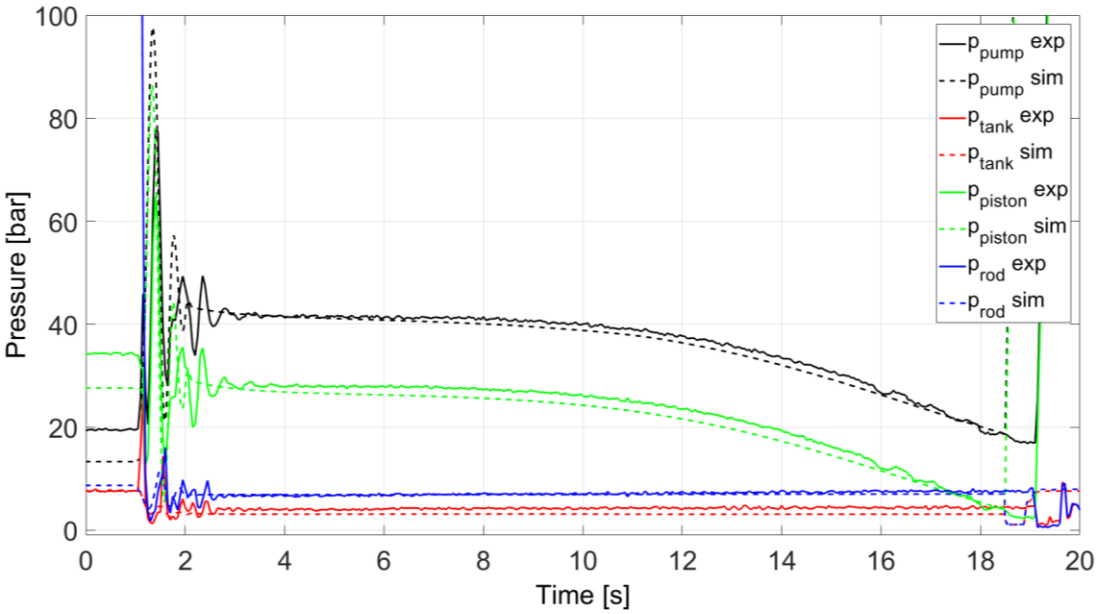

Figure 5-22: Comparison of experimental and simulation results for the OB unfolding movement.

The simulation results match consistently the experimental results; both the pressure levels and the actuation time required for the full extension are well represented. The pressure levels

match all over the actuation and this means that the dynamic model of the mechanical arms recreates properly the forces acting on the actuators. In conclusion, the developed model is a valid "virtual test-rig" which can be used for the development of the control algorithm and the diagnostics system.

5.7.2 Optimization of the Feedback Parameters

The numerical model was used for the optimization of the feedback parameters on the outer boom unfolding cycle presented in Figure 5-11. The optimization was performed with the ES algorithm (presented in section § 5.5) which requires the definition of a first guess for the two control parameters: the proportional gain K_P and the integral gain K_I. The optimization was performed starting with the two parameters at 0, therefore, for the first iteration the control was a pure feedforward control. The piston pressure and the rod pressure obtained with the feedforward control are reported in Figure 5-23.

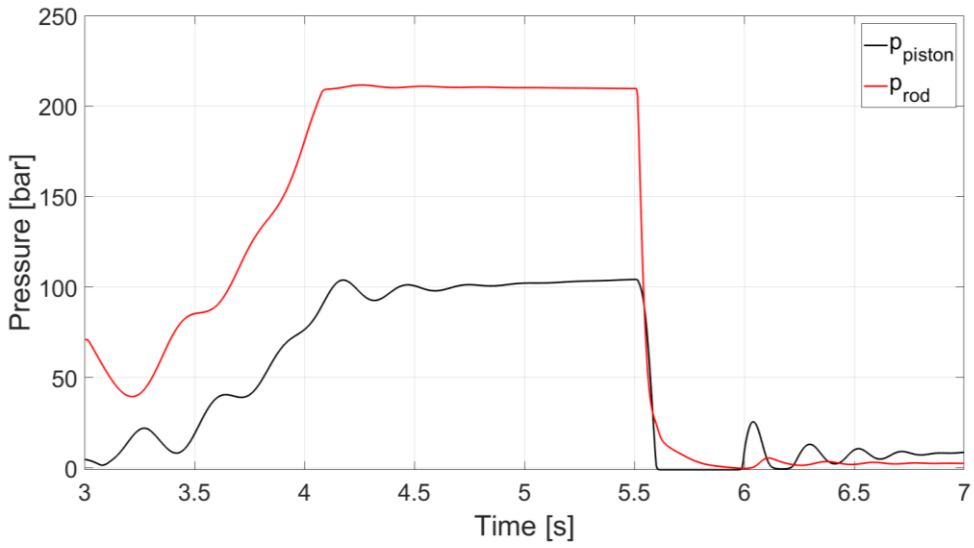

Figure 5-23: Piston pressure and rod pressure with the feedforward control.

The rod pressure is limited by the pressure relief valve because the feedforward control defines an opening for the meter-out valve which is too small for the considered actuation. This error is due to the approximations introduced in the feedforward model described in section § 5.4 which is simpler than the numerical model developed in the AMESim® environment. This mismatch will for sure exist in the application on the actual machine, even if a refined feedforward model is adopted, because the actual machine is not perfectly representable by a numerical model and

even a small approximation can lead to a consistent discrepancy. The convergence plots for the cost function J, and the control parameters K_P and K_I are reported in Figure 5-24. The value of the cost function J is normalized with its value in case of feedforward control, therefore the value of J is 1 for the first iteration.

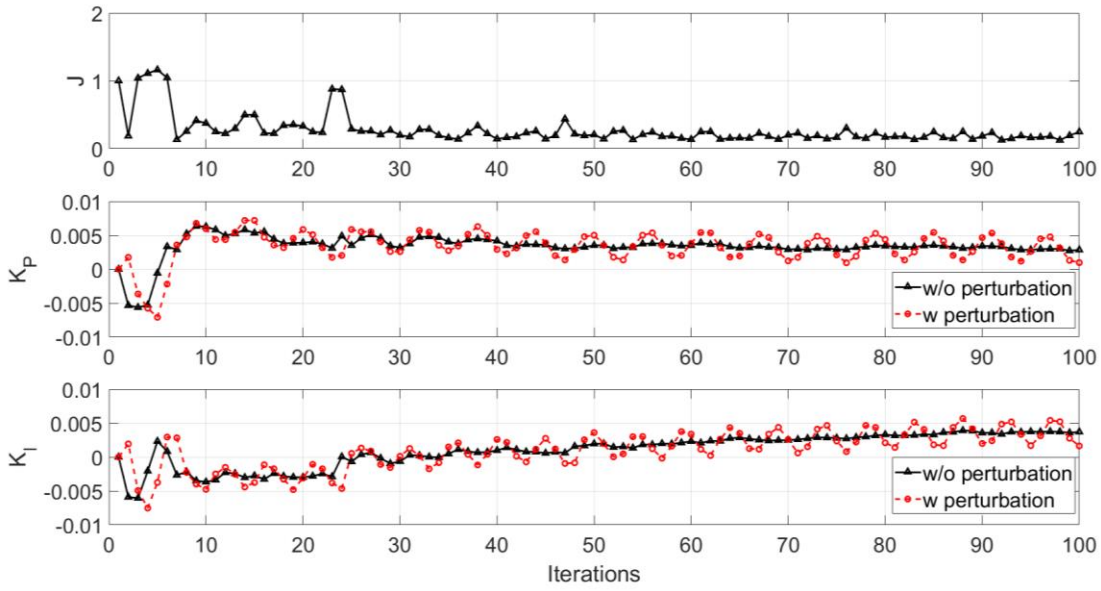

Figure 5-24: Convergence plots for the cost function J and the feedback parameters K_P and K_I.

The plots show that after 100 iterations the control parameters reached the convergence and the value of the cost function is heavily reduced. The optimized values of the control parameters are the result of the integration (black curves in the figure) before the application of the additive perturbation (red curves). The repetition of the reference cycle with the optimized feedback control leads to the values of the piston and rod pressure reported in Figure 5-25.

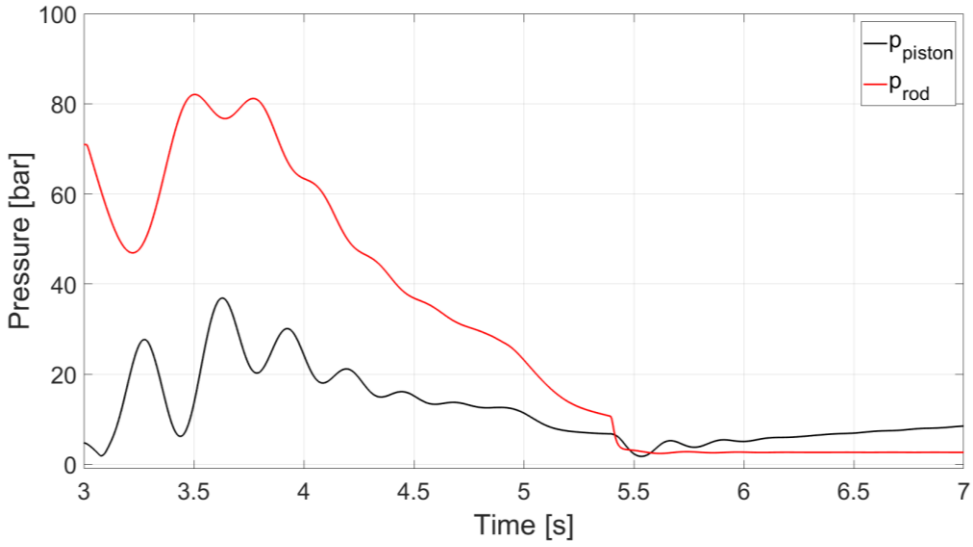

Figure 5-25: Piston pressure and rod pressure with the optimized feedback control.

The introduction of the feedback control allows to maintain the controllability of the actuator since the piston side of the actuator is kept pressurized and the cavitation is avoided. At the same time, the value of the piston pressure is kept close to the reference value of 10 bar all along the actuation and therefore the cycle is accomplished in an efficient way. In this work the control parameters were optimized for a specific cycle, the same procedure can be repeated for other cycles and a gain scheduler can be implemented online so as to select the optimal values of the parameters for each actuation. The proposed optimization algorithm can also be implemented online to adapt the control parameters to the machine changes, due to aging, degradation or incipient faults.

5.7.3 Diagnostics Results

The cost functions used for the optimization of the control parameters are performance indicators and are considered as inputs of the diagnostics algorithm. The sensibility of the cost functions to the considered faults was estimated by performing a series of simulation with an increasing fault intensity. Only single faults scenarios were considered and for each fault 15 simulations were carried out. The volumetric efficiency was decreased linearly from the healthy value of 0.95 to the value of 0.65. The Coulomb friction in the post-compensator valve and in the unloading valve was increased with constant step from the healthy value of 1 N to 20 N. The cylinder Coulomb friction was increased with constant step from the healthy value of 1000 N to

7500 N. The cost functions CF_1 and CF_2 for the 60 simulations are reported in Figure 5-26; the simulations were performed with the optimal value of the control parameters.

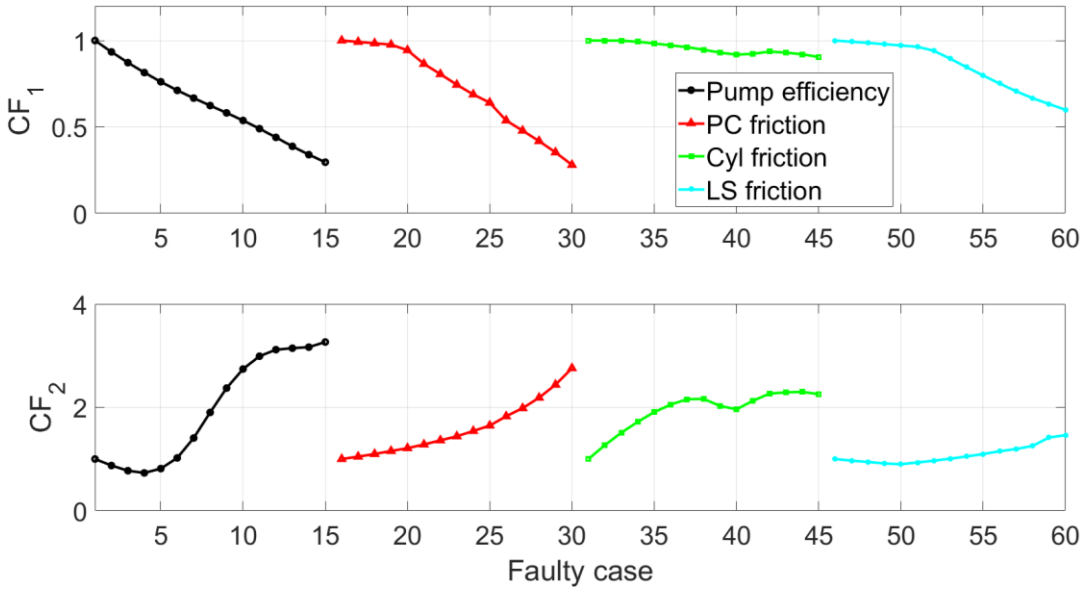

Figure 5-26: Value of the cost functions in faulty conditions.

For all the considered faults, the value of the cost function CF_1, proportional to the actuation efficiency tends to decrease, while the value of the cost function CF_2, relative to the risk of cavitation, tends to increase. The considered faults seem to increase the efficiency of the system, but in most cases, this is obtained through the cavitation in the piston side and the consequent loss of controllability of the actuator. The reduction of the pump volumetric efficiency induces a reduction of the flow rate, therefore, the meter-out valve opening calculated by the control algorithm is bigger than actually required and the actuator pressures reduce; the reduction of the piston pressure explains the trend of the two cost functions. The two faults related to an increased vale friction show a similar trend, but with different intensities. In both cases the increased friction slows the valve dynamic down and, consequently, the risk of cavitation increases in the first part of the actuation because the meter-out valve response remains the same. The increased Coulomb friction in the cylinder reduces the time where an overrunning load is present, and this explains the slight decrease of CF_1; the cost function CF_2 instead increases because the increased stiction force augments the cavitation at the beginning of the actuation.

The two cost functions are sensible to the considered faults and therefore can be considered as valuable input parameters for the diagnostic algorithm. However, all the considered faults induce

a similar trend and therefore also other parameters need to be considered if the objective is to distinguish among different faults. For the training of the NN, besides the cost functions, four features for each acquired signal were considered as presented in section § 5.6.2. The input features are 71 for the full set of sensors (Figure 5-15) and 43 for the reduced set (Figure 5-16).

The results of the NN trained with the full set of sensors on the training data are reported in Figure 5-27. The first five simulation refer to the healthy case and the next twenty simulations refer to fault 1, the following twenty to fault 2 and so on. Within the twenty simulations of each fault, the first five refer to level 1, the next five to level 2 and so on. The blue markers indicate the target values used for the network training while the red markers indicate the network outputs. The network output 1 refers to the fault 1, the output 2 to fault 2 and so on.

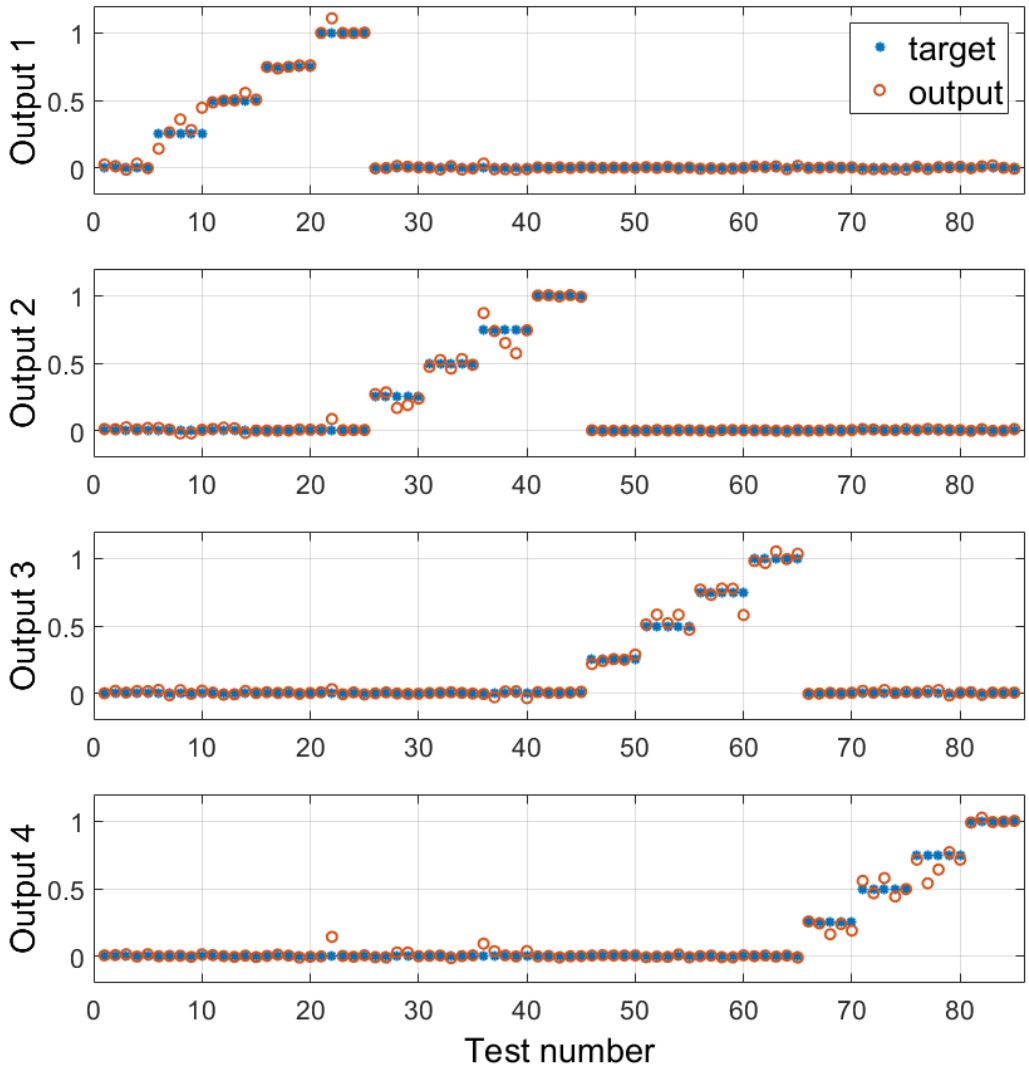

Figure 5-27: Results of the neural network trained with the full set of sensors.

The results demonstrate that the neural network is able to identify the considered faults and their intensity. These results represent the response of the network to the same data set considered for the network training, therefore the performance of the network must be verified on a different set of tests. Figure 5-28 reports the results of the network when the features obtained from the validation tests presented in section § 5.6.3 are used as inputs.

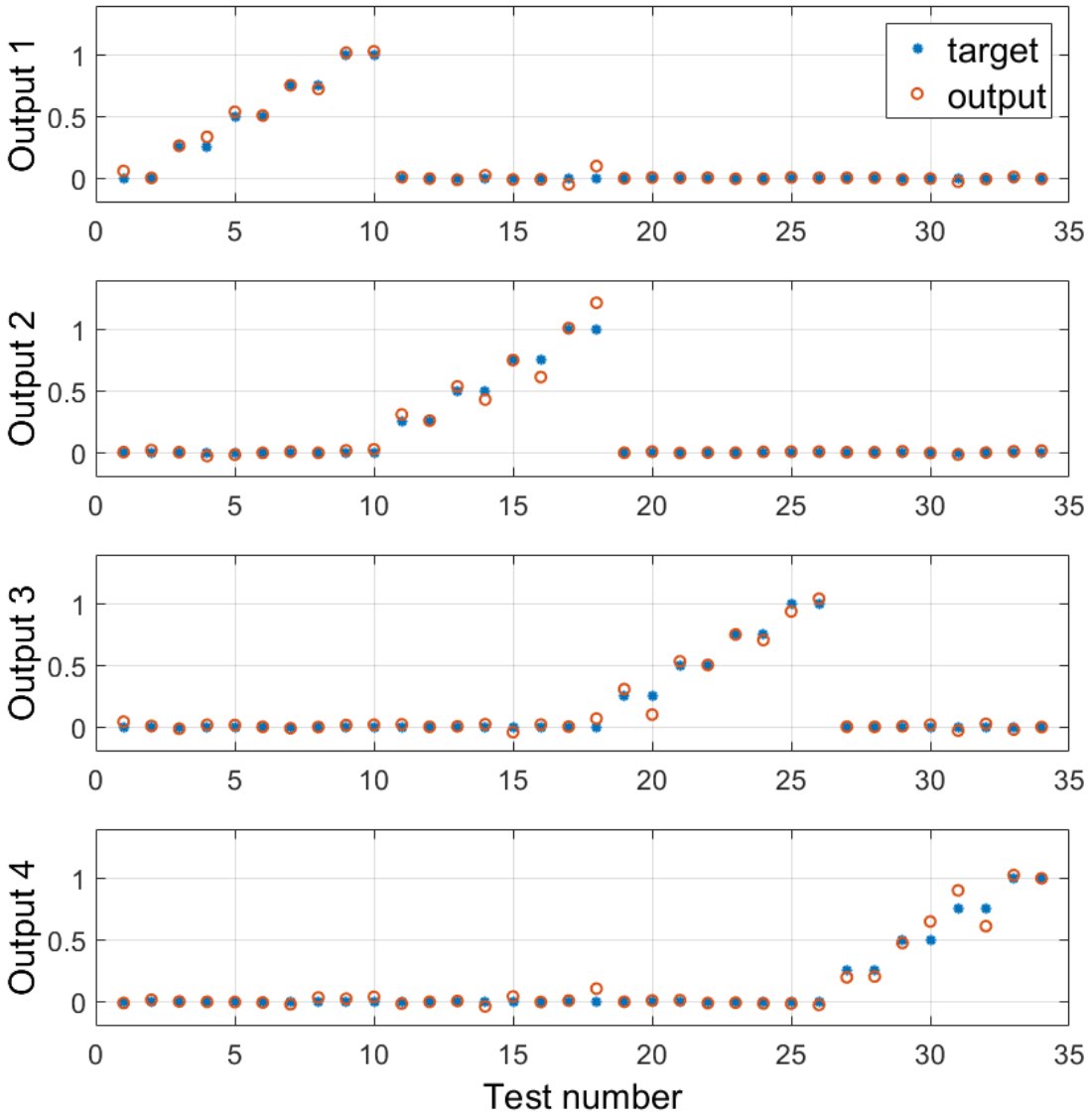

Figure 5-28: Validation results of the neural network trained with the first set of sensors.

The match between the target values, i.e. the expected output, and the output values indicates that the NN is capable of identify not only the faults, but also their intensity also for the validation tests. This result demonstrates that the NN is correctly trained without overfitting.

The full set of sensors considers also some sensors which are expensive and difficult to install on the actual machine. A second NN with the same structure was trained with the data acquired with the reduced set of sensors. The results of the network on the training data set are reported in Figure 5-29; this figure must be interpreted as Figure 5-27 and Figure 5-28.

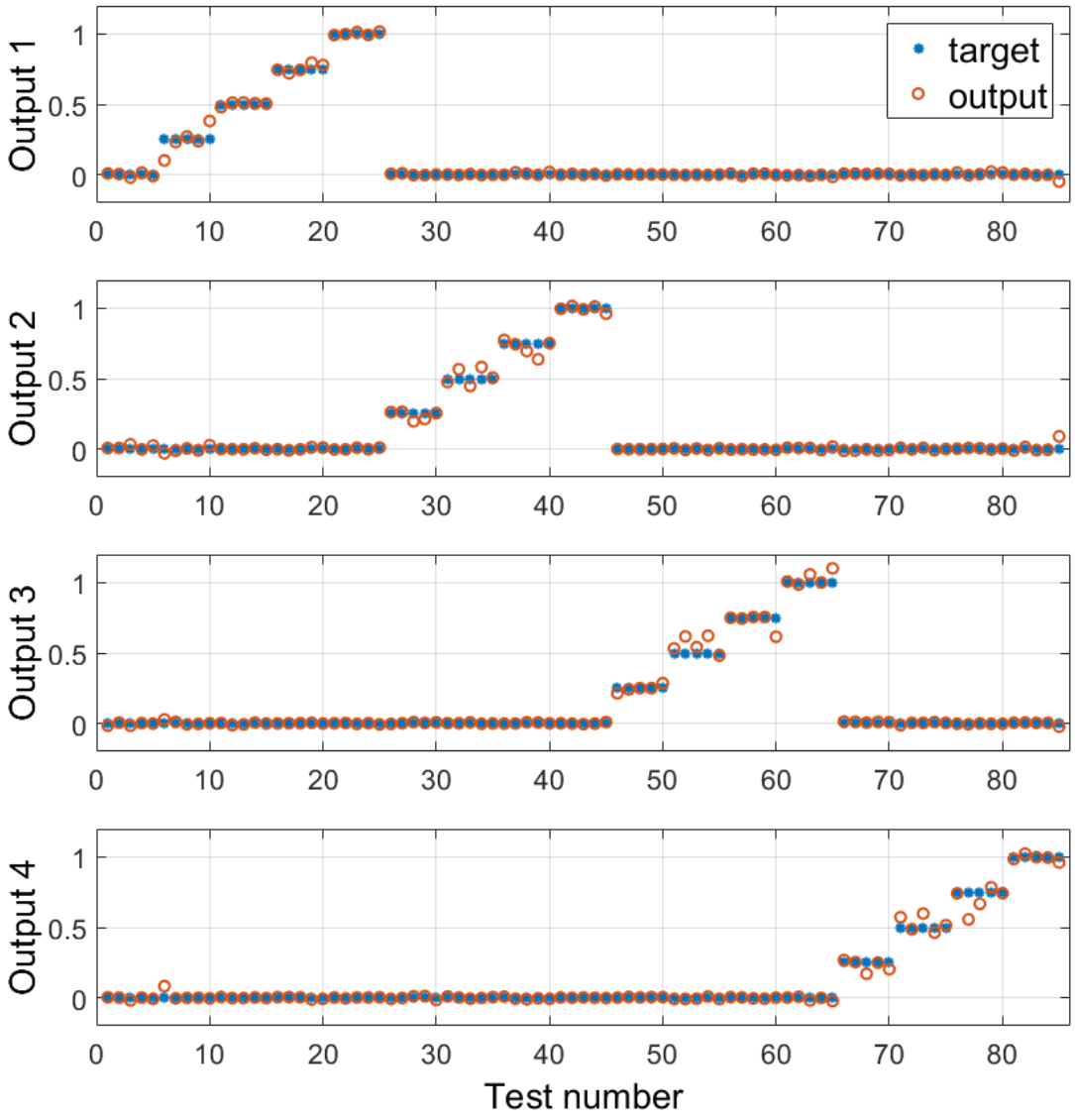

Figure 5-29: Results of the neural network trained with the reduced set of sensors.

Also for the reduced set of sensors the match between target values and output values is clear, but these results are obtained with the same data set used for the training and therefore the NN must be validated on a different set of tests. The results of the NN on the validation data set are reported in Figure 5-30.

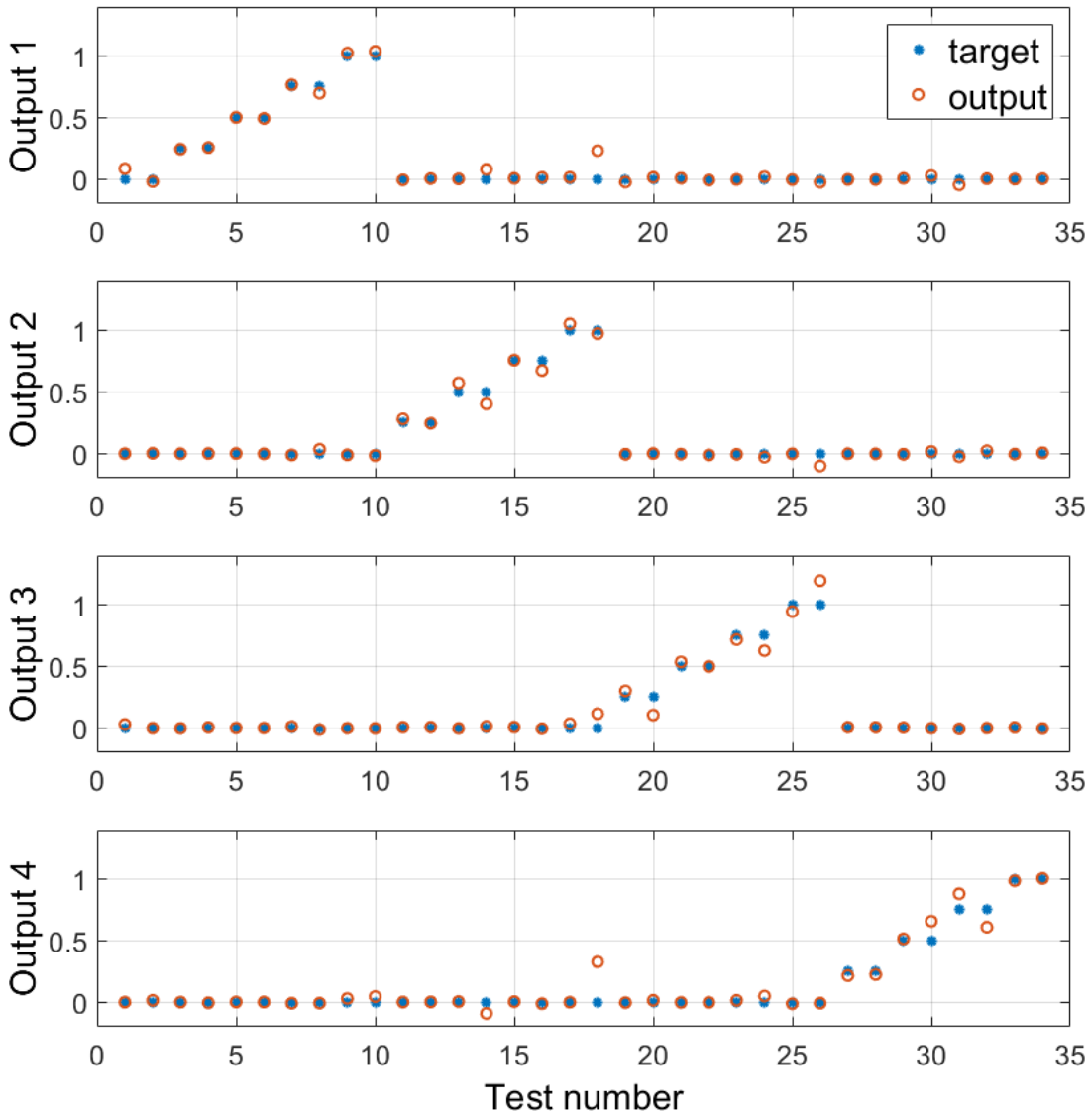

Figure 5-30: Validation results of the neural network trained with the reduced set of sensors.

The match between the expected outputs, target values, and the NN output is consistent also with the reduced set of sensors which requires only the installation of seven pressure sensors. This result is important because demonstrates that an effective system diagnosis can be performed without the installation of expensive and cumbersome sensors.

5.8 Discussion and Future Works

This chapter presented an intelligent system for EH machines which combines an advanced control strategy with a diagnostic and prognostics system. In this activity, the case of a hydraulic

crane was considered, but the developed approach can potentially be applied to any independent metering EH system.

The case study of the hydraulic crane is particularly interesting because in some actuations the load is resistive and in other actuations the load is overrunning. The hydraulic system is of LSPC type and the adoption of an independent metering valve introduced an additional degree of freedom at the meter-out valve. In case of overrunning loads, the meter-out valve must be properly controlled in order to keep the inlet side of the actuator pressurized and therefore maintain the actuator controllability. The control proposed in this Thesis is based on a feedforward part which calculates the required meter-out valve opening. Simulation results demonstrated that the sole feedforward control fails because of the unavoidable simplification in the feedforward model; therefore, a feedback control was added to introduce the required corrective action. The feedback control is based on a PI regulator and the feedback signal is the pressure of the inlet side of the considered actuator. The control performance depends on the value of the feedback gains; the ES optimization algorithm was proposed to define the best pair of control parameters for each actuation. The parameters optimization was demonstrated on a reference cycle, but it can be repeated to define the best control parameters on a wide set of operating conditions. This control algorithm can potentially be applied online to adapt the value of the control parameters to the changes which the machine experiences during its life.

The numerical model of the reference machine, validated on the basis of experimental results, was also exploited to simulate the presence of four common faults in hydraulic machines. The value of the cost functions calculated for the optimization process was used as features for the fault identification. The results demonstrated that the cost functions are sensible to the considered faults and therefore can used as inputs for the diagnostic algorithm. The proposed diagnostic algorithm is based on a static NN which was trained with the results of simulations performed in healthy and faulty conditions. The cost functions are useful for the fault identification, but do not allow to distinguish among different faults; therefore, other features extracted from signal acquired from the system were also considered as inputs of the neural network. Two different set of sensors were considered, a full set of sensors (13 sensors) and a reduced set of sensors (7 sensors). The full set of sensors included some expensive and cumbersome sensors which can difficultly be installed in an actual application; the reduced set instead considered only pressure sensors, which are simple to install. The presented results demonstrated that the performance of the NN trained with the reduced set of sensors are as good as the results obtained with the full set. This result is very important because demonstrates that the fault identification can be performed without the installation of expensive sensors. The proposed diagnostic algorithm returned also a

reliable indication of the fault intensity and this is a key feature which constitute the starting point for the development of a prognostic algorithm.

In this activity, only single fault scenarios were considered. In actual application more than one fault can occur at the same time, therefore, the performance of the proposed diagnostic algorithm needs to be tested on multiple faults cases. If two faults share similar effects, the NN is not able to distinguish between the two faults and returns a wrong diagnosis. To avoid this issue, the features used for the NN training must be selected to be influenced only by one fault, i.e. each feature is relative to a precise fault; to achieve that a proper methodology for the features extraction needs to be implemented. Another future development of this activity is the definition of the minimum set of sensors which is required for the identification of the faults of interest. In this Thesis, it is demonstrated that even a reduced set of sensors can lead to consistent results. The definition of the minimum set of sensors would make the algorithm more cost-effective and therefore more appealing. Finally, the performance of the proposed intelligent system for the control and prognostics must be verified by considering experimental results, which are noisier and with greater stochasticity than the simulation results.

List of references

5.1. T. Torikka, Evaluation of Analysis Methods for Fault Diagnosis on axial-piston pumps, The Twelfth Scandinavian International Conference on Fluid Power, May 18-20, 2011, Tampere, Finland.

5.2. Y. Gao, Q. Zhang, A Wavelet Packet and Residual Analysis Based Method for Hydraulic Pump Health Diagnosis, Proceedings of the Institution of Mechanical Engineers, Part D: Journal of Automobile Engineering, Vol. 220 (2006), issue 6, pp: 735-745.

5.3. N. Helwig, E. Pignanelli, A. Schütze, Condition Monitoring of a Complex Hydraulic System using Multivariate Statistics, Instrumentation and Measurement Technology Conference (I2MTC), May 11-14, 2015, Pisa, Italy.

5.4. A. El-Betar, M. Abdelhamed, A. El-Assal, R. Abdelsatar, Fault Diagnosis of a Hydraulic Power System Using an Artificial Neural Network, JKAU: Eng. Sci., Vol. 17 (2006), No. 1, pp: 117 – 137.

5.5. D. Cristofori, A. Vacca, K. Ariyur, A Novel Pressure-Feedback Based Adaptive Control Method to Damp Instabilities in Hydraulic Machines, SAE International Journal of Commercial Vehicles, vol. 5, no. 2 (October 2012), pp. 586-596, 2012.

5.6. R. Bianchi, A. Alexander, A. Vacca, Active Vibration Damping for Construction Machines Based on Frequency Identification, SAE Technical Paper 2016-01-8121, 2016.

5.7. R. Bianchi, G. F. Ritelli, A. Vacca, Payload oscillation reduction in load-handling machines: A frequency-based approach, Proceedings of the Institution of Mechanical Engineers, Part I: Journal of Systems and Control Engineering, 2017.

5.8. Amir Shenouda & Wayne Book (2008) Optimal Mode Switching for a Hydraulic Actuator Controlled with Four-Valve Independent Metering Configuration, International Journal of Fluid Power, 9:1, 35-43.

5.9. M. Borghi, F. Mancarella, B. Zardin, Energy Dissipation of The Hydraulic Circuit of Remote Auxiliary Utilities of an Agricultural Tractor, Fluid Power and Motion Control 2010.

5.10. S. Liu, B. Yao, Energy-Saving Control of Single-Rod Hydraulic Cylinders with Programmable Valves and Improved Working Mode Selection, SAE International Off-Highway Congress, Las Vegas, Nevada, March 19-21, 2002.

5.11. L. Lu, B. Yao, Energy-Saving Adaptive Robust Control of a Hydraulic Manipulator Using Five Cartridge Valves with an Accumulator, IEEE Transactions on Industrial Electronics, Vol. 61, No. 12, December 2014.

5.12. H. C. Pedersen, T. Andersen, T. Skouboe, M. S. Jacobsen, Investigation and Comparison of Separate Meter-in separate Meter-out Control Strategies, Proceedings of the ASME/BATH 2013 Symposium on Fluid Power & Motion Control, October 6-9, 2013, Sarasota, Florida, USA.

5.13. F. Campanini, R. Bianchi, A. Vacca, P. Casoli, Optimized control for an independent metering valve with integrated diagnostic features, Proceedings of the ASME/BATH 2017 Symposium on Fluid Power & Motion Control FPMC2017 October 16-19, 2017, Sarasota, Florida, United States.

5.14. LMS Imagine.Lab Amesim version 15 2016 – Reference Manual.

5.15. K. B. Ariyur, M. Krstic, Real-Time Optimization by Extremum-Seeking Control, John Wiley & Sons, Inc., Hoboken, NJ, 2003.

Chapter 6 - Summary and Conclusions

The main goal of this Thesis was the development of PHM solutions suitable for hydraulic systems and components. The proposed solutions were demonstrated for the case studies of a variable displacement axial-piston pump and a truck loading crane.

The activity conducted on the axial-piston pump was aimed at the development of a "smart pump" which can provide information about its health status. The pump overall efficiency is an important performance parameter and a thermodynamic method for its estimation was proposed. This approach is based on the first principle of thermodynamics and requires the measurement of the pressure and the temperature at the hydraulic ports. Pressure sensors and temperature sensors are cheap and easy to install, and this makes the thermodynamic approach suitable for the online monitoring. In case of pumps with external drainage, the method requires also the estimation of the ratio of the drainage flow rate and the delivery flow rate; a solution was proposed to avoid the use of expensive flowmeters and keep this method suitable for the online monitoring of hydraulic machines with external drainage. The method requires the knowledge of the fluid properties, but this does not represent a limit; in this Thesis a fluid model was derived from experimental data. A critical point of this method is the measurement uncertainty which was accurately measured according to the relevant standards. The greatest contribution to the combined uncertainty on the overall efficiency is due to the measurement of the temperature difference between the suction and the delivery ports; high accuracy temperature sensors must be used to keep the combined uncertainty at reasonable levels. In this Thesis, high accuracy Pt 100 with a standard uncertainty of ± 0.2 K were used. The thermodynamic method was experimentally validated by means of a comparison with the standard method, based on the direct measurement of the input mechanical power. The uncertainty of the thermodynamic method becomes higher when the delivery pressure

reduces to low values, but it is comparable to that of the standard method at medium and high delivery pressures. The results of tests performed in dynamic conditions demonstrated that the proposed method is unable to return a valid estimate of the overall efficiency when the pump operating conditions change rapidly; this method requires steady state conditions or slowly changing operating conditions. This aspect hinders the use of this method for the online monitoring in many applications in mobile machinery; for these applications a suitable diagnostic phase or cycle must be defined. The method was tested on pumps with incipient faults and it was able to quantify the reduction of efficiency due to two important faults: worn slippers and port plate eroded by cavitation. All the tests were performed by using positive displacement flowmeters for the evaluation of the ratio of the drainage and the delivery flow rates. A solution to avoid the use of flowmeters was presented; this solution is based on an alternative and cheap sensor for the measurement of the drainage flow rate and the estimate of the delivery flow rate from the ideal flow. The idea is to measure the drainage flow rate through the measurement of the differential pressure between the intrados and the extrados of a curve installed at the drainage port. A prototype of this sensor is currently under study and it will be implemented and tested on healthy and faulty pumps in the future developments of this activity. With this solution the proposed method becomes a powerful tool for the online monitoring of hydraulic pumps and hydraulic motors.

A methodology for the analysis of acceleration signals was proposed and applied for the extraction of features for the diagnostics of the axial-piston pump. This methodology is based on the theory of cyclostationarity and decomposes the signal in the contributions due to different sources. The proposed methodology focuses only on the CS1 and CS2 components since they are the most significant in roto-dynamic machines, and proposes tools for their analysis. The CS1 component is extracted by computing the SA which requires an angular sampling. In this activity, a relative encored was used, but this solution is unsuitable for the online monitoring. An alternative solution is based on the time sampling of the acceleration signal and its angular resampling exploiting a tacho signal. This solution will be considered in the future developments of this activity. The MCR algorithm was proposed for the extraction of the CS2 component at a specific cyclic frequency so as to avoid interferences with other CS2 components or the background noise. This methodology was applied to the accelerations signals acquired from two sensors with the pump in healthy and faulty conditions. The two considered faults are worn slippers and port plate eroded by cavitation. The fault related to worn slippers was highlighted clearly both in the CS1 and CS2 analysis. The considered fault related to the port plate eroded by cavitation was a light incipient fault and it was not evident from the CS1 analysis. The application

of the CS2 tools highlighted higher values for the CS2 components at the piston cyclic frequency and at a specific spectral frequency range. The application of the MCR algorithm introduced some benefits, but was not essential for the identification of the considered faults. The MCR algorithm is very useful for the identification of those faults, such as a bearing faults, whose CS2 components are masked by CS2 components with higher intensity. In future works, a wider set of incipient faults will be considered and the proposed MCR algorithm will be exploited. The results demonstrated that the proposed methodology is effective for the identification of incipient faults in an axial-piston pump, but it can be applied to other roto-dynamic machines. In future works, the features extracted with the proposed method will be used as inputs of an automatic diagnostic system. In this Thesis, the extracted features were visualized and compared manually; this approach becomes inapplicable with a wider data set and an automatic methodology for the feature reduction will be developed. A problem related to the proposed method is the high computational effort required for the calculation of the CS2 parameters. Once the reduced set of significant features is defined, the methodology can be used to calculate only these features, thus reducing the computational effort and making this approach suitable for online monitoring in many onboard applications.

The activity on the truck loading crane aimed at combining an advanced control strategy with diagnostic and prognostic features. The reference machine was equipped with an independent metering valve and a control scheme for the meter-out valve was proposed. The control algorithm considers a feedforward action and a feedback action. The feedforward action is based on a model of the hydraulic system and requires the knowledge of some system parameters. These system parameters are known with some uncertainty and therefore a feedback action is required to compensate for this uncertainty and reduce the steady state error. A PI controller is used for the feedback control and the pressure of the inlet side of the actuator is used as feedback variable. The gains of the feedback control were optimized by means of the ES algorithm and two cost functions were defined. The unfolding cycle of the outer boom actuator was considered as reference cycle for the control and for the diagnostics. A simulation model of the crane was developed and was validated against experimental results; this model was exploited to demonstrate the performance of the control and to simulate the system in faulty conditions. Simulation results demonstrated that the proposed control is able to manage overrunning loads and guarantee an efficient actuation. The results in faulty conditions demonstrated that the optimization cost functions are sensible to the considered faults and can be used to detect the presence of a fault in the system; however, they are not sufficient for the fault identification. A diagnostic approach based on a NN was proposed. Besides the cost functions, features extracted

in the time domain were considered as inputs of the NN. Two set of sensors were considered and the classification results of the NN demonstrated that an effective classification can be performed even with a reduced set of sensors that includes only pressure sensors, which are cheap and easy to install. The NN was trained with the Levenberg–Marquardt algorithm and was able to return an output proportional to the fault intensity. This last feature is important not only for diagnostics, but also for prognostics. In this Thesis, only single-fault scenarios were considered and in future works the proposed methodology will be tested in presence of multiple faults. When several faults are present at the same time, the extraction of specific features for each fault is required to compute a correct diagnosis and this point will be addressed. Another development of this activity is the identification of the minimum set of sensors required for the fault identification; the identification of the minimum set of sensors will make the diagnostics and prognostics system more cost-effective and attractive. This methodology, developed in simulations, will be tested on the actual machine by introducing faulty components. Actual measurements are noisier and with a greater stochasticity which represent additional challenges for the proposed PHM approach.

In conclusion, this Thesis gives a contribution to the development of PHM systems in the field of FP, both for systems and components. The results obtained are encouraging and create the basis for future developments. The research in the field of PHM is complex, but it is required for the development of the “smart” hydraulic components and the “smart” hydraulic systems of the next generation.

Acknowledgments

The author would like to thank the company Casappa® S.p.A. for the support provided throughout the activity of this Thesis.

The author would like to thank Prof. Paolo Casoli for the opportunity to get involved in a Ph.D. Course on such an interesting topic. The author would like to express his gratitude to Prof. Andrea Vacca (Purdue University) for the opportunity given to join his group at the MAHA Fluid Power Research Lab as a visiting scholar. A special thanks to my colleagues: Luca Riccò, Andrea Bedotti and Mirko Pastori.

The greater thanks are for my family and, in particular, for my brother Enrico who was always by my side during the three years of this Ph.D. Course.